

DYNAMIC MODELING, GUIDANCE, AND CONTROL OF
HOMING MISSILES

A THESIS SUBMITTED TO
THE GRADUATE SCHOOL OF NATURAL AND APPLIED SCIENCES
OF
MIDDLE EAST TECHNICAL UNIVERSITY

BY

BÜLENT ÖZKAN

IN PARTIAL FULFILLMENT OF THE REQUIREMENTS
FOR
THE DEGREE OF DOCTOR OF PHILOSOPHY
IN
MECHANICAL ENGINEERING

SEPTEMBER 2005

Approval of the Graduate School of Natural and Applied Sciences

Prof. Dr. Canan ÖZGEN
Director

I certify that this thesis satisfies all the requirements as a thesis for the degree of Doctor of Philosophy.

Prof. Dr. S. Kemal İDER
Head of Department

This is to certify that we have read this thesis and that in our opinion it is fully adequate, in scope and quality, as a thesis for the degree of Doctor of Philosophy.

Dr. Gökmen MAHMUTYAZICIOĞLU
Co-Supervisor

Prof. Dr. M. Kemal ÖZGÖREN
Supervisor

Examining Committee Members

Prof. Dr. Bülent E. PLATİN	(METU, ME)	_____
Prof. Dr. M. Kemal ÖZGÖREN	(METU, ME)	_____
Prof. Dr. M. Kemal LEBLEBİCİOĞLU	(METU, EEE)	_____
Dr. Gökmen MAHMUTYAZICIOĞLU	(TÜBİTAK-SAGE)	_____
Prof. Dr. Yücel ERCAN	(ETU, ME)	_____

I hereby declare that all information in this document has been obtained and presented in accordance with academic rules and ethical conduct. I also declare that, as required by these rules and conduct, I have fully cited and referenced all material and results that are not original to this work.

Name, Last Name : Bülent ÖZKAN
Signature :

ABSTRACT

DYNAMIC MODELING, GUIDANCE, AND CONTROL OF HOMING MISSILES

ÖZKAN, Bülent

Ph. D., Department of Mechanical Engineering

Supervisor: Prof. Dr. M. Kemal ÖZGÖREN

Co-Supervisor: Dr. Gökmen MAHMUTYAZICIOĞLU

September 2005, 236 pages

In this study, the dynamic modeling, guidance, and control of a missile with two relatively rotating parts are dealt with. The two parts of the missile are connected to each other by means of a roller bearing. In the first part of the study, the governing differential equations of motion of the mentioned missile are derived. Then, regarding the relative rotation between the bodies, the aerodynamic model of the missile is constructed by means of the Missile Datcom software available in TÜBİTAK-SAGE. After obtaining the required aerodynamic stability derivatives using the generated aerodynamic data, the necessary transfer functions are determined based on the equations of motion of the missile. Next, the guidance laws that are considered in this study are formulated. Here, the Linear Homing Guidance and the Parabolic Homing Guidance laws are introduced as alternatives to the Proportional Navigation Guidance law. On this occasion, the spatial derivation of

the Proportional Navigation Guidance law is also done. Afterwards, the roll, pitch and yaw autopilots are designed using the determined transfer functions. As the roll autopilot is constructed to regulate the roll angle of the front body of the missile which is the controlled part, the pitch and yaw autopilots are designed to realize the command signals generated by the guidance laws. The guidance commands are in the form of either the lateral acceleration components or the flight path angles of the missile. Then, the target kinematics is modeled for a typical surface target. As a complementary part of the work, the design of a target state estimator is made as a first order fading memory filter. Finally, the entire guidance and control system is built by integrating all the models mentioned above. Using the entire system model, the computer simulations are carried out using the Matlab-Simulink software and the proposed guidance laws are compared with the Proportional Navigation Guidance law. The comparison is repeated for a selected single-body missile as well. Consequently, the simulation results are discussed and the study is evaluated.

Keywords: Homing missiles, two-part missile, missile dynamics, missile aerodynamics, guidance, proportional navigation, linear homing, parabolic homing, missile control, autopilot design, acceleration autopilot, rate autopilot, angle autopilot, anti-windup, surface target model, target state estimation

ÖZ

HEDEF İZLEYİCİ FÜZELERİN DİNAMİK MODELLEMESİ, GÜDÜM VE DENETİMİ

ÖZKAN, Bülent

Doktora, Makina Mühendisliği Bölümü

Tez Yöneticisi: Prof. Dr. M. Kemal ÖZGÖREN

Ortak Tez Yöneticisi: Dr. Gökmen MAHMUTYAZICIOĞLU

Eylül 2005, 236 sayfa

Bu çalışmada, birbirine göre bağıl dönüş yapabilen ve bağlantıları bir rulman aracılığıyla sağlanan iki parçadan oluşan bir füzenin dinamik modellemesi, güdüm ve denetimi ele alınmıştır. Çalışmanın ilk kısmında füzenin hareketini tanımlayan türevsel denklemler türetilmiş, ardından TUBİTAK-SAGE’de mevcut olan Missile-Datcom yazılımı kullanılarak füzenin aerodinamik modeli çıkarılmıştır. Bulunan aerodinamik katsayılar kullanılarak aerodinamik kararlılık türevlerinin elde edilmesinin ardından, denetim sisteminin tasarımında kullanılacak iletim işlevleri füze hareket denklemlerinden türetilmiştir. Daha sonra, çalışmada kullanılacak güdüm kuralları formüle edilmiştir. Bu kapsamda, Doğrusal Hedef Takibi (DHT) ve Parabolik Hedef Takibi (PHT) güdüm kuralları Oransal Seyrüsefer güdüm kuralına alternatif olarak sunulmuş, ayrıca Oransal Seyrüsefer güdüm kuralının üç boyutlu uzaydaki genel ifadesi türetilmiştir. Bu çalışmanın ardından,

daha önce türetilen iletim işlevleri kullanılarak yuvarlanma, yunuslama ve yandönme otopilotlarının tasarımı yapılmıştır. Burada, yuvarlanma otopilotu füzenin denetimi yapılan ön gövdesinin yuvarlanma açısını sıfırlayacak şekilde tasarlanırken, yuvarlanma ve yandönme otopilotları kullanılarak, ele alınan güdüm kuralı tarafından üretilen güdüm komutlarının gerçekleştirilmesi amaçlanmıştır. Bahsedilen güdüm komutları, füzenin yanal ivme bileşenlerini veya füze uçuş yörüngesi açılarının denetimini sağlayacak şekilde oluşturulmuştur. Ele alınan tipik bir yer hedefi için hedef kinematiğinin modellenmesinin ardından, hedef durum kestirimcisi olarak kullanılmak üzere birinci mertebeden sabit katsayılı sayısal bir filtre tasarlanmıştır. Nihayet, tasarlanan modeller biraraya getirilerek genel füze güdüm ve kontrol sistemi modeli oluşturulmuş ve bu model kullanılarak, ele alınan güdüm kuralları için Matlab-Simulink ortamında bilgisayar benzetimleri gerçekleştirilmiştir. Benzetim çalışmaları, karşılaştırma amaçlı olarak ele alınan tek parçalı genel bir füze modeli için tekrarlanmıştır. Çalışmanın son bölümünde, elde edilen benzetim sonuçları tartışılmış ve genel olarak bu tez kapsamında yapılan çalışmalar değerlendirilmiştir.

Anahtar Kelimeler: Hedef izleyici füzeler, iki parçalı füze, füze dinamiği, füze aerodinamiği, güdüm, oransal seyrüsefer, doğrusal hedef izleme, parabolik hedef izleme, füze denetimi, otopilot tasarımı, ivme otopilotu, açısal hız otopilotu, açı otopilotu, doyumsal hata büyümesinin önlenmesi, yüzey hedefi modeli, hedef durum kestirimi

To My Parents

and

My Wife...

ACKNOWLEDGMENTS

First, I would like to express my sincere appreciation to my supervisor, Prof. Dr. M. Kemal ÖZGÖREN for his helpful suggestions, prompt feedbacks and endless patience. If he had not helped me, I could not complete this thesis. I am grateful to him.

If the guidance and help of Dr. Gökmen MAHMUTYAZICIOĞLU and Dr. Ömer TANRIKULU had not been with me, I think my job would be much harder. I extend my thanks to them.

I would like to express my thanks to my Thesis Supervising Committee members, Prof. Dr. Bülent E. PLATİN and Prof. Dr. M. Kemal LEBLEBİCİOĞLU for their constructive comments and guidance throughout my study.

My special thanks go to Dr. Mutlu D. CÖMERT and Mr. Erdiñ N. YILDIZ for their understanding and help in this study.

Also, I would like to thank my colleagues and my friends Mr. Dursun ÖNER, Mr. Ali E. TURGUT, Mr. Kutluk B. ARIKAN, Mr. Serkan GÜROĞLU, Mr. Yusuf BAŞIBÜYÜK, Mr. Vedat EKÜTEKİN, Mrs. Burcu SÖYLEMEZ (DÖNMEZ), Mr. Alper AKMEŞE, Mr. İsmet OĞRAŞ, Mr. Fahri İŞIKTAŞ, Dr. L. Oktay GÖNÇ, Dr. A. Serkan GÖZÜBÜYÜK and the other friends in TÜBİTAK-SAGE for their friendship and help.

The support of TÜBİTAK-SAGE in this thesis especially in the part of the aerodynamic modeling is also acknowledged.

My greatest thanks go to my parents, Fatma ÖZKAN and Mehmet ÖZKAN, and especially my wife, Nuray ÖZKAN, for their endless support, patience and understanding. If they had not been with me, I could not achieve anything. I love them very much.

Above all, I would like to thank Allah (c.c.), the creator of all things, for giving me the strength and ability to conduct this study.

TABLE OF CONTENTS

PLAGIARISM	iii
ABSTRACT	iv
ÖZ	vi
ACKNOWLEDGMENTS	ix
TABLE OF CONTENTS	xi
LIST OF TABLES	xvi
LIST OF FIGURES	xvii
LIST OF SYMBOLS	xxi
LIST OF ABBREVIATIONS	xxxvi
1. INTRODUCTION.....	1
1.1. General	1
1.2. Studies on the Dynamic Modeling of Missiles in the Literature	3
1.3. Studies on the Guidance of Missiles in the Literature	5
1.3.1 Command to Line-of-Sight Guidance.....	10
1.3.2 Beam Riding Guidance	11
1.3.3 Homing Guidance	12
1.3.3.1 Conventional Homing Guidance Methods.....	15
1.3.3.1.1 Pursuit Guidance	15
1.3.3.1.2 Constant Bearing Guidance.....	17
1.3.3.1.3 Proportional Navigation Guidance.....	18
1.3.3.1.4 Predictive Guidance	21

1.3.3.2	Homing Guidance Methods based on Optimal Control Theory ..	21
1.3.3.3	Homing Guidance Methods based on Game Theory	22
1.3.3.4	Homing Guidance Methods based on Robust Control Techniques	23
1.3.3.4.1	Homing Guidance Methods based on Sliding Mode Control Theory	24
1.3.3.4.2	H_∞ Guidance Methods based on H_∞ Norm Criterion	25
1.3.3.5	Homing Guidance Methods with Applications of Artificial Intelligence Techniques	26
1.3.3.5.1	Homing Guidance using Neural Networks	26
1.3.3.5.2	Homing Guidance using Fuzzy Logic Control Methods	27
1.3.3.6	Integrated Homing Guidance and Control Methods	28
1.4.	Studies on the Control of Missiles in the Literature	29
1.4.1	Classical Control Methods	34
1.4.2	Modern Control Methods	34
1.4.3	Robust Control Methods	35
1.4.3.1	Control Methods based on the Lyapunov's Theorem	35
1.4.3.1.1	Backstepping Control.....	35
1.4.3.1.2	Sliding Mode Control.....	37
1.4.3.2	Control Methods based on H_∞ Norm	37
1.4.4	Intelligent Control Methods	38
1.4.4.1	Neural Network Based Control Methods.....	38
1.4.4.2	Fuzzy Logic Based Control Methods.....	40
1.5.	Studies on the Estimation of Target Motion in the Literature	40
1.5.1	Simple Digital Fading Memory Filters	41
1.5.2	Kalman Filters	42
1.6.	Scope of the Thesis	42

2. MISSILE MODEL	46
2.1. Missile Dynamic Model	46
2.1.1. Missile Kinematics	46
2.1.2. Equations of Motion of the Missile	56
2.2. Missile Aerodynamic Model	64
2.3. Missile Transfer Functions	73
2.3.1 Roll Dynamics	74
2.3.2 Pitch Dynamics	75
2.3.3 Yaw Dynamics	79
2.4. Control Actuation System Modeling	82
2.5. Measuring Instruments Models	87
2.6. Wind Model	87
3. MISSILE GUIDANCE	90
3.1. Considered Guidance Methods	90
3.1.1. Proportional Navigation Guidance Law	90
3.1.1.1. Spatial Derivation of the Proportional Navigation Guidance Law	91
3.1.1.2. Planar Interpretation of the Proportional Navigation Guidance Law	105
3.1.2. Linear Homing Guidance Law	108
3.1.2.1. Spatial Derivation of the Linear Homing Guidance Law	108
3.1.2.2. Planar Interpretation of the Linear Homing Guidance Law	111
3.1.3. Parabolic Homing Guidance Law	116
3.1.3.1. Spatial Derivation of the Parabolic Homing Guidance Law	116
3.1.3.2. Planar Interpretation of the Parabolic Homing Guidance Law	120
3.2. Missile-Target Engagement Kinematics	121

4. MISSILE CONTROL	124
4.1. Missile Autopilot.....	124
4.1.1. Roll Autopilot	124
4.1.2. Transversal Autopilots	127
4.1.2.1. Acceleration Autopilots	127
4.1.2.2. Rate Autopilots	131
4.1.2.3. Angle Autopilots	134
4.2. Anti-Windup Scheme.....	144
4.3. Roll Resolving Scheme	148
5. TARGET MOTION ESTIMATION.....	149
5.1. Target Model.....	149
5.2. Seeker Model	151
5.2.1. Atmospheric Transmittance	152
5.2.2. Seeker Performance	153
5.2.3. Seeker Dome Materials	154
5.2.4. Seeker Types	155
5.2.4.1. Gimballed Seekers	155
5.2.4.2. Strapdown Seekers.....	157
5.2.4.3. Comparison of Gimballed and Strapdown Seeker Models....	158
Gimballed Seeker	158
Strapdown Seeker.....	158
Mounting.....	158
FOV	158
Cost	159
5.2.5. Seeker Detector Model.....	159
5.3. Target State Estimator.....	161

6. CASE STUDIES	166
6.1. Considered Models.....	166
6.2. Aerodynamic Data	168
6.3. Guidance and Control System Models.....	169
6.4. Simulation Results	172
7. DISCUSSION AND CONCLUSION.....	203
REFERENCES.....	213
POLYNOMIALS THAT CAN BE USED IN POLE PLACEMENT	228
CURRICULUM VITAE	232

LIST OF TABLES

Table 1. Comparison of Gimballed and Strapdown Seeker Models.....	158
Table 2. International Visibility Code	163
Table 3. Parameters of the Two-Part Missiles	167
Table 4. Parameters of the Single-Part Missile.....	168
Table 8. Test Configurations.....	173
Table 9. Test Scenarios	173
Table 10. Initial Conditions	174
Table 11. Simulation Results	176
Table 12. Simulation Results for the Target Parameter Uncertainties for S1-C2 Situation	195
Table 13. Simulation Results for the Target Parameter Uncertainties for S2-C2 Situation	196
Table 14. Simulation Results against a Faster Target.....	197
Table 15. Simulation Results with Varying-Bandwidth Autopilots of the C2 Configuration for $t_F = 0.5$ s	198
Table 16. Simulation Results with Varying-Bandwidth Autopilots of the C2 Configuration for $t_F = 1$ s	198
Table 17. Simulation Results for the S1 Scenario for $u_w = v_w = -1$ m/s and $w_w = 0$	201
Table 18. Simulation Results for the S1 Scenario for $u_w = v_w = -7$ m/s and $w_w = 0$	202

LIST OF FIGURES

Figure 1.1. Command to Line-of-Sight Guidance	11
Figure 1.2. Beam Rider Guidance	12
Figure 1.3. Velocity Pursuit Guidance.....	16
Figure 1.4. Constant Bearing Guidance	17
Figure 1.5. Proportional Navigation Guidance	19
Figure 1. 6. Fuzzy Logic Controller Architecture	28
Figure 1.7. Canard-Controlled Missile	30
Figure 1.8. Wing-Controlled Missile	30
Figure 1.9. Tail-Controlled Missile.....	31
Figure 1.10. Fin Arrangements in Aerodynamically Controlled Missiles.....	31
Figure 1.11. Gimbal-Controlled Missile	32
Figure 1.12. Direct Thrust -Controlled Missile.....	33
Figure 1.13. Jet Vane-Controlled Missile	33
Figure 1.14. Side Jets-Controlled Missile.....	33
Figure 2.1. Considered Missile Model.....	47
Figure 2.2. Demonstration of Angle of Attack and Side-Slip Angle	69
Figure 2.3. Considered Fin Arrangement from the Rear View of the Missile.....	70
Figure 2.4. Control Actuation System Block Diagram.....	85
Figure 3.1. Missile-Target Engagement Geometry.....	91

Figure 3.2. Horizontal Plane of the Wind Frame	99
Figure 3.3. Vertical Plane of the Wind Frame	100
Figure 3.4. Planar Pure Proportional Navigation Geometry	106
Figure 3.5. Planar True Proportional Navigation Geometry	107
Figure 3.6. Linear Homing Guidance Law Geometry	108
Figure 3.7. Planar Linear Homing Guidance Law Geometry	113
Figure 3.8. Parabolic Homing Guidance Law Geometry	117
Figure 4.1. Pitch Acceleration Control System.....	127
Figure 4.2. Flight Path Angle Rate Control System.....	131
Figure 4.3. Flight Path Angle Control System.....	137
Figure 4.4. Anti-Windup Scheme	145
Figure 5.1. Horizontal Engagement Geometry	150
Figure 5.2. Basic Seeker Angle Definitions for the Pitch Plane Motion	152
Figure 5.3. Gimbaled Seeker Model	156
Figure 5.4. Strapdown Seeker Model.....	158
Figure 5.5. Target Spot on a Four-Quadrant Detector	161
Figure 6. 1. Unit Step Response of the Acceleration Control System	170
Figure 6. 2. Unit Step Response of the Angle Control System.....	170
Figure 6. 3. Unit Step Response of the Acceleration Control System with Nonlinear Missile Dynamics.....	171

Figure 6. 4. Unit Step Response of the Angle Control System with Nonlinear Missile Dynamics.....	172
Figure 6. 5. Horizontal Missile-Target Engagement in the S1-C1 Situation.....	177
Figure 6. 6. Vertical Missile-Target Engagement in the S1-C1 Situation	177
Figure 6. 7. Horizontal Missile-Target Engagement in the S1-C2 Situation.....	178
Figure 6. 8. Vertical Missile-Target Engagement in the S1-C2 Situation	178
Figure 6. 9. Horizontal Missile-Target Engagement in the S1-C3 Situation.....	179
Figure 6. 10. Vertical Missile-Target Engagement in the S1-C3 Situation	179
Figure 6. 11. Horizontal Missile-Target Engagement in the S2-C1 Situation.....	180
Figure 6. 12. Vertical Missile-Target Engagement in the S2-C1 Situation	180
Figure 6. 13. Horizontal Missile-Target Engagement in the S2-C2 Situation.....	181
Figure 6. 14. Vertical Missile-Target Engagement in the S2-C2 Situation	181
Figure 6. 15. Horizontal Missile-Target Engagement in the S2-C3 Situation.....	182
Figure 6. 16. Vertical Missile-Target Engagement in the S2-C3 Situation	182
Figure 6. 17. Horizontal Missile-Target Engagement in the S3-C1 Situation.....	183
Figure 6. 18. Vertical Missile-Target Engagement in the S3-C1 Situation	183
Figure 6. 19. Horizontal Missile-Target Engagement in the S3-C2 Situation.....	184
Figure 6. 20. Vertical Missile-Target Engagement in the S3-C2 Situation	184
Figure 6. 21. Horizontal Missile-Target Engagement in the S3-C3 Situation.....	185
Figure 6. 22. Vertical Missile-Target Engagement in the S3-C3 Situation	185
Figure 6. 23. Horizontal Missile-Target Engagement in the S4-C1 Situation.....	186
Figure 6. 24. Vertical Missile-Target Engagement in the S4-C1 Situation	186
Figure 6. 25. Horizontal Missile-Target Engagement in the S4-C2 Situation.....	187
Figure 6. 26. Vertical Missile-Target Engagement in the S4-C2 Situation	187
Figure 6. 27. Horizontal Missile-Target Engagement in the S4-C3 Situation.....	188

Figure 6. 28. Vertical Missile-Target Engagement in the S4-C3 Situation	188
Figure 6. 29. Change of the Resultant Command Acceleration for S1-C1 Situation	189
Figure 6. 30. Change of the Resultant Command Acceleration for S1-C2 Situation	189
Figure 6. 31. Change of the Resultant Command Acceleration for S1-C3 Situation	190
Figure 6. 32. Change of the Resultant Command Acceleration for S2-C1 Situation	190
Figure 6. 33. Change of the Resultant Command Acceleration for S2-C2 Situation	191
Figure 6. 34. Change of the Resultant Command Acceleration for S2-C3 Situation	191
Figure 6. 35. Change of the Resultant Command Acceleration for S3-C1 Situation	192
Figure 6. 36. Change of the Resultant Command Acceleration for S3-C2 Situation	192
Figure 6. 37. Change of the Resultant Command Acceleration for S3-C3 Situation	193
Figure 6. 38. Change of the Resultant Command Acceleration for S4-C1 Situation	193
Figure 6. 39. Change of the Resultant Command Acceleration for S4-C2 Situation	194
Figure 6. 40. Change of the Resultant Command Acceleration for S4-C3 Situation	194
Figure 6. 41. Change of the Pitch Autopilot Bandwidth for S2-C2 Situation for $t_F = 1$ s	199
Figure 6. 42. Change of the Resultant Command Acceleration for S2-C2 Situation for $t_F = 1$ s	200
Figure 6. 43. Horizontal Missile-Target Engagement in the S2-C2 Situation for $t_F = 1$ s	200

LIST OF SYMBOLS

Basic Latin Letters

\vec{a}_c	: Commanded Acceleration Vector
$\vec{a}_c^{(k)}$: Column Representation of \vec{a}_c in F_k ($k=b, w$)
a_{wj}^c	: Component of \vec{a}_c along $\vec{u}_j^{(w)}$ Direction ($j=1, 2, 3$)
$\vec{a}_{P/Q}$: Acceleration Vector of Point P with respect to Point Q
a_{cp}	: Pitch Plane Component of the Control Acceleration
a_{cy}	: Yaw Plane Component of the Control Acceleration
A_d	: Detector Area
a_M^n	: Normal Acceleration Component of the Missile in the Pitch Plane
a_M^t	: Tangential Acceleration Component of the Missile in the Pitch Plane
a_T^n	: Normal Acceleration Component of the Target in the Pitch Plane
a_T^t	: Tangential Acceleration Component of the Target in the Pitch Plane
a_x	: Component of \vec{a}_{C_M/O_e} along $\vec{u}_1^{(b)}$ Direction
a_y	: Component of \vec{a}_{C_M/O_e} along $\vec{u}_2^{(b)}$ Direction
a_z	: Component of \vec{a}_{C_M/O_e} along $\vec{u}_3^{(b)}$ Direction
a_{zd}	: Desired Value of a_z

- b_{α} : Pressure Center Offset
- b_{δ} : Static Offset of the Hinge Locations
- $B_j(s)$: j'th Order Butterworth Polynomial in the Laplace Domain
(j=2, 3, 4)
- B_m : Viscous Damping Coefficient of the Control Actuation
System Rotor
- b_t : Viscous Friction Coefficient of the Bearing between Body 1
and Body 2
- $\hat{C}^{(a,b)}$: Transformation Matrix from F_a to F_b
- C_i : Mass Center of Body i (i=1, 2)
- C_{li} : Aerodynamic Moment Coefficient of Body i along $\bar{u}_1^{(b)}$
Direction (i=1, 2)
- C_M : Mass Center of Entire Missile
- C_m : Aerodynamic Moment Coefficient of the Entire Missile along
 $\bar{u}_2^{(b)}$ Direction
- C_n : Aerodynamic Moment Coefficient of the Entire Missile along
 $\bar{u}_3^{(b)}$ Direction
- C_x : Aerodynamic Force Coefficient of the Entire Missile along
 $\bar{u}_1^{(b)}$ Direction
- C_y : Aerodynamic Force Coefficient of the Entire Missile along
 $\bar{u}_2^{(b)}$ Direction
- C_z : Aerodynamic Force Coefficient of the Entire Missile along
 $\bar{u}_3^{(b)}$ Direction
- D^* : Specific Detectivity
- D_a : Time Derivative with respect to Reference Frame F_a

d_{12}	: Distance between Points C_1 and C_2
d_M	: Missile Diameter
d_{miss}	: Resultant Miss Distance
e_γ	: Error of the Flight Path Angle Rate Control System
F_0	: Earth-Fixed Reference Frame
\vec{F}_{Ai}	: Aerodynamic Force Vector Acting on Body i ($i=1, 2$)
F_b	: Reference Frame of Body 1 and the Entire Missile
\vec{F}_{ij}	: Reaction Force Vector Applied by Body i on Body j ($i, j=1, 2$)
F_r	: Line-of-Sight Frame
F_s	: Reference Frame of Body 2
\vec{F}_{T2}	: Thrust Force Vector Acting on Body 2
F_w	: Wind Frame
\vec{g}	: Gravity Vector
$\vec{g}^{(b)}$: Column Representation of the Gravity Vector in F_b
g	: Magnitude of the Gravity Vector
$G_{\alpha\delta}(s)$: Transfer Function from δ to α
$G_c(s)$: Controller Transfer Function
$G_D(s)$: Transfer Function of the Seeker Detector
g_x	: Component of \vec{g} along $\vec{u}_1^{(b)}$ Direction
g_y	: Component of \vec{g} along $\vec{u}_2^{(b)}$ Direction
g_z	: Component of \vec{g} along $\vec{u}_3^{(b)}$ Direction
\hat{I}	: Identity Matrix

I_{ai}	: Axial Moment of Inertia Component of Body i ($i=1, 2$)
i_n	: Standard Deviation of the Noise on the Detector Current
I_{ti}	: Transverse Moment of Inertia Component of Body i ($i=1, 2$)
\tilde{J}_{C_i}	: Inertia Dyadic of Body i ($i=1, 2$)
$\hat{J}_{C_i}^{(b)}$: Inertia Matrix of Body i expressed in F_b i ($i=1, 2$)
J_e	: Equivalent Moment of Inertia of the Control Actuation System
J_f	: Moment of Inertia of the Control Fin
J_M	: Moment of Inertia of the Rotor of the DC Motor
K	: i. Proportional Gain of the Control Actuation System ii. Detector Gain
\bar{k}	: Column of the Controller Gains
K_b	: DC Motor Constant
K_D	: Detector Amplifying Gain
k_ϕ	: Controller Parameter for Roll Attitude of the Roll Autopilot
K_g	: Glint Coefficient
K_γ	: Proportional Gain of the Flight Path Angle Rate Autopilot
k_γ	: Flight Path Angle Gain of the Flight Path Angle Autopilot
K_{HM}	: Hinge Moment Ratio
k_i	: Integral Gain of the Flight Path Angle Autopilot
K_p	: i. Proportional Gain for the Pitch Angle Autopilot ii. Potentiometer Gain
k_p	: Controller Parameter for Roll Rate of the Roll Autopilot

K_q	: Pitch Damping Gain of the Pitch Angle Autopilot
k_q	: Pitch Rate Gain of the Flight Path Angle Autopilot
$K_{q\gamma}$: Pitch Damping Gain of the Flight Path Angle Rate Autopilot
K_R	: Radome Refraction Factor
K_r	: Receiver Coefficient
K_σ	: Scattering Coefficient
K_T	: DC Motor Torque Constant
k_θ	: Pitch Attitude Gain of the Flight Path Angle Autopilot
L	: Component of the Total Aerodynamic Moment Vector along $\bar{u}_1^{(b)}$ Direction
L_1	: Component of \bar{M}_{A1} along $\bar{u}_1^{(b)}$ Direction
L_2	: Component of \bar{M}_{A2} along $\bar{u}_1^{(s)}$ Direction
L_{T2}	: Component of \bar{M}_{T2} along $\bar{u}_1^{(s)}$ Direction
M	: i. Component of the Total Aerodynamic Moment Vector along $\bar{u}_2^{(b)}$ Direction ii. Missile
m	: Mass of the Entire Missile
M_1	: Component of \bar{M}_{a1} along $\bar{u}_2^{(b)}$ Direction
M_2	: Component of \bar{M}_{a2} along $\bar{u}_2^{(s)}$ Direction
\bar{M}_{Ai}	: Aerodynamic Moment Vector acting on Body i ($i=1, 2$)
m_i	: Mass of Body i ($i=1, 2$)
M_∞	: Mach Number

\vec{M}_{ij}	: Reaction Moment Vector applied by Body i on Body j (i, j=1, 2)
\vec{M}_{T2}	: Thrust Misalignment Moment Vector acting on Body 2
M_{T2}	: Component of \vec{M}_{T2} along $\vec{u}_2^{(s)}$ Direction
\tilde{N}	: Effective Navigation Ratio Dyadic
N	: i. Component of the Total Aerodynamic Moment Vector along $\vec{u}_3^{(b)}$ Direction ii. Gearbox Ratio iii. Total Noise
N_1	: Component of \vec{M}_{a1} along $\vec{u}_3^{(b)}$ Direction
N_2	: Component of \vec{M}_{a2} along $\vec{u}_3^{(s)}$ Direction
N_j	: Effective Navigation Ratio along $\vec{u}_j^{(w)}$ Direction (j=2, 3)
n_g	: Standard Deviation of the Glint Noise
n_R	: Standard Deviation of the Radome Refraction Noise
n_r	: Standard Deviation of the Receiver Noise
n_s	: Standard Deviation of the System Noise
N_{T2}	: Component of \vec{M}_{T2} along $\vec{u}_3^{(s)}$ Direction
O_e	: Origin of the Earth-fixed Frame
P	: Predicted Intercept Point
p	: i. Roll Rate of the Entire Missile ii. Pitch Plane
p_i	: Roll Rate of Body i (i=1, 2)
q	: Pitch Rate of the Entire Missile

q_i	: Pitch Rate of Body i ($i=1, 2$)
q_∞	: Dynamic Pressure Acting on the Entire Missile
$q_{\infty i}$: Dynamic Pressure acting on Body i ($i=1, 2$)
R	: Responsivity
r	: i. Yaw Rate of the Entire Missile ii. Reference Input
R_A	: Effective Resistance between Points A and B
R_i	: Incident Radiation
r_i	: Yaw Rate of Body i ($i=1, 2$)
\vec{r}_{M/O_e}	: Position Vector of the Missile with respect to Point O_e
$\vec{r}_{P/Q}$: Position Vector of Point P with respect to Point Q
r_s	: Detectable Range of the Seeker
$R_{S/N}$: Signal-to-Noise Ratio
\vec{r}_{T/O_e}	: Position Vector of the Target with respect to Point O_e
$\vec{r}_{T/M}$: Relative Distance Vector from the Missile to the Target
s	: Laplace Operator
S_M	: Cross-sectional Area of the Missile
s_s	: Size of the Target Spot on the Seeker Detector
T	: i. Ambient Temperature ii. Target iii. Tracker Time Constant
T_0	: Temperature at Sea Level
t_0	: Initial Time

T_a	: Anti-Windup Time Constant
T_d	: Derivative Time Constant of the Control Actuation System
T_D	: Tracker Delay
t_F	: Final Time
T_γ	: Integral Time Constant of the Flight Path Angle Rate Autopilot
T_{HM}'	: Hinge Moment reduced on the Output Shaft of the Control Actuation System
T_i	: Integral Time Constant of the Control Actuation System
T_m	: Torque generated by the Control Actuation System
T_p	: Integral Time Constant of the Pitch Autopilot
T_{sj}	: Sampling Time ($j=y$ and p)
u	: Component of \vec{v}_{C_M/O_e} along $\vec{u}_1^{(b)}$ Direction
u_i	: Component of \vec{v}_{C_i/O_e} along $\vec{u}_1^{(b)}$ Direction ($i=1, 2$)
$\vec{u}_j^{(k)}$: j 'th Unit Vector of the reference frame F_k ($j=1, 2, 3$ and $k=0, b, r, s, w$)
v	: Component of \vec{v}_{C_M/O_e} along $\vec{u}_2^{(b)}$ Direction
V_A	: Voltage at Point A
\vec{v}_c	: Missile-Target Closing Velocity Vector
v_c	: Magnitude of the Missile-Target Closing Velocity Vector
v_i	: Component of \vec{v}_{C_i/O_e} along $\vec{u}_2^{(b)}$ Direction ($i=1, 2$)
v_M	: Magnitude of the Missile Velocity Vector
$\vec{v}_{Mactual}$: Actual Velocity Vector of the Missile

- \vec{v}_{Mideal} : Ideal Velocity Vector of the Missile
- \vec{v}_{M/O_e} : Velocity Vector of the Missile with respect to Point O_e
- V_p : Volume of the Scattering Particles
- $\vec{v}_{\text{P}/Q}$: Velocity Vector of Point P with respect to Point Q
- v_s : Speed of Sound
- v_T : Magnitude of the Target Velocity Vector
- v_{T0} : Initial Target Velocity
- \vec{v}_{T/O_e} : Velocity Vector of the Target with respect to Point O_e
- v_{Tx} : Component of the Target Velocity Vector along along $\vec{u}_1^{(0)}$ Direction
- v_{Ty} : Component of the Target Velocity Vector along along $\vec{u}_2^{(0)}$ Direction
- v_{Tz} : Component of the Target Velocity Vector along along $\vec{u}_3^{(0)}$ Direction
- v_{wx} : Component of the Wind Velocity Vector along $\vec{u}_1^{(0)}$ Direction
- v_{wy} : Component of the Wind Velocity Vector along $\vec{u}_2^{(0)}$ Direction
- v_{wz} : Component of the Wind Velocity Vector along $\vec{u}_3^{(0)}$ Direction
- w : Component of \vec{v}_{C_M/O_e} along $\vec{u}_3^{(b)}$ Direction
- w_i : Component of \vec{v}_{C_i/O_e} along $\vec{u}_3^{(b)}$ Direction ($i=1, 2$)
- X : Component of the Total Aerodynamic Force Vector along $\vec{u}_1^{(b)}$ Direction

X_1	: Component of \vec{F}_{A1} along $\vec{u}_1^{(b)}$ Direction
X_2	: Component of \vec{F}_{A2} along $\vec{u}_1^{(s)}$ Direction
\bar{x}_e	: Column of the Extended State Variables
x_i	: Additional State Variable
x_M	: i. Distance between Points C_1 and C_M ii. Component of the Missile Position Vector along $\vec{u}_1^{(0)}$ Direction
x_{miss}	: Component of the Final Miss Distance of the Missile along $\vec{u}_1^{(0)}$ Direction
x_T	: Component of the Target Position Vector along $\vec{u}_1^{(0)}$ Direction
x_{T0}	: Component of the Initial Target Position Vector along $\vec{u}_1^{(0)}$ Direction
X_{T2}	: Component of \vec{F}_{T2} along $\vec{u}_1^{(s)}$ Direction
Y	: Component of the Total Aerodynamic Force Vector along $\vec{u}_2^{(b)}$ Direction
y	: Yaw Plane
Y_1	: Component of \vec{F}_{A1} along $\vec{u}_2^{(b)}$ Direction
Y_2	: Component of \vec{F}_{A2} along $\vec{u}_2^{(s)}$ Direction
y_M	: Component of the Missile Position Vector along $\vec{u}_2^{(0)}$ Direction
y_{miss}	: Component of the Final Miss Distance of the Missile along $\vec{u}_2^{(0)}$ Direction
y_T	: Component of the Target Position Vector along $\vec{u}_2^{(0)}$ Direction

y_{T0}	: Component of the Initial Target Position Vector along $\bar{u}_2^{(0)}$ Direction
Y_{T2}	: Component of \vec{F}_{T2} along $\bar{u}_2^{(s)}$ Direction
Z	: Component of the Total Aerodynamic Force Vector along $\bar{u}_3^{(b)}$ Direction
Z_1	: Component of \vec{F}_{A1} along $\bar{u}_3^{(b)}$ Direction
Z_2	: Component of \vec{F}_{A2} along $\bar{u}_3^{(s)}$ Direction
z_M	: Component of the Missile Position Vector along $\bar{u}_3^{(0)}$ Direction
z_T	: Component of the Target Position Vector along $\bar{u}_3^{(0)}$ Direction
z_{T0}	: Component of the Initial Target Position Vector along $\bar{u}_3^{(0)}$ Direction
Z_{T2}	: Component of \vec{F}_{T2} along $\bar{u}_3^{(s)}$ Direction

Greek Letters

α	: Angle of Attack
$\bar{\alpha}_{b/0}$: Relative Angular Acceleration Vector of F_b with respect to F_0
β	: Side-Slip Angle
β_j	: Memory Length (j=y and p)
δ_a	: Aileron Deflection
δ_c	: Control Actuation System Command
δ_e	: Elevator Deflection

δ_f	: Fin Deflection
δ_{fd}	: Desired Fin Deflection
Δf_e	: Differential Noise Frequency
ΔI	: Intensity Difference between the Target and its Background
δ_m	: Angular Deflection of the Control Actuation System Output Shaft
$\Delta \vec{r}$: Relative Distance Vector between the Missile and Target
$\Delta \vec{r}^{(0)}$: Column Representation of the Relative Distance Vector between the Missile and Target in F_a
δ_r	: Rudder Deflection
ΔT	: Differential Temperature
ΔT_n	: Noise Equivalent Differential Temperature
Δt	: Duration from the Initial Time to the Final Time
$\Delta \theta_{FOV}$: Sensor Half-Instantaneous Field of View Deviation
ε	: Boresight Angle
ε_D	: Detector Output Signal
ε_p	: Pitch Plane Boresight Angle
ε_y	: Yaw Plane Boresight Angle
ϕ	: Roll Attitude of the Entire Missile
ϕ_{ld}	: Desired Roll Attitude of Body 1
ϕ_{lss}	: Steady-State Value of the Roll Attitude of Body 1
ϕ_i	: Roll Attitude of Body I (i=1, 2)
ϕ_s	: Spin Angle of Body 2 about $\vec{u}_1^{(b)}$ Axis
γ_m	: Flight Path Angle Component of the Missile in the Pitch Plane

γ_m^c	: Command to the Flight Path Angle Component of the Missile in the Pitch Plane
γ_{md}	: Desired Value of the Flight Path Angle Component of the Missile in the Pitch Plane
γ_{mss}	: Steady-State Value of the Flight Path Angle Component of the Missile in the Pitch Plane
γ_{mdss}	: Steady-State Value of the Desired Flight Path Angle Component of the Missile in the Pitch Plane
γ_t	: Flight Path Angle Component of the Target in the Pitch Plane
η_m	: Flight Path Angle Component of the Missile in the Yaw Plane
η_m^c	: Command to the Flight Path Angle Component of the Missile in the Yaw Plane
η_t	: Heading Angle of the Target
η_{t0}	: Initial Heading Angle of the Target
λ	: Line-of-Sight Angle
$\hat{\lambda}_{j(k-1)}$: Line-of-Sight Estimate at Instant 'k-1' (j=y and p)
λ_{jk}^*	: Line-of-Sight Measurement of the Seeker at Instant k (j=y and p)
$\hat{\lambda}_{jk}$: Line-of-Sight Estimate at Instant k (j=y and p)
λ_p	: Pitch Component of the Line-of-Sight Angle
λ_y	: Yaw Component of the Line-of-Sight Angle
μ	: Acceleration Ratio
$\vec{\omega}_{b/0}$: Angular Velocity Vector of F_b with respect to F_0
$\tilde{\omega}_{b/0}^{(b)}$: Tilda Matrix of $\vec{\omega}_{b/0}$ expressed in F_b

ω_c	: Desired Bandwidth
ω_n	: Undamped Natural Frequency
$\vec{\omega}_{r/0}$: Line-of-Sight Angular Velocity Vector
$\vec{\omega}_{s/0}$: Angular Velocity Vector of F_s with respect to F_0
Ω	: Error Angle between the Apparent and True Line-of-Sight Angles
π	: Pi Number ($\cong 3.14$)
ρ	: i. Air Density ii. Seeker Resolution
σ	: Scattering
θ	: Pitch Attitude of the Entire Missile
$\theta_{(1/2)FOV}^3$: Sensor Half-Instantaneous Field of View Angle
θ_i	: Pitch Attitude of Body I ($i=1, 2$)
θ_s	: i. Pitch Plane Seeker Angle ii. Seeker Angle Limit in the Pitch Plane
$\dot{\theta}_s^*$: Desired Angular Rate of the Seeker Centerline
$\tau_{atm-ave}^R$: Average Atmospheric Attenuation Coefficient
Ψ	: Yaw Attitude of the Entire Missile
Ψ_i	: Yaw Attitude of Body I ($i=1, 2$)
Ψ_s	: i. Yaw Plane Seeker Angle ii. Seeker Angle Limit in the Yaw Plane
ζ	: Damping Ratio

Overhead Symbols

- : First Time Derivative
- • : Second Time Derivative
- \rightarrow : Vector
- $-$: Column
- \wedge : Matrix
- \sim : Skew-Symmetric Matrix
- $*$: Desired Value

LIST OF ABBREVIATIONS

AAF	:	Acceleration Advantage Factor
AAM	:	Air-to-Air Missiles
AOA	:	Angle-of-Attack
APKWS	:	Advanced Precision Kill Weapon System
APNG	:	Augmented Proportional Navigation Guidance
ASM	:	Air-to-Surface Missiles
BRG	:	Beam Rider Guidance
CAS	:	Control Actuation System
CG	:	Center of Gravity
CIWS	:	Closed-In Weapon System
CLOS	:	Command to Line-of-Sight
ENR	:	Effective Navigation Ratio
FOV	:	Field of View
FPA	:	Flight Path Angle
HG	:	Homing Guidance
IFOV	:	Instantaneous Field of View
IMU	:	Inertial Measurement Unit
INS	:	Inertial Navigation System
IR	:	Infrared
KF	:	Kalman Filter
LHG	:	Linear Homing Guidance
LOS	:	Line-of-Sight

PHG	:	Parabolic Homing Guidance
PI	:	Proportional plus Integral
PID	:	Proportional plus Integral plus Derivative
PNG	:	Proportional Navigation Guidance
PPNG	:	Pure Proportional Navigation Guidance
RF	:	Radio-Frequency
SAM	:	Surface-to-Air Missiles
SMC	:	Sliding Mode Control
SMG	:	Sliding Mode Guidance
SSA	:	Side-Slip Angle
SSM	:	Surface-to-Surface Missiles
TPNG	:	True Proportional Navigation Guidance
TV	:	Television
TVC	:	Thrust Vector Control
VPG	:	Velocity Pursuit Guidance

CHAPTER 1

INTRODUCTION

1.1. General

A missile can be defined as any object that can be thrown, projected or propelled toward a target [1]. In other words, a missile is a projectile carrying a payload (usually a warhead) which is guided onto a target by manual or automatic means [2]. Obviously, it is primarily used as a weapon in order to give damage to the target.

Missiles can be classified into different categories. Depending on how they are oriented toward the target, the following two major categories come into the picture [1]:

- Unguided Missiles
- Guided Missiles

Unguided missiles, whether initially or continuously propelled, can be oriented toward their targets only before they are fired. After firing, they get completely out of control. Therefore, they can be used with acceptable effectiveness only for short distance and stationary targets; because, for moving targets or for targets at longer distances, the hitting accuracy drops more and more due to various reasons such as aiming errors, crosswinds, curvature and rotation of the Earth, etc.

The unguided missiles are especially ineffective against moving targets unless such targets are particularly close and slowly moving. Guided missiles, on the other hand, can be used effectively both for distant and arbitrarily moving targets because the motion of a guided missile keeps being observed or reckoned and any deviation from a commanded motion is corrected during its flight [1].

The guided missiles can be categorized into two groups depending on the operational range [3]:

- Tactical Missiles
- Strategic, or Ballistic, or Cruise Missiles

Tactical missiles are used in short and medium range scenarios and they are in general guided to the target by some kind of sensors such as seekers. Strategic missiles are different from the tactical ones because they travel much longer distances and are designed to intercept stationary targets whose location is known precisely [3].

Depending on their missions, the missiles can be divided into four subsets [4]:

- Surface-to-Surface Missiles (SSM)
- Surface-to-Air Missiles (SAM)
- Air-to-Air Missiles (AAM)
- Air-to-Surface Missiles (ASM)

An SSM is fired from a surface launcher against a surface target such as a tank, while the target is an air target such as an aircraft in the case of a SAM.

An AAM or an ASM is thrown from an air platform such as an aircraft or helicopter toward an air and surface target, respectively.

Regarding the guided missiles, the guidance and control problem involves four sequential stages:

- Dynamic Modeling
- Guidance
- Control
- Target Motion Estimation

In the dynamic modeling stage, the missile is modeled so as to get the relationships among the selected input and the output variables. Then, the guidance algorithm is developed in order to guide the missile toward the intended target for an expected interception. Once the guidance algorithm is constructed, the next step is to design a control system based on the dynamic model of the missile so that it obeys the command signals generated by the guidance unit. The last stage is the estimation of the kinematic parameters of the target. For this task, it is conventional to use a state estimator algorithm such as Kalman filter or fading memory filter.

1.2. Studies on the Dynamic Modeling of Missiles in the Literature

In order to design a control algorithm, it is a primary requirement to obtain the relationships among the forces/moments acting on the missile and the kinematic state, i.e., position and velocity, of the missile. The external forces and moments acting on a missile are those generated by the aerodynamic effects including control surfaces, the propulsion including control thrusters and the gravity [5]. As the results of these effects, the components of the position vector of the missile along

the downrange, crossrange and altitude directions change as well as the yaw, pitch and roll attitudes.

It turns out that it is easier to model the inertial forces and moments than the aerodynamic force and moment components. The aerodynamic force and moment terms are dependent both on the present and past values of the kinematic parameters of the missile. In order to model the aerodynamics of the symmetric missiles, one of the widely used methods is the Maple-Synge analysis [6]. With this method, the aerodynamic force and moment coefficients are related to the kinematic flight parameters by means of certain functions. For the sake of designing an autopilot, these coefficients are in general expressed as linear functions of angle of attack (AOA), side-slip angle (SSA), or skid angle, effective fin deflections and body angular velocity components [7], [8], [9], [10], [11]. Also, some analytical methods have been developed in order to predict the nonlinear aerodynamic forces and moments acting on a missile undergoing steady and unsteady maneuvers [12]. Some researchers have turned to neural networks as a means of explicitly accounting for uncertain aerodynamic effects [13]. In modeling the aerodynamic forces and moments, the effect of aerodynamic drag on the missile is usually ignored because it causes only a slow change in the speed. As a result of this, the missile speed is treated to be almost constant throughout the after-boost phase [14].

In the sense of the existence of the thrust effect, the motion of the missile can be primarily divided into two successive phases:

- Boost Phase
- After-Boost Phase

As its name implies, the boost phase comprises the flight of the missile from the firing instant to the end of the thrust. Because the thrust that is supplied by the solid propellant in the rocket motor causes the missile to move ahead, the

dynamics of the missiles in the boost phase can be modeled considering the nonzero effect of the thrust force and thus the changing mass [1], [8]. In the after-boost phase, the inertial parameters of the missiles, i.e., its mass and moment of inertia components, remain unchanged.

Although almost all of the guided missiles are single-body structures, there are also rarely seen two-body structures. An example is the so-called “Advanced Precision Kill Weapon System (APKWS)”. In this structure, the guidance section is mounted onto the motor section using a deroll bearing which permits the motor to roll freely while the guidance section is roll stabilized. The roll bearing causes unusual dynamic properties for this missile design because the airframe has two separate sections rolling at different rates. This fact creates additional dynamic coupling between the pitch and yaw channels of the missile [15]. Like APKWS, the missile model dealt with in this thesis is also a two-body structure whose parts are connected to each other by means of a roller bearing.

1.3. Studies on the Guidance of Missiles in the Literature

“Guidance” can be defined as the strategy of steering a missile toward a possible intercept with a target, while “control” can be defined as the tactics of using the missile control actuators to implement the strategy dictated by the guidance unit [5]. The primary functions of the elements that make up the guidance system include sensing, information processing and correction [4].

In the sense of guidance, the flight of a missile can be divided into three main phases [4]:

- i. Boost or Launch Phase
- ii. Midcourse Phase
- iii. Terminal Phase

As mentioned above, the boost phase covers the flight of the missile from the firing instant to the end of the thrust.

The midcourse phase begins after the boost phase and remains till the detection of the intended target by the seeker. Actually, the duration of the midcourse phase is dependent on the instant of the target detection. In midcourse guidance, it is intended to guide the missile to the vicinity of the target as soon as possible. While the midcourse guidance is usually utilized in strategic or long range missiles, it is not employed in short range tactical missiles most of the times [5], [16], [17], [18], [19], [20] .

Once the target is detected by the seeker, the terminal guidance phase is initiated. In this phase, using the target state information acquired by the seeker, the missile is directed to the target by means of the considered guidance law and then the missile tries to follow the target in order to achieve the planned interception.

In addition to the usual classification above, two more phases are emphasized in some studies. The first one of them is the “gathering phase” that is defined as an intermediate phase between the boost and midcourse stages. In this phase, the control of the missile is tried to be gained or captured right after the boost phase [2]. The second additional phase is termed as “shaping phase” that is actually defined as a transition between the midcourse and terminal phases to provide a smooth transition from the midcourse phase to the terminal phase [3].

In the sense of the aimed target, guidance can be normally divided into two groups [5]:

- i. Indirect or Non-Target Related Guidance
- ii. Direct or Target Related Guidance

In indirect guidance, the missile navigates to some predetermined point at which a target related guidance can begin [5]. The indirect guidance can be classified in the following manner [21]:

- Preset Guidance
- Inertial Guidance
- Terrestrial Guidance
- Celestial Guidance

In the Preset Guidance, the path to the intended target is predetermined and then inserted into the missile. In this approach, the missile makes the path corrections according to a pre-determined sequence of the steering commands given in an open-loop manner [4], [9]. Unlike the Preset Guidance, the missile senses the deviations from the desired path and makes the necessary adjustments in the Inertial Guidance [9]. In the Terrestrial Guidance, the missile compares the actual terrain with the predicted terrain profile and then performs the required adjustments. On the other hand, these comparisons and adjustments are made with respect to the fixed distant stars in the Celestial Guidance approach.

In the direct guidance, the missile navigates according to the target state information acquired by the seeker. However, due to some internal and/or external errors, the missile may not be able to accomplish the intercept to the target with fuel accuracy and hence the existence of a terminal miss distance may be inevitable [3]. In a direct guidance problem, the chief contributors to the miss distance are indicated in the following list [3], [5], [22]:

- Initial heading error of the missile
- Target maneuvers
- Seeker errors
- Target state estimation lag
- Autopilot lag
- Structural limits of the missile

The heading error is defined as the angle representing the deviation of the missile's velocity vector from the collision course. When the initial value of the heading error is different from zero, the missile tries to compensate the difference and this attempt causes a delay for sitting on the collision course. So, this contributes positively to the miss distance at the termination of the engagement.

Another significant factor of the miss distance is the target maneuver. Compared to a stationary target, it is more difficult first to detect and then to track a moving target. Especially the interception with maneuvering targets that have nonzero lateral acceleration is a quite challenging problem [17], [23].

Also, the disturbing effects such as the noises affecting the electro-optical part of the seeker and the radome refraction that occurs depending on the shape of the radome cause the seeker to generate the target information in a corrupted form. This in turn results in an increase in the miss distance [5].

Moreover, the time lags originating from the target estimation system and the autopilot dynamics may contribute to the terminal miss distance. As usual, it is a

remedy for this problem to keep the ratio between the flight time of the missile and the control system time constant as large as possible [3].

In the case that the missile can not realize the guidance commands generated by the guidance system due to saturation, a miss from the target becomes inevitable at the end of the engagement. In the endo-atmospheric interceptors that fly within the atmosphere, angle of attack constraints limit the maximum achievable accelerations at high altitudes in order to avoid stall problems whereas the missile structure restricts achievable acceleration levels at the lower altitudes [3], [17].

As proposed by Zarchan, the terminal miss distance of tactical missiles can be estimated using the method of adjoints. In this method, first, the block diagram of the overall guidance and control system is drawn based on the linearized missile dynamics. Then, the corresponding adjoint model is constructed by converting all system inputs to impulses, reversing all the signal flows and redefining the nodes of the block diagram as summing junctions. Afterwards, taking the target maneuver and the initial heading error of the missile as the impulsive inputs, the terminal miss distance values corresponding to each of the inputs can be determined by running the adjoint model for a specified engagement duration. However, this method can not be applied to nonlinear guidance and control models [3], [24].

Depending on the target tracking way, the direct guidance methods can be divided into four major groups [1], [4], [25]:

- Command to Line-of-Sight Guidance
- Beam Riding Guidance
- Homing Guidance

1.3.1 Command to Line-of-Sight Guidance

Command to Line-of-Sight (CLOS) Guidance is one of the two members of the Line-of-Sight (LOS) guidance methods [3], [5], [18]. In the literature, the LOS guidance methods are also called three-point methods. This is because the launcher, the missile and the target constitute the three points of the guidance triangle [4].

In the CLOS Guidance, an uplink is employed to transmit guidance signals from a ground controller to the missile [1], [2], [18]. In other words, both the guidance and control units of the missile are located off the missile, i.e., on the ground. Based on the type of transmission, the following designations can be made [1]:

- Wire Guidance
- Radio Guidance
- Radar Guidance

In the case of wire guidance, as the name implies, the transmission is made through a thin unwinding wire whereas the transmission is supplied by radio and radar signals in the radio and radar guidance systems, respectively [1], [4]. The illustrative representation of the CLOS Guidance is shown in Figure 1.1.

Although the CLOS method can be used in short-range missile-target engagement scenarios, its success gradually decreases as the missile and target go away from the trackers.

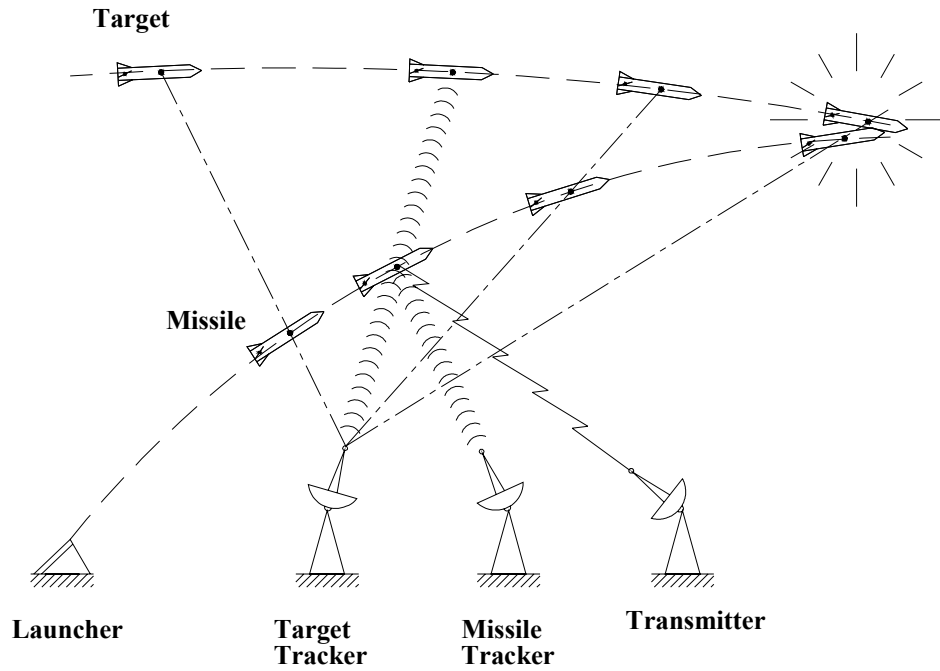


Figure 1.1. Command to Line-of-Sight Guidance

1.3.2 Beam Riding Guidance

The other member of the LOS guidance methods is the Beam Riding Guidance (BRG). In the BRG approach, the missile is configured with a sensor and optics in order first to detect and then to track the beam from the target tracker to the target [18]. In BRG, the objective is to make the missile fly along a radar or laser beam that is continuously pointed at the target so as to keep the missile on the straight line of the beam throughout its trajectory [1], [3], [5], [18]. If the beam is always on the target and the missile is always on the beam, an intercept will be inevitable [3]. Unlike the CLOS guidance, the error off the beam is detected in the missile in the BRG method [25]. Also, since the sensor is located away from the nose of the missile, the nose can be shaped so as to minimize aerodynamic drag [4]. However, the capability of BRG is limited with short-range missile-target engagement situations [18]. Another disadvantage of BRG is that the angle tracking errors in the guidance beam such as the errors caused by the gunner jitter result in

position errors that are directly proportional to the range between the target tracker and the target [4]. The illustrative representation of BRG is shown in Figure 1.2.

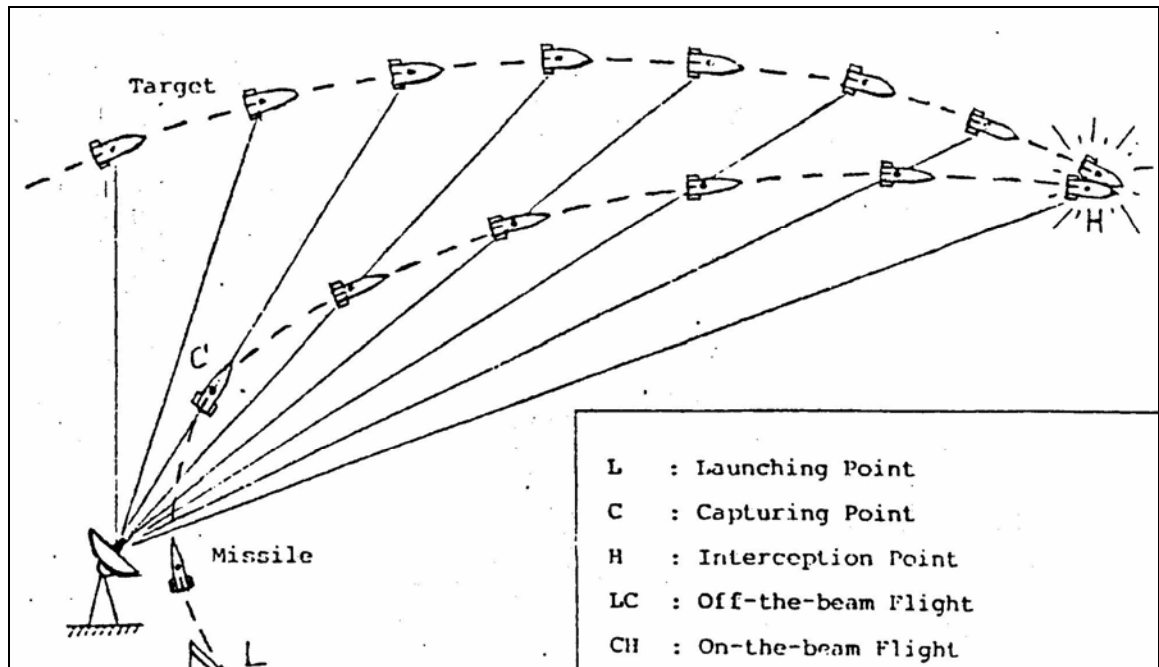


Figure 1.2. Beam Rider Guidance [1]

1.3.3 Homing Guidance

Homing Guidance (HG) is defined as a method by which a missile steers itself toward a target by means of a self contained guidance unit which generates the commanded motion based on some characteristics of the target [1]. Simply, a homing missile operates on signals reaching it from the target [4]. As a missile per se, a homing guided missile is more sophisticated compared to missiles guided by the CLOS Guidance or BRG because a homing guided missile carries all the additional equipment required by the guidance unit, the self motion measuring unit and the target tracking unit. However, a homing guided missile is much more convenient to use because it requires minimal amount of equipment at the launching site and after launching one can simply forget it since it fulfills its duty on its own

[1]. This kind of missiles are called *fire and forget*, or *launch and leave type missiles* [4]. Another advantage of HG over the CLOS Guidance and BRG is that the measurement accuracy of the relative motion of the target with respect to the missile increases in HG but decreases in the others as the missile approaches the target [1], [26].

In HG, the onboard target tracking unit requires some kind of a homing method by which the target becomes detectable. The four possible homing methods can be listed as given below [1]:

- Active Homing
- Semiactive Homing
- Passive Homing
- Homing by Map Matching

In active homing method, the missile carries two devices: One for transmitting some kind of radiation and the other for receiving the portion of this radiation reflected from the target. This way, the missile illuminates the target by its own “flashlight” in order to make it visible to its tracking unit. Once the target becomes visible, then the missile homes on it to destroy it. The homing radiation can be in various forms such as radio waves, light waves, infrared (IR) waves, and even sound waves [1].

In semicative homing approach, the homing radiation is already transmitted from another source and the missile is equipped only with a receiver to pick up the radiation reflected from the target. The source which transmits the radiation is usually placed at the launching site [1]. With the semiactive homing, the high-power radar illuminator or the laser designator extends the range [4].

In the passive homing method, no transmitting device is required for the homing radiation because its source is target itself. The missile is again equipped only with a receiver to pick up the radiation emitted from the target. As noted, the passive homing is the simplest and thus the mostly used HG method. In this method, a radar antenna, a radio transmitter or the hot engine of an aircraft constitutes very convenient targets [1].

In the homing by map matching, the missile carries a camera which continuously views the terrain below. These views are compared with the map stored in a memory device. A particular view is detected as the target when its features match the stored map. Then, the guidance unit gets locked on this view and the missile homes on the piece of terrain having this view [1], [4].

Looking at the literature, the HG methods can be seen to have the following type of varieties:

- i. Conventional Homing Guidance Methods
- ii. Homing Guidance Methods based on Optimal Control Theory
- iii. Homing Guidance Methods based on Game Theory
- iv. Homing Guidance Methods based on Robust Control Techniques
- vi. Homing Guidance Methods with Applications of Artificial Intelligence Techniques
- vii. Integrated Homing Guidance and Control Methods

1.3.3.1 Conventional Homing Guidance Methods

The guidance laws under this title are the ones that date back to very first guided missiles developed in 1940's and 1950's. The reasons that they have been so successful are mainly due to their simplicity to implement and also their robust performance [5].

The widely-used conventional HG strategies can be listed as follows [1], [3], [5], [18]:

- Pursuit Guidance
- Constant Bearing Guidance
- Proportional Navigation Guidance
- Predictive Guidance

1.3.3.1.1 Pursuit Guidance

In Pursuit Guidance, it is intended to nullify the relative LOS angle between the missile and the target. However, the Pursuit Guidance laws have limited capability to engage maneuvering targets [18].

The Pursuit Guidance has two basic variants [18]:

- Body Pursuit or Attitude Pursuit Guidance
- Velocity Pursuit Guidance

In the Body Pursuit approach, the longitudinal axis, or the centerline, of the missile is directed at the target. In order to track the target, the seeker should have a wide field-of-view (FOV) [18].

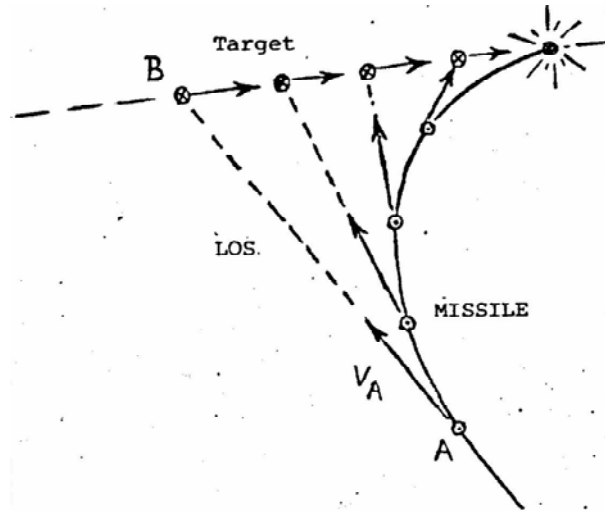


Figure 1.3. Velocity Pursuit Guidance [1]

The conceptual idea behind the Velocity Pursuit Guidance (VPG) is that the missile should always head for the current position of the target [5]. In other words, the missile velocity vector is kept pointed at the target to get aligned with the LOS in this approach [1], [18]. This strategy that resembles to the one a dog follows as it chases, say, a rabbit will result in an intercept provided that the missile velocity is greater than the target velocity [1], [4], [5]. The required information for VPG is limited to the bearing angle that is defined as the difference between the flight path angle (FPA) of the missile and the LOS angle, and the direction of the missile velocity. The bearing angle information can be obtained from a seeker onboard the missile. VPG is usually implemented to the laser-guided bombs where a simple seeker is mounted on a vane that automatically aligns with the missile velocity vector relative to the wind. The VPG law results in a high lateral acceleration demand; in most cases almost infinite at the final phase of the intercept. As the missile can not generate infinite acceleration, the result is a finite miss distance [5].

Unlike the Body Pursuit, a seeker with a narrower FOV is sufficient in the implementation of VPG [18]. The illustrative representation of VPG is shown in Figure 1.2.

1.3.3.1.2 Constant Bearing Guidance

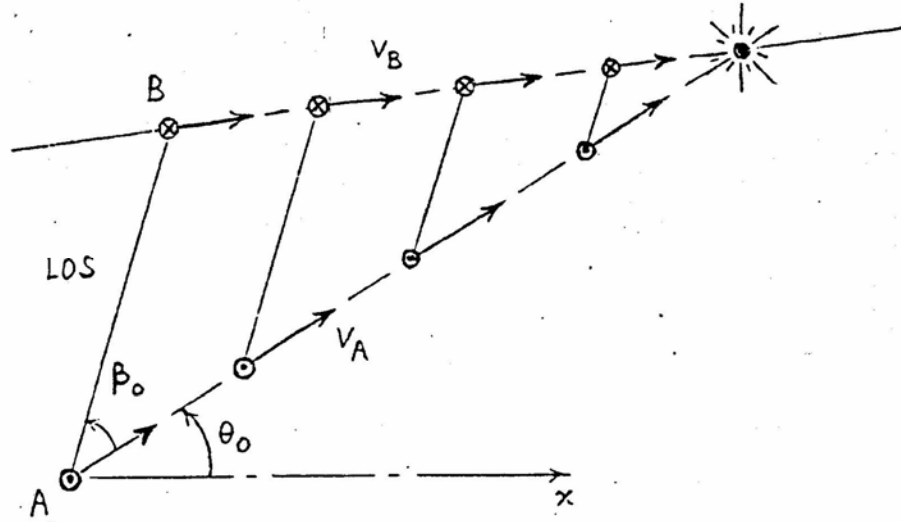


Figure 1.4. Constant Bearing Guidance [1]

In the Constant Bearing strategy, the bearing angle is forced to have a constant nonzero value [1]. In other words, it is intended to keep the missile at a constant bearing to the target at all the time [5]. With a judicious choice of this constant value, it is possible to minimize the swerving motion of the missile. Thus, the requirements on the strength and the maneuvering energy can be reduced. However, unless the target is moving uniformly, or at least almost uniformly, it will not be easy to find that constant value for the bearing angle [1]. Therefore, the success of this approach is strongly dependent on the correct prediction of this angle [4]. Here, it should be noted that the VPG strategy in which the bearing angle is tried to be kept at zero is a special case of the constant bearing strategy [1]. The illustrative representation of the constant bearing guidance is shown in Figure 1.4.

In the figure, as A and B denote the missile and the target, v_A and v_B show the velocity vectors of the missile and the target.

1.3.3.1.3 Proportional Navigation Guidance

The Lark missile which had its first successful test in December 1950 was the first missile using the Proportional Navigation Guidance (PNG) method. Since that time, PNG has been used in most of the world's tactical radar, IR and television (TV) guided missiles. The popularity of this interceptor guidance law comes from its simplicity, effectiveness and ease of implementation [3].

Originally, the PNG law issues angular rate or acceleration commands perpendicular to the instantaneous missile-target LOS in accordance with an effective navigation ratio (ENR) [3], [17], [18], [27], [28]. In order to determine the optimal value for ENR depending on the application, several studies have been conducted [29]. In a planar case, the lateral acceleration command of the missile can be generated by multiplying the angular rate command with the closing velocity. Here, the closing velocity is defined as the difference between the magnitudes of the missile and target velocity vectors [18]. In tactical radar homing missiles employing PNG, the seeker provides an effective measurement of the LOS angular rate and a Doppler radar provides the closing velocity information. However, in laser guided missiles, the LOS angular rate is measured whereas the closing velocity is estimated. Once the missile seeker detects the target, the PNG law begins forcing the missile to home on the target. If there are no dynamics and uncertainties in a PNG homing loop, then the resultant miss distance should always be zero [3].

In application, the missile employing PNG is not fired at the target but is fired in a direction to lead the target. This way, it is provided for the missile to be on a collision triangle with the target [3], [17].

The schematic representation of the missile-target engagement in PNG is given in Figure 1.5.

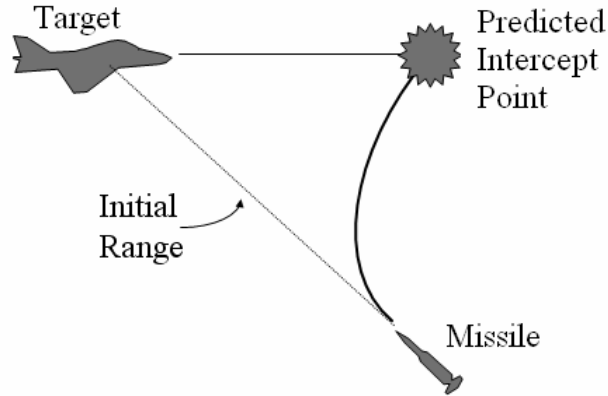


Figure 1.5. Proportional Navigation Guidance [30]

Unlike the Pursuit Guidance, the LOS angular rate is tried to be nullified while closing on the target in PNG [1], [18], [31]. Actually, this provides an advantage to PNG over the Pursuit Guidance methods because the course corrections are made in earlier stages of the flight [4], [32], [33].

Depending on the direction of the generated acceleration command, PNG is usually classified into two sub-groups [18]:

- True Proportional Navigation Guidance (TPNG)
- Pure Proportional Navigation Guidance (PPNG)

In TPNG which is the original form of PNG, the acceleration command is produced perpendicular to the LOS. Thus, regarding the planar engagement situation, the acceleration command generated according to the TPNG approach has the components both in the direction of the missile velocity vector and in the direction normal to the velocity vector. However, it becomes not possible for the missile control system to realize the acceleration demand along the velocity vector

due to the lack of a controllable thrust. Thus, a modified type of TPNG is introduced: PPNG. In PPNG, the acceleration command is generated to be perpendicular to the missile velocity vector. Since PPNG does not have any acceleration demand along the velocity vector, it can be realizable by the missile control system [18]. However, as TPNG, PPNG is effective against non-maneuvering targets. Considering maneuvering targets, the efficiency of the PPNG law can be improved using a varying ENR [34].

Although most of the studies in the literature about PNG consider the planar missile-target engagement model, the three dimensional extension of the PNG law is also derived especially for the engagement case with highly maneuvering targets [9], [18], [35], [36], [37]. In spite of the fact that the optimality of PNG against non-maneuvering targets was proven many years later from its derivation, the PNG law is not very effective in the presence of target maneuvers and often leads to unacceptable miss distances especially when the guidance system time constant is too large or the flight time is very short [3], [38]. Then, increasing the effective navigation ratio and decreasing the guidance system time constant work in the direction of reducing the terminal miss distance due to target maneuver. As the effective navigation ratio is increased, the initial values of the acceleration commands become larger, but the commands get smaller near the end of the flight. Against non-constant target maneuvers, larger effective navigation ratios result in smaller miss distances. On the contrary, increasing the effective navigation ratio also causes the miss distance due to noise and parasitic effects to grow. Here, another significant property of the noise and parasitic effects is that they place a practical lower limit on the minimum attainable guidance system time constant [3].

If the target acceleration can be measured or at least estimated, it becomes possible to augment the PNG law by adding the target acceleration term to compensate the acceleration of the maneuvering target [5]. In the literature, this form of PNG is called Augmented Proportional Navigation Guidance (APNG) that causes the missile to yield less final miss distance as well as reduced acceleration

commands [3], [4], [28]. On the other hand, the target acceleration information is not directly available in most cases, especially in laser guided missiles [3], [39], [40]. In such cases, one of the best ways is to estimate the target acceleration using the available measurements.

1.3.3.1.4 Predictive Guidance

Predictive Guidance is based on the prediction of the future location of the intended target. Once this prediction is done, the next task is to turn the heading of the missile in order to form a collision triangle with the target. During the engagement, the predicted intercept is updated at certain instants with respect to the target state information acquired by the seeker [3], [23], [27]. Actually, the Linear Homing Guidance (LHG) and the Parabolic Homing Guidance (PHG) methods proposed in this thesis are two different forms of the Predictive Guidance. In LHG, the missile trajectory to the target is assigned as a linear path while PHG considers a parabolic trajectory. In both of the methods, the predicted intercept point is continuously updated according to the current state information of the target.

1.3.3.2 Homing Guidance Methods based on Optimal Control Theory

The objective of the optimal control theory is to determine the control signals that will cause a process to satisfy the physical constraints and at the same time to minimize or maximize some cost function [41]. In the guidance sense, the cost function is designed in a quadratic form so as to minimize the terminal miss distance, the maximum achievable lateral acceleration and the intercept time at certain weights. Although the derived optimal control theory based methods are used in computer simulations and some satisfactory results are obtained, they have not been yet implemented in the guidance applications in the real world [42], [43], [44], [45], [46], [47].

1.3.3.3 Homing Guidance Methods based on Game Theory

A pursuit-evasion game is about how to guide one or a group of pursuers to catch one or a group of moving evaders. In the game theory, a game consists of three parts: players, actions and lost functions. The solutions to a game are normally the policies for the players. With these policies, an equilibrium state will be achieved and the players will have no regrets [48]. In other words, each player tries to minimize his own performance index [49], [50]. The methods to solve the pursuit-evasion problems involve the following approaches [48]:

- Approach for Problems with Differential Motion Models
- Approach using Worst Case Analysis
- Approach using Probabilistic Analysis

If motion models of players in the pursuit-evasion game are differential equations, then the game is called a differential game. The objective of a differential game is to find the saddle-point equilibria with respect to the game policy [48].

In the worst case analysis, it is assumed that only the game environment is known to the pursuers, and the evaders work as Nature which knows any information such as the location of the pursuers, the environment and even the policy of the pursuers [48].

In the probabilistic analysis, the evaders are considered to be no superior to the pursuers, which might only have limited range and uncertain sensors, and not know the environment [48].

The modern approach to missile guidance is based on the optimal control theory and the differential games. Actually, while the optimal control theory

involves one-sided optimization, i.e., the optimization of the missile parameters, the differential games involve two-sided optimization, i.e., the optimization of both the missile and the target parameters [51]. According to the comparison studies based on extensive simulations, the interceptor guidance laws derived from a differential game formulation are superior to those obtained using optimal control theory. In spite of the results of these comparisons, the differential game guidance laws have not yet been adopted by the missile industry. This conservative attitude can be explained by that the already existing interceptor missiles have a sufficient maneuverability advantage over the presumed targets even with the simple but efficient conventional guidance laws. Moreover, applying the optimal pursuer strategy of the perfect information game as the guidance law of the interceptor using a typical estimator yields very disappointing results. The miss distance is never zero and there is a high sensitivity to the structure of the unknown target maneuver [42].

1.3.3.4 Homing Guidance Methods based on Robust Control Techniques

The issue of robust control is to design a controller such that the closed loop system remains stable for all the possible plant uncertainties and disturbances. For this purpose, the bounds of the uncertainties and the disturbances should be known. In the robust guidance methods, the uncertainties in the missile parameters and the target maneuver are tried to be compensated as well as the effects of the noise and the disturbances on the missile guidance system [49], [52].

The most widely used two robust guidance methods are the following ones:

- Guidance Methods based on Sliding Mode Control Theory
- Guidance Methods based on H_∞ Norm Criterion

1.3.3.4.1 Homing Guidance Methods based on Sliding Mode Control Theory

In the Sliding Mode Control (SMC), the states of the system to be controlled are moved from their initial values to a switching surface so that the system restricted to this surface produces the desired behavior. The next step is to choose a control, which will drive the system trajectories onto the switching surface and constrain them to slide along this surface, for all the subsequent time. In this scheme, the robustness can be achieved owing to the fact that the switching surface describes a stable homogeneous behavior and it can be configured independently of the parameters and the inputs of the system [14]. However, driving the system toward and keeping it on the sliding surface may not be so easy. Although the stability of the system is guaranteed as long as it remains on the sliding surface, SMC has the drawback of chattering because of the signum functions it involves. The most common method for solving the chattering problem is to allow a larger error zone around the switching surface by replacing the signum functions with their continuous approximations. This method, however, does not ensure the convergence of the state trajectories of the system to the sliding surface and thus may cause some steady-state error [53].

In the guidance field, SMC is proposed in the form of Sliding Mode Guidance (SMG) law. Considering the missile-target engagement kinematics and choosing the relative position components as the state variables, the SMG laws are derived on the sliding surface of the zero LOS angular rate based on the Lyapunov method [37], [54]. According to Moon, although this method is quite useful against non-maneuvering targets, the guidance gains become much larger when the target is maneuvering and this may cause a rapid chattering within the boundary layer. Thus, the resulting guidance commands may not be realizable by the missile. This in turn causes the terminal miss distance to be unacceptably different from zero. On the other hand, this method could not be employed on realistic guidance applications [37].

1.3.3.4.2 H_∞ Guidance Methods based on H_∞ Norm Criterion

For an $n \times 1$ column matrix $\bar{x} = [x_1 \ x_2 \ x_3 \ \dots \ x_n]^T$, the H_∞ norm is defined as

$$\|\bar{x}\|_\infty = \max\{|x_k|, 1 \leq k \leq n\} \quad (1.1)$$

In H_∞ control, as x_k corresponds to the magnitude of the transfer function between the considered input and output variables at the k 'th frequency when it is dealt with in the frequency domain, it is aimed at obtaining a controller such that $\|\bar{x}\|_\infty$ is minimized [52]. If the transfer function is evaluated in the time domain, then x_k denotes its magnitude at the k 'th instant.

This method can be applied to the missile guidance considering the missile-target engagement kinematics. In this scheme, the target acceleration components are chosen as the disturbances and the relative position variables are designated as the outputs. Then, regarding the linearized engagement geometry, the transfer functions between the disturbance terms and the output variables are obtained. For each of the transfer functions, the guidance gains are determined to minimize the corresponding H_∞ norm [54], [55], [56]. In order to apply this method, the upper bounds of the target acceleration components should be known or at least estimated. If the acceleration level of the intended target is greater than the estimation, then the terminal miss distance may not be nullified. Also, when the guidance problem is dealt with in the three-dimensional space especially in the case of maneuvering targets, the linearization of the missile-target engagement kinematics, and hence the determination of the guidance gains become quite difficult. Hence, the H_∞ norm criterion based methods have not been employed on the real applications.

1.3.3.5 Homing Guidance Methods with Applications of Artificial Intelligence Techniques

Intelligent control can be defined as a control approach involving environment discovery, future prediction, method learning, skill development and independent decision making. Neural networks, fuzzy logic, expert learning schemes, genetic algorithms, genetic programming and any combination of these constitute the tools of the intelligent control [57].

In the missile guidance area, the most widely used tools of intelligent control are the neural networks and the fuzzy logic control methods.

1.3.3.5.1 Homing Guidance using Neural Networks

Artificial neural networks are circuits, computer algorithms or mathematical representations loosely inspired by the massively connected set of neurons that form the biological neural networks [58]. Because of their parallel structures with distributed storage and processing of massive amounts of information and their learning ability made possible by adjusting the network interconnection weights and biases based on certain learning algorithms, the neural networks have been used in the solutions of control problems [17], [38], [59].

In a neural network guidance scheme, the appropriate ones of the line-of-sight (LOS) angle, the LOS angular rate, the time derivative of the LOS angular rate, the missile velocity and the target acceleration components are used to construct the input sets of the dedicated neural network. The output variable is the lateral acceleration command in most cases. The training data are obtained by the computer simulations performed using different guidance schemes that produce minimum terminal miss distance and smallest command accelerations. In general, the network is trained before the implementation and the weights are determined in an off-line manner. Also, generating the training data using the guidance schemes

employing the PNG law with different effective navigation ratios (ENR), the output of the neural network can be selected as the ENR value as well [38]. The neural network guidance methods are quite effective provided that the values of the input variables remain within the bounds considered in the training data. On the other hand, as the ranges of the inputs are enlarged, it will take too much time both to generate the data and to train the network using these data. Hence, the homing guidance methods based on the neural networks have not been utilized in the missile industry.

1.3.3.5.2 Homing Guidance using Fuzzy Logic Control Methods

Fuzzy logic control is a methodology to make decisions according to the constructed rule tables and to generate control commands. Basically, a fuzzy logic control system consists of three successive stages [58]:

- Fuzzification
- Inference Mechanism
- Defuzzification

Fuzzification is the process of transforming the numerical inputs into a form that can be used by the inference mechanism. The inference mechanism uses information about the current inputs formed by fuzzification, decides which rules apply in the current situation and forms conclusions about what the plant input should be. Finally, defuzzification converts the conclusions reached by the inference mechanism into a numeric input for the plant [58]. The schematic representation of a fuzzy logic control architecture is shown in Figure 1. 6.

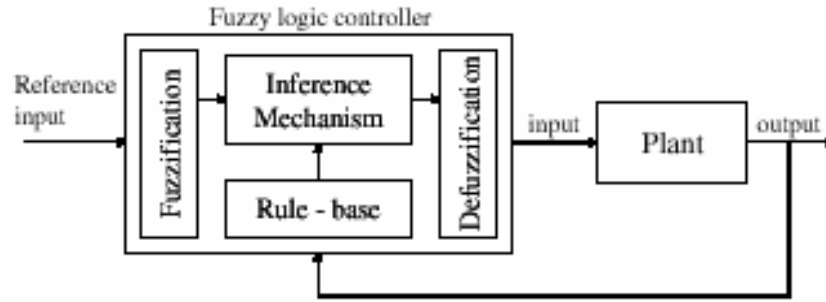


Figure 1. 6. Fuzzy Logic Controller Architecture [11]

Like the neural network guidance algorithms, the reference inputs of the fuzzy guidance schemes are selected from the combinations of the LOS angle, the LOS angular rate, the time derivative of the LOS angular rate, the missile velocity and the target acceleration components. In general, the input sets are formed using the LOS angle and the LOS angular rate. Usually, the output of the fuzzy guidance scheme is the lateral acceleration commands to the missile [11], [38]. Mishra claims that smaller miss distance and less acceleration commands than the Proportional Navigation Guidance (PNG) can be attained using a fuzzy guidance scheme [38]. Also, according to Vural, a fuzzy logic based guidance law can perform as well as the PNG [11]. On the other hand, the success of a fuzzy guidance scheme is directly dependent on the statement of the rules. If the rules are not properly set, then the fuzzy guidance algorithm can not lead the missile to hit the intended target.

1.3.3.6 Integrated Homing Guidance and Control Methods

Constructing a missile guidance and control algorithm, the guidance, control and target motion estimation systems are usually designed separately and then integrated to the missile. Since these systems in general have different bandwidths, there exists a time lag in the response of the overall guidance and control system [60]. In order to decrease this lag, the integrated guidance and control algorithms

are proposed [22]. However, since the dimension of the nonlinear guidance and control problem is increased, it becomes difficult to construct such a scheme such that the stability of the missile is maintained [22]. For such reasons, these kinds of structures can not be easily implemented on realistic guidance and control problems.

1.4. Studies on the Control of Missiles in the Literature

The mission of a missile control system, or a missile autopilot, is to ensure the stability, high performance and that the missile flies in accordance to the demands of the guidance law [5], [38], [61], [62]. Figuratively speaking, the guidance unit is the *commander* and the control unit is the *executive officer* who forces the missile to obey the *orders* of the commander [1].

In order for the minimum terminal miss distance, the dynamics of the control system should be as fast as possible. That is, the autopilot time constant should be as small as possible [22].

In most of the missile control systems, the controlled variables are selected to be the lateral acceleration components of the missile. Depending on the type of the guidance command, the controlled variables may also be the body rates (yaw, pitch and roll rates), body angles (yaw, pitch and roll angles), wind frame angles (angle of attack and side-slip angles), or their rates.

In the guided missiles, the necessary steering actions are achieved by various motion control elements such as the ones listed below [1], [63]:

- Aerodynamic Control Surfaces
- Thrust Vector Deflectors
- Side Jets or Reaction Jets

Aerodynamic control surfaces can be in the form of canards, wings, and tails depending on their locations on the missile [1], [63].

In the canard-controlled missiles, the control fins, or canards, are mounted on the nose part of the missile as shown in Figure 1.7. They are light in weight and can be simply packaged. The drag acting on their bodies is smaller because of their smaller sizes. Also, small canards create less downwash effect. On the other hand, they contribute very little to the necessary lift which is mainly derived from the body angle of attack (AOA) in this type of missiles [63].

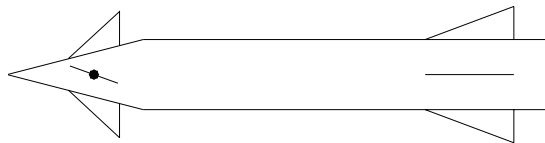


Figure 1.7. Canard-Controlled Missile

In the wing-controlled missiles, the control fins are mounted near the mass center of the missile (CG) as shown in Figure 1.8. This type of control provides fast response of body lateral acceleration [63].

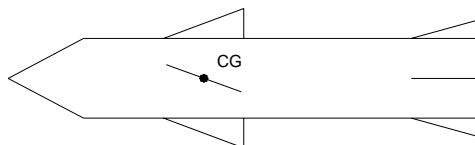


Figure 1.8. Wing-Controlled Missile

The third type of aerodynamic control surfaces are tail fins. As the name implies, these control surfaces are placed at the tail section of the missile as shown in Figure 1.9. Their main advantage over the canard and wing types is more linear aerodynamic characteristics due to the absence of the downwash effect. However, the space available to put the control section is limited due to the rocket motor and the nozzle. Beyond this disadvantage, the most important drawback of the tail-controlled missiles is that their first reaction is opposite to the desired motion command [63]. Actually, this results from the non-minimum phase characteristics of the tail-controlled missiles [64].

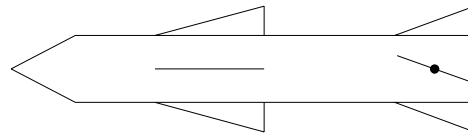


Figure 1.9. Tail-Controlled Missile

The fin arrangement in an aerodynamically controlled missile can be one of the cruciform, triform and monowing configurations. As shown in Figure 1.10, they are formed by four, three and two fins that are equally spaced. As the cruciform configuration is the most common one among all, the monowing configuration is in general chosen for cruise type missiles, e.g. NACE missile. However, although they provide a high lift, the monowing-type missiles have a large maneuver delay. Considering the triform arrangement, it is a rarely used fin arrangement, e.g. in Pershing missile [63].

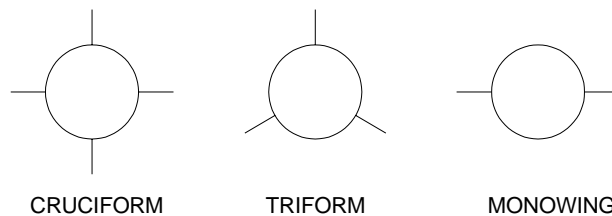


Figure 1.10. Fin Arrangements in Aerodynamically Controlled Missiles

In the case where the control of the missile is achieved by means of aerodynamic control surfaces, the desired deflections for them are supplied by a control actuation system (CAS) [2]. Depending on the type of the energy transmission mechanism, a CAS can be hydraulic, pneumatic or electromechanical. The hydraulic type actuators are used in the applications that require high torques. Despite their limited torque capability, pneumatic actuators may be preferred because of their simplicity and low-cost. On the other hand, the electromechanical type actuators give the best results in the low-torque rotary applications [2], [65].

In the cases where the thrust vector deflectors are used in motion control elements, the flight of the missile is controlled by controlling the direction of the thrust. In the literature, this type of control is known as the Thrust Vector Control (TVC). In general, TVC can be implemented in three different ways [63]:

- Gimbal Control
- Direct Thrust Control
- Jet Vane Control

In the gimbal control, the missile is controlled by means of the rotation of a gimballed nozzle. On the other hand, the control is done by means of the orifices on the fixed nozzle in the direct thrust control. In the jet-vane control method, the thrust is directed by means of the vanes hinged at the aft end section of the nozzle. In all of these methods, the roll motion of the missile can not be controlled [63]. Their schematic representations are given in Figure 1.11, Figure 1.12 and Figure 1.13.



Figure 1.11. Gimbal-Controlled Missile

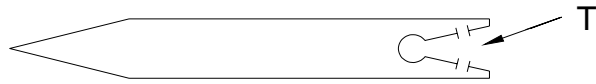


Figure 1.12. Direct Thrust -Controlled Missile

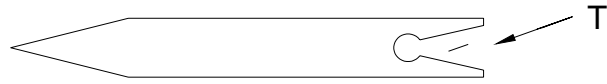


Figure 1.13. Jet Vane-Controlled Missile

In the control of missile with side jets, the small rockets put around the missile body are fired in order to make the missile behave in accordance with the commands generated by the guidance algorithm. As the control strategy, usually on-off or bang-bang control is applied for the control of missiles with side jets. If the jet nozzles are located in a canted configuration, the side jet control can provide the missile with a roll motion, too [63]. Also, since the conventional aerodynamic surfaces may no longer be effective at extreme AOA values, additional control with side jets is a good choice [62], [66]. A side jet-controlled missile is depicted as shown in Figure 1.14.

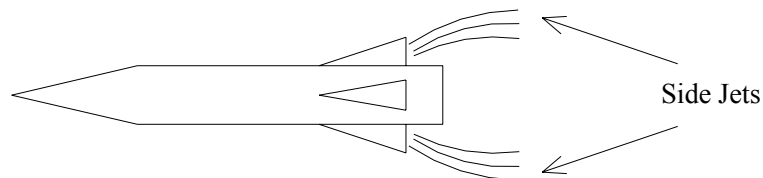


Figure 1.14. Side Jets-Controlled Missile

The strategies utilized in missile control may be discussed under the following headings:

- i. Classical Control Methods
- ii. Modern Control Methods
- iii. Robust Control Methods
- iv. Intelligent Control Methods

1.4.1 Classical Control Methods

If the roll motion of the missile is stabilized, then its motion in its yaw and pitch planes will become decoupled. In such a structure, where the motion equations are almost linear for not so large wind angles and control surface deflections, the autopilots can be designed easily using the classical control techniques. In this sense, usually PI (proportional plus integral) or PID (proportional plus integral plus derivative) control with synthetic pitch and yaw damping is used in the design of the yaw and pitch autopilots. In the resulting control system, the desired poles are in general set according to the pole placement technique. In order to keep these poles at the desired locations against the changing operating conditions, the mostly used way is the gain scheduling method [62], [67]. In this approach, the controller gains are continuously adjusted with respect to the current flight conditions so as to maintain the desired locations of the poles of the closed loop control system.

1.4.2 Modern Control Methods

Most of the modern control strategies fall into one of the following two categories: They are either state feedback or output feedback strategies [68]. Many of the linear and nonlinear design methods assume that the full state information is available [69]. However, it is not always possible to implement a state feedback based control law as all the states may not be available for measurement. In such a case, the output feedback is a viable alternative usually coupled with a Kalman filter

to estimate the full state. On the other hand, the use of the state and output feedback strategies is limited in the control of the missiles. As an example, in a specific problem where the missile is fired from the ground in vertical position, the state feedback control can be used in order to maintain the vertical position of the missile throughout its flight.

1.4.3 Robust Control Methods

Regarding the uncertainties in the missile parameters and the disturbances influencing the missile dynamics, the robust control methods appear as a viable solution [70]. In the design of a missile autopilot, the most widely used robust control methods can be divided into two main groups:

- Control Methods based on the Lyapunov's Theorem
- Control Methods based on H_∞ Norm

1.4.3.1 Control Methods based on the Lyapunov's Theorem

In the control methods under this title, the control law is generated with respect to a properly selected Lyapunov function. Basically, two kinds of such methods appear in the literature:

- Backstepping Control
- Sliding Mode Control

1.4.3.1.1 Backstepping Control

The backstepping control is a recursive control technique. In order to design a controller using the backstepping method, the dynamic equations of the system to

be controlled should be expressed in the “strict feedback form”. For example, if x_1 , x_2 and x_3 denote the state variables of a system and u represents its control input, the dynamic equations of the system can be expressed in the strict feedback form as [71], [72], [73]

$$\dot{x}_1 = x_2 + f_1(x_1) \quad (1.2)$$

$$\dot{x}_2 = x_3 + f_2(x_1, x_2) \quad (1.3)$$

$$\dot{x}_3 = u + f_3(x_1, x_2, x_3) \quad (1.4)$$

In this technique, each of the differential equations given above is stabilized with the following state variable as the control variable. Namely, at the first stage, x_2 is used as the control variable for the x_1 dynamics in equation (1.2). Then, x_3 serves as the control variable of the x_2 dynamics given in equation (1.3). After stabilizing the x_1 and x_2 dynamics, the actual control input u is determined from equation (1.4) as a function of x_1 , x_2 and x_3 . In each stage, the corresponding stabilizing control law is obtained using an appropriate method such as using a proper Lyapunov function. Since a stabilizing feedback control law is derived at each stage and then the process goes one step back until the actual control input is determined, this method is called “backstepping” [71], [74].

The backstepping method is used in the missile autopilot design as well. According to the design procedure proposed by Sharma and Ward, selecting the pitch rate, the pitch angle and the flight path angle as the state variables and the elevator deflection as the control input, the differential equations describing the pitch motion of the missile can be expressed in terms of these state variables and the input variable. Then, these equations are expressed in the strict feedback form as explained above and the actual control input is determined by following the

backstepping design procedure [75]. Sharma and Ward claim that the autopilot designed using the backstepping method is robust to the uncertainties in both the missile parameters and the aerodynamic terms. Also, the stability of the resulting control system can be guaranteed according to Liu [71]. On the other hand, since the control input is needed to be updated according to the changing flight parameters, the implementation of this procedure may take a long time. In the practical guidance applications, the backstepping method is rarely used.

1.4.3.1.2 Sliding Mode Control

Specifying properly the sliding surface parameters and the thickness of the boundary layer introduced around the sliding surface in order to restrict the amount of the chattering, a robust autopilot can be designed using the sliding mode control (SMC) method. In the study conducted by Menon and Ohlmeyer, the design of a pitch autopilot using the SMC method is explained. In the mentioned design, the pitch rate and the angle of attack are chosen as the state variables and the elevator deflection is selected as the control input [74], [76]. Although they claim that this method produces quite successful results, the SMC approach is not chosen most of the time. This is because the SMC system will be slower than any classical control system since the sliding surface is needed to be adapted to varying flight conditions.

1.4.3.2 Control Methods based on H_∞ Norm

The H_∞ autopilot design is based on the linearized missile dynamics and it can be carried out in either frequency domain or time domain in the form of state space formulation [70]. In this approach, first the state variables and the inputs are defined. Then, the linearized dynamic equations are expressed in terms of the selected state and input variables. After deriving the transfer functions between the input and the state variables, the H_∞ norm of each transfer function can be defined as

$$\|\bar{x}\|_{\infty} = \max\{|x_k|, 1 \leq k \leq n\} \quad (1.5)$$

Thus, the final task is to obtain a controller such that $\|\bar{x}\|_{\infty}$ is minimized [52]. In the autopilot design, the state variables are selected to be the body rates (yaw, pitch and roll rates), the body angles (yaw, pitch and roll angle) and the wind frame angles (angle of attack and side-slip angle). As usual, the input variables are the rudder, elevator, and aileron deflections. Regarding the pitch autopilot design, \bar{x} is constructed using the transfer functions from the elevator deflection to the pitch rate, the pitch angle and the angle of attack. Then, the controller is tried to be determined so as to minimize $\|\bar{x}\|_{\infty}$. Since the algorithm involves the uncertainties in the missile parameters and the disturbances acting on the control system within certain bounds, the designed control system is robust to the parameter uncertainties and the disturbances. However, the determination of an appropriate controller is an iterative and hence a time consuming process. Thus, this method is not chosen in practical guidance implementations [52].

1.4.4 Intelligent Control Methods

The intelligent methods in missile control can be grouped as follows:

- Neural Network Based Control Methods
- Fuzzy Logic Based Control Methods

1.4.4.1 Neural Network Based Control Methods

In general, the neural network controller in a control system is utilized as an inverse plant model. In this structure, first the neural network is constructed by deciding the numbers of the input and the output nodes as well as the number of the neurons in the hidden layer. Then, performing a suitably planned simulation set, the

selected output variables of the plant are measured for several types of the plant inputs. Using the measured values, the data set is formed for the training of the neural network controller such that the values of the plant outputs constitute the input data set while the values of the plant inputs are its output data set. Next, the neural network is trained using this data set to determine the values of the weighting factors [38].

In the missile autopilot design, the lateral acceleration components of the missile, the body rates, the body angles, the wind frame angles and the missile velocity are usually selected as the output variables. Carrying out successive computer simulations using the considered missile model, the values of these output values are measured for the different values of the input variables (the rudder, elevator and aileron deflections) at different Mach numbers. Then, the collected data are fed into the neural network in order to train it. Thus, the trained neural network can be used as a controller in the missile control system. In order to increase the performance of the neural network controller, the training data space should be enlarged. The neural network controllers give satisfactory results provided that the flight parameters of the missile remain within the bounds considered in the training data set. However, the data generation process is very long as well as the training duration. Also, there is no acceptable criterion to check the stability of a neural network control system [59]. In order to guarantee the stability of the neural control systems, Lin and Chen proposed a hybrid control scheme in which a fixed-gain controller operates in parallel with the neural network controller. However, this method seems not to be practical because it dictates an online tuning of the weighting factors over the operating range [38]. Also, for non-minimum systems, the neural network controller used as an inverse plant model becomes unstable [38], [77], [78], [79]. Therefore, the use of this method is not a good choice in the control of missiles.

1.4.4.2 Fuzzy Logic Based Control Methods

In a missile control system, a fuzzy logic controller can be utilized to generate the control commands for the fin deflections. In general, the error term between the reference input and the actual output of the control system, and the first derivative of the error term are designated as the inputs of the fuzzy logic controller. Then, depending on the established inference rules, the fin deflection commands are produced as the outputs. Actually, the success of a fuzzy controller is directly dependent on the statement of the inference rules. In the derivation of these rules, the input and output data of some properly working controllers can be used as the reference. Also, like the neural network controller, the lack of satisfactory formal techniques for studying the stability of the fuzzy logic based control systems is a major drawback. In order to increase the performance of the fuzzy controllers, Dash and Panda propose a fuzzy logic structure in which the input and output membership functions are adaptable to the parameter variations. However, they can not guarantee the stability of the overall control system [38], [80], [81], [82]. For this reason, the fuzzy logic control is not practical for the implementation on the real missile guidance applications.

1.5. Studies on the Estimation of Target Motion in the Literature

The third leg of the guidance and control system design for a missile is the development of an algorithm to estimate the states of the target required for the implementation of the guidance law under consideration. In a homing guidance problem, a target state estimator deals with two major problems: highly maneuvering targets and low-observability from the LOS measurements [83].

The dynamic nature of the estimation process has an important effect on the homing performance [45]. According to the results of the relevant computer simulations made by Shinar and Shima, the largest error source on a missile guidance system appears as the inherent delay in estimating the target acceleration.

Therefore, the entire estimation process is roughly approximated by a pure time delay in the measurement of the target acceleration [42].

In the guidance and control field, there are basically two sorts of target state estimators in practical use [84]:

- Simple Digital Fading Memory Filters
- Kalman Filters

1.5.1 Simple Digital Fading Memory Filters

The missile seeker provides a noisy measurement of the LOS angle. Therefore, the use of a simple digital fading memory filter, or a constant gain filter, as a part of the missile guidance system is one of the simplest and the most effective ways to get an estimate of the LOS angle and the LOS angular rate from the noisy measurement. In this filter structure, the value of the column \bar{x} at the k 'th instant can be estimated as

$$\bar{x}_{\text{est}}(k) = \bar{x}_{\text{est}}(k-1) + \hat{K} [\bar{x}_{\text{mes}}(k) - \bar{x}_{\text{est}}(k-1)] \quad (1.6)$$

where $\hat{K} = \tau \hat{K}_D$; $0 < \tau < 1$ and \bar{x}_{mes} is the measured value of \bar{x} . Also, τ is called the memory length. If τ is zero, then the current estimate is just equal to the current measurement. Conversely, if it is one, it yields an estimate the same as the previous one. In general, the first order simple digital fading memory filters are used, as described above [3]. However, it is possible to use higher order filters too, if desired.

1.5.2 Kalman Filters

A Kalman Filter (KF) is one of the best choices in estimating the maneuvering level of the intended target [23]. More generally, it is a well-known recursive state estimator for linear systems [85]. In a KF type state estimator, the data available from the seeker and the inertial navigation system (INS) together with a model of the target behavior are used to generate the target state vector, which typically includes the target position, velocity and acceleration vectors [86]. However, for a KF to be truly optimal, the statistics of the measurement and process noise must be known [3], [87]. Unlike the constant-gain simple digital fading memory filter, a KF has a time-varying gain matrix. Yet, in most of the applications, a simple digital fading memory filter gives very satisfactory results.

1.6. Scope of the Thesis

In almost all of the guidance and control studies in the literature, the missile is modeled as a single-body structure. Therefore, the same dynamic model is used in the similar studies by changing the numerical values of the missile parameters. In this study, a two-body missile is dealt with. Namely, the missile is considered as an air-to-surface missile (ASM) consisting of two separate bodies that are connected to each other by means of a roller bearing. In this configuration, the guidance and control sections are located in the front body and the rear body carrying the rocket motor is left uncontrolled. Since the free roll motion of the rear body affects the aerodynamics of the entire missile, the missile aerodynamics is modeled considering the motion of the rear body. In this model, the necessary stability derivatives are obtained as functions of the Mach number and the spin angle that is defined as the difference between the roll angles of the front and rear bodies. Then, the complete dynamic model of the missile is derived along with the necessary transfer functions.

In this study, the three-dimensional formulation of the Proportional Navigation Guidance (PNG) law is done. Another contribution of this study is the derivation of the Linear Homing Guidance (LHG) and the Parabolic Homing Guidance (PHG) laws. Then, all these three methods are implemented on both the considered missile model for the uncanted and canted tail wing configurations, and a generic single-body missile model. Also, the acceleration, rate and angular autopilots are designed in order to realize the guidance commands generated by these guidance laws on the considered missile models.

Finally, the overall guidance and control models are constructed by integrating the obtained models and then numerous computer simulations are carried out to test the performance of the system in different scenarios.

The thesis comprises seven chapters. In Chapter 1, the results of an extensive literature survey about the guidance and control of homing missiles is presented. Also, the scope of the thesis is given.

In Chapter 2, first, the missile model considered in this study is described as a missile combined of two bodies connected to each other by means of a roller bearing. Afterwards, the kinematic relationships are obtained for each of the bodies and then they are written in terms of the kinematic parameters of the entire missile which are defined with respect to the mass center of the entire missile. Next, the equations of motions of the bodies are derived separately. Using the reaction force and moment components between the bodies through the roller bearing, these equations are combined and hence the seven equations of motion of the entire missile are obtained. In modeling, the bearing friction is assumed wholly in the viscous region. Next, the aerodynamics of the entire missile is modeled for different Mach numbers and the relative spin angle values. Based on the resulting dynamic model, the transfer functions required for the design of the governing control systems are obtained. Furthermore, choosing electro-mechanical type actuators, the

control actuation system model is constructed. Eventually, the models for the measuring instruments and the wind are supplied.

In Chapter 3, the guidance methods implemented in the computer simulations of this study are explained. First, the spatial derivation of the widely-used Proportional Navigation Guidance (PNG) law is completed. After PNG, two additional candidate guidance laws are proposed: Linear Homing Guidance (LHG) and Parabolic Homing Guidance (PHG) laws. In LHG, the guidance commands are generated in the form of the flight path angle components to drive the missile to the predicted intercept point with the target by following a linear path. In PHG, the guidance commands are produced for the lateral acceleration components of the missile and the desired trajectory toward the predicted intercept point is shaped to be a parabola rather than a straight line. In the final section of the chapter, the kinematic relationships for the missile-target engagement geometry are derived.

In Chapter 4, first, the roll and the two transversal autopilots of the missile are designed based on the transfer functions obtained in Chapter 2. Here, the transversal autopilots include the acceleration, angular rate and angle autopilots. When PNG or PHG is employed as the guidance law, the acceleration or the rate autopilot is used whereas the angle autopilot is needed for the execution of the guidance commands of the LHG law. After the design of the autopilots, the concept of anti-windup scheme used along with the controller is explained. Lastly, the roll resolving scheme is presented, which is employed to decouple the yaw and pitch channels in case of a nonzero roll motion.

In Chapter 5, the target is modeled as a surface target so as to use in the forthcoming computer simulations and the necessary kinematic equations are determined. Afterwards, the properties of the seeker suitable for the engagement purpose are explained in addition to the external contributors affecting the performance of the seeker. Then, the basic seeker types are introduced and a control system is designed for the control of the gimballed type seeker. Having compared

the mentioned seeker types, the chapter is concluded by the design of an estimator that is to be used in the estimation of the target states.

In Chapter 6, the numerical parameters used in the models are first given and the models created in the Matlab-Simulink environment are introduced. After the formation of the test configurations as well as the sets of the initial conditions, the results of the performed computer simulations are presented in the form of tables and figures. The interpretation of the obtained results is also made for all of the simulated configurations.

In Chapter 7, the performance of the designed guidance and control schemes are discussed. Also, the results of the relevant computer simulations are evaluated in accordance with the considered guidance and control schemes. Finally, some future work recommendations are made.

CHAPTER 2

MISSILE MODEL

In this chapter, first, the missile model considered in this study is described. Next, completing the kinematic analysis of the considered missile model, its governing differential equations of motion are derived. Afterwards, the necessary transfer functions to be used in the control system design stage have been determined based on the derived equations of motion. Then, the control actuation system model is constructed. Eventually, the models for the measuring instruments and the wind are given.

2.1. Missile Dynamic Model

In this study, a missile is considered such that its body is combined of two parts which are connected to each other by means of a free-rotating bearing. In this structure, the front body carries the guidance and control sections of the entire missile while the rear body involves the fixed tail wings and the rocket motor that supplies the missile with thrust required in the boost phase.

2.1.1. Missile Kinematics

As shown in Figure 2.1, C_1 and C_2 are used to represent the mass centers of the front and rear bodies which are called body 1 and body 2, respectively, while

C_M represents the mass center of the entire missile. Denoting the reference frame of body 1 as F_b which is attached to the missile at point C_1 , the relevant rotating frame based Euler angle sequence can be written for body 1 in the following manner:

$$\begin{array}{ccccc} \vec{u}_3^{(0)} & \vec{u}_2^{(m)} & \vec{u}_1^{(n)} & & \\ F_0 \rightarrow F_m \rightarrow F_n \rightarrow F_b & & & & \\ \psi_1 & \theta_1 & \phi_1 & & \end{array}$$

Here, F_0 denotes the Earth-fixed reference frame whose origin is point O_e while F_m and F_n show the intermediate reference frames between F_0 and F_b . Also, ψ_1 , θ_1 and ϕ_1 stand for the Euler angles in the yaw, pitch and roll directions of body 1, respectively. As a general note for the reference frames, they are all taken to be orthogonal and right-handed.

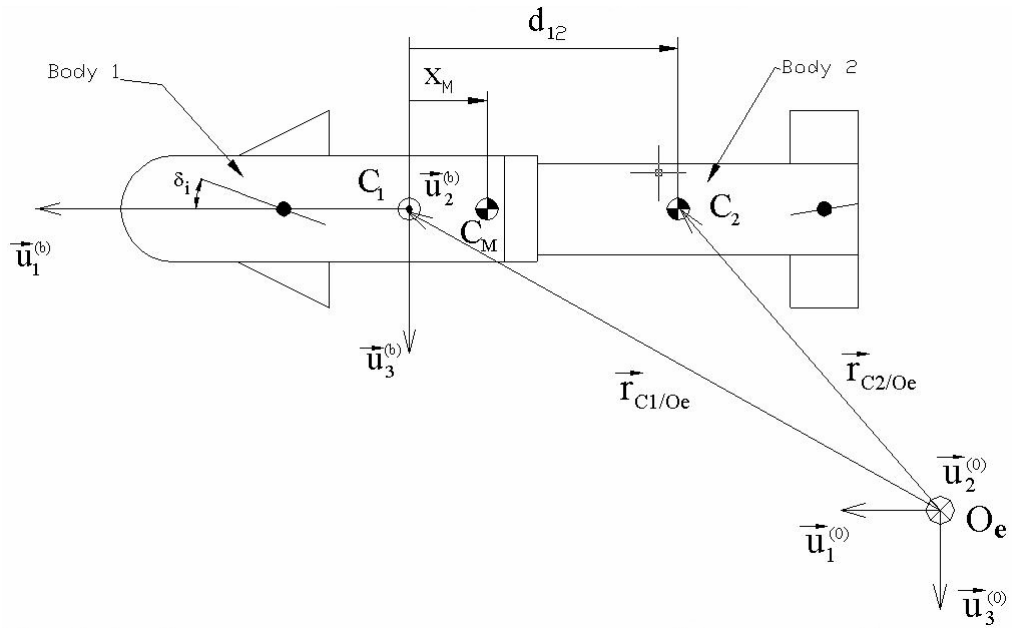


Figure 2.1. Considered Missile Model

Considering the rotation sequence given above, the overall rotation matrix can be written for body 1 using the basic rotation matrices as follows:

$$\hat{C}^{(0,b)} = \hat{C}^{(0,m)}\hat{C}^{(m,n)}\hat{C}^{(n,b)} = \hat{R}_3(\psi_1)\hat{R}_2(\theta_1)\hat{R}_1(\phi_1) \quad (2.1)$$

In equation (2.1), the basic rotation matrices for the rotations about the yaw, pitch and roll axes are defined as follows:

$$\hat{C}^{(0,m)} = \begin{bmatrix} \cos(\psi_1) & -\sin(\psi_1) & 0 \\ \sin(\psi_1) & \cos(\psi_1) & 0 \\ 0 & 0 & 1 \end{bmatrix} \quad (2.2)$$

$$\hat{C}^{(m,n)} = \begin{bmatrix} \cos(\theta_1) & 0 & \sin(\theta_1) \\ 0 & 1 & 0 \\ -\sin(\theta_1) & 0 & \cos(\theta_1) \end{bmatrix} \quad (2.3)$$

$$\hat{C}^{(n,b)} = \begin{bmatrix} 1 & 0 & 0 \\ 0 & \cos(\phi_1) & -\sin(\phi_1) \\ 0 & \sin(\phi_1) & \cos(\phi_1) \end{bmatrix} \quad (2.4)$$

The angular velocity vector of body 1 with respect to F_0 can be determined in terms of the rates of the Euler angles as follows:

$$\bar{\omega}_{b/0} = \dot{\psi}_1 \bar{u}_3^{(0)} + \dot{\theta}_1 \bar{u}_2^{(m)} + \dot{\phi}_1 \bar{u}_1^{(n)} \quad (2.5)$$

Defining the expression of $\bar{\omega}_{b/0}$ in F_b as $\bar{\omega}_{b/0}^{(b)} = [\bar{p}_1 \quad \bar{q}_1 \quad \bar{r}_1]^T$, the roll, pitch and yaw rates of body 1 can be written in terms of the Euler angles and their rates as

$$p_1 = \dot{\phi}_1 - \dot{\psi}_1 \sin(\theta_1) \quad (2.6)$$

$$q_1 = \dot{\theta}_1 \cos(\phi_1) + \dot{\psi}_1 \cos(\theta_1) \sin(\phi_1) \quad (2.7)$$

$$r_1 = -\dot{\theta}_1 \sin(\phi_1) + \dot{\psi}_1 \cos(\theta_1) \cos(\phi_1) \quad (2.8)$$

Reversely, once p_1, q_1 and r_1 are given, the rates of the Euler angles can be obtained from equations (2.6) through (2.8) in the following fashion, provided that $\cos(\theta_1) \neq 0$:

$$\dot{\psi}_1 = [q_1 \sin(\phi_1) + r_1 \cos(\phi_1)] / \cos(\theta_1) \quad (2.9)$$

$$\dot{\theta}_1 = q_1 \cos(\phi_1) - r_1 \sin(\phi_1) \quad (2.10)$$

$$\dot{\phi}_1 = p_1 + [q_1 \sin(\phi_1) + r_1 \cos(\phi_1)] \tan(\theta_1) \quad (2.11)$$

Also, the angular acceleration vector of body 1 with respect to F_0 can be determined by taking the time derivative of $\vec{\omega}_{b/0}$ in F_0 as follows:

$$\vec{\alpha}_{b/0} = D_0(\vec{\omega}_{b/0}) \quad (2.12)$$

where D_0 denotes the time derivative operator with respect to F_0 .

Expressing $\vec{\alpha}_{b/0}$ in F_b and noting that

$$D_0(\vec{\omega}_{b/0}) = D_b(\vec{\omega}_{b/0}) + \vec{\omega}_{b/0} \times \vec{\omega}_{b/0} = D_b(\vec{\omega}_{b/0}),$$

the components of the resulting column $\vec{\alpha}_{b/0}^{(b)}$ can be obtained simply as

$$\bar{\alpha}_{b/0}^{(b)} = \begin{bmatrix} \dot{p}_1 \\ \dot{q}_1 \\ \dot{r}_1 \end{bmatrix} \quad (2.13)$$

where

$$\dot{p}_1 = \ddot{\phi}_1 - \ddot{\psi}_1 \sin(\theta_1) - \dot{\psi}_1 \dot{\theta}_1 \cos(\theta_1)$$

$$\dot{q}_1 = \ddot{\theta}_1 \cos(\phi_1) + [\ddot{\psi}_1 \sin(\phi_1) + \dot{\psi}_1 \dot{\phi}_1 \cos(\phi_1)] \cos(\theta_1) - \dot{\theta}_1 [\dot{\phi}_1 + \dot{\psi}_1 \sin(\theta_1)] \sin(\phi_1)$$

$$\dot{r}_1 = -\ddot{\theta}_1 \sin(\phi_1) + [\ddot{\psi}_1 \cos(\phi_1) - \dot{\psi}_1 \dot{\phi}_1 \sin(\phi_1)] \cos(\theta_1) - \dot{\theta}_1 [\dot{\phi}_1 + \dot{\psi}_1 \sin(\theta_1)] \cos(\phi_1)$$

Since body 1 is the controlled body, the body-fixed frame of the entire missile can be taken to be coincident with F_b . Therefore, from now on, the following simpler notation will be used:

$$p = p_1 \quad (2.14)$$

$$q = q_1 \quad (2.15)$$

$$r = r_1 \quad (2.16)$$

Assuming that C_M lies on $\bar{u}_1^{(b)}$ axis like C_1 and C_2 , the distance between C_1 and C_M (x_M) can be determined as follows:

$$x_M = \frac{m_2}{m} d_{12} \quad (2.17)$$

where m and m_2 stand for the masses of the entire missile and body 2, and d_{12} denotes the distance between points C_1 and C_2 .

Here, it should be noted that d_{12} varies in accordance with the mass decay of body 2 due to the propulsion during the boost phase. On the other hand, since the guidance and control of the missile is performed after the boost phase, this distance is taken to be constant.

The velocity vectors of C_1 and C_M with respect to O_e can be related as

$$\vec{v}_{C_1/O_e} = \vec{v}_{C_M/O_e} + x_M [\vec{\omega}_{b/o} \times \vec{u}_1^{(b)}] \quad (2.18)$$

Equation (2.18) can be expressed in F_b in the following manner:

$$\bar{v}_{C_1/O_e}^{(b)} = \bar{v}_{C_M/O_e}^{(b)} + x_M [\tilde{\omega}_{b/o}^{(b)} \bar{u}_1] \quad (2.19)$$

where $\bar{v}_{C_1/O_e}^{(b)} = [u_1 \quad v_1 \quad w_1]^T$ and $\tilde{\omega}_{b/o}^{(b)} = \begin{bmatrix} 0 & -r & q \\ r & 0 & -p \\ -q & p & 0 \end{bmatrix}$.

Then, with $\bar{v}_{C_M/O_e}^{(b)} = [u \quad v \quad w]^T$, equation (2.19) yields the following expressions:

$$u_1 = u \quad (2.20)$$

$$v_1 = v + x_M r \quad (2.21)$$

$$w_1 = w - x_M q \quad (2.22)$$

Taking the time derivatives of equations (2.20) through (2.22), the following relationships are obtained in the acceleration level:

$$\dot{u}_1 - r v_1 + q w_1 = \dot{u} - r v + q w - x_M (q^2 + r^2) \quad (2.23)$$

$$\dot{v}_1 + r u_1 - p w_1 = \dot{v} + r u - p w + x_M (\dot{r} + p q) \quad (2.24)$$

$$\dot{w}_1 - q u_1 + p v_1 = \dot{w} - q u + p v - x_M (\dot{q} - p r) \quad (2.25)$$

Since the roll bearing between body 1 and body 2 restricts their relative lateral motions, both bodies show the same behaviour in the yaw and pitch directions. Conversely, they have independent relative rotations about the roll axis $\vec{u}_1^{(b)}$. Due to the relative motion of the bodies about $\vec{u}_1^{(b)}$ axis, the following rotation sequence occurs between body 1 and body 2:

$$\begin{array}{c} \vec{u}_1^{(b)} \\ F_b \rightarrow F_s \\ \phi_s \end{array}$$

In the sequence above, F_s represents the reference frame of body 2 whose origin is put at point C_2 as shown in Figure 2.1. Also, ϕ_s stands for the spin angle of body 2 about $\vec{u}_1^{(b)}$ axis and it is defined as

$$\phi_s = \phi_2 - \phi_1 \quad (2.26)$$

From here, the rotation matrix from F_b to F_s can be written as

$$\hat{C}^{(b,s)} = \begin{bmatrix} 1 & 0 & 0 \\ 0 & \cos(\phi_s) & -\sin(\phi_s) \\ 0 & \sin(\phi_s) & \cos(\phi_s) \end{bmatrix} \quad (2.27)$$

Hence, the angular velocity vector of body 2 with respect to F_b can be expressed as

$$\vec{\omega}_{s/b} = \dot{\phi}_s \vec{u}_1^{(b)} \quad (2.28)$$

Having determined the relative angular velocity vector between body 1 and body 2, the angular velocity vector of body 2 with respect to F_θ can be written as

$$\vec{\omega}_{s/0} = \vec{\omega}_{s/b} + \vec{\omega}_{b/0} \quad (2.29)$$

Defining the expressions of the angular velocity and the angular acceleration vectors of body 2 in F_s as $\vec{\omega}_{s/0}^{(s)} = [p_2 \quad q_2 \quad r_2]^T$ and $\vec{\alpha}_{s/0}^{(s)} = [\dot{p}_2 \quad \dot{q}_2 \quad \dot{r}_2]^T$, they can be written in F_b that corresponds to the non-spinning reference frame of body 2 as well in the following manner:

$$\vec{\omega}_{s/0}^{(b)} = \hat{C}^{(b,s)} \vec{\omega}_{s/0}^{(s)} \quad (2.30)$$

$$\vec{\alpha}_{s/0}^{(b)} = \hat{C}^{(b,s)} \dot{\vec{\omega}}_{s/0}^{(s)} \quad (2.31)$$

The components of $\vec{\omega}_{s/0}^{(b)}$ and $\vec{\alpha}_{s/0}^{(b)}$ can be defined as

$$\vec{\omega}_{s/0}^{(b)} = \begin{bmatrix} p'_2 \\ q'_2 \\ r'_2 \end{bmatrix} \quad (2.32)$$

$$\vec{\alpha}_{s/0}^{(b)} = \begin{bmatrix} \dot{p}'_2 \\ \dot{q}'_2 + \dot{\phi}_s r'_2 \\ \dot{r}'_2 - \dot{\phi}_s q'_2 \end{bmatrix} \quad (2.33)$$

where $\mathbf{p}'_2 = \mathbf{p}_2$, $\mathbf{q}'_2 = \mathbf{q}_2 \cos(\phi_s) - \mathbf{r}_2 \sin(\phi_s)$, $\mathbf{r}'_2 = \mathbf{r}_2 \cos(\phi_s) + \mathbf{q}_2 \sin(\phi_s)$, $\dot{\mathbf{p}}'_2 = \dot{\mathbf{p}}_2$, $\dot{\mathbf{q}}'_2 = \dot{\mathbf{q}}_2 \cos(\phi_s) - \dot{\mathbf{r}}_2 \sin(\phi_s)$ and $\dot{\mathbf{r}}'_2 = \dot{\mathbf{r}}_2 \cos(\phi_s) + \dot{\mathbf{q}}_2 \sin(\phi_s)$.

Equations (2.28) and (2.29) can be written in F_b as follows:

$$\overline{\omega}_{s/b}^{(b)} = \dot{\phi}_s \bar{\mathbf{u}}_1 \quad (2.34)$$

$$\overline{\omega}_{s/0}^{(b)} = \overline{\omega}_{s/b}^{(b)} + \overline{\omega}_{b/0}^{(b)} \quad (2.35)$$

Putting equations (2.32) and (2.34) into equation (2.35), the following kinematic constraint equations arise among the angular velocity components of the body 2 and the entire missile:

$$\mathbf{p}_2 = \mathbf{p} + \dot{\phi}_s \quad (2.36)$$

$$\mathbf{q}'_2 = \mathbf{q} \quad (2.37)$$

$$\mathbf{r}'_2 = \mathbf{r} \quad (2.38)$$

From equation (2.31), the constraint equations among the angular acceleration components of the bodies can be obtained as

$$\dot{\mathbf{p}}_2 = \dot{\mathbf{p}} + \ddot{\phi}_s \quad (2.39)$$

$$\dot{\mathbf{q}}'_2 = \dot{\mathbf{q}} \quad (2.40)$$

$$\dot{\mathbf{r}}'_2 = \dot{\mathbf{r}} \quad (2.41)$$

Considering point C_2 , the velocity vector of C_M with respect to O_e can be written as

$$\vec{v}_{C_2/O_e} = \vec{v}_{C_M/O_e} - (d_{12} - x_M) [\vec{\omega}_{b/0} \times \vec{u}_1^{(b)}] \quad (2.42)$$

Defining $\bar{v}_{C_2/O_e}^{(s)} = [u_2 \quad v_2 \quad w_2]^T$, the expression of equation (2.42) in F_b yields the following scalar expressions:

$$u'_2 = u \quad (2.43)$$

$$v'_2 = v - (d_{12} - x_M)r \quad (2.44)$$

$$w'_2 = w + (d_{12} - x_M)q \quad (2.45)$$

where $u'_2 = u_2$, $v'_2 = v_2 \cos(\phi_s) - w_2 \sin(\phi_s)$ and $w'_2 = w_2 \cos(\phi_s) + v_2 \sin(\phi_s)$.

The time derivative of equations (2.43) through (2.45) gives the following expressions:

$$\dot{u}'_2 - r v'_2 + q w'_2 = \dot{u} - r v + q w + (d_{12} - x_M)(q^2 + r^2) \quad (2.46)$$

$$\dot{v}'_2 + r u'_2 - p w'_2 = \dot{v} + r u - p w - (d_{12} - x_M)(\dot{r} + p q) \quad (2.47)$$

$$\dot{w}'_2 - q u'_2 + p v'_2 = \dot{w} - q u + p v + (d_{12} - x_M)(\dot{q} - p r) \quad (2.48)$$

2.1.2. Equations of Motion of the Missile

Having completed the kinematic analysis, the equations of motion of the missile can be derived using the Newton-Euler equations, which express the force and moment balance on each body. The Newton-Euler equations for body 1 are

$$\vec{F}_{A1} + \vec{F}_{21} + m_1 \vec{g} = m_1 \vec{a}_{C_1/O_e} \quad (2.49)$$

$$\vec{M}_{A1} + \vec{M}_{21} + \vec{r}_{B/C_1} \times \vec{F}_{21} = \check{J}_{C_1} \cdot \vec{\alpha}_{b/0} + \vec{\omega}_{b/0} \times \check{J}_{C_1} \cdot \vec{\omega}_{b/0} \quad (2.50)$$

Similarly, the Newton-Euler equations for body 2 are

$$\vec{F}_{A2} + \vec{F}_{T2} + \vec{F}_{12} + m_2 \vec{g} = m_2 \vec{a}_{C_2/O_e} \quad (2.51)$$

$$\vec{M}_{A2} + \vec{M}_{T2} + \vec{M}_{12} + \vec{r}_{B/C_2} \times \vec{F}_{12} = \check{J}_{C_2} \cdot \vec{\alpha}_{s/0} + \vec{\omega}_{s/0} \times \check{J}_{C_2} \cdot \vec{\omega}_{s/0} \quad (2.52)$$

In equations (2.49) through (2.52), the following definitions are made for $i, j=1$ and 2 :

$\vec{F}_{Ai}, \vec{M}_{Ai}$: Aerodynamic force and moment vectors acting on body i

$\vec{F}_{ij}, \vec{M}_{ij}$: Reaction force and moment vectors applied by body i on body j

$\vec{F}_{T2}, \vec{M}_{T2}$: Thrust force and thrust misalignment moment vectors acting on body 2

m_i : Mass of body i

$\check{\mathbf{J}}_{C_i}$: Inertia dyadic of body i about its own mass center

$\vec{\mathbf{g}}$: Acceleration of gravity

$\vec{\mathbf{r}}_{B/C_i}$: Position vector between the mass center of body i and the midpoint of the bearing (point B)

Looking at equations (2.49) through (2.52), it is seen that the thrust force and moment terms occur in the equations of body 2. That is because the rocket motor that supplies the required thrust throughout the boost phase is mounted on body 2. Also, the vectors $\vec{\mathbf{r}}_{B/C_1}$ and $\vec{\mathbf{r}}_{B/C_2}$ can be expressed as

$$\vec{\mathbf{r}}_{B/C_1} = -d_1 \vec{\mathbf{u}}_1^{(b)} \quad (2.53)$$

$$\vec{\mathbf{r}}_{B/C_2} = d_2 \vec{\mathbf{u}}_1^{(b)} \quad (2.54)$$

where d_i shows the distance between the points C_i and B ($i=1$ and 2) and $d_{12} = d_1 + d_2$.

Expressing equations (2.49) through (2.52) in F_b results in the following matrix equations:

$$\overline{\mathbf{F}}_{A1}^{(b)} + \overline{\mathbf{F}}_{21}^{(b)} + m_1 \vec{\mathbf{g}}^{(b)} = m_1 \vec{\mathbf{a}}_{C_1/O_e}^{(b)} \quad (2.55)$$

$$\overline{\mathbf{M}}_{A1}^{(b)} + \overline{\mathbf{M}}_{21}^{(b)} - d_1 \tilde{\mathbf{u}}_1 \overline{\mathbf{F}}_{21}^{(b)} = \hat{\mathbf{J}}_{C_1}^{(b)} \overline{\boldsymbol{\alpha}}_{b/0}^{(b)} + \tilde{\boldsymbol{\omega}}_{b/0}^{(b)} \hat{\mathbf{J}}_{C_1}^{(b)} \overline{\boldsymbol{\omega}}_{b/0}^{(b)} \quad (2.56)$$

$$\overline{\mathbf{F}}_{A2}^{(b)} + \overline{\mathbf{F}}_{T2}^{(b)} + \overline{\mathbf{F}}_{12}^{(b)} + m_2 \vec{\mathbf{g}}^{(b)} = m_2 \vec{\mathbf{a}}_{C_2/O_e}^{(b)} \quad (2.57)$$

$$\overline{\mathbf{M}}_{A2}^{(b)} + \overline{\mathbf{M}}_{T2}^{(b)} + \overline{\mathbf{M}}_{12}^{(b)} + d_2 \tilde{\mathbf{u}}_1 \overline{\mathbf{F}}_{12}^{(b)} = \hat{\mathbf{J}}_{C_2}^{(b)} \overline{\boldsymbol{\alpha}}_{s/0}^{(b)} + \tilde{\boldsymbol{\omega}}_{s/0}^{(b)} \hat{\mathbf{J}}_{C_2}^{(b)} \overline{\boldsymbol{\omega}}_{s/0}^{(b)} \quad (2.58)$$

In equations (2.55) through (2.58), the force and moment columns for the aerodynamic and thrust effects are defined as follows:

$$\bar{\mathbf{F}}_{A1}^{(b)} = \begin{bmatrix} X_1 \\ Y_1 \\ Z_1 \end{bmatrix} \quad (2.59)$$

$$\bar{\mathbf{M}}_{A1}^{(b)} = \begin{bmatrix} L_1 \\ M_1 \\ N_1 \end{bmatrix} \quad (2.60)$$

$$\bar{\mathbf{F}}_{A2}^{(b)} = \begin{bmatrix} X_2 \\ Y'_2 \\ Z'_2 \end{bmatrix} \quad (2.61)$$

$$\bar{\mathbf{M}}_{A2}^{(b)} = \begin{bmatrix} L_2 \\ M'_2 \\ N'_2 \end{bmatrix} \quad (2.62)$$

$$\bar{\mathbf{F}}_{T2}^{(b)} = \begin{bmatrix} X_{T2} \\ Y'_{T2} \\ Z'_{T2} \end{bmatrix} \quad (2.63)$$

$$\bar{\mathbf{M}}_{T2}^{(b)} = \begin{bmatrix} L_{T2} \\ M'_{T2} \\ N'_{T2} \end{bmatrix} \quad (2.64)$$

In equations (2.61) through (2.64), the terms in the columns are obtained by making the transformations of the relevant columns from F_s to F_b in the following manner:

$$\bar{F}_{A2}^{(b)} = \hat{C}^{(b,s)} \bar{F}_{A2}^{(s)} \quad (2.65)$$

$$\bar{M}_{A2}^{(b)} = \hat{C}^{(b,s)} \bar{M}_{A2}^{(s)} \quad (2.66)$$

$$\bar{F}_{T2}^{(b)} = \hat{C}^{(b,s)} \bar{F}_{T2}^{(s)} \quad (2.67)$$

$$\bar{M}_{T2}^{(b)} = \hat{C}^{(b,s)} \bar{M}_{T2}^{(s)} \quad (2.68)$$

where

$$\bar{F}_{A2}^{(s)} = [X_2 \quad Y_2 \quad Z_2]^T, \quad \bar{M}_{A2}^{(s)} = [L_2 \quad M_2 \quad N_2]^T, \quad \bar{F}_{T2}^{(s)} = [X_{T2} \quad Y_{T2} \quad Z_{T2}]^T \quad \text{and}$$

$$\bar{M}_{T2}^{(s)} = [L_{T2} \quad M_{T2} \quad N_{T2}]^T.$$

Hence, equations (2.65) through (2.68) lead to the following expressions:

$$X'_2 = X_2 \quad (2.69)$$

$$Y'_2 = Y_2 \cos(\phi_s) - Z_2 \sin(\phi_s) \quad (2.70)$$

$$Z'_2 = Z_2 \cos(\phi_s) + Y_2 \sin(\phi_s) \quad (2.71)$$

$$L'_2 = L_2 \quad (2.72)$$

$$M'_2 = M_2 \cos(\phi_s) - N_2 \sin(\phi_s) \quad (2.73)$$

$$N'_2 = N_2 \cos(\phi_s) + M_2 \sin(\phi_s) \quad (2.74)$$

$$X'_{T2} = X_{T2} \quad (2.75)$$

$$Y'_{T2} = Y_{T2} \cos(\phi_s) - Z_{T2} \sin(\phi_s) \quad (2.76)$$

$$Z'_{T2} = Z_{T2} \cos(\phi_s) + Y_{T2} \sin(\phi_s) \quad (2.77)$$

$$L'_{T2} = L_{T2} \quad (2.78)$$

$$M'_{T2} = M_{T2} \cos(\phi_s) - N_{T2} \sin(\phi_s) \quad (2.79)$$

$$N'_{T2} = N_{T2} \cos(\phi_s) + M_{T2} \sin(\phi_s) \quad (2.80)$$

Next, $\bar{F}_{12}^{(b)}$ can be picked up from equation (2.57) as follows:

$$\bar{F}_{12}^{(b)} = m_2 \bar{a}_{C_2/O_e}^{(b)} - [\bar{F}_{A2}^{(b)} + \bar{F}_{T2}^{(b)} + m_2 \bar{g}^{(b)}] \quad (2.81)$$

Notice that $\bar{F}_{21}^{(b)} = -\bar{F}_{12}^{(b)}$. Hence, putting equation (2.81) into equation (2.55) yields the following equation:

$$\bar{F}_A^{(b)} + \bar{F}_{T2}^{(b)} + m \bar{g}^{(b)} = m_1 \bar{a}_{C_1/O_e}^{(b)} + m_2 \bar{a}_{C_2/O_e}^{(b)} \quad (2.82)$$

where $\bar{F}_A^{(b)} = \bar{F}_{A1}^{(b)} + \bar{F}_{A2}^{(b)}$ and $m = m_1 + m_2$.

Also, since the acceleration of gravity is expressed in F_θ as $\bar{g} = g \bar{u}_3^{(0)}$ ($g = 9.81 \text{ m/s}^2$), its representation in F_b becomes

$$\bar{g}^{(b)} = \hat{C}^{(b,0)} \bar{g}^{(0)} \quad (2.83)$$

Because of the orthonormality property of the overall rotation matrix $\hat{C}^{(0,b)}$, $\hat{C}^{(b,0)} = [\hat{C}^{(0,b)}]^{-1} = [\hat{C}^{(0,b)}]^T$. Using this property, equation (2.83) can also be written as

$$\bar{g}^{(b)} = g [\hat{C}^{(0,b)}]^T \bar{u}_3 \quad (2.84)$$

Making the necessary manipulations, equation (2.84) leads to

$$\bar{g}^{(b)} = \begin{bmatrix} g_x \\ g_y \\ g_z \end{bmatrix} \quad (2.85)$$

where $g_x = -g \sin(\theta_1)$, $g_y = g \cos(\theta_1) \sin(\phi_1)$ and $g_z = g \cos(\theta_1) \cos(\phi_1)$.

Proceeding further, the acceleration columns for the mass centers of body 1 and body 2 can be expressed in terms of their angular and linear velocity components as

$$\bar{a}_{C_1/O_e}^{(b)} = \dot{\bar{v}}_{C_1/O_e}^{(b)} + \tilde{\omega}_{b/0}^{(b)} \bar{v}_{C_1/O_e}^{(b)} \quad (2.86)$$

$$\bar{a}_{C_2/O_e}^{(b)} = \dot{\bar{v}}_{C_2/O_e}^{(b)} + \tilde{\omega}_{s/0}^{(b)} \bar{v}_{C_2/O_e}^{(b)} \quad (2.87)$$

Defining $\bar{a}_{C_i/O_e}^{(b)} = [a_{ix} \quad a_{iy} \quad a_{iz}]^T$ for $i=1$ and 2 , equations (2.86) and (2.87) yield the following equations:

$$a_{1x} = \dot{u} - r v + q w - x_M (q^2 + r^2) \quad (2.88)$$

$$a_{1y} = \dot{v} + r u - p w + x_M (\dot{r} + p q) \quad (2.89)$$

$$a_{1z} = \dot{w} - q u + p v - x_M (\dot{q} - p r) \quad (2.90)$$

$$a_{2x} = \dot{u} - r v + q w + (d_{12} - x_M)(q^2 + r^2) \quad (2.91)$$

$$a_{2y} = \dot{v} + r u - p w - (d_{12} - x_M)(\dot{r} + p q) \quad (2.92)$$

$$a_{2z} = \dot{w} - q u + p v + (d_{12} - x_M)(\dot{q} - p r) \quad (2.93)$$

Hence, putting equations (2.59), (2.61), (2.63), (2.83), (2.86) and (2.87) into equation (2.82) and then making the necessary operations, the translational equations for the entire missile motion can be obtained as given below:

$$\dot{u} - r v + q w = \frac{1}{m}(X + X_T) + g_x \quad (2.94)$$

$$\dot{v} + r u - p w = \frac{1}{m}(Y + Y_T) + g_y \quad (2.95)$$

$$\dot{w} - q u + p v = \frac{1}{m}(Z + Z_T) + g_z \quad (2.96)$$

where $X = X_1 + X_2$, $Y = Y_1 + Y'_2$, $Z = Z_1 + Z'_2$, $X_T = X_{T2}$, $Y_T = Y'_{T2}$ and

$$Z_T = Z'_{T2}.$$

The moment equations can be handled in the same manner. Since the bodies are connected to each other through the roller bearing, there exists no reaction moment about their body axis $[\bar{u}_1^{(b)}]$ except bearing friction. Thus, for the columns of the reaction moments between the bodies can be expressed as follows:

$$\overline{M}_k^{(b)} = \begin{bmatrix} M_{kx} \\ M_{ky} \\ M_{kz} \end{bmatrix} \quad (2.97)$$

where $k=12$ and 21 .

Modeling the bearing friction as viscous friction with the coefficient b_t , the moment component M_{21x} in equation (2.97) can be introduced as

$$M_{21x} = b_t \dot{\phi}_s \quad (2.98)$$

Also, as I_{ai} and I_{ti} stand for the axial and transverse moment of inertia components of body i ($i=1$ and 2), and regarding the rotational symmetries of the bodies, the inertia dyadics of the bodies can be expressed in their own reference frames as follows:

$$\hat{\mathbf{J}}_{C_1}^{(b)} = \begin{bmatrix} \mathbf{I}_{a1} & 0 & 0 \\ 0 & \mathbf{I}_{t1} & 0 \\ 0 & 0 & \mathbf{I}_{t1} \end{bmatrix} \quad (2.99)$$

$$\hat{\mathbf{J}}_{C_2}^{(s)} = \begin{bmatrix} \mathbf{I}_{a2} & 0 & 0 \\ 0 & \mathbf{I}_{t2} & 0 \\ 0 & 0 & \mathbf{I}_{t2} \end{bmatrix} \quad (2.100)$$

The inertia matrix of body 2 can be expressed in F_b as follows:

$$\hat{\mathbf{J}}_{C_2}^{(b)} = \hat{\mathbf{C}}^{(b,s)} \hat{\mathbf{J}}_{C_2}^{(s)} \hat{\mathbf{C}}^{(s,b)} \quad (2.101)$$

From equation (2.101), $\hat{\mathbf{J}}_{C_2}^{(b)}$ appears in the following form:

$$\hat{\mathbf{J}}_{C_2}^{(b)} = \begin{bmatrix} \mathbf{I}_{a2} & 0 & 0 \\ 0 & \mathbf{I}_{t2} & 0 \\ 0 & 0 & \mathbf{I}_{t2} \end{bmatrix} \quad (2.102)$$

Here, it should be noted that $\hat{\mathbf{J}}_{C_2}^{(b)} = \hat{\mathbf{J}}_{C_2}^{(s)}$ due to the symmetry of body 2 about $\bar{\mathbf{u}}_1^{(b)}$.

Eventually, substituting equations (2.14), (2.15), (2.16), (2.30), (2.31), (2.60), (2.62), (2.64), (2.81), (2.97), (2.98), (2.99) and (2.102) into equations (2.56) and (2.58), and making the necessary arrangements, the moment equations of the entire missile can be obtained. Hence, regarding equations (2.94) through (2.96), the governing equations of motion of the missile can be written as

$$\dot{u} - r v + q w = \frac{1}{m}(X + X_T) + g_x \quad (2.103)$$

$$\dot{v} + r u - p w = \frac{1}{m}(Y + Y_T) + g_y \quad (2.104)$$

$$\dot{w} - q u + p v = \frac{1}{m}(Z + Z_T) + g_z \quad (2.105)$$

$$\dot{p} = \frac{1}{I_{a1}}(L_1 + b_t \dot{\phi}_s) \quad (2.106)$$

$$\dot{p}_2 = \frac{1}{I_{a2}}(L_2 + L_T - b_t \dot{\phi}_s) \quad (2.107)$$

$$\dot{q} - p r (1 - \mu_1) + p_2 r \gamma_2 = \frac{1}{I'_t}(M + M_T - \lambda_2 Z_T) \quad (2.108)$$

$$\dot{r} + p q (1 - \mu_1) - p_2 q \gamma_2 = \frac{1}{I'_t}(N + N_T + \lambda_2 Y_T) \quad (2.109)$$

where $\dot{p}_2 = \dot{p} + \ddot{\phi}_s$, $\mu_1 = \frac{m_1}{m}$, $I'_t = I_t - \left(\frac{m_1 m_2}{m} \right) d_{12}^2$, $\gamma_2 = \frac{I_{a2}}{I'_t}$, $\lambda_2 = d_{12} - x_M$,

$M = M_1 + M'_2 + x_M Z_1 - \lambda_2 Z'_2$, $N = N_1 + N'_2 - x_M Y_1 + \lambda_2 Y'_2$, $M_T = M'_{T2}$ and

$N_T = N'_{T2}$.

2.2. Missile Aerodynamic Model

There are no difficulties in terms of the mathematical modeling of the inertial and gravitational forces as indicated by the above equations of motion. One of the fundamental problems in flight mechanics is the mathematical modeling of the relationships between aerodynamic forces and moments (\vec{F}_A, \vec{M}_A) and motion

of the missile $(\vec{v}_{C_i/0_e}, \vec{\omega}_{b_i/0})$ for $i = 1$ and 2 . In general, aerodynamic forces and moments that instantaneously act on a missile depend not only on the instantaneous kinematic state of the missile, but also on its previous motion. In other words, the missile and the air surrounding it constitute a dynamic system with memory. Hence, a generalized aerodynamic force component F is a *functional* of the translational and rotational velocity components. That is,

$$F = F[u(\tau), v(\tau), w(\tau), p(\tau), q(\tau), r(\tau) : 0 \leq \tau \leq t] \quad (2.110)$$

The memory effect is significant in subsonic flight speeds; in case of sudden changes in translational or rotational velocities; in case of oscillatory motion with high frequency; in cases where viscous effects are important such as boundary layer separation; or in cases where aerodynamic heating effects are significant. On the other hand, in most ordinary cases, the aerodynamic memory effect is negligible and hence the generalized aerodynamic force component F can be safely assumed to be a *function* of instantaneous translational and rotational velocity components [6]:

$$F = F(u, v, w, p, q, r) \quad (2.111)$$

With this assumption, the aerodynamic force components in equations (2.103) through (2.109) can be formulated as given below:

$$X = C_x q_\infty S_M \quad (2.112)$$

$$Y = C_y q_\infty S_M \quad (2.113)$$

$$Z = C_z q_\infty S_M \quad (2.114)$$

$$L_i = C_{li} q_\infty S_M d_M \quad (2.115)$$

$$M = C_m q_\infty S_M d_M \quad (2.116)$$

$$N = C_n q_\infty S_M d_M \quad (2.117)$$

where the relevant symbols are as explained below:

X, Y, Z : Components of the aerodynamic force acting on the missile in $\bar{u}_1^{(b)}$, $\bar{u}_2^{(b)}$ and $\bar{u}_3^{(b)}$ directions

L_i : Component of the aerodynamic roll moment acting on body i in $\bar{u}_1^{(b)}$ direction

M, N : Components of the aerodynamic pitch and yaw moments acting on the missile in $\bar{u}_2^{(b)}$ and $\bar{u}_3^{(b)}$ directions

S_M : Cross-sectional area of the missile

d_M : Missile diameter

$q_{\infty i}$: Dynamic pressure acting on body i

q_∞ : Dynamic pressure acting on the entire missile body

$q_{\infty i}$, q_∞ and S_M can be obtained as

$$q_{\infty i} = \frac{1}{2} \rho v_{C_i/O_e}^2 \quad (2.118)$$

$$q_\infty = \frac{1}{2} \rho v_M^2 \quad (2.119)$$

$$S_M = \frac{\pi}{4} d_M^2 \quad (2.120)$$

In equations (2.118) and (2.119), ρ and v_{C_i/O_e} stand for the air density and resulting velocity of the mass center of body i . Also, v_M represents the resulting velocity of the mass center of the entire missile.

The air density changes with the altitude as given below [10]:

$$\rho = \begin{cases} \rho_0 (1 - 0.00002256h)^{4.256} & \text{if } h \leq 10000 \text{ m} \\ 0.412 e^{-0.000151(h-10000)} & \text{if } h > 10000 \text{ m} \end{cases} \quad (2.121)$$

where h (in meters) and ρ_0 denote the altitude and air density at the sea level and $\rho_0 = 1.223 \text{ kg/m}^3$.

v_{C_i/O_e} and v_M are determined using their components as

$$v_{C_i/O_e} = \sqrt{u_i^2 + v_i^2 + w_i^2} \quad (2.122)$$

$$v_M = \sqrt{u^2 + v^2 + w^2} \quad (2.123)$$

The aerodynamic force and moment coefficients are basically functions of Mach number (M_∞) which is a dimensionless number defined as the ratio of the missile velocity to the speed of sound at the altitude at which the vehicle is at flight. Thus, M_∞ can be formulated as

$$M_\infty = \frac{v_M}{v_s} \quad (2.124)$$

In equation (2.124), v_s is the speed of sound and can be calculated using the following formula:

$$v_s = \sqrt{k R T} \quad (2.125)$$

In equation (2.125), k is the specific heat ratio of the air which is taken to be equal to 1.4 and R is the universal gas constant which is taken to be equal to 287 J/kg K . T is the ambient temperature which also changes with altitude, and can be expressed in the following manner:

$$T = \begin{cases} T_0 (1 - 0.00002256 h) & \text{if } h \leq 10000 \text{ m} \\ 0.7744 T_0 & \text{if } h > 10000 \text{ m} \end{cases} \quad (2.126)$$

In equation (2.126), T_0 is the temperature at the sea level and it is taken as 293 K, in this work.

Throughout the flight, two angles are defined to describe the aerodynamic effects acting on the missile: the angle of attack (α) and the side-slip angle (β). In some sources, α and β are also called wind angles. The lift and drag components of the aerodynamic forces are oriented by α and β . From Figure 2.2, α and β can be obtained as follows:

$$\alpha = \arctan\left(\frac{w}{u}\right) \quad (2.127)$$

$$\beta = \arcsin\left(\frac{v}{v_M}\right) \quad (2.128)$$

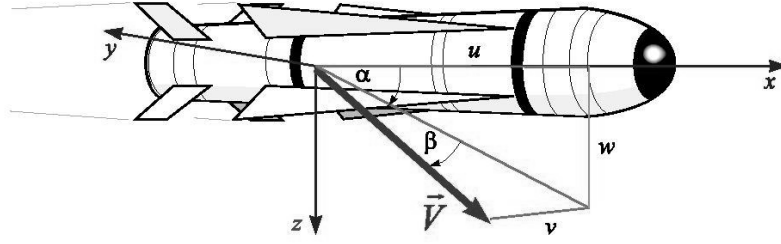


Figure 2.2. Demonstration of Angle of Attack and Side-Slip Angle [10]

Since the values of the velocity components v and w are much smaller when compared with the u value, u can be taken to be equal to v_M . Hence, equations (2.127) and (2.128) can be approximated as follows in accordance with the assumption that α and β are small angles:

$$\alpha \cong \frac{w}{u} \quad (2.129)$$

$$\beta \cong \frac{v}{u} \quad (2.130)$$

Considering the missile model in this study, the aerodynamic coefficients C_j ($j=x, y, z, l_i, m$ and n) in equations (2.112) through (2.117) are also functions of the flight parameters such as α , β , the control surface deflections (δ_a, δ_e and δ_r), the body angular rates (p, q and r), the time rates of α and β , the spin angle (ϕ_s) and the rate of the spin angle ($\dot{\phi}_s$) in addition to M_∞ . The subscripts e, r and a of the δ terms denote the elevator, rudder, and aileron deflections, respectively. These deflections are provided by the control surfaces and are defined in terms of the fin deflections in the following manner:

$$\delta_a = \frac{\delta_1 + \delta_3}{2} \quad (2.131)$$

$$\delta_e = \frac{\delta_2 - \delta_4}{2} \quad (2.132)$$

$$\delta_r = \frac{\delta_1 - \delta_3}{2} \quad (2.133)$$

In equations (2.131) through (2.133), δ_i shows the deflection of control fin i for $i=1, 2, 3$ and 4 . The fin arrangement of the considered cruciform missile is given in Figure 2.3 with the positive rotation senses of the fins.

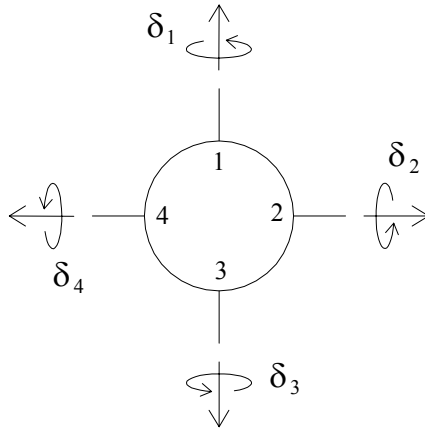


Figure 2.3. Considered Fin Arrangement from the Rear View of the Missile

Then, for each j , C_j can be expressed as a function of the mentioned flight parameters in the following manner [10]:

$$C_j = C_j(M, \alpha, \beta, \delta_e, \delta_r, \delta_a, p, q, r, \dot{\alpha}, \dot{\beta}, \dot{\phi}_s, \dot{\phi}_s) \quad (2.134)$$

In fact, C_j is a nonlinear function of the parameters mentioned above. For instance, using the Maple-Synge method, a wider expansion of the coefficient C_m can be made as follows for a rocket with fixed fins [6]:

$$\begin{aligned}
C_m = & C_{m_\alpha} \alpha + C_{m_{\alpha^2}} \delta^2 \alpha + C_{m_\beta} \beta + C_{m_{\beta^2}} \delta^2 \beta - C_{m_{\delta^2\gamma}}^{(I)} \alpha (\alpha^2 - 3\beta^2) \\
& + C_{m_{\delta^2\gamma}}^{(R)} \beta (\beta^2 - 3\alpha^2) - C_{m_{\delta^4\gamma-}}^{(I)} \alpha (\alpha^4 - 2\alpha^2 \beta^2 - 3\beta^4) \\
& + C_{m_{\delta^4\gamma-}}^{(R)} \beta (\beta^4 - 2\alpha^2 \beta^2 - 3\alpha^4) - C_{m_{\delta^4\gamma+}}^{(I)} \alpha (\alpha^4 - 10\alpha^2 \beta^2 + 5\beta^4) \\
& + C_{m_{\delta^4\gamma+}}^{(R)} \beta (\beta^4 - 10\alpha^2 \beta^2 + 10\alpha^4) - C_{m_{\delta^4}}^{(I)} \delta^4 \alpha + C_{m_{\delta^4}}^{(R)} \delta^4 \beta
\end{aligned} \quad (2.135)$$

On the other hand, for the autopilot design issue, the aerodynamic coefficients can be linearized as [11]

$$C_x = C_{x0} \quad (2.136)$$

$$C_y = C_{y_\beta} \beta + C_{y_\delta} \delta_r + C_{y_r} \frac{d_M}{2 v_M} r \quad (2.137)$$

$$C_z = C_{z_\alpha} \alpha + C_{z_\delta} \delta_e + C_{z_q} \frac{d_M}{2 v_M} q \quad (2.138)$$

$$C_{li} = C_{l_\delta} \delta_a + C_{l_{pi}} \frac{d_M}{2 v_M} p_i \quad (2.139)$$

$$C_m = C_{m_\alpha} \alpha + C_{m_\delta} \delta_e + C_{m_q} \frac{d_M}{2 v_M} q \quad (2.140)$$

$$C_n = C_{n_\beta} \beta + C_{n_\delta} \delta_r + C_{n_r} \frac{d_M}{2 v_M} r \quad (2.141)$$

In equations (2.136) through (2.141), C_{y_β} , C_{y_δ} , C_{y_r} , C_{z_α} , C_{z_δ} , C_{z_q} , C_{l_δ} , $C_{l_{pi}}$, C_{m_α} , C_{m_δ} , C_{m_q} , C_{n_β} , C_{n_δ} and C_{n_r} are called stability derivatives, and they are functions of M_∞ and ϕ_s . Here, for instance, the static stability C_{m_α} is defined

as the slope of the pitching moment coefficient (C_m) versus angle of attack (α). For a statically stable missile, C_{m_α} is negative.

As a property of the symmetric cruciform missiles, the following relationships exist between the aerodynamic stability derivatives of the missile. Here, it should be noticed that these equalities come from the distances between the hinges of the control fins and the mass center of the entire missile.

$$C_{m_\alpha} = b_\alpha C_{z_\alpha} \quad (2.142)$$

$$C_{m_\delta} = b_\delta C_{z_\delta} \quad (2.143)$$

In the above equations, b_α stands for the pressure center offset and b_δ is the parameter related to the position of the hinge locations of the control fins with respect to the missile mass center.

In this study, the aerodynamic coefficients are generated for the selected ranges of the Mach number (M_∞), the angle of attack (α), the elevator deflection (δ_e) and the spin angle (ϕ_s). In the data generation, the Missile Datcom software that is available in TÜBİTAK-SAGE is used. Since this software can be used for only single-body missile structures, the considered two-part missile is modeled as a single body whose control fins have a fixed relative rotation at an angle ϕ_s with respect to its tail fins. Then, the simulation model is run for the discrete values of ϕ_s from zero to 90 degrees and the aerodynamic coefficients C_x , C_z , C_{ll} and C_m are determined for the considered ϕ_s values. After the generation of the aerodynamic coefficients, the stability derivatives are found by fitting the linear polynomials given in equations (2.136), (2.138), (2.139) and (2.140) to the data. Hence, sets of the aerodynamic stability derivatives are constructed such that each set contains the data for a specific Mach number and a spin angle. The stability

derivatives found for the pitch motion of the missile are then used as the yaw motion stability derivatives by regarding the rotational symmetry of the missile. In the computer simulations, the current value of the stability derivatives are taken from the look-up tables depending on the current values of M_∞ and ϕ_s .

2.3. Missile Transfer Functions

In order to design the roll, pitch and yaw autopilots, the transfer functions between the selected inputs and are needed. These transfer functions are naturally based on a linearized model of the missile. Since the flight of the missile after the boost is accounted, the thrust force and thrust misalignment moment effects on the missile will vanish. That is, $X_T = Y_T = Z_T = L_T = M_T = N_T = 0$. Also, the gravity can be taken as an external disturbance on the missile, i.e., g_x , g_y and g_z can be left without compensation. Hence, the equations of motion of the missile given in equations (2.103) through (2.109) turn into the following forms:

$$\dot{u} - r v + q w = \frac{X}{m} \quad (2.144)$$

$$\dot{v} + r u - p w = \frac{Y}{m} \quad (2.145)$$

$$\dot{w} - q u + p v = \frac{Z}{m} \quad (2.146)$$

$$\dot{p} = \frac{1}{I_{a1}} (L_1 + b_t \dot{\phi}_s) \quad (2.147)$$

$$\dot{p}_2 = \frac{1}{I_{a2}} (L_2 - b_t \dot{\phi}_s) \quad (2.148)$$

$$\dot{q} - p r (1 - \mu_1) + p_2 r \gamma_2 = \frac{M}{I_t} \quad (2.149)$$

$$\dot{r} + p q (1 - \mu_1) - p_2 q \gamma_2 = \frac{N}{I_t} \quad (2.150)$$

2.3.1 Roll Dynamics

The roll dynamics of the missile is described by equations (2.147) and (2.148). Substituting equations (2.115) and (2.139) into equations (2.147) and (2.148), the roll dynamics of the missile can be expressed in a handy form as follows:

$$\dot{p} = \frac{1}{I_{a1}} [C_{\delta 1} \delta_a + (C_{p1} - b_t) p + b_t p_2] \quad (2.151)$$

$$\dot{p}_2 = \frac{1}{I_{a2}} [C_{\delta 2} \delta_a + (C_{p2} - b_t) p_2 + b_t p] \quad (2.152)$$

where $C_{\delta 1} = q_\infty S_M d_M C_{l\delta}$, $C_{p1} = \frac{q_\infty S_M d_M^2}{2 v_M} C_{lp}$, $C_{\delta 2} = q_\infty S_M d_M C_{l\delta 2}$ and

$$C_{p2} = \frac{q_\infty S_M d_M^2}{2 v_M} C_{lp2}.$$

For the missile model considered, the fins on body 2, which constitute the tail fins of the entire missile, are uncontrolled, i.e., they remain at a fixed orientation. If the tail fins of the missile are in a canted configuration, i.e., if they are fixed at an orientation different from zero, then body 2 will have a rotation at a rate that depends on the amount of the cant angle, i.e., the fixed orientation angle, of the tail fins during the flight of the missile after the boost. On the contrary, in the zero cant angle configuration, the rotation of body 2 will be damped in a short while

after the boost. Since the rotation of the tail fins can not be manipulated, body 2 becomes uncontrolled during the flight. However, due to the aerodynamic interaction and the bearing coupling between the bodies, the rotation of body 2 will influence the roll motion of body 1. That is, the roll motion of body 2 will act as an external disturbance on body 1. Thus, in the roll autopilot design, the roll rate of body 2 can be accounted as a disturbance upon the roll dynamics of body 1. In this case, regarding the roll attitude of the missile as well, the roll dynamics that is to be controlled can be expressed by the following equations:

$$\dot{\phi}_1 = p \quad (2.153)$$

$$\dot{p} = L_{\delta} \delta_a + L_{p1} p + L_{p2} p_2 \quad (2.154)$$

where $L_{\delta} = \frac{C_{\delta l}}{I_{a1}}$, $L_{p1} = \frac{C_{p1} - b_t}{I_{a1}}$ and $L_{p2} = \frac{b_t}{I_{a1}}$.

Taking the Laplace transforms of equations (2.153) and (2.154), and making the necessary arrangements, the transfer function from δ_a to ϕ_1 is obtained in the following manner:

$$\frac{\phi_1(s)}{\delta_a(s)} = \frac{L_{\delta}}{s(s - L_{p1})} \quad (2.155)$$

2.3.2 Pitch Dynamics

Assuming that the roll motion of body 1 is compensated by the roll autopilot which is at least three times faster than the yaw and pitch autopilots, i.e., $\phi_1 = p \cong 0$, and regarding the roll rate of body 2 (p_2) as an external disturbance, equations (2.146) and (2.149) that describe the motion of the missile on its pitch plane can be simplified into the following equations:

$$\dot{w} - q u = \frac{Z}{m} \quad (2.156)$$

$$\dot{q} = \frac{M}{I_t} \quad (2.157)$$

Also, since the pitch plane motion of the missile is of concern, equation (2.10) reduces to

$$\dot{\theta}_1 = q \quad (2.158)$$

From equation (2.129), the following relationship can be written between w and α :

$$w \cong u \alpha \quad (2.159)$$

Since the velocity components v and w are much smaller than u , u can be taken to be nearly equal to v_M . Regarding the flight of the missile after the boost, the changes in v_M can be neglected. Hence, u can be assumed to be constant in time. With this assumption, taking the time derivative of equation (2.159) yields the following expression in the acceleration level:

$$\dot{w} \cong u \dot{\alpha} \quad (2.160)$$

Then, plugging equations (2.138), (2.140) and (2.160) into equations (2.156) and (2.157) and making the necessary arrangements, the following equations are obtained to identify the pitch dynamics of the missile:

$$\dot{\alpha} = \frac{Z_\alpha}{u} \alpha + \left(\frac{Z_q}{u} + 1 \right) q + \frac{Z_\delta}{u} \delta_e \quad (2.161)$$

$$\dot{q} = M_\alpha \alpha + M_q q + M_\delta \delta_e \quad (2.162)$$

where

$$Z_\alpha = \frac{q_\infty S_M}{m} C_{z_\alpha}, \quad Z_\delta = \frac{q_\infty S_M}{m} C_{z_\delta}, \quad Z_q = \frac{q_\infty S_M d_M}{2 m v_M} C_{z_q}, \quad M_\alpha = \frac{q_\infty S_M d_M}{I'_t} C_{m_\alpha},$$

$$M_\delta = \frac{q_\infty S_M d_M}{I'_t} C_{m_\delta} \quad \text{and} \quad M_q = \frac{q_\infty S_M d_M^2}{2 I'_t v_M} C_{m_q}.$$

Taking the Laplace transform of equations (2.161) and (2.162) and making the necessary arrangements, the transfer functions from δ_e to α and from δ_e to q are found as

$$G_{\alpha\delta}(s) = \frac{\alpha(s)}{\delta_e(s)} = \frac{n_{\alpha 1} s + n_{\alpha 0}}{s^2 + d_{p1} s + d_{p0}} \quad (2.163)$$

$$G_{q\delta}(s) = \frac{q(s)}{\delta_e(s)} = \frac{n_{q1} s + n_{q0}}{s^2 + d_{p1} s + d_{p0}} \quad (2.164)$$

where

$$d_{p0} = \frac{Z_\alpha}{u} M_q - \left(\frac{Z_q}{u} + 1 \right) M_\alpha, \quad d_{p1} = - \left(\frac{Z_\alpha}{u} + M_q \right), \quad n_{\alpha 0} = \left(\frac{Z_q}{u} + 1 \right) M_\delta - \frac{Z_\delta}{u} M_q$$

$$n_{\alpha 1} = \frac{Z_\delta}{u}, \quad n_{q0} = \frac{1}{u} (Z_\delta M_\alpha - Z_\alpha M_\delta) \quad \text{and} \quad n_{q1} = M_\delta.$$

As a general convention, α is defined as the difference of the pitch attitude (θ_1) from the pitch plane component of the missile flight path angle (γ_m) as

$$\alpha = \theta_1 - \gamma_m \quad (2.165)$$

Applying the Laplace transform to equation (2.165) and dividing the resulting expression by δ_e , the transfer function from δ_e to $\dot{\gamma}_m$ can be obtained as

$$G_{\dot{\gamma}\delta}(s) = \frac{\dot{\gamma}_m(s)}{\delta_e(s)} = \frac{-n_{\alpha 1} s^2 + n_{\alpha q} s + n_{q0}}{s^2 + d_{p1} s + d_{p0}} \quad (2.166)$$

where $n_{\alpha q} = n_{q1} - n_{\alpha 0}$.

Furthermore, the transfer function from δ_e to γ_m can also be obtained by dividing the transfer function in equation (2.166) by the Laplace operator “s” as

$$G_{\gamma\delta}(s) = \frac{\gamma_m(s)}{\delta_e(s)} = \frac{-n_{\alpha 1} s^2 + n_{\alpha q} s + n_{q0}}{s(s^2 + d_{p1} s + d_{p0})} \quad (2.167)$$

In the case that the pitch motion of the missile is to be controlled via an acceleration autopilot, the relationship between the elevator deflection (δ_e) and the lateral acceleration component in the pitch plane (a_z) should be known. In fact, a_z can be written in terms of the angular and linear velocity components of the missile as follows:

$$a_z = \dot{w} - q u + p v \quad (2.168)$$

With the assumption that p is kept small by the roll autopilot, equation (2.168) shrinks into the following form:

$$a_z = \dot{w} - q u \quad (2.169)$$

Then, inserting equation (2.160) into equation (2.169), taking the Laplace transform of the resulting equation and dividing it by δ_e , the transfer function from δ_e to a_z happens to be

$$G_{a\delta}(s) = \frac{a_z(s)}{\delta_e(s)} = \frac{n_{z2}s^2 + n_{z1}s + n_{z0}}{s^2 + d_{p1}s + d_{p0}} \quad (2.170)$$

where $n_{z0} = Z_\alpha M_\delta - Z_\delta M_\alpha$, $n_{z1} = Z_q M_\delta - Z_\delta M_q$ and $n_{z2} = Z_\delta$.

2.3.3 Yaw Dynamics

Since the considered missile has rotational symmetry, the equations for the yaw dynamics can be derived in a manner similar to the pitch dynamics. Thus, using the same assumptions held for the pitch dynamics, the differential equations describing the yaw motion of the missile can be written from equations (2.104) and (2.109) in the following manner.

$$\dot{v} + r u = \frac{Y}{m} \quad (2.171)$$

$$\dot{r} = \frac{N}{I_t} \quad (2.172)$$

Regarding the yaw plane motion of the missile, equation (2.9) simplifies as

$$\dot{\psi} = \frac{r}{\cos(\theta_1)} \quad (2.173)$$

From equation (2.130), the following relationship can be written between v and β :

$$v \cong u \beta \quad (2.174)$$

Neglecting the change of u in time and taking the time derivative of equation (2.174), the following expression is obtained in acceleration level:

$$\dot{v} \cong u \dot{\beta} \quad (2.175)$$

Then, plugging equations (2.137), (2.141) and (2.175) into equations (2.171) and (2.172) and making the necessary arrangements, the following equations are obtained to identify the yaw dynamics of the missile:

$$\dot{\beta} = \frac{Y_{\beta}}{u} \beta + \left(\frac{Y_r}{u} - 1 \right) r + \frac{Y_{\delta}}{u} \delta_r \quad (2.176)$$

$$\dot{r} = N_{\beta} \beta + N_r r + N_{\delta} \delta_r \quad (2.177)$$

where

$$Y_{\beta} = \frac{q_{\infty} S_M}{m} C_{y_{\beta}}, \quad Y_{\delta} = \frac{q_{\infty} S_M}{m} C_{y_{\delta}}, \quad Y_r = \frac{q_{\infty} S_M d_M}{2 m v_M} C_{y_r}, \quad N_{\beta} = \frac{q_{\infty} S_M d_M}{I_t'} C_{n_{\beta}},$$

$$N_{\delta} = \frac{q_{\infty} S_M d_M}{I_t'} C_{n_{\delta}} \quad \text{and} \quad N_r = \frac{q_{\infty} S_M d_M^2}{2 I_t' v_M} C_{n_r}.$$

Taking the Laplace transform of equations (2.176) and (2.177) and making the necessary arrangements, the transfer functions from δ_r to β and from δ_r to r are found as

$$G_{\beta\delta}(s) = \frac{\beta(s)}{\delta_r(s)} = \frac{n_{\beta 1} s + n_{\beta 0}}{s^2 + d_{y1} s + d_{y0}} \quad (2.178)$$

$$G_{r\delta}(s) = \frac{r(s)}{\delta_r(s)} = \frac{n_{r1} s + n_{r0}}{s^2 + d_{y1} s + d_{y0}} \quad (2.179)$$

where

$$d_{y0} = \frac{Y_\beta}{u} N_r - \left(\frac{Y_r}{u} - 1 \right) N_\beta, d_{y1} = - \left(\frac{Y_\beta}{u} + N_r \right), n_{\beta 0} = \left(\frac{Y_r}{u} - 1 \right) N_\delta - \frac{Y_\delta}{u} N_r$$

$$n_{\beta 1} = \frac{Y_\delta}{u}, n_{r0} = \frac{1}{u} (Y_\delta N_\beta - Y_\beta N_\delta) \text{ and } n_{r1} = N_\delta.$$

The lateral acceleration component in the yaw plane can be written in terms of the angular and linear velocity components of the missile as follows:

$$a_y = \dot{v} + r u - p w \quad (2.180)$$

With the assumption that p is kept small by the roll autopilot, equation (2.180) takes the following form:

$$a_y = \dot{v} + r u \quad (2.181)$$

Substituting equation (2.175) into equation (2.181), taking the Laplace transform of the resulting equation and dividing it by δ_r , the transfer function from δ_r to a_y happens to be

$$G_{a\delta}(s) = \frac{a_y(s)}{\delta_r(s)} = \frac{n_{y2} s^2 + n_{y1} s + n_{y0}}{s^2 + d_{y1} s + d_{y0}} \quad (2.182)$$

where $n_{y0} = Y_\delta N_\beta - Y_\beta N_\delta$, $n_{y1} = Y_r N_\delta + Y_\delta N_r$ and $n_{y2} = Y_\delta$

The transfer functions from δ_r to the yaw plane components of the missile flight path angle and its rate can be derived in the same manner as done for the pitch dynamics.

2.4. Control Actuation System Modeling

In a missile control system, a control actuation system (CAS) is used to convert the command signals for the desired fin deflections into realizable mechanical responses in order to deflect the fins so as to steer the missile towards the target.

In this study, electro-mechanical type actuators are selected to drive the control fins. In this structure, the output shaft of a servomotor type actuator is connected to the fin to be controlled through a coupling. During the motion of the missile under control, the actuator operates against the inertia and friction loads arising from the rotation of the rotor portion of the servomotor and the inertia loads of the gearbox and the fin. Also, due to aerodynamic force components acting on the center of pressure of the fin, each fin is subjected to a hinge moment effect. Thus, the equation of motion of the servomotor can be written as follows:

$$J_e \ddot{\delta}_m + B_m \dot{\delta}_m + T'_{HM} = T_m \quad (2.183)$$

where, for the servomotor, the following definitions are made:

δ_m : Angular deflection of the output shaft

J_e : Equivalent moment of inertia

B_m : Viscous damping coefficient of the rotor

T'_{HM} : Hinge moment reduced on the output shaft

T_m : Generated torque

In equation (2.183), J_e is defined as follows:

$$J_e = J_m + \frac{J_f}{N^2} \quad (2.184)$$

where

J_m : Moment of inertia of the rotor of the servomotor

J_f : Moment of inertia of the fin

N : Gearbox reduction ratio ($N \geq 1$)

Since T_{HM} is defined on the shaft between the gearbox and fin, it can be moved onto the servomotor output shaft that lies between the servomotor and gearbox in the following manner:

$$T'_{HM} = \frac{T_{HM}}{N} \quad (2.185)$$

The hinge moment (T_{HM}) is a moment proportional to the angular deflection of the fin. As δ_f and K_{HM} stand for the angular deflection of the fin and hinge moment ratio, T_{HM} can be formulated as

$$T_{HM} = K_{HM} \delta_f \quad (2.186)$$

The command signals to the CAS are sent in the form of electrical voltages by the autopilot. As the letters A and B denote the input and output ports of the CAS, the following equation holds between the voltages at points A and B (V_A and V_B):

$$V_B = V_A - R_A i \quad (2.187)$$

where R_A and i represent the effective resistance of the circuit between points A and B, and the electrical flow from point A to point B.

Also, the following relationships can be written between $\dot{\delta}_m$ and V_B , and between T_m and i :

$$\dot{\delta}_m = \frac{V_B}{K_b} \quad (2.188)$$

$$T_m = K_T i \quad (2.189)$$

In the above equations, K_b and K_T are called as the DC motor constant and the DC motor torque constant and actually they are equal to each other in values, i.e., $K_b = K_T$.

Substituting equations (2.188) and (2.189) into equation (2.187) and making the necessary arrangements, the expression giving T_m is found as follows:

$$T_m = \left(\frac{K_T}{R_A} \right) V_A - \left(\frac{K_T K_b}{R_A} \right) \dot{\delta}_m \quad (2.190)$$

Inserting equation (2.190) into equation (2.183), the following equation comes into the picture:

$$J_e \ddot{\delta}_m + B_e \dot{\delta}_m = \left(\frac{K_T}{R_A} \right) V_A - T'_{HM} \quad (2.191)$$

where $B_e = B_m + \frac{K_T K_b}{R_A}$.

Equation (2.191) can be expressed in Laplace domain as

$$\left(J_e s^2 + B_e\right) \dot{\delta}_m(s) = \left(\frac{K_T}{R_A}\right) V_A(s) - T'_{HM}(s) \quad (2.192)$$

Having determined the relationship among V_A , T'_{HM} and $\dot{\delta}_m$ as in equation (2.192), the CAS can be constructed in order to obey the commanded fin deflection signals sent by the autopilot. Regarding an integrator part to nullify the steady-state error in the fin deflection, a PID (proportional plus integral plus derivative) type controller with the proportional gain K , the integral time constant T_i and the derivative time constant T_d can be utilized. Thus, the resulting type 1 control system can be built as in Figure 2.4.

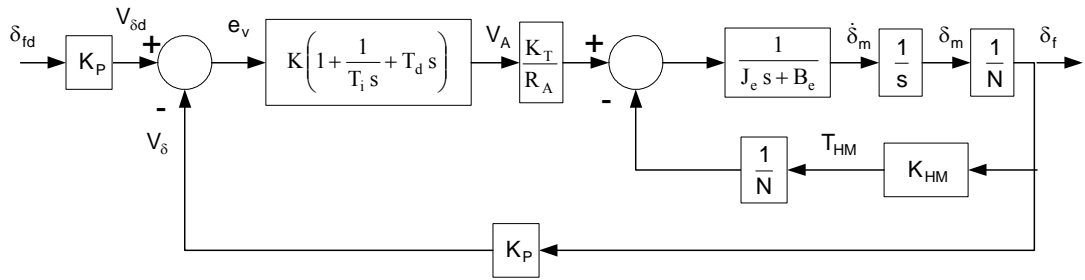


Figure 2.4. Control Actuation System Block Diagram

Using the block diagram algebra, as δ_{fd} denotes the desired fin deflection, the closed loop transfer function of the CAS can be obtained from Figure 2.4 as follows:

$$\frac{\delta_f(s)}{\delta_{fd}(s)} = \frac{n_2 s^2 + n_1 s + 1}{d_3 s^3 + d_2 s^2 + d_1 s + 1} \quad (2.193)$$

where $n_1 = T_i$, $n_2 = T_i T_d$, $d_1 = T_i \left(\frac{K_{HM} R_A}{N K_T K_p K} + 1 \right)$, $d_2 = T_i \left(\frac{N R_A B_e}{K_T K_p K} + T_d \right)$
and $d_3 = \frac{N R_A T_i J_e}{K_T K_p K}$.

The controller parameters K , T_i and T_d can be determined by applying the pole placement technique to the control system. Before the placement of poles as desired, the characteristic polynomial of the control system can be picked from equation (2.193) as follows:

$$D(s) = d_3 s^3 + d_2 s^2 + d_1 s + 1 \quad (2.194)$$

Since the order of $D(s)$ in equation (2.194) is three which is just equal to the number of controller parameters to be obtained, a third-order polynomial can be used to place the poles to the desired locations. Among several available polynomials, the third-order Butterworth polynomial $[B_3(s)]$ can be selected as [Appendix]:

$$B_3(s) = \left(\frac{1}{\omega_c^3} \right) s^3 + \left(\frac{2}{\omega_c^2} \right) s^2 + \left(\frac{2}{\omega_c} \right) s + 1 \quad (2.195)$$

where ω_c stands for the desired bandwidth the control systems is expected to satisfy.

Equating equations (2.194) and (2.195) term by term, the controller gains can be obtained as

$$K = K_{HM} \left(2 N J_e \omega_c^2 - \frac{K_{HM}}{N} \right) \quad (2.196)$$

$$T_i = \frac{1}{\omega_c} \left(2 - \frac{K_{HM}}{N^2 J_e \omega_c^2} \right) \quad (2.197)$$

$$T_d = \frac{2 J_e \omega_c - B_e}{2 J_e \omega_c^2 - \frac{K_{HM}}{N^2}} \quad (2.198)$$

2.5. Measuring Instruments Models

Both guidance and control units require information about the motion of the missile. The guidance unit requires this information for generating the commanded motion and the control unit requires this information for its feedback control law. The mentioned information is provided by the navigational measurement instruments such as gyroscopes and accelerometers [7]. In this scheme, gyroscopes and accelerometers measure the angular rates and the linear acceleration components of the missile. In this study, they are modeled as second order systems with the following transfer function:

$$G(s) = \frac{\omega_n^2}{s^2 + 2\zeta\omega_n s + \omega_n^2} \quad (2.199)$$

where ω_n and ζ stand for the undamped natural frequency and the damping ratio.

In the gyroscope model, the non-g sensitive drift, the g-sensitive drift and the noise (as random noise) are modeled as the typical error sources. Also, the bias and the noise are imparted to the accelerometer model as the error sources.

2.6. Wind Model

The atmospheric winds acting on the missile create an aerodynamic disturbance on the missile causing it to deviate from its nominal trajectory.

Therefore, it is necessary to model this effect for the computer simulations. Denoting the components of the wind in the Earth-fixed frame coordinates x, y and z represented by the unit vectors $\bar{u}_1^{(0)}$, $\bar{u}_2^{(0)}$ and $\bar{u}_3^{(0)}$ as v_{wx} , v_{wy} and v_{wz} , respectively, they can be transformed into F_b as follows [7]:

$$\begin{bmatrix} u_w \\ v_w \\ w_w \end{bmatrix} = \hat{C}^{(b,o)} \begin{bmatrix} v_{wx} \\ v_{wy} \\ v_{wz} \end{bmatrix} \quad (2.200)$$

where, regarding $\hat{C}^{(b,0)} = [\hat{C}^{(0,b)}]^T$,

$$\hat{C}^{(0,b)} = \begin{bmatrix} c_{11} & c_{12} & c_{13} \\ c_{21} & c_{22} & c_{23} \\ c_{31} & c_{32} & c_{33} \end{bmatrix}$$

$$c_{11} = \cos(\psi_1) \cos(\theta_1)$$

$$c_{12} = \cos(\psi_1) \sin(\theta_1) \sin(\phi_1) - \sin(\psi_1) \cos(\phi_1)$$

$$c_{13} = \cos(\psi_1) \sin(\theta_1) \cos(\phi_1) + \sin(\psi_1) \sin(\phi_1)$$

$$c_{21} = \sin(\psi_1) \cos(\theta_1)$$

$$c_{22} = \sin(\psi_1) \sin(\theta_1) \sin(\phi_1) + \cos(\psi_1) \cos(\phi_1)$$

$$c_{23} = \sin(\psi_1) \sin(\theta_1) \cos(\phi_1) - \cos(\psi_1) \sin(\phi_1)$$

$$c_{31} = -\sin(\theta_1)$$

$$c_{32} = \cos(\theta_1) \sin(\phi_1)$$

$$c_{33} = \cos(\theta_1) \cos(\phi_1)$$

Taking into account the effect of the wind, the resultant velocity components of the missile appear as follows:

$$u_R = u - u_w \quad (2.201)$$

$$v_R = v - v_w \quad (2.202)$$

$$w_R = w - w_w \quad (2.203)$$

CHAPTER 3

MISSILE GUIDANCE

In this chapter, the guidance methods implemented in the computer simulations of this study are explained. Also, the kinematic parameters that should be computed for the missile-target engagement scenario are derived.

3.1. Considered Guidance Methods

In this study, the Proportional Navigation Guidance (PNG) law is utilized as well as the Linear Homing Guidance (LHG) and the Parabolic Homing Guidance (PHG) laws. Although the PNG law is the most commonly used algorithm in the guidance field, the LHG and PHG concepts are developed as alternatives.

3.1.1. Proportional Navigation Guidance Law

The PNG law is the most popular guidance law that has been applied for over fifty years. Actually, its popularity comes from its effectiveness and ease of implementation. Originally, the PNG law issues angular rate commands or acceleration commands perpendicular to the instantaneous missile-target line-of-sight (LOS). However, considering the acceleration commands, when these commands are transformed into the missile reference frame (F_b), they yield an axial component as well as transversal components. Due to the lack of a controllable

thrust, the axial acceleration requirement can not be met. For this reason, it becomes quite useful to generate the command accelerations perpendicular to the missile velocity vector instead of the LOS. In the literature, the former type of the PNG is termed as the True Proportional Navigation Guidance while the latter one is defined as the Pure Proportional Navigation Guidance.

3.1.1.1. Spatial Derivation of the Proportional Navigation Guidance Law

In the guidance studies, the missile-target engagement problem is in general dealt with in the pitch plane. Thus, the guidance laws are formulated for the planar intercept geometry. On the other hand, the spatial formulations of the guidance laws are also done. One of them is the three dimensional PNG law. However, in almost all of these derivations, the guidance commands are generated in the line-of-sight (LOS) frame. Hence, when they are transformed into the wind frame, the resulting expressions become quite complex [9], [18], [35], [36], [37].

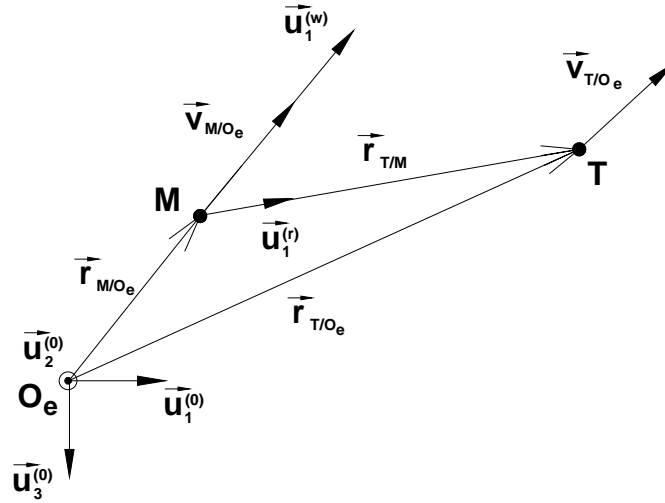


Figure 3.1. Missile-Target Engagement Geometry

As shown in Figure 3.1, the missile velocity vector (\vec{v}_{M/O_e}) is arranged to be along the first axis of the wind frame (F_w) whose direction is shown by the unit

vector $\vec{u}_1^{(w)}$. Moreover, the LOS vector ($\vec{r}_{T/M}$) is aligned with the unit vector of the LOS frame (F_r) whose direction is shown by the unit vector $\vec{u}_1^{(r)}$. That is, \vec{v}_{M/O_e} and $\vec{r}_{T/M}$ can be written as

$$\vec{v}_{M/O_e} = v_M \vec{u}_1^{(w)} \quad (3.1)$$

$$\vec{r}_{T/M} = r_{T/M} \vec{u}_1^{(r)} \quad (3.2)$$

where O_e denotes the origin of the Earth-fixed frame (F_0).

Here, F_w and F_r that are both right-handed and orthogonal can be formed by the following rotation sequences:

$$\begin{array}{cccc} \vec{u}_3^{(0)} & \vec{u}_2^{(a)} & \vec{u}_1^{(c)} & \\ F_0 \rightarrow F_a \rightarrow F_c \rightarrow F_w & & & \\ \eta_m & \gamma_m & \rho_m & \end{array}$$

$$\begin{array}{ccc} \vec{u}_3^{(0)} & \vec{u}_2^{(d)} & \\ F_0 \rightarrow F_d \rightarrow F_r & & \\ \lambda_y & \lambda_p & \end{array}$$

In the first sequence given above, η_m and γ_m denote the flight path angles of the missile that describe the orientation of \vec{v}_{M/O_e} with respect to the F_0 . Here, ρ_m stands for the roll angle of F_w . In the second sequence, λ_y and λ_p stand for the yaw and pitch angles of the LOS. F_a , F_c and F_d show the intermediate reference frames.

Regarding these sequences, the overall rotation matrix from F_θ to F_w can be written as

$$\hat{C}^{(0,w)} = \hat{C}^{(0,a)} \hat{C}^{(a,c)} \hat{C}^{(c,w)} = \hat{R}_3(\eta_m) \hat{R}_2(\gamma_m) \hat{R}_1(\rho_m) \quad (3.3)$$

Writing the third, second and first basic rotation matrices in equation (3.3) explicitly and multiplying them in the indicated order, $\hat{C}^{(0,w)}$ is obtained as

$$\hat{C}^{(0,w)} = \begin{bmatrix} c_{w11} & c_{w12} & c_{w13} \\ c_{w21} & c_{w22} & c_{w23} \\ c_{w31} & c_{w32} & c_{w33} \end{bmatrix} \quad (3.4)$$

where

$$c_{w11} = \cos(\eta_m) \cos(\gamma_m)$$

$$c_{w12} = \cos(\eta_m) \sin(\gamma_m) \sin(\rho_m) - \sin(\eta_m) \cos(\rho_m)$$

$$c_{w13} = \cos(\eta_m) \sin(\gamma_m) \cos(\rho_m) + \sin(\eta_m) \sin(\rho_m)$$

$$c_{w21} = \sin(\eta_m) \cos(\gamma_m)$$

$$c_{w22} = \sin(\eta_m) \sin(\gamma_m) \sin(\rho_m) + \cos(\eta_m) \cos(\rho_m)$$

$$c_{w23} = \sin(\eta_m) \sin(\gamma_m) \cos(\rho_m) - \cos(\eta_m) \sin(\rho_m)$$

$$c_{w31} = -\sin(\gamma_m)$$

$$c_{w32} = \cos(\gamma_m) \sin(\rho_m)$$

$$c_{w33} = \cos(\gamma_m) \cos(\rho_m)$$

Similarly, the overall rotation matrix from F_θ to F_r can be expressed as

$$\hat{C}^{(0,r)} = \hat{C}^{(0,d)} \hat{C}^{(d,r)} = \hat{R}_3(\lambda_y) \hat{R}_2(\lambda_p) \quad (3.5)$$

Again writing the third and second basic rotation matrices in equation (3.5) explicitly and working out their product, $\hat{C}^{(0,r)}$ is obtained as

$$\hat{C}^{(0,r)} = \begin{bmatrix} \cos(\lambda_y) \cos(\lambda_p) & -\sin(\lambda_y) & \cos(\lambda_y) \sin(\lambda_p) \\ \sin(\lambda_y) \cos(\lambda_p) & \cos(\lambda_y) & \sin(\lambda_y) \sin(\lambda_p) \\ -\sin(\lambda_p) & 0 & \cos(\lambda_p) \end{bmatrix} \quad (3.6)$$

After these preparations, the PNG law can be formulated so as to supply the commanded acceleration vector (\vec{a}_c) in the following manner:

$$\vec{a}_c = \check{N} \cdot \vec{\omega}_{r/0} \times \vec{v}_c \quad (3.7)$$

In equation (3.7), \check{N} , $\vec{\omega}_{r/0}$, and \vec{v}_c represent the effective navigation ratio dyadic, the LOS angular velocity vector and the missile-target closing velocity vector, respectively. Among them, \check{N} can be expressed as

$$\check{N} = N_2 \vec{u}_2^{(w)} \vec{u}_2^{(w)} + N_3 \vec{u}_3^{(w)} \vec{u}_3^{(w)} \quad (3.8)$$

where N_i is the effective navigation ratio associated with the $\vec{u}_i^{(w)}$ direction ($i=2$ and 3). In order to ensure good dynamic performance, values such as $N_i=3, 4$ or 5 happen to be quite satisfactory [5].

The angular velocity vector of the LOS frame ($\vec{\omega}_{r/0}$) can be written with respect to the rotation sequence from F_θ to F_r as follows:

$$\vec{\omega}_{r/0} = \dot{\lambda}_y \vec{u}_3^{(0)} + \dot{\lambda}_p \vec{u}_2^{(d)} \quad (3.9)$$

Noting that $\vec{u}_2^{(d)} = \vec{u}_2^{(r)}$, equation (3.9) can be expressed in F_r as

$$\vec{\omega}_{r/0}^{(r)} = \dot{\lambda}_y \vec{u}_3^{(0/r)} + \dot{\lambda}_p \vec{u}_2 \quad (3.10)$$

Equation (3.10) can be rewritten as follows:

$$\vec{\omega}_{r/0}^{(r)} = \dot{\lambda}_y \hat{C}^{(r,0)} \vec{u}_3 + \dot{\lambda}_p \vec{u}_2 \quad (3.11)$$

where $\vec{u}_2 = [0 \ 1 \ 0]^T$ and $\vec{u}_3 = [0 \ 0 \ 1]^T$.

Noting also that $\hat{C}^{(r,0)} = [\hat{C}^{(0,r)}]^{-1} = [\hat{C}^{(0,r)}]^T$, equation (3.11) becomes

$$\vec{\omega}_{r/0}^{(r)} = \dot{\lambda}_y [\hat{C}^{(0,r)}]^T \vec{u}_3 + \dot{\lambda}_p \vec{u}_2 \quad (3.12)$$

Substituting equation (3.6) into equation (3.12) and making the necessary arrangements, equation (3.12) turns into the following form:

$$\vec{\omega}_{r/0}^{(r)} = \omega_{r1}^r \vec{u}_1 + \omega_{r2}^r \vec{u}_2 + \omega_{r3}^r \vec{u}_3 \quad (3.13)$$

where $\omega_{r1}^r = -\dot{\lambda}_y \sin(\lambda_p)$, $\omega_{r2}^r = \dot{\lambda}_p$ and $\omega_{r3}^r = \dot{\lambda}_y \cos(\lambda_p)$.

From equation (3.13), $\vec{\omega}_{r/0}$ can be expressed with the unit vectors of F_r as

$$\vec{\omega}_{r/0} = \omega_{r1}^r \vec{u}_1^{(r)} + \omega_{r2}^r \vec{u}_2^{(r)} + \omega_{r3}^r \vec{u}_3^{(r)} \quad (3.14)$$

Alternatively, the representation of $\bar{\omega}_{r/0}$ in F_w can be obtained by pre-multiplying the column $\bar{\omega}_{r/0}^{(r)}$ in equation (3.13) by $\hat{C}^{(w,r)}$. That is,

$$\bar{\omega}_{r/0}^{(w)} = \hat{C}^{(w,r)} \bar{\omega}_{r/0}^{(r)} \quad (3.15)$$

In equation (3.15), $\hat{C}^{(w,r)}$ can be composed as

$$\hat{C}^{(w,r)} = \hat{C}^{(w,0)} \hat{C}^{(0,r)} \quad (3.16)$$

Using the property that $\hat{C}^{(w,0)} = [\hat{C}^{(0,w)}]^{-1} = [\hat{C}^{(0,w)}]^T$, equation (3.16) can also be written as

$$\hat{C}^{(w,r)} = [\hat{C}^{(0,w)}]^T \hat{C}^{(0,r)} \quad (3.17)$$

Substituting equations (3.4) and (3.6) into equation (3.17), and carrying out the necessary matrix operations, $\hat{C}^{(w,r)}$ can be expressed as follows:

$$\hat{C}^{(w,r)} = \begin{bmatrix} c_{\omega 11} & c_{\omega 12} & c_{\omega 13} \\ c_{\omega 21} & c_{\omega 22} & c_{\omega 23} \\ c_{\omega 31} & c_{\omega 32} & c_{\omega 33} \end{bmatrix} \quad (3.18)$$

where

$$c_{\omega 11} = \cos(\gamma_m) \cos(\lambda_p) \cos(\lambda_y - \eta_m) + \sin(\gamma_m) \sin(\lambda_p)$$

$$c_{\omega 12} = -\cos(\gamma_m) \sin(\lambda_y - \eta_m)$$

$$c_{\omega 13} = \cos(\gamma_m) \sin(\lambda_p) \cos(\lambda_y - \eta_m) - \sin(\gamma_m) \cos(\lambda_p)$$

$$c_{\omega 21} = \cos(\rho_m) \cos(\lambda_p) \sin(\lambda_y - \eta_m) + \sin(\gamma_m) \sin(\rho_m) \cos(\lambda_p) \cos(\lambda_y - \eta_m) \\ - \cos(\gamma_m) \sin(\rho_m) \sin(\lambda_p)$$

$$c_{\omega 22} = \cos(\rho_m) \cos(\lambda_y - \eta_m) - \sin(\gamma_m) \sin(\rho_m) \sin(\lambda_y - \eta_m)$$

$$c_{\omega 23} = \cos(\rho_m) \sin(\lambda_p) \sin(\lambda_y - \eta_m) + \sin(\gamma_m) \sin(\rho_m) \sin(\lambda_p) \cos(\lambda_y - \eta_m) \\ + \cos(\gamma_m) \sin(\rho_m) \cos(\lambda_p)$$

$$c_{\omega 31} = -\sin(\rho_m) \cos(\lambda_p) \sin(\lambda_y - \eta_m) + \sin(\gamma_m) \cos(\rho_m) \cos(\lambda_p) \cos(\lambda_y - \eta_m) \\ - \cos(\gamma_m) \cos(\rho_m) \sin(\lambda_p)$$

$$c_{\omega 32} = -\sin(\rho_m) \cos(\lambda_y - \eta_m) - \sin(\gamma_m) \cos(\rho_m) \sin(\lambda_y - \eta_m)$$

$$c_{\omega 33} = -\sin(\rho_m) \sin(\lambda_p) \sin(\lambda_y - \eta_m) + \sin(\gamma_m) \cos(\rho_m) \sin(\lambda_p) \cos(\lambda_y - \eta_m) \\ + \cos(\gamma_m) \cos(\rho_m) \cos(\lambda_p)$$

Inserting equation (3.18) into equation (3.15), the expression of $\vec{\omega}_{r/0}$ in F_w becomes

$$\vec{\omega}_{r/0}^{(w)} = \omega_{r1}^w \bar{u}_1 + \omega_{r2}^w \bar{u}_2 + \omega_{r3}^w \bar{u}_3 \quad (3.19)$$

where

$$\omega_{r1}^w = c_{\omega 11} \omega_{r1}^r + c_{\omega 12} \omega_{r2}^r + c_{\omega 13} \omega_{r3}^r$$

$$\omega_{r2}^w = c_{\omega 21} \omega_{r1}^r + c_{\omega 22} \omega_{r2}^r + c_{\omega 23} \omega_{r3}^r$$

$$\omega_{r3}^w = c_{\omega 31} \omega_{r1}^r + c_{\omega 32} \omega_{r2}^r + c_{\omega 33} \omega_{r3}^r$$

From equation (3.19), $\vec{\omega}_{r/0}$ can be expressed with the unit vectors of F_w as

$$\vec{\omega}_{r/0} = \omega_{r1}^w \bar{u}_1^{(w)} + \omega_{r2}^w \bar{u}_2^{(w)} + \omega_{r3}^w \bar{u}_3^{(w)} \quad (3.20)$$

The closing velocity vector (\vec{v}_c) between the missile and the target is defined as the difference between the missile and target velocity vectors (\vec{v}_{M/O_e} and \vec{v}_{T/O_e}). That is,

$$\vec{v}_c = \vec{v}_{M/T} = \vec{v}_{M/O_e} - \vec{v}_{T/O_e} \quad (3.21)$$

Since a surface target is concerned with in this study, the magnitude of \vec{v}_{M/O_e} is much larger than the magnitude of \vec{v}_{T/O_e} . Therefore, \vec{v}_{M/O_e} can be used instead of \vec{v}_c in the PNG implementation. With this approximation, the PNG law given in equation (3.7) takes the following form:

$$\vec{a}_c = \ddot{N} \cdot \vec{\omega}_{r/0} \times \vec{v}_{M/O_e} \quad (3.22)$$

Hence, inserting equations (3.1), (3.8) and (3.20) into equation (3.22), and carrying out the necessary manipulations, the command acceleration vector becomes

$$\vec{a}_c = a_{w1}^c \vec{u}_1^{(w)} + a_{w2}^c \vec{u}_2^{(w)} + a_{w3}^c \vec{u}_3^{(w)} \quad (3.23)$$

where

$$a_{w1}^c = 0$$

$$a_{w2}^c = N_2 v_M \left[\dot{\lambda}_y \cos(\gamma_m) \cos(\rho_m) - \dot{\lambda}_p \sin(\rho_m) \cos(\lambda_y - \eta_m) \right. \\ \left. - \dot{\lambda}_p \sin(\gamma_m) \cos(\rho_m) \sin(\lambda_y - \eta_m) \right]$$

$$a_{w3}^c = -N_3 v_M \left[\dot{\lambda}_y \cos(\gamma_m) \sin(\rho_m) + \dot{\lambda}_p \cos(\rho_m) \cos(\lambda_y - \eta_m) \right. \\ \left. - \dot{\lambda}_p \sin(\gamma_m) \sin(\rho_m) \sin(\lambda_y - \eta_m) \right]$$

As seen from equation (3.23), \vec{a}_c has no components in the direction of \vec{v}_{M/O_e} , i.e., in $\vec{u}_1^{(w)}$ direction.

Assuming $\rho_m = 0$, the command accelerations a_{w2}^c and a_{w3}^c in equation (3.23) turn into the following forms:

$$a_{w2}^c = N_2 v_M [\dot{\lambda}_y \cos(\gamma_m) - \dot{\lambda}_p \sin(\gamma_m) \sin(\lambda_y - \eta_m)] \quad (3.24)$$

$$a_{w3}^c = -N_3 v_M \dot{\lambda}_p \cos(\lambda_y - \eta_m) \quad (3.25)$$

The schematic representations of a_{w2}^c and a_{w3}^c in the horizontal and vertical planes of F_w are as shown in Figure 3.2 and Figure 3.3.

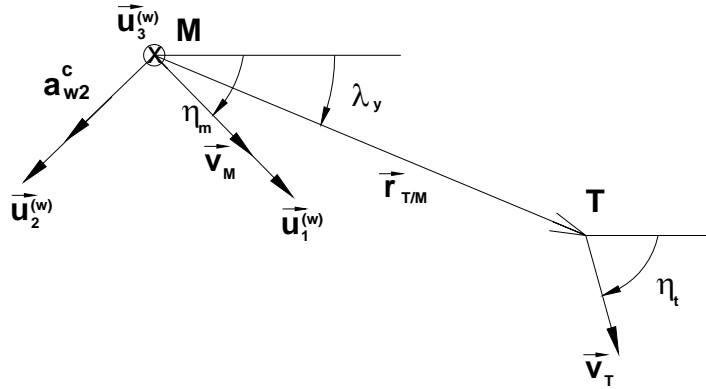


Figure 3.2. Horizontal Plane of the Wind Frame

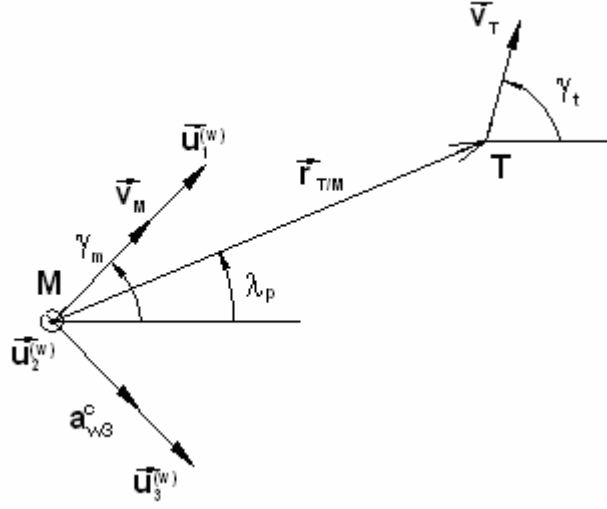


Figure 3.3. Vertical Plane of the Wind Frame

In order to implement the commanded guidance accelerations to the missile control systems as reference signals, it is more suitable to express the measured acceleration components of the missile in F_w . Thus, defining the expression of the missile acceleration vector in F_b as $\vec{a}_{M/O_e}^{(b)} = [a_x \quad a_y \quad a_z]^T$, the following equation can be written:

$$\vec{a}_{M/O_e}^{(w)} = \hat{C}^{(w,b)} \vec{a}_{M/O_e}^{(b)} \quad (3.26)$$

where $\hat{C}^{(w,b)}$ is the transformation matrix from F_w to F_b .

As consistent with the preceding sequences, the rotation sequence from F_w to F_b can be expressed as follows:

$$\begin{array}{ccccccc} & -\vec{u}_3^{(w)} & \vec{u}_2^{(h)} & \vec{u}_1^{(k)} & & & \\ F_w & \rightarrow & F_h & \rightarrow & F_k & \rightarrow & F_b \\ & \beta & \alpha & & \phi_s & & \end{array}$$

In the sequence above, α and β represent the angle of attack and the side-slip angle of the missile, and ϕ_s denotes the spin angle. Also, F_h and F_k stand for the intermediate reference frame between F_w and F_b .

From the sequence given above, $\hat{C}^{(w,b)}$ can be obtained as

$$\hat{C}^{(w,b)} = \begin{bmatrix} c_{b11} & c_{b12} & c_{b13} \\ c_{b21} & c_{b22} & c_{b23} \\ c_{b31} & c_{b32} & c_{b33} \end{bmatrix} \quad (3.27)$$

where

$$c_{b11} = \cos(\beta)\cos(\alpha)$$

$$c_{b12} = \cos(\beta)\sin(\alpha)\sin(\phi_s) + \sin(\beta)\cos(\phi_s)$$

$$c_{b13} = \cos(\beta)\sin(\alpha)\cos(\phi_s) - \sin(\beta)\sin(\phi_s)$$

$$c_{b21} = -\sin(\beta)\cos(\alpha)$$

$$c_{b22} = -\sin(\beta)\sin(\alpha)\sin(\phi_s) + \cos(\beta)\cos(\phi_s)$$

$$c_{b23} = -\sin(\beta)\sin(\alpha)\cos(\phi_s) - \cos(\beta)\sin(\phi_s)$$

$$c_{b31} = -\sin(\alpha)$$

$$c_{b32} = \cos(\alpha)\sin(\phi_s)$$

$$c_{b33} = \cos(\alpha)\cos(\phi_s)$$

Hence, substituting equation (3.27) into equation (3.26), the expression of \bar{a}_{M/O_e} in F_w appears as

$$\bar{\mathbf{a}}_{M/O_e}^{(w)} = \begin{bmatrix} \mathbf{a}_{M1}^w \\ \mathbf{a}_{M2}^w \\ \mathbf{a}_{M3}^w \end{bmatrix} \quad (3.28)$$

where

$$\mathbf{a}_{M1}^w = \mathbf{a}_x \cos(\beta) \cos(\alpha) + \mathbf{a}_y [\cos(\beta) \sin(\alpha) \sin(\phi_s) + \sin(\beta) \cos(\phi_s)] \\ + \mathbf{a}_z [\cos(\beta) \sin(\alpha) \cos(\phi_s) - \sin(\beta) \sin(\phi_s)]$$

$$\mathbf{a}_{M2}^w = -\mathbf{a}_x \sin(\beta) \cos(\alpha) + \mathbf{a}_y [-\sin(\beta) \sin(\alpha) \sin(\phi_s) + \cos(\beta) \cos(\phi_s)] \\ + \mathbf{a}_z [-\sin(\beta) \sin(\alpha) \cos(\phi_s) - \cos(\beta) \sin(\phi_s)]$$

$$\mathbf{a}_{M3}^w = -\mathbf{a}_x \sin(\alpha) + \mathbf{a}_y \cos(\alpha) \sin(\phi_s) + \mathbf{a}_z \cos(\alpha) \cos(\phi_s)$$

Since ρ_m is assumed to be zero and the roll attitude of the missile is compensated by the roll autopilot, ϕ_s can also be treated as zero. Hence, the expressions for \mathbf{a}_{M1}^w , \mathbf{a}_{M2}^w and \mathbf{a}_{M3}^w simplify to the following ones:

$$\mathbf{a}_{M1}^w = \mathbf{a}_x \cos(\beta) \cos(\alpha) + \mathbf{a}_y \sin(\beta) + \mathbf{a}_z \cos(\beta) \sin(\alpha) \quad (3.29)$$

$$\mathbf{a}_{M2}^w = -\mathbf{a}_x \sin(\beta) \cos(\alpha) + \mathbf{a}_y \cos(\beta) - \mathbf{a}_z \sin(\beta) \sin(\alpha) \quad (3.30)$$

$$\mathbf{a}_{M3}^w = -\mathbf{a}_x \sin(\alpha) + \mathbf{a}_z \cos(\alpha) \quad (3.31)$$

The guidance commands generated in terms of the acceleration components can also be derived in terms of the rates of the flight path angles. To do this, the acceleration vector of the missile ($\bar{\mathbf{a}}_{M/O_e}$) can be expressed as follows:

$$\bar{\mathbf{a}}_{M/O_e} = D_0 (\bar{\mathbf{v}}_{M/O_e}) \quad (3.32)$$

where D_0 denotes the time derivative operator with respect to F_0 .

Substituting equation (3.1) into equation (3.32) and then using the transport theorem, equation (3.32) can be expanded as

$$\bar{\mathbf{a}}_{M/O_e} = D_w \left(\mathbf{v}_M \bar{\mathbf{u}}_1^{(w)} \right) + \mathbf{v}_M \bar{\boldsymbol{\omega}}_{w/0} \times \bar{\mathbf{u}}_1^{(w)} \quad (3.33)$$

In equation (3.33), the angular velocity vector $\bar{\boldsymbol{\omega}}_{w/0}$ can be written as

$$\bar{\boldsymbol{\omega}}_{w/0} = \dot{\eta}_m \bar{\mathbf{u}}_3^{(0)} + \dot{\gamma}_m \bar{\mathbf{u}}_2^{(a)} + \dot{\rho}_m \bar{\mathbf{u}}_1^{(c)} \quad (3.34)$$

Carrying out the same vector and matrix calculations as done above, $\bar{\boldsymbol{\omega}}_{w/0}$ is expressed as

$$\bar{\boldsymbol{\omega}}_{w/0} = \omega_{w1}^w \bar{\mathbf{u}}_1^{(w)} + \omega_{w2}^w \bar{\mathbf{u}}_2^{(w)} + \omega_{w3}^w \bar{\mathbf{u}}_3^{(w)} \quad (3.35)$$

where

$$\omega_{w1}^w = -\dot{\eta}_m \sin(\gamma_m) + \dot{\rho}_m$$

$$\omega_{w2}^w = \dot{\eta}_m \cos(\gamma_m) \sin(\rho_m) + \dot{\gamma}_m \cos(\rho_m)$$

$$\omega_{w3}^w = \dot{\eta}_m \cos(\gamma_m) \cos(\rho_m) - \dot{\gamma}_m \sin(\rho_m)$$

Hence, substituting equation (3.35) into equation (3.33), $\bar{\mathbf{a}}_{M/O_e}$ can be obtained as

$$\bar{\mathbf{a}}_{M/O_e} = \mathbf{a}_{w1} \bar{\mathbf{u}}_1^{(w)} + \mathbf{a}_{w2} \bar{\mathbf{u}}_2^{(w)} + \mathbf{a}_{w3} \bar{\mathbf{u}}_3^{(w)} \quad (3.36)$$

where

$$a_{w1} = \dot{v}_M$$

$$a_{w2} = v_M [\dot{\eta}_m \cos(\gamma_m) \cos(\rho_m) - \dot{\gamma}_m \sin(\rho_m)]$$

$$a_{w3} = -v_M [\dot{\eta}_m \cos(\gamma_m) \sin(\rho_m) + \dot{\gamma}_m \cos(\rho_m)]$$

Matching equations (3.23) and (3.36) term by term, the command values of \dot{v}_M , $\dot{\eta}_m$ and $\dot{\gamma}_m$ appear as

$$\dot{v}_M^c = 0 \quad (3.37)$$

$$\begin{aligned} \dot{\eta}_m^c = [N_2 \cos^2(\rho_m) + N_3 \sin^2(\rho_m)] [\dot{\lambda}_y \cos(\gamma_m) - \dot{\lambda}_p \sin(\gamma_m) \sin(\lambda_y - \eta_m)] \\ + (N_3 - N_2) \dot{\lambda}_p \cos(\rho_m) \sin(\rho_m) \cos(\lambda_y - \eta_m) \end{aligned} \quad (3.38)$$

$$\begin{aligned} \dot{\gamma}_m^c = [N_2 \sin^2(\rho_m) + N_3 \cos^2(\rho_m)] \dot{\lambda}_p \cos(\lambda_y - \eta_m) \\ + (N_3 - N_2) [\dot{\lambda}_y \cos(\gamma_m) - \dot{\lambda}_p \sin(\gamma_m) \sin(\lambda_y - \eta_m)] \cos(\rho_m) \sin(\rho_m) \end{aligned} \quad (3.39)$$

Looking at equation (3.37), it imposes the condition that v_M^c is constant in time. Since the guidance law is applied after the burnout, the change in the actual speed v_M is caused by the aerodynamic drag acting on the missile. Actually, the amount of this change during the flight is not very significant. Therefore, it is reasonable to command \dot{v}_M^c to be zero.

If the effective navigation ratios are taken to be equal, i.e., $N_2 = N_3 = N$, then equations (3.34) and (3.35) simplify to a large extent as

$$\dot{\eta}_m^c = N \left[\dot{\lambda}_y - \dot{\lambda}_p \tan(\gamma_m) \sin(\lambda_y - \eta_m) \right] \quad (3.40)$$

$$\dot{\gamma}_m^c = N \dot{\lambda}_p \cos(\lambda_y - \eta_m) \quad (3.41)$$

Note as a significant feature that these simplified expressions are independent of the roll angle ρ_m .

3.1.1.2. Planar Interpretation of the Proportional Navigation Guidance Law

Regarding the planar engagement scenarios, the commanded guidance expressions shrink into more concise forms. Namely, for the guidance problem handled in the yaw plane only, the guidance command (a_{cy}) will be determined from the a_{w2}^c component of \vec{a}_c in equation (3.23) by setting $\gamma_m = \rho_m = 0$ as follows:

$$a_{cy} = N_2 v_M \dot{\lambda}_y \quad (3.42)$$

Similarly, the acceleration command in the pitch plane can be obtained from the a_{w3}^c component for $\lambda_y = \eta_m = \rho_m = 0$ in the following manner:

$$a_{cp} = -N_3 v_M \dot{\lambda}_p \quad (3.43)$$

As explained above, a_{cy} and a_{cp} are generated to be perpendicular to \vec{v}_{M/O_e} . In the literature, this kind of PNG is called Pure Proportional Navigation Guidance (PPNG). The schematic representation of the PPNG geometry for the pitch plane motion is shown in Figure 3.4.

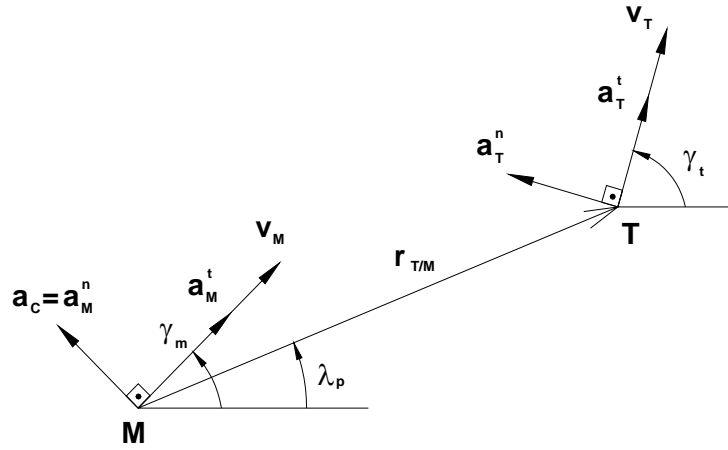


Figure 3.4. Planar Pure Proportional Navigation Geometry

In the original derivation of the PNG law, the guidance commands are formed to be perpendicular to the LOS. To make a distinction between the PPNG, this approach is termed as True Proportional Navigation Guidance (TPNG) later. However, since the axial component of the command acceleration in F_b imposed by the TPNG can not be met by the missile because of the lack of a controllable thrust, this method is not implementable. The schematic representation of the TPNG geometry in the pitch plane is given in Figure 3.5.

Both in Figure 3.4 and Figure 3.5, a_M^t and a_M^n denote the tangential and normal acceleration components of the missile in the pitch plane while a_T^t and a_T^n represent the tangential and normal acceleration components of the target.

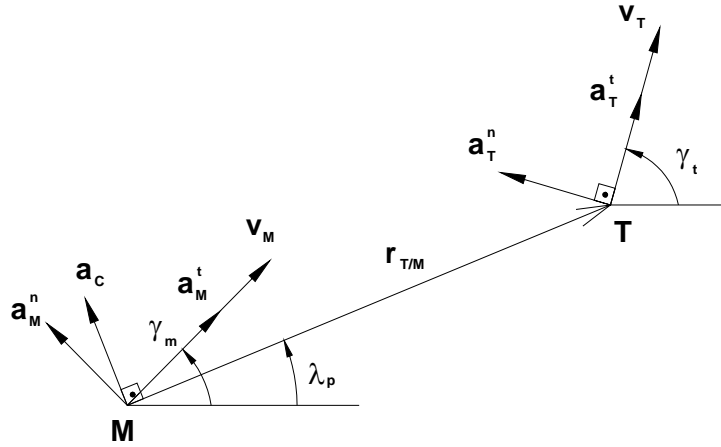


Figure 3.5. Planar True Proportional Navigation Geometry

In equations (3.42) and (3.43), when $N_i = 1$ ($i=2$ and 3), the PNG turns into the Velocity Pursuit Guidance (VPG). Thus, the yaw and pitch plane components of the acceleration commands can be generated with respect to the VPG law in the following manner:

$$a_{cy} = v_M \dot{\lambda}_y \quad (3.44)$$

$$a_{cp} = -v_M \dot{\lambda}_p \quad (3.45)$$

It turns out that the PNG law is very effective against stationary or non-maneuvering targets. However, its performance degrades somewhat when maneuvering targets are involved. Thus, it is modified by adding half of the normal acceleration component of the target (a_T^n) to the present guidance law [3]. Then, the resulting law is termed as Augmented Proportional Navigation Guidance (APNG) law. The APNG law can be formulated for the pitch plane motion as follows:

$$a_{cp} = -N_3 \left(\dot{\lambda}_p v_M + \frac{a_T^n}{2} \right) \quad (3.46)$$

3.1.2. Linear Homing Guidance Law

In this approach, it is intended to keep the missile always on the collision triangle that is formed by the missile, the target, and the predicted intercept point. For this purpose, the most appropriate way is to orient the missile velocity vector toward the predicted intercept point at which the missile-target collision will occur after a while. Then, the resulting guidance commands will be in the form of the flight path angles of the missile.

3.1.2.1. Spatial Derivation of the Linear Homing Guidance Law

The missile-target engagement geometry for the LHG law is depicted in Figure 3.6.

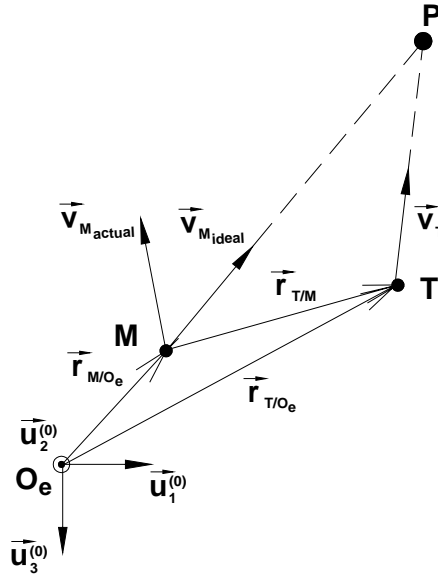


Figure 3.6. Linear Homing Guidance Law Geometry

In Figure 3.6, M, T and P stand for the missile, the target, and the predicted intercept point, respectively. Also, $\vec{v}_{M_{actual}}$ shows the velocity vector of the missile at the beginning of the guidance. The velocity vector of the missile in order to be on

the collision triangle is then indicated by \vec{v}_{Mideal} . Once \vec{v}_{Mactual} is turned into \vec{v}_{Mideal} , it means that the missile is on the collision triangle so as to collide the intended target at point P. In applying this method, unless the target has a velocity vector constant in both magnitude and direction, \vec{v}_{Mideal} should be updated continuously in order to guarantee the intercept.

As Δt denotes the duration from the initial time (t_0) to the end of the intercept (t_F), the desired position vectors of the missile and target at point P can be written as

$$\vec{r}_j(t_F) = \vec{r}_j(t_0) + \vec{v}_{j/O_e} \Delta t \quad (3.47)$$

where $j=M$ and T .

In order for the missile to hit the target, they must be at the same point at time t_F . That is, $\vec{r}_T(t_F) = \vec{r}_M(t_F)$. Hence, from equation (3.47), this condition can be expressed more explicitly as

$$\vec{r}_T + \vec{v}_T \Delta t = \vec{r}_M + \vec{v}_M \Delta t \quad (3.48)$$

where $\vec{r}_T = \vec{r}_T(t_0)$, $\vec{v}_T = \vec{v}_{T/O_e}$, $\vec{r}_M = \vec{r}_M(t_0)$, and $\vec{v}_M = \vec{v}_{M/O_e}$.

In equation (3.48), it is obvious that \vec{v}_M should be equal to \vec{v}_{Mideal} for a successful intercept.

The vectors in equation (3.48) can be written in terms of their components in F_0 as follows:

$$\vec{r}_j = x_j \vec{u}_1^{(0)} + y_j \vec{u}_2^{(0)} + z_j \vec{u}_3^{(0)} \quad (3.49)$$

$$\vec{v}_j = v_{jx} \vec{u}_1^{(0)} + v_{jy} \vec{u}_2^{(0)} + v_{jz} \vec{u}_3^{(0)} \quad (3.50)$$

where $j=M$ and T .

Hence, equation (3.48) can be expressed in F_θ as

$$\vec{v}_T^{(0)} \Delta t = \Delta \vec{r}^{(0)} + \hat{C}^{(0,w)} \vec{v}_M^{(w)} \Delta t \quad (3.51)$$

where $\Delta \vec{r}^{(0)} = \vec{r}_M^{(0)} - \vec{r}_T^{(0)} = \Delta x \vec{u}_1 + \Delta y \vec{u}_2 + \Delta z \vec{u}_3$; $\Delta x = x_M - x_T$, $\Delta y = y_M - y_T$ and $\Delta z = z_M - z_T$.

Noting that $\vec{v}_M^{(w)} = v_M \vec{u}_1$, equation (3.51) yields the following expressions:

$$v_M \Delta t \cos(\eta_m) \cos(\gamma_m) = v_{Tx} \Delta t - \Delta x \quad (3.52)$$

$$v_M \Delta t \sin(\eta_m) \cos(\gamma_m) = v_{Ty} \Delta t - \Delta y \quad (3.53)$$

$$v_M \Delta t \sin(\gamma_m) = -v_{Tz} \Delta t + \Delta z \quad (3.54)$$

Taking the squares of the both sides of equations (3.48) through (3.50) and then adding them up, the following quadratic equation comes out for solving Δt :

$$(v_M^2 - v_T^2) \Delta t^2 + 2\sigma \Delta t - \Delta r^2 = 0 \quad (3.55)$$

where

$$\Delta r^2 = \Delta x^2 + \Delta y^2 + \Delta z^2, \quad \sigma = v_{Tx} \Delta x + v_{Ty} \Delta y + v_{Tz} \Delta z \quad \text{and} \quad v_T^2 = v_{Tx}^2 + v_{Ty}^2 + v_{Tz}^2.$$

Equation (3.55) has only one positive solution for Δt , which is

$$\Delta t = \frac{\sqrt{\sigma^2 + (v_M^2 - v_T^2)\Delta r^2} - \sigma}{v_M^2 - v_T^2} \quad (3.56)$$

Having determined Δt , the division of equation (3.53) by equation (3.52) gives the guidance command for η_m^c as follows, if $\cos(\gamma_m) \neq 0$:

$$\eta_m^c = \arctan\left(\frac{v_{Ty} \Delta t - \Delta y}{v_{Tx} \Delta t - \Delta x}\right) \quad (3.57)$$

Then, γ_m^c can be obtained from equations (3.52) through (3.54) as

$$\gamma_m^c = \arctan\left[\frac{\Delta z - v_{Tz} \Delta t}{(v_{Tx} \Delta t - \Delta x)\cos(\eta_m) + (v_{Ty} \Delta t - \Delta y)\sin(\eta_m)}\right] \quad (3.58)$$

3.1.2.2. Planar Interpretation of the Linear Homing Guidance Law

Considering the missile-target engagement scenario in the pitch plane, equations (3.52) and (3.54) turn into the following expressions by putting $\eta_m = 0$ while equation (3.53) vanishes:

$$v_M \Delta t \cos(\gamma_m) = v_{Tx} \Delta t - \Delta x \quad (3.59)$$

$$v_M \Delta t \sin(\gamma_m) = -v_{Tz} \Delta t + \Delta z \quad (3.60)$$

From Figure 3.4, v_{Tx} and v_{Tz} can be written in terms of v_T and the target flight path angle (γ_t) as follows:

$$v_{Tx} = v_T \cos(\gamma_t) \quad (3.61)$$

$$v_{Tz} = v_T \sin(\gamma_t) \quad (3.62)$$

Then, substituting equations (3.61) and (3.62) into equations (3.59) and (3.60), the following fractional expression arises

$$\frac{\Delta x}{\Delta z} = \frac{v_T \cos(\gamma_t) - v_M \cos(\gamma_m)}{v_T \sin(\gamma_t) + v_M \sin(\gamma_m)} \quad (3.63)$$

From Figure 3.4, Δx and Δz can be expressed in terms of $r_{T/M}$ and λ_p as

$$\Delta x = r_{T/M} \cos(\lambda_p) \quad (3.64)$$

$$\Delta z = r_{T/M} \sin(\lambda_p) \quad (3.65)$$

Inserting equations (3.64) and (3.65) into equation (3.63) and arranging the resulting expression, the guidance command γ_m^c can be found as

$$\gamma_m^c = \lambda_p + a \sin \left[\frac{v_T}{v_M} \sin(\gamma_t - \lambda_p) \right] \quad (3.66)$$

Actually, the expression in equation (3.66) can also be obtained by applying the sine law to the planar engagement geometry considered within the pitch plane as shown in Figure 3.7. In Figure 3.7, θ_L shows the lead angle that is defined as

$$\theta_L = \gamma_m - \lambda_p \quad (3.67)$$

From Figure 3.7, the sine law leads to

$$\frac{v_M}{\sin(\gamma_t - \lambda_p)} = \frac{v_T}{\sin(\gamma_m - \lambda_p)} \quad (3.68)$$

As seen, the solution of equation (3.68) for γ_m^c yields equation (3.66).

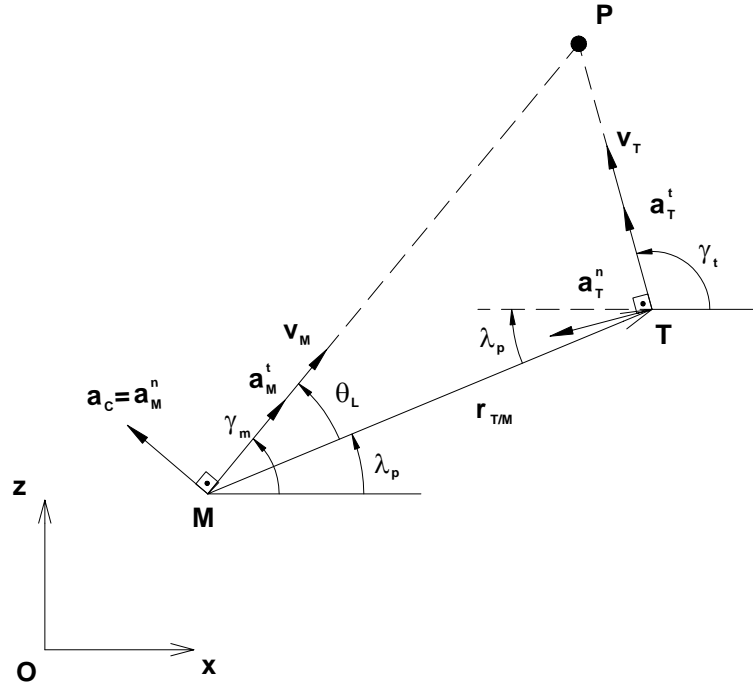


Figure 3.7. Planar Linear Homing Guidance Law Geometry

Equation (3.68) can also be written as

$$v_M \sin(\gamma_m - \lambda_p) = v_T \sin(\gamma_t - \lambda_p) \quad (3.69)$$

Assuming that the angular differences $\gamma_m - \lambda_p$ and $\gamma_t - \lambda_p$ are small, equation (3.69) can be approximated as

$$v_M (\gamma_m - \lambda_p) \cong v_T (\gamma_t - \lambda_p) \quad (3.70)$$

Taking the time derivative of both sides of equation (3.70) and making the necessary arrangements, the following equality is obtained:

$$a_M^t (\gamma_m - \lambda_p) + a_M^n - v_M \dot{\lambda}_p = a_T^t (\gamma_t - \lambda_p) + a_T^n - v_T \dot{\lambda}_p \quad (3.71)$$

where $a_M^t = \dot{v}_M$, $a_M^n = v_M \dot{\gamma}_m$, $a_T^t = \dot{v}_T$ and $a_T^n = v_T \dot{\gamma}_t$.

Since the guidance problem is dealt with in the flight phase after the burnout, \bar{v}_M remains almost constant. Hence, the term a_M^t can be ignored. Moreover, concerning the target motion with a constant velocity, a_T^t can be neglected, too. Thus, setting $a_M^t = a_T^t = 0$ in equation (3.71), it becomes

$$a_M^n - v_M \dot{\lambda}_p = a_T^n - v_T \dot{\lambda}_p \quad (3.72)$$

Noting that $v_c = v_M - v_T$, equation (3.72) can be rearranged as

$$a_c = a_M^n = v_c \dot{\lambda}_p + a_T^n \quad (3.73)$$

As seen in equation (3.73), in order to be on the collision triangle, the normal acceleration of the target (a_T^n) should be added to the product of the closing velocity (v_c) and line-of-sight angular rate ($\dot{\lambda}_p$) to generate the normal acceleration command of the missile. Actually, without the addition of a_T^n , the resulting guidance law in equation (3.73) converts into the VPG law. Thus, it can be inferred that the VPG law can not make the missile drive into the collision triangle unless a_T^n is taken into account.

Then, defining the acceleration advantage factor as $\mu = \frac{a_M^n}{a_T^n}$, equation (3.73)

can be expressed as

$$a_c = N v_c \dot{\lambda}_p \quad (3.74)$$

where $N = \frac{\mu}{\mu - 1}$.

As seen in equation (3.74), the LHG is turned into the PNG law as N stands for the effective navigation ratio. From the definition of N in the PNG law, if $N=3$, then $\mu = 1.5$ and if $N=4$, then $\mu = 1.3$. On the other hand, N goes to infinity when μ becomes unity and takes negative values for values of μ smaller than 1. Actually, this condition says that in order for the missile to catch the target, its acceleration advantage must be strictly greater than unity.

Moreover, equation (3.73) may also be rendered into that of the Augmented Proportional Navigation Guidance (APNG). Namely, as k is constant parameter, adding the $k a_T^n$ multiplication to the both sides of equation (3.73) and making the necessary arrangements, the following equation is obtained:

$$a_c = N_a v_c \dot{\lambda}_p + k_a a_T^n \quad (3.75)$$

where $N_a = \frac{\mu}{\mu + k - 1}$ and $k_a = \frac{\mu k}{\mu + k - 1}$.

Since k_a is heuristically taken to be 0.5 in the APNG formulation, k can be obtained in terms of μ as

$$k = \frac{\mu - 1}{2\mu - 1} \quad (3.76)$$

Hence, using equation (3.76), N_a can be found as

$$N_a = \frac{2\mu - 1}{2(\mu - 1)} \quad (3.77)$$

For example, for $N=3$, $\mu = 1.25$ is obtained from equation (3.77).

3.1.3. Parabolic Homing Guidance Law

In this method, the missile is driven to the predicted intercept point with the target by means of a parabolic trajectory. In order to keep the missile on the planned trajectory, the necessary guidance commands are generated in the form of lateral acceleration components. Actually, this method differs from the LHG law with the shape of the planned trajectory. In other words, while the LHG poses a linear path toward the predicted intercept point, the Parabolic Homing Guidance (PHG) law upgrades the trajectory to a parabola.

3.1.3.1. Spatial Derivation of the Parabolic Homing Guidance Law

In this approach, for both the missile and the target, the assumed future trajectories for predicting the intercept are parabolic as depicted in Figure 3.8.

The derivation of the PHG law can be done similarly to the derivation of the LHG law. Thus, with Δt being the duration from t_0 to t_F , the desired position vectors of the missile and the target at point P can be written as

$$\vec{r}_j(t_F) = \vec{r}_j(t_0) + \vec{v}_{j/O_e} \Delta t + \frac{1}{2} \vec{a}_{j/O_e} \Delta t^2 \quad (3.78)$$

where $j=M$ and T .

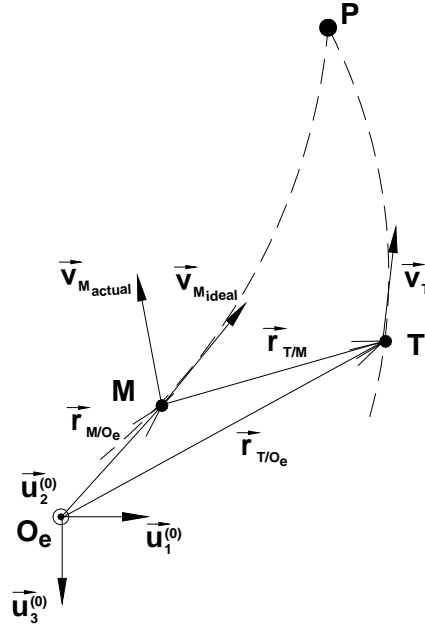


Figure 3.8. Parabolic Homing Guidance Law Geometry

As noticed, the only difference of equation (3.78) from equation (3.47) is the contribution of the acceleration vector.

Hence, in order for the missile to hit the target, the condition that $\vec{r}_T(t_F) = \vec{r}_M(t_F)$ must be satisfied. This condition can be obtained from equation (3.78) as

$$\vec{r}_T + \vec{v}_T \Delta t + \frac{1}{2} \vec{a}_T \Delta t^2 = \vec{r}_M + \vec{v}_M \Delta t + \frac{1}{2} \vec{a}_M \Delta t^2 \quad (3.79)$$

where $\vec{r}_T = \vec{r}_T(t_0)$, $\vec{v}_T = \vec{v}_{T/O_e}$, $\vec{a}_T = \vec{a}_{T/O_e}$, $\vec{r}_M = \vec{r}_M(t_0)$, $\vec{v}_M = \vec{v}_{M/O_e}$ and $\vec{a}_M = \vec{a}_{M/O_e}$.

Expressing equation (3.79) in F_θ and then substituting equations (3.4), (3.49) and (3.50) into the resulting equations along with $\bar{v}_M^{(w)} = v_M \bar{u}_1$, the following equations are obtained:

$$v_{Tx} \Delta t + \frac{1}{2} a_{Tx} \Delta t^2 = \Delta x + v_M \Delta t \cos(\eta_m) \cos(\gamma_m) + \frac{1}{2} [-a_{w2} \sin(\eta_m) + a_{w3} \cos(\eta_m) \sin(\gamma_m)] \Delta t^2 \quad (3.80)$$

$$v_{Ty} \Delta t + \frac{1}{2} a_{Ty} \Delta t^2 = \Delta y + v_M \Delta t \sin(\eta_m) \cos(\gamma_m) + \frac{1}{2} [a_{w2} \cos(\eta_m) + a_{w3} \sin(\eta_m) \sin(\gamma_m)] \Delta t^2 \quad (3.81)$$

$$v_{Tz} \Delta t + \frac{1}{2} a_{Tz} \Delta t^2 = \Delta z - v_M \Delta t \sin(\gamma_m) + \frac{1}{2} a_{w3} \Delta t^2 \cos(\gamma_m) \quad (3.82)$$

where $\bar{a}_T^{(0)} = a_{Tx} \bar{u}_1 + a_{Ty} \bar{u}_2 + a_{Tz} \bar{u}_3$ and $\bar{a}_M^{(w)} = a_{w1} \bar{u}_1 + a_{w2} \bar{u}_2 + a_{w3} \bar{u}_3$.

Making the necessary manipulations among equations (3.80) through (3.82), the following quadratic equation arises for the solution of Δt :

$$\left(\frac{A}{2} \right) \Delta t^2 + B \Delta t + C = 0 \quad (3.83)$$

where

$$A = -[a_{Tx} \cos(\eta_m) + a_{Ty} \sin(\eta_m)] \cos(\gamma_m) + a_{Tz} \sin(\gamma_m)$$

$$B = -[v_{Tx} \cos(\eta_m) + v_{Ty} \sin(\eta_m)] \cos(\gamma_m) + v_{Tz} \sin(\gamma_m) + v_M$$

$$C = [\Delta x \cos(\eta_m) + \Delta y \sin(\eta_m)] \cos(\gamma_m) - \Delta z \sin(\gamma_m)$$

Then, the positive solution for Δt can be determined from equation (3.83) as follows, if $A \neq 0$:

$$\Delta t = \frac{-B + \sigma \sqrt{B^2 - 2AC}}{A} \quad (3.84)$$

$$\text{where } \sigma = \begin{cases} 1 & , \text{ for } A > 0 \text{ and } C < 0, \text{ or } A < 0 \text{ and } C < 0 \\ -1 & , \text{ for } A < 0 \text{ and } C > 0 \end{cases} .$$

Here, it should be noted that no positive solution occurs for Δt if $A > 0$ and $C > 0$. Also, to get a real solution, the condition that $B^2 - 2AC \geq 0$ must be satisfied in equation (3.84).

If $A = 0$, equation (3.83) reduces into a linear equation in terms of Δt and the solution is obtained simply as

$$\Delta t = \frac{-C}{B} \quad (3.85)$$

Note that A and B can not be zero simultaneously. Otherwise, no equation remains for Δt .

Having determined Δt , the guidance commands for a_{w2} and a_{w3} can be determined from equations (3.80) through (3.81) in the following manner:

$$a_{w2}^c = -d_1 \sin(\eta_m) + d_2 \cos(\eta_m) \quad (3.86)$$

$$a_{w3}^c = (d_1 + d_2) \sin(\gamma_m) + d_3 \cos(\gamma_m) \quad (3.87)$$

where

$$d_1 = 2 \left[\frac{v_{Tx} - v_M \cos(\eta_m) \cos(\gamma_m)}{\Delta t} - \frac{\Delta x}{\Delta t^2} \right] + a_{Tx}$$

$$d_2 = 2 \left[\frac{v_{Ty} - v_M \sin(\eta_m) \cos(\gamma_m)}{\Delta t} - \frac{\Delta y}{\Delta t^2} \right] + a_{Ty}$$

$$d_3 = 2 \left[\frac{v_{Tz} + v_M \sin(\gamma_m)}{\Delta t} - \frac{\Delta z}{\Delta t^2} \right] + a_{Tz}$$

3.1.3.2. Planar Interpretation of the Parabolic Homing Guidance Law

Considering the missile-target engagement in the pitch plane, setting $\eta_m = \Delta y = a_{w2} = a_{Tx} = 0$, equations (3.80) and (3.82) reduce to the following ones while equation (3.74) vanishes:

$$a_{w3} \Delta t^2 \sin(\gamma_m) = 2 \left[(v_{Tx} - v_M \cos(\gamma_m)) \Delta t - \Delta x \right] + a_{Tx} \Delta t^2 \quad (3.88)$$

$$a_{w3} \Delta t^2 \cos(\gamma_m) = 2 \left[(v_{Tz} + v_M \sin(\gamma_m)) \Delta t - \Delta z \right] + a_{Tz} \Delta t^2 \quad (3.89)$$

Thus, the quadratic equation (3.83) is reduced into the following form:

$$\left(\frac{A_p}{2} \right) \Delta t^2 + B_p \Delta t + C_p = 0 \quad (3.90)$$

where

$$A_p = -a_{Tx} \cos(\gamma_m) + a_{Tz} \sin(\gamma_m)$$

$$B_p = -v_{Tx} \cos(\gamma_m) + v_{Tz} \sin(\gamma_m) + v_M$$

$$C_p = \Delta x \cos(\gamma_m) - \Delta z \sin(\gamma_m)$$

Hence, Δt is given by one of the following equations depending on whether A_p is zero or not:

$$\Delta t = \frac{-C_p}{B_p} \quad (3.91)$$

$$\Delta t = \frac{-B_p + \sigma_p \sqrt{B_p^2 - 2 A_p C_p}}{A_p} \quad (3.92)$$

$$\text{where } \sigma_p = \begin{cases} 1 & , \text{ for } A_p > 0 \text{ and } C_p < 0, \text{ or } A_p < 0 \text{ and } C_p < 0 \\ -1 & , \text{ for } A_p < 0 \text{ and } C_p > 0 \end{cases}.$$

Similar to its spatial derivation, no positive solution occurs for Δt if $A_p > 0$ and $C_p > 0$. Also, the condition $B_p^2 - 2 A_p C_p \geq 0$ must be satisfied for a real Δt .

Regarding $a_{Tx} = a_T \sin(\gamma_t)$ and $a_{Tz} = a_T \cos(\gamma_t)$ in the pitch plane, the guidance command for a_{w3} is obtained as

$$a_{w3}^c = \frac{2 \left[v_T \Delta t \sin(\gamma_m - \gamma_t) - r_{T/M} \sin(\gamma_m - \lambda_p) \right]}{\Delta t^2} + a_T \cos(\gamma_m - \gamma_t) \quad (3.93)$$

3.2. Missile-Target Engagement Kinematics

Considering the engagement kinematics illustrated in Figure 3.1, the following relationship can be written between the position vectors of the missile and target with respect to point O_e , the origin of F_0 :

$$\vec{r}_{T/O_e} = \vec{r}_{M/O_e} + \vec{r}_{T/M} \quad (3.94)$$

The relative distance vector $\Delta \vec{r}$ can be defined as

$$\Delta \vec{r} = \vec{r}_{T/O_e} - \vec{r}_{M/O_e} \quad (3.95)$$

where $\Delta \vec{r} = \Delta x \vec{u}_1^{(0)} + \Delta y \vec{u}_2^{(0)} + \Delta z \vec{u}_3^{(0)}$.

Expressing equation (3.95) in F_θ and then substituting equations (3.2) and (3.6) into the resulting equation, the following expressions can be obtained:

$$r_{T/M} \cos(\lambda_y) \cos(\lambda_p) = \Delta x \quad (3.96)$$

$$r_{T/M} \sin(\lambda_y) \cos(\lambda_p) = \Delta y \quad (3.97)$$

$$-r_{T/M} \sin(\lambda_p) = \Delta z \quad (3.98)$$

Dividing equation (3.97) by equation (3.96), λ_y is found as follows, if $\cos(\lambda_p) \neq 0$:

$$\lambda_y = \arctan\left(\frac{\Delta y}{\Delta x}\right) \quad (3.99)$$

Then, λ_p can be found from equations (3.96) and (3.98) as

$$\lambda_p = \arctan\left(\frac{-\Delta z \cos(\lambda_y)}{\Delta x}\right) \quad (3.100)$$

Taking the squares of equations (3.96) through (3.98) and then adding them up, the magnitude of the relative distance between the missile and target ($r_{T/M}$) can be determined as follows:

$$r_{T/M} = |\vec{r}_{T/M}| = \sqrt{\Delta x^2 + \Delta y^2 + \Delta z^2} \quad (3.101)$$

Since the missile is thought to be fired against a surface target, $\Delta z = 0$ condition will be satisfied at the end of the engagement. Thus, at this final point, i.e., at $t = t_F$, the values of Δx and Δy will give the two components of the final miss distance of the missile (x_{miss} and y_{miss}) as

$$x_{\text{miss}} = \Delta x(t_F) \quad (3.102)$$

$$y_{\text{miss}} = \Delta y(t_F) \quad (3.103)$$

Hence, the resultant miss distance (d_{miss}) can be obtained from equations (3.102) and (3.103) as

$$d_{\text{miss}} = \sqrt{\Delta x^2(t_F) + \Delta y^2(t_F)} \quad (3.104)$$

CHAPTER 4

MISSILE CONTROL

In this chapter, first the roll and the transversal autopilots of the missile are designed based on the transfer functions obtained in Chapter 2. Here, the transversal autopilots include the acceleration, the angular rate and the angle autopilots. Then, the concept of the anti-windup scheme used along with the controller is explained. Lastly, the roll resolving scheme employed to decouple the yaw and the pitch channels in the case of nonzero roll motion is presented.

4.1. Missile Autopilot

In order to control the motion of the missile in its pitch and yaw planes as well as in the roll direction, three different autopilots are needed: roll, pitch and yaw autopilots. Regarding the transfer functions of the missile obtained according to its equations of motion, the mentioned autopilots can be properly designed.

4.1.1. Roll Autopilot

Due to the thrust forces and the thrust misalignment moments, the missile gains a roll motion around the $\bar{u}_1^{(b)}$ axis. After the boost phase, this roll motion is damped within a period of time. The length of the period changes depending on the orientations of the fixed tail fins of the missile. Namely, if the tail fins are mounted in a canted configuration, i.e., if they are fixed at an

orientation with nonzero angles, then the roll motion will last much longer than the period of the uncanted configuration. In the autopilot design, it will be quite useful to compensate the roll motion of the missile prior to the control of its pitch and yaw motions. In other words, either the roll attitude or roll rate should be nullified at the beginning of the control. In this study, the roll control system is designed to regulate the roll attitude, or roll angle, of the missile. In fact, the mentioned roll attitude belongs to body 1. Designing the roll autopilot, the uncontrolled roll motion of body 2 is taken as an external disturbance on the roll motion of body 1 as explained in Chapter 2.

Considering equations (2.197) and (2.198), the following state feedback control law can be written for the roll attitude of body 1:

$$u_r = k_\phi (\phi_{1d} - \phi_1) - k_p p \quad (4.1)$$

where k_ϕ and k_p are the controller gains.

Then, substituting equation (4.1) into equations (2.197) and (2.198), the closed-loop transfer function of the roll motion of the missile is determined as

$$\frac{\phi_1(s)}{\phi_d(s)} = \frac{1}{c_{\phi 2} s^2 + c_{\phi 1} s + 1} \quad (4.2)$$

where $c_{\phi 1} = \frac{L_\delta k_p - L_{p1}}{L_\delta k_\phi}$ and $c_{\phi 2} = \frac{1}{L_\delta k_\phi}$.

The resulting control system is a type 1 control system. Its characteristic polynomial appears as

$$D_r(s) = c_{\phi 2} s^2 + c_{\phi 1} s + 1 \quad (4.3)$$

The controller gains (k_ϕ and k_p) can be obtained by placing the two poles of the closed-loop control system to the desired locations on the left-hand-side of the complex plane. For this purpose, a second-order Butterworth polynomial given above can be used [Appendix]:

$$B_2(s) = \left(\frac{1}{\omega_c^2} \right) s^2 + \left(\frac{\sqrt{2}}{\omega_c} \right) s + 1 \quad (4.4)$$

where ω_c stands for the desired bandwidth the control system.

Hence, equating the polynomials $D_r(s)$ and $B_2(s)$ in equations (4.3) and (4.4) term by term and making the intermediate operations, k_ϕ and k_p can be found as

$$k_\phi = \frac{\omega_c^2}{L_\delta} \quad (4.5)$$

$$k_p = \frac{\sqrt{2} \omega_c + L_{p1}}{L_\delta} \quad (4.6)$$

During the flight of the missile, the aerodynamic stability derivatives vary in accordance with the Mach number (M_∞), angle of attack (α), side-slip angle (β), aileron deflection (δ_a) and the spin angle (ϕ_s). In order to keep the roll stability of the missile, the roll control system must adapt to the changes of these parameters. Thus, k_ϕ and k_p values given in equations (4.5) and (4.6) should be updated depending on the current values of these parameters throughout the controlled flight of the missile.

4.1.2. Transversal Autopilots

After the boost, the missile velocity can not be changed due to the lack of the required thrust. Thus, the control of the missile can be achieved by manipulating either the orientation of the velocity vector or the lateral acceleration components. Assuming that the bandwidth of the roll autopilot is at least three times the bandwidth of the pitch and yaw autopilots, and hence the roll motion of the missile is regulated prior to the control in the pitch and yaw planes, the equations describing the pitch and yaw motions become decoupled. Therefore, the pitch and yaw autopilots can be designed separately.

4.1.2.1. Acceleration Autopilots

In order to execute the lateral acceleration commands coming from the guidance unit in the pitch plane, the control system can be designed considering the classical PI (proportional plus integral) control action with the contribution of the pitch damping. Denoting the proportional, integral and pitch damping gains as K_p , T_p and K_q , the mentioned control system can be constructed as given in Figure 4.1.

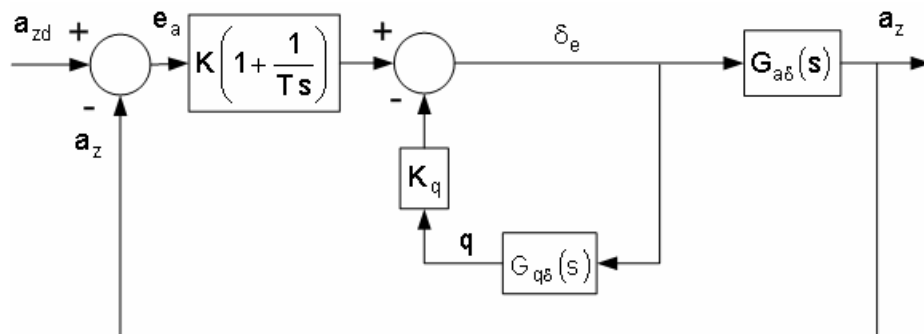


Figure 4.1. Pitch Acceleration Control System

Applying the block diagram algebra to the block diagram in Figure 4.1 with the inclusion of $G_{q\delta}(s)$ and $G_{a\delta}(s)$ given in equations (2.164) and (2.170), the closed loop transfer function between the actual and the desired lateral accelerations is obtained as

$$\frac{a_z(s)}{a_{zd}(s)} = \frac{(T_p s + 1)(n_{p2} s^2 + n_{p1} s + 1)}{a_{p3} s^3 + a_{p2} s^2 + a_{p1} s + 1} \quad (4.7)$$

where

$$n_{p1} = \frac{n_{z1}}{n_{z0}}$$

$$n_{p2} = \frac{n_{z2}}{n_{z0}},$$

$$a_{p1} = \frac{T_p (d_{p0} + K_q n_{q0} + K_p n_{z0}) + K_p n_{z1}}{K_p n_{z0}}$$

$$a_{p2} = \frac{T_p (d_{p1} + K_q n_{q1} + K_p n_{z1}) + K_p n_{z2}}{K_p n_{z0}}$$

$$a_{p3} = \frac{T_p (1 + K_p n_{z2})}{K_p n_{z0}}.$$

For the control system whose type number is one, the characteristic polynomial of the transfer function in equation (4.7) is

$$D_p(s) = a_{p3} s^3 + a_{p2} s^2 + a_{p1} s + 1 \quad (4.8)$$

In order to determine K_p , T_p and K_q , the third-order Butterworth polynomial given below can be used [Appendix]:

$$B_3(s) = \left(\frac{1}{\omega_c^3} \right) s^3 + \left(\frac{2}{\omega_c^2} \right) s^2 + \left(\frac{2}{\omega_c} \right) s + 1 \quad (4.9)$$

Introducing $\sigma_p = \frac{T_p}{K_p}$ and $\eta_p = \frac{T_p K_q}{K_p}$, σ_p , η_p and T_p can be

obtained by matching equations (4.8) and (4.9) term by term as follows:

$$\begin{bmatrix} \sigma_p \\ \eta_p \\ T_p \end{bmatrix} = \hat{M}_p^{-1} \bar{b}_p \quad (4.10)$$

$$\text{where } \hat{M}_p = \begin{bmatrix} 1 & 0 & n_{z2} \\ d_{p1} & n_{q1} & n_{z1} \\ d_{p0} & n_{q0} & n_{z0} \end{bmatrix} \text{ and } \bar{b}_p = \begin{bmatrix} \frac{n_{z0}}{\omega_c^3} & \frac{2n_{z0}}{\omega_c^2} - n_{z2} & \frac{2n_{z0}}{\omega_c} - n_{z1} \end{bmatrix}^T$$

In order for σ_p , η_p and T_p to take finite values, \hat{M}_p^{-1} must exist. In other words, the determinant of the matrix \hat{M}_p must be nonzero. From here, the following singularity condition for the proposed control system can be obtained by equating the determinant of the matrix \hat{M}_p to zero:

$$M_\delta^2 Z_\alpha (u + Z_q) + Z_\alpha Z_\delta \left(\frac{M_\delta Z_\alpha - M_\alpha Z_\delta}{u} - M_\alpha M_q \right) = 0 \quad (4.11)$$

It seems that the above condition can not be encountered in practice. Therefore, the control parameters can be determined without any problem.

Having determined σ_p , η_p and T_p from equation (4.10), the controller gains K_p and K_q can be calculated as shown below:

$$K_p = \frac{T_p}{\sigma_p} \quad (4.12)$$

$$K_q = \frac{\eta_p K_p}{T_p} \quad (4.13)$$

For adaptation of the control system to the changing flight conditions, the values of K_p , T_p and K_q should be updated continuously according to the current values of M_∞ , α , δ_e and ϕ_s .

As shown in equation (4.7), the numerator dynamics of the transfer function of the missile acceleration control system is represented by the following polynomial:

$$N_p(s) = (T_p s + 1)(n_{p2} s^2 + n_{p1} s + 1) \quad (4.14)$$

The roots of $N_p(s)$ in equation (4.14) will give the zeros of the control system. If all of the zeros have negative real parts, then the control system will be of minimum phase, otherwise nonminimum phase. Looking at the zeros of $N_p(s)$, the system will be of nonminimum phase if either of the following conditions is satisfied:

$$T_p < 0 \quad (4.15)$$

$$M_q Z_\delta - Z_q M_\delta < 0 \quad (4.16)$$

Having designed the pitch control system, the yaw control system can be designed in the same manner because of the rotational symmetry of the missile. In the design, considering the transfer functions $G_{r\delta}(s)$ and $G_{a\delta}(s)$ given in equations (2.179) and (2.182), the same control system as the previous one can be built up.

Because of the rotational symmetry of the entire missile body, the following equalities can be established among the stability derivatives of the pitch and yaw dynamics of the missile:

$$C_{y\beta} = C_{z\alpha} \quad (4.17)$$

$$C_{y\delta} = -C_{z\delta} \quad (4.18)$$

$$C_{yr} = -C_{zq} \quad (4.19)$$

$$C_{n\beta} = -C_{m\alpha} \quad (4.20)$$

$$C_{n\delta} = C_{m\delta} \quad (4.21)$$

$$C_{nr} = C_{mq} \quad (4.22)$$

4.1.2.2. Rate Autopilots

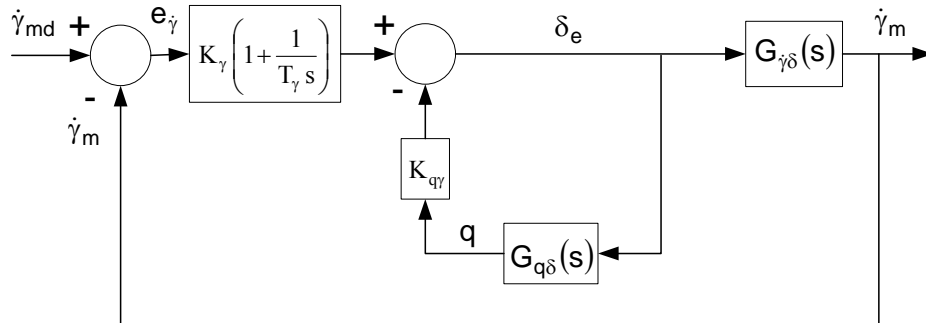


Figure 4.2. Flight Path Angle Rate Control System

The pitch (yaw) rate autopilot can be designed similarly to the acceleration autopilot so as to control the rate of the flight path angle of the missile in the pitch (yaw) plane. Thus, the mentioned control system can be constructed with the pitch damping added PI control law as shown in Figure 4.2.

The transfer functions $G_{q\delta}(s)$ and $G_{\dot{\gamma}\delta}(s)$ in Figure 4.2 are already given in equations (2.164) and (2.166). Thus, applying the block diagram algebra, the closed-loop transfer function of the resulting type 1 control system from the desired flight path angle rate ($\dot{\gamma}_{md}$) to the actual flight path angle rate ($\dot{\gamma}_m$) is obtained as

$$\frac{\dot{\gamma}_m(s)}{\dot{\gamma}_{md}(s)} = \frac{(T_\gamma s + 1)(n_{\dot{\gamma}2} s^2 + n_{\dot{\gamma}1} s + 1)}{d_{\dot{\gamma}3} s^3 + d_{\dot{\gamma}2} s^2 + d_{\dot{\gamma}1} s + 1} \quad (4.23)$$

where

$$n_{\dot{\gamma}1} = \frac{n_{\alpha q}}{n_{q0}}$$

$$n_{\dot{\gamma}2} = -\frac{n_{\alpha 1}}{n_{q0}}$$

$$d_{\dot{\gamma}1} = \frac{T_\gamma d_{p0} + T_\gamma K_{q\gamma} n_{q0} + K_\gamma T_\gamma n_{q0} + K_\gamma n_{\alpha q}}{K_\gamma n_{q0}}$$

$$d_{\dot{\gamma}2} = \frac{T_\gamma d_{p1} + T_\gamma K_{q\gamma} n_{q1} + K_\gamma T_\gamma n_{\alpha q} - K_\gamma n_{\alpha 1}}{K_\gamma n_{q0}}$$

$$d_{\dot{\gamma}3} = \frac{T_\gamma - K_\gamma T_\gamma n_{\alpha 1}}{K_\gamma n_{q0}}.$$

The characteristic polynomial of the closed-loop transfer function in equation (4.23) is seen to be

$$D(s) = d_{\gamma 3} s^3 + d_{\gamma 2} s^2 + d_{\gamma 1} s + 1 \quad (4.24)$$

In the determination of the controller gains K_γ , T_γ and $K_{q\gamma}$, the pole placement technique can be applied. Hence, equating the polynomial given in equation (4.9) to $D(s)$ in equation (4.24) term by term, the following matrix expression is obtained:

$$\begin{bmatrix} \sigma_\gamma \\ \eta_\gamma \\ T_\gamma \end{bmatrix} = \hat{M}_\gamma^{-1} \bar{b}_\gamma \quad (4.25)$$

where $\hat{M}_\gamma = \begin{bmatrix} 1 & 0 & -n_{\alpha 1} \\ d_{p1} & n_{q1} & n_{\alpha q} \\ d_{p0} & n_{q0} & n_{q0} \end{bmatrix}$, $\bar{b}_k = \left[\frac{n_{q0}}{\omega_c^3} \quad \frac{2n_{q0}}{\omega_c^2} + n_{\alpha 1} \quad \frac{2n_{q0}}{\omega_c} - n_{\alpha q} \right]^T$,

$\sigma_\gamma = \frac{T_\gamma}{K_\gamma}$ and $\eta_\gamma = \frac{T_\gamma K_{q\gamma}}{K_\gamma}$.

The singularity condition of equation (4.25) arises as

$$\frac{Z_\alpha}{M_\alpha u} + \frac{M_q (Z_\alpha + Z_\delta)}{M_\delta Z_\alpha} + \frac{Z_q + u}{Z_\alpha} - \frac{M_\alpha (Z_q + u) - M_q Z_\alpha}{M_\alpha Z_\delta - M_\delta Z_\alpha} = 0 \quad (4.26)$$

This condition does not seem to be encountered in practice. Therefore, it can be said that finite values can be determined for the parameters $\sigma_\gamma, \eta_\gamma$ and T_γ from equation (4.25). After obtaining these parameters, the controller gains K_γ and $K_{q\gamma}$ can be calculated as

$$K_{\gamma} = \frac{T_{\gamma}}{\sigma_{\gamma}} \quad (4.27)$$

$$K_{q\gamma} = \frac{\eta_{\gamma} K_{\gamma}}{T_{\gamma}} \quad (4.28)$$

In order to keep the stability of the control system, K_{γ} , T_{γ} and $K_{q\gamma}$ should be updated continuously depending on the current values of M_{∞} , α , δ_e and ϕ_s .

Also, the numerator dynamics of the closed-loop transfer function appears as

$$N(s) = (T_{\gamma} s + 1)(n_{\dot{\gamma}2} s^2 + n_{\dot{\gamma}1} s + 1) \quad (4.29)$$

Solving for the zeros of $N(s)$, the system will be of nonminimum phase if either of the following conditions is satisfied:

$$T_{\gamma} < 0 \quad (4.30)$$

$$(Z_q + Z_{\alpha} + u)M_{\delta} - (M_{\alpha} + M_q) < 0 \quad (4.31)$$

4.1.2.3. Angle Autopilots

Another way of controlling the motion of a missile after the boost phase is to control the orientation of its velocity vector, i.e., its flight path angles. In order to design a control system that tracks the flight path angle commands generated by the guidance unit, the equations of motion of the missile should be rearranged in a compatible form. Assuming that the roll motion of the missile is already compensated, the pitch and the yaw motions can be handled separately.

Thus, they can be treated as planar motions. Because of the rotational symmetry of the missile, it will be sufficient to design the angle control system for either of the pitch and the yaw planes, and then adapt the results to the other one.

Hence, considering the roll-free motion of the missile in the pitch plane and taking the gravity effect as an external disturbance, the component of the missile acceleration in $\bar{u}_3^{(b)}$ direction and the time derivative of the pitch rate can be obtained as

$$a_z = \frac{Z}{m} \quad (4.32)$$

$$\dot{q} = \frac{M}{I_t'} \quad (4.33)$$

Also, in the pitch plane motion, a_z is equal to the multiplication of the missile velocity (v_M) and flight path angle rate ($\dot{\gamma}_m$) as

$$a_z = v_M \dot{\gamma}_m \quad (4.34)$$

Then, substituting equations (2.114), (2.116), (2.138), (2.140), (2.165) and (4.34) into equations (4.32) and (4.33), the following expressions are found:

$$\dot{\gamma}_m = -Z_\alpha \gamma_m + Z_\alpha \theta + Z_q q + Z_\delta \delta_e \quad (4.35)$$

$$\dot{q} = -M_\alpha \gamma_m + M_\alpha \theta + M_q q + M_\delta \delta_e \quad (4.36)$$

where $\theta = \theta_1$, $Z_\alpha = \frac{q_\infty S_M}{m v_M} C_{z_\alpha}$, $Z_q = \frac{q_\infty S_M d_M}{m v_M^2} C_{z_q}$, $Z_\delta = \frac{q_\infty S_M}{m v_M} C_{z_\delta}$,
 $M_\alpha = \frac{q_\infty S_M d_M}{I'_t} C_{m_\alpha}$, $M_q = \frac{q_\infty S_M d_M^2}{2 I'_t v_M} C_{m_q}$ and $M_\delta = \frac{q_\infty S_M d_M}{I'_t} C_{m_\delta}$.

Thus, equations (4.35) and (4.36) can be expressed in matrix form along with the equality $\dot{\theta} = q$ as follows:

$$\begin{bmatrix} \dot{\gamma}_m \\ \dot{\theta} \\ \dot{q} \end{bmatrix} = \begin{bmatrix} -Z_\alpha & Z_\alpha & Z_q \\ 0 & 0 & 1 \\ -M_\alpha & M_\alpha & M_q \end{bmatrix} \begin{bmatrix} \gamma_m \\ \theta \\ q \end{bmatrix} + \begin{bmatrix} Z_\delta \\ 0 \\ M_\delta \end{bmatrix} \delta_e \quad (4.37)$$

In this scheme, the integration of the error between the desired and the actual (measured) values of the control variable (γ_m) is also used to generate the control input to the plant. Thus, the error integration term can be designated an additional state variable called x_i . In other words, the error of the control system (e_γ) is just the time derivative of the new state variable x_i as

$$\dot{x}_i = e_\gamma = \gamma_{md} - \gamma_m \quad (4.38)$$

For this control system, the following state feedback control law can be designed to control γ_m :

$$u = \delta_e = k_\gamma (\gamma_{md} - \gamma_m) - k_\theta \theta - k_q q + k_i x_i \quad (4.39)$$

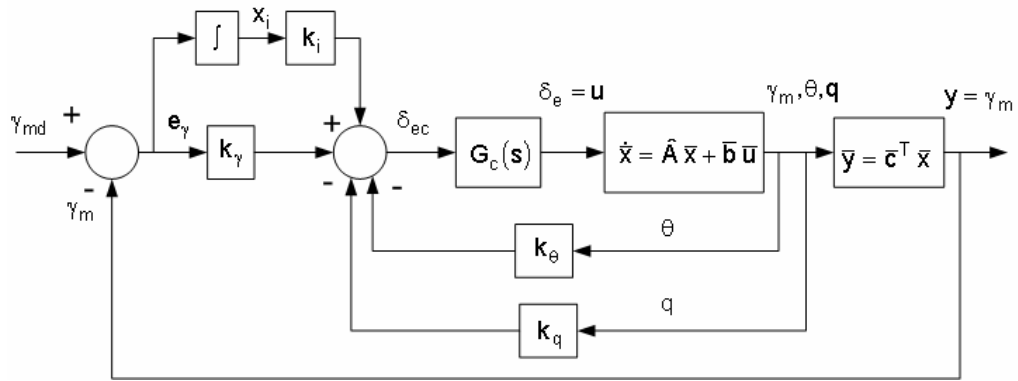


Figure 4.3. Flight Path Angle Control System

Hence, the flight path angle control system can be constructed as shown by the block diagram in Figure 4.3.

Inserting equation (4.39) into equation (4.37) and gathering the resulting equation with equation (4.38), the state-space representation of the augmented control system appears as

$$\dot{\bar{\mathbf{x}}}_e = \hat{\mathbf{A}}_e \bar{\mathbf{x}}_e + \bar{\mathbf{b}}_e r \quad (4.40)$$

where

$$r = \gamma_{md}$$

$$\bar{\mathbf{x}}_e = [\gamma_m \quad \theta \quad q \quad x_i]^T$$

$$\hat{\mathbf{A}}_e = \begin{bmatrix} z_\gamma & z_\theta & z_q & Z_\delta k_i \\ 0 & 0 & 1 & 0 \\ m_\gamma & m_\theta & m_q & M_\delta k_i \\ -1 & 0 & 0 & 0 \end{bmatrix}$$

$$z_\gamma = -Z_\alpha - Z_\delta k_\gamma$$

$$z_\theta = Z_\alpha - Z_\delta k_\theta$$

$$z_q = Z_q - Z_\delta k_q$$

$$m_\gamma = -M_\alpha - M_\delta k_\gamma$$

$$m_\theta = M_\alpha - M_\delta k_\theta$$

$$m_q = M_q - M_\delta k_q$$

$$\bar{b}_e = [Z_\delta k_\gamma \quad 0 \quad M_\delta k_\gamma \quad 1]^T$$

Also, since the state variable to be controlled is the pitch plane component of the missile flight path angle (γ_m), the output equation can be formed as

$$\bar{y} = \bar{c}_e^T \bar{x}_e \quad (4.41)$$

where $\bar{c}_e = [1 \quad 0 \quad 0 \quad 0]^T$.

Eventually, taking the Laplace transforms of equations (4.40) and (4.41), the closed-loop transfer function of the control system between the desired and the actual values of the flight path angle (γ_{md} and γ_m) can be determined from the resulting expressions in the following manner:

$$\frac{\gamma_m(s)}{\gamma_{md}(s)} = \frac{n_{\gamma 3} s^3 + n_{\gamma 2} s^2 + n_{\gamma 1} s + 1}{d_{\gamma 4} s^4 + d_{\gamma 3} s^3 + d_{\gamma 2} s^2 + d_{\gamma 1} s + 1} \quad (4.42)$$

where

$$n_{\gamma 1} = \frac{k_{\gamma}}{k_i} + \frac{a_{\delta q}}{a_{\alpha \delta}}$$

$$n_{\gamma 2} = \frac{a_{\delta q} k_{\gamma}}{a_{\alpha \delta} k_i} + \frac{Z_{\delta}}{a_{\alpha \delta}}$$

$$n_{\gamma 3} = \frac{Z_{\delta} k_{\gamma}}{a_{\alpha \delta} k_i}$$

$$d_{\gamma 1} = \frac{k_{\theta} + k_{\gamma}}{k_i} + \frac{a_{\delta q}}{a_{\alpha \delta}}$$

$$d_{\gamma 2} = \frac{M_{\alpha} + M_{\delta} k_{\theta} - a_{\alpha q} + a_{\alpha \delta} k_q + a_{\delta q} k_{\gamma} + Z_{\delta} k_i}{a_{\alpha \delta} k_i}$$

$$d_{\gamma 3} = \frac{M_{\delta} k_q + Z_{\delta} k_{\gamma} - (M_q + Z_{\alpha})}{a_{\alpha \delta} k_i}$$

$$d_{\gamma 4} = \frac{1}{a_{\alpha \delta} k_i}$$

In the abbreviations in equation (4.42), the following definitions are made:

$$a_{\alpha \delta} = M_{\delta} Z_{\alpha} - M_{\alpha} Z_{\delta} \quad (4.43)$$

$$a_{\delta q} = M_{\delta} Z_q - M_q Z_{\delta} \quad (4.44)$$

$$a_{\alpha q} = M_q Z_{\alpha} - M_{\alpha} Z_q \quad (4.45)$$

Here, the type number of the designed control system is equal to one.

Also, the characteristic polynomial of the transfer function in equation (4.42) is as follows:

$$D(s) = d_{\gamma 4} s^4 + d_{\gamma 3} s^3 + d_{\gamma 2} s^2 + d_{\gamma 1} s + 1 \quad (4.46)$$

In order to determine the controller gains k_γ , k_θ , k_q and k_i , the fourth-order Butterworth polynomial given below can be used in the pole placement:

$$B_4(s) = \left(\frac{1}{\omega_c^4} \right) s^4 + \left(\frac{2.613}{\omega_c^3} \right) s^3 + \left(\frac{3.414}{\omega_c^2} \right) s^2 + \left(\frac{2.613}{\omega_c} \right) s + 1 \quad (4.47)$$

Matching equations (4.46) and (4.47) term by term, the matrix equation to solve k_γ , k_θ , k_q and k_i appears as

$$\begin{bmatrix} k_\gamma \\ k_\theta \\ k_q \\ k_i \end{bmatrix} = \hat{M}_k^{-1} \bar{b}_k \quad (4.48)$$

where

$$\hat{M}_k = \begin{bmatrix} 0 & 0 & 0 & a_{\alpha\delta} \\ Z_\delta & 0 & M_\delta & -\frac{2.613 a_{\alpha\delta}}{\omega_c^3} \\ a_{\delta q} & M_\delta & a_{\alpha\delta} & Z_\delta - \frac{3.414 a_{\alpha\delta}}{\omega_c^2} \\ a_{\alpha\delta} & a_{\alpha\delta} & 0 & a_{\alpha q} - \frac{2.613 a_{\alpha\delta}}{\omega_c} \end{bmatrix}$$

$$\bar{b}_k = [\omega_c^4 \quad M_q + Z_\alpha \quad a_{\alpha q} - M_\alpha \quad 0]^T$$

In order to keep the stability of the control system, k_γ , k_θ , k_q and k_i should be updated continuously depending on the current values of M_∞ , α , δ_e and ϕ_δ .

Equating the determinant of \hat{M}_k to zero, the following equality arises:

$$a_{\alpha\delta} M_\delta = 0 \quad (4.49)$$

Thus, equation (4.49) yields the following two singularity conditions:

$$C_{m_\delta} = 0 \quad (4.50)$$

$$C_{m_\alpha} C_{z_\delta} - C_{m_\delta} C_{z_\alpha} = 0 \quad (4.51)$$

In order to control a missile aerodynamically, i.e., to control it by means of control fins in a certain arrangement, the aerodynamic stability derivative contributing to the fin deflection (C_{m_δ}) must be nonzero. Therefore, unless the missile under consideration is controlled by a way other than aerodynamic control, the first condition in equation (4.50) can not be held.

Putting the relationships $C_{m_\alpha} = b_\alpha C_{z_\alpha}$ and $C_{m_\delta} = b_\delta C_{z_\delta}$, where b_α and b_δ are the pressure center offset and the static offset term relating to the hinge locations of the elevators and rudders, into equation (4.51), the second singularity condition reduces to the following equality:

$$b_\alpha = b_\delta \quad (4.52)$$

Considering the missile geometry, b_α can not be equal to b_δ . Therefore, this condition is not encountered in practice.

Regarding the yaw plane motion of the missile, the side-slip angle and the component of the missile acceleration in $\bar{u}_2^{(b)}$ direction are defined in the yaw plane as

$$\beta = (\eta_m - \psi)\cos(\theta_1) \quad (4.53)$$

$$a_y = v_M \dot{\eta}_m \cos(\gamma_m) \quad (4.54)$$

Then, considering equations (2.113), (2.117), (2.137), (2.141), (4.53) and (4.54) along with the equality $\dot{\psi}_1 = \frac{r}{\cos(\theta_1)}$, the transfer function of the closed-loop transfer function of the flight path angle control system in the yaw plane can be obtained as follows using the same state feedback structure with an integrator as the flight path angle control system in the pitch plane:

$$\frac{\eta_m(s)}{\eta_{md}(s)} = \frac{n_{\eta 3} s^3 + n_{\eta 2} s^2 + n_{\eta 1} s + 1}{d_{\eta 4} s^4 + d_{\eta 3} s^3 + d_{\eta 2} s^2 + d_{\eta 1} s + 1} \quad (4.55)$$

where

$$n_{\eta 1} = \frac{k_\eta}{k_i} + \frac{a_{\delta r}}{a_{\beta \delta}}$$

$$n_{\eta 2} = \frac{a_{\delta r} k_\eta \cos(\theta_1)}{a_{\beta \delta} k_i} + \frac{Y_\delta \cos(\theta_1)}{a_{\beta \delta}}$$

$$n_{\eta 3} = \frac{Y_{\delta} k_{\eta} \cos(\theta_1)}{a_{\beta\delta} k_i}$$

$$d_{\eta 1} = \frac{k_{\psi} + k_{\eta}}{k_i} + \frac{a_{\delta r} \cos(\theta_1)}{a_{\beta\delta}}$$

$$d_{\eta 2} = \frac{N_{\beta} + N_{\delta} k_{\psi} + (a_{\beta r} + a_{\beta\delta} k_r + a_{\delta r} k_{\eta} + Y_{\delta} k_i) \cos(\theta_1)}{a_{\beta\delta} k_i}$$

$$d_{\eta 3} = \frac{[N_{\delta} k_r + Y_{\delta} k_{\eta} - (N_r + Y_{\beta})] \cos(\theta_1)}{a_{\beta\delta} k_i}$$

$$d_{\eta 4} = \frac{\cos(\theta_1)}{a_{\beta\delta} k_i}$$

As k_{η} , k_{ψ} , k_r and k_i stand for the controller gains, the following definitions are used in equation (4.55):

$$a_{\beta\delta} = N'_{\beta} Y'_{\delta} - N_{\delta} Y'_{\beta} \quad (4.56)$$

$$a_{\delta r} = N_{\delta} Y'_r - N_r Y'_{\delta} \quad (4.57)$$

$$a_{\beta r} = N_r Y'_{\beta} - N'_{\beta} Y'_r \quad (4.58)$$

where

$$Y'_{\beta} = \frac{Y_{\beta} \cos(\theta_1)}{v_M \cos(\gamma_m)}, \quad Y'_{\delta} = \frac{Y_{\delta}}{v_M \cos(\gamma_m)}, \quad Y'_r = \frac{Y_r}{v_M \cos(\gamma_m)} Y_r \quad \text{and}$$

$$N'_{\beta} = N_{\beta} \cos(\theta_1).$$

Then, the controller gains of the pitch angle and the yaw plane flight path angle control systems can be determined in the same manner as for the pitch plane flight path angle control system.

4.2. Anti-Windup Scheme

Many dynamic systems behave “almost” linearly under certain operating conditions and therefore linear control theory is widely applicable. However quite often, e.g. when operating a system on its limits, different kinds of nonlinearities may degrade the stability and performance properties to such an extent that they are no longer acceptable. These nonlinearities must then be taken into account when designing and implementing the controller. Actuator nonlinearities, such as amplitude and rate limiters, appearing at the plant input, are examples of such nonlinearities [88]. In fact, in the presence of saturation, the phenomenon known as the integrator windup arises [89]. In the case of a windup, the input signals to the actuator exceeds the acceptable level of the actuator [90]. Thus, the real plant input may differ from the controller output. This discrepancy not only leads to the deterioration of the system behavior [91], but it also causes the error integral to attain large magnitudes, which leads to an abrupt and jerky behavior of the control input after the release of the saturation. Probably the most widely used remedy to this problem is the so-called “anti-windup compensation”.

Anti-windup compensators are widely used in practice for the control of systems with saturating actuators. An anti-windup compensator consists of a nominal (most often linear) controller appended with an anti-windup compensation. An important property of the anti-windup compensation is that it leaves the loop unaffected as long as saturation does not occur. Consequently, the control action provided by the anti-windup compensator is identical to that of the nominal controller as long as the control signals operate within the saturation limits [88].

Anti-windup was originally used for preventing the integrator state in PID (proportional plus integral plus derivative) controllers from growing large, which may cause overshoots and limit cycles [88]. The typical method to deal with the integrator windup problem is to tune the controller ignoring the actuator saturation and subsequently to add an anti-windup compensator to prevent the degradation of performance. Basically, the compensator design techniques belong to two different approaches [89]:

- Conditional Integration
- Back-Calculation

In the former approach, the value of the integrator is frozen when the actuator output is equal to the actuator input [89]. In the latter method, the difference between the controller output and the actual process input is fed back to the integral term [89], [91]. This way, the contribution of the integral state to the manipulated variable is removed until the difference becomes zero.

In this study, the back-calculation method is applied to the designed control system. As an example, the implementation of the mentioned method on the acceleration control system is shown in Figure 4.4.

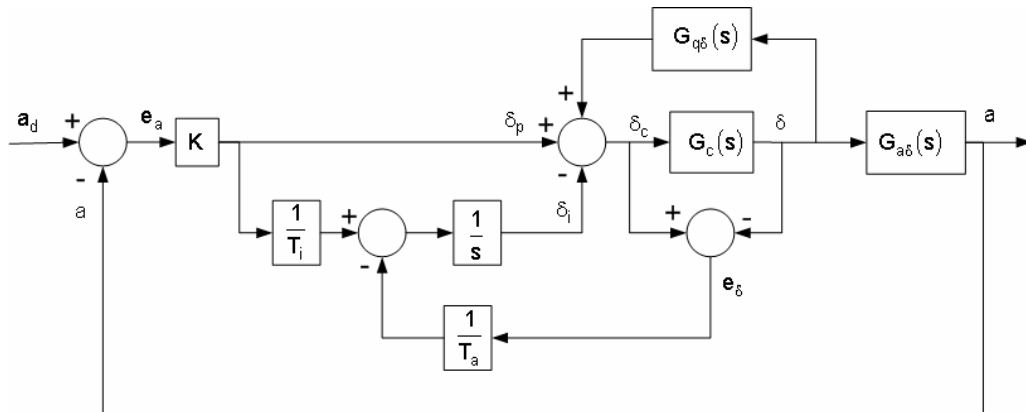


Figure 4.4. Anti-Windup Scheme

From Figure 4.4, the cumulative command signal produced by the autopilot (δ_c) is combined of the proportional (δ_p) and the integral (δ_i) portions as indicated below:

$$\delta_c = \delta_p + \delta_i \quad (4.59)$$

Looking at the block diagram in Figure 4.4, δ_p and δ_i are equal to the following quantities:

$$\delta_p = K e_a \quad (4.60)$$

$$\delta_i = \left[K e_a \left(\frac{1}{T_i} \right) - e_\delta \left(\frac{1}{T_a} \right) \right] \frac{1}{s} \quad (4.61)$$

In equations (4.60) and (4.61), K , T_i and T_a represent the proportional gain, the integral time constant and the anti-windup time constant of the control system. Also, e_a and e_δ denote the errors of the entire control system and the control actuation system (CAS) shown by the transfer function $G_c(s)$.

With the anti-windup scheme, it is intended to nullify δ_i either when $\delta_c < \delta_{\min}$ or when $\delta_c > \delta_{\max}$ where δ_{\min} and δ_{\max} stand for the lower and upper limits on the fin deflection that can be realized by the CAS. When this nullification occurs, equation (4.61) results in

$$\frac{e_\delta}{T_a} = \frac{K e_a}{T_i} \quad (4.62)$$

Once the condition in equation (4.62) holds, the integrator will not contribute to the command signal anymore. In application, this condition can be satisfied in two different ways:

i. T_a is set in order to be equal to T_i .

ii. T_a is scheduled continuously such that $T_a = \frac{e_\delta}{K e_a} T_i$. This way,

without waiting for the occurrence of the condition $e_\delta = K e_a$, the integrator output can be made zero whenever either of the conditions $\delta_c < \delta_{\min}$ and $\delta_c > \delta_{\max}$ holds.

As an alternative approach, the integrator output can be nullified as soon as the actuation system error (e_δ) becomes nonzero. This scheme can be formulated as follows [89]:

$$\delta_i = \frac{K e_a}{T_i s} [1 - \text{sgn}(|e_\delta|)] \quad (4.63)$$

In equation (4.63), the signum function is defined as

$$\text{sgn}(x) = \begin{cases} -1 & , \text{ if } x < 0 \\ 0 & , \text{ if } x = 0 \\ 1 & , \text{ if } x > 0 \end{cases} \quad (4.64)$$

According to equation (4.63), as soon as e_δ takes a nonzero value, δ_i will vanish immediately. Conversely, as long as e_δ keeps being zero, δ_i will remain nonzero and keep contributing to the command signal to the CAS.

4.3. Roll Resolving Scheme

During its flight, the missile might roll due to disturbances such as asymmetrical winds and manufacturing errors that cause misalignments. Even if the missile is roll position stabilized, a certain amount of offset in the roll attitude (ϕ_1) might be unavoidable. In this case, the fin deflection commands received from the autopilots need to be compensated to allow for this effect. If it is not done, the pitch and yaw control channels get mixed up and it becomes impossible to control the missile in either direction. Supposing that the missile rolls with an angle ϕ_1 at a certain time instant, the commands sent to the fins for the three actuators 1, 3, and, 2 and 4 together have to be modified as follows [7]:

$$\delta_{1c} = -\delta_{ec} \sin(\phi_1) + \delta_{rc} \cos(\phi_1) + \delta_{ac} \quad (4.65)$$

$$\delta_{3c} = \delta_{ec} \sin(\phi_1) - \delta_{rc} \cos(\phi_1) + \delta_{ac} \quad (4.66)$$

$$\delta_{24c} = \delta_{ec} \cos(\phi_1) + \delta_{rc} \sin(\phi_1) \quad (4.67)$$

CHAPTER 5

TARGET MOTION ESTIMATION

This chapter begins with the modeling of the target considered in this study. Then, the properties of the seeker suitable for the engagement purpose are explained in addition to the external contributors affecting its performance. After introducing the basic seeker types, they are compared according to certain criteria. The chapter is concluded by the design of an estimator that is to be used in the estimation of the target states.

5.1. Target Model

In this study, the considered missile is taken to be an air-to-surface missile. In other words, it is fired from an air platform against a surface target. Moreover, the mission of the missile is defined in short range.

Regarding a surface target, the kinematic parameters describing its motion on the horizontal plane are the normal and tangential acceleration components, (a_T^n and a_T^t), the target velocity (v_T) and the heading angle (η_t). They are depicted in Figure 5.1. In this figure, the capital letters M and T denote the missile and the target.

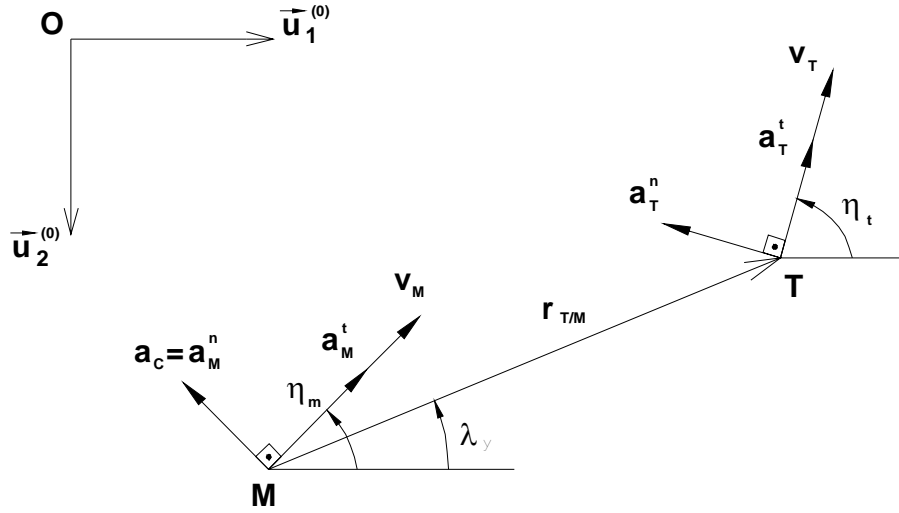


Figure 5.1. Horizontal Engagement Geometry

Specifying a_T^n and a_T^t as well as the initial values of the target velocity and the heading angle (v_{T0} and η_{t0}), v_T and η_t can be obtained as functions of time by means of the following integrals:

$$v_T(t) = v_{T0} + \int_{t_0}^t a_T^t(s) ds \quad (5.1)$$

$$\eta_t(t) = \eta_{t0} + \int_{t_0}^t \frac{a_T^n(s)}{v_T(s)} ds \quad (5.2)$$

Afterwards, regarding its initial position components (x_{T0} and y_{T0}), the position of the target can be described by the following equations as functions of time:

$$x_T(t) = x_{T0} + \int_{t_0}^t v_T(s) \cos(\eta_t(s)) ds \quad (5.3)$$

$$y_T(t) = y_{T0} + \int_{t_0}^t v_T(s) \sin(\eta_t(s)) ds \quad (5.4)$$

Actually, the motion surface of the target is not planar. However, in order to simplify the engagement problem, the altitude of the target is taken to be constant in the computer simulations as given below:

$$z_T(t) = z_{T0} \quad (5.5)$$

5.2. Seeker Model

In order to guide a missile for a successful intercept with an enemy target, it is vital to get the correct information about the motion of the target during the flight. In homing guidance schemes, that information is provided by seekers [23].

In all the homing guidance laws, the line of sight (LOS) angles (azimuth and elevation) should be correctly measured. Considering the pitch plane motion of the missile, the schematic representation of the LOS angle is given in Figure 5.2 along with the other basic seeker angles. In this figure, θ , θ_s , λ_p , ε and Ω denote the pitch angle of the missile, the seeker angle in the pitch plane, the pitch plane LOS angle, the boresight angle, and the error angle between the apparent and true LOS angles, respectively. Here, the apparent LOS is resulted from the refraction of the true LOS by the radome of the missile. The similar angle definitions can be made for the yaw plane motion as well.

The measurement capability of seekers is restricted due to some physical, optical and electronic limitations such as limited field-of-view (FOV), atmospheric transmittance and noise effects. Actually, a seeker is a combination of optical, electronic and mechanical components. Therefore, the seeker modeling process includes the integration of the models of all the optical, electronic and mechanical subsystems.

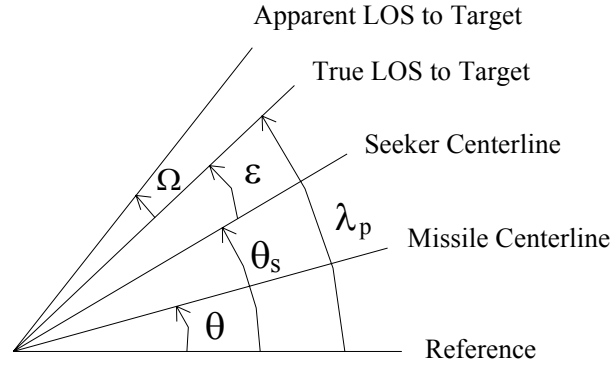


Figure 5.2. Basic Seeker Angle Definitions for the Pitch Plane Motion

5.2.1. Atmospheric Transmittance

Atmospheric transmittance is basically described by means of two main criteria: extinction and visibility. The extinction is the total reduction of radiation along the LOS. This includes both absorption and scattering [65], [92]. The absorption of radiation is caused by the molecular constituents of the atmosphere, i.e., water vapor, carbon dioxide and ozone. The concentration of these molecules depends on the temperature, the pressure, the geographical location, the altitude and the weather conditions [65]. On the other hand, the scattering simply alters the radiation propagation direction and any radiation scattered out of the LOS contributes extinction [92]. As the functions of the incident radiation (R_i) and the volume of the scattering particles (V_p), the scattering (σ) can be obtained as

$$\sigma = K_{\sigma} R_i V_p^2 \quad (5.6)$$

where K_{σ} denotes the scattering coefficient.

The other criterion in evaluating the atmospheric transmittance is visibility. The visibility depends on the aerosol distribution and it is very

sensitive to the local meteorological conditions such as snow and rain. It is also dependent upon the view angle with respect to the sun. As the sun angle approaches the view angle, the forward scattering into the LOS increases and the visibility decreases [92].

5.2.2. Seeker Performance

Essentially, the seeker performance depends on both resolution and sensitivity. Here, the resolution is the measure of obtaining the finest signal and the sensitivity deals with the smallest signal that can be detected. Using the resolution information of a seeker (ρ), the range from the target to the missile ($r_{T/M}$) can be estimated from the size of the target spot on the seeker detector (s_s) as

$$r_{T/M} \cong \frac{s_s}{\rho} \quad (5.7)$$

The sensitivity of the seeker is generally identified using the signal-to-noise ratio ($R_{S/N}$). $R_{S/N}$ can be expressed in terms of the average atmospheric attenuation coefficient ($\tau_{atm-ave}^R$), the intensity difference between the target and its background (ΔI), and the standard deviation of the system noise (n_s) as given below:

$$R_{S/N} = \frac{\tau_{atm-ave}^R \Delta I}{n_s} \quad (5.8)$$

In the infrared imaging systems, ΔI is specified by a differential temperature (ΔT) and the system noise is taken as the noise equivalent

differential temperature (ΔT_n). That is, $R_{S/N}$ can be redefined for infrared systems as [92]

$$R_{S/N} = \frac{\tau_{\text{atm-ave}}^R \Delta T}{\Delta T_n} \quad (5.9)$$

Another factor influencing the performance of a seeker is the radome refraction. The radome refraction is the function of the geometry of a radome. Namely, although the ogive shape is preferable in the radome design to reduce the aerodynamic drag effect on the missile, it is the worst choice in the sense of the radome refraction. Conversely, the minimum refraction on the signals coming from the target to the seeker aperture occurs when the radome is in the semi-spherical shape [23]. As K_R denotes the radome refraction factor, the standard deviation of the radome refraction noise (n_R) can be estimated in the pitch plane as

$$n_R = K_R \theta_s \quad (5.10)$$

5.2.3. Seeker Dome Materials

The seeker dome materials are grouped based on their best applicability to multimode [radio-frequency (RF)/infrared (IR)], RF-only and mid-wave IR-only seekers. Measures of merit are the dielectric constant, combined mid-wave/long wave infrared bandpass, transverse strength, thermal expansion, erosion resistance and maximum short-duration temperature. Dome materials that are especially suited for combined radar and infrared seekers are zinc sulfide and zinc selenide. The zinc sulfide has advantages in the dielectric constant, transverse strength and rain erosion [93].

5.2.4. Seeker Types

Basically, two types of seekers are used in guidance applications:

- Gimballed Seekers
- Strapdown or Body-Fixed Seekers

5.2.4.1. Gimballed Seekers

Because of the field-of-view (FOV) limitations of seekers, the gimballed seekers are preferred if it is desired to increase the FOV range. In this scheme, the seeker is mounted on a platform supported by two orthogonal gimbals and stabilized by means of rate gyro feedbacks. This way, the FOV range of the seeker is increased considerably. Also, the LOS angle and the LOS angular rate can be measured directly independently of the missile motion.

A simplified model of a planarly working gimballed seeker structure is shown in Figure 5.3. In this figure, N , $G_D(s)$, K_D , T_D , $G(s)$ and K_R represent the total noise, the detector transfer function, the detector amplifying gain, the tracker delay, the transfer function of the gimbal control system and the radome refraction factor, respectively. Also, regarding the pitch plane, ε_D and $\dot{\theta}_s^*$ stand for the detector output signal and the desired seeker angular rate. In this model, the aim is to measure the pitch plane LOS rate ($\dot{\lambda}_p$). The same gimballed seeker model can be adapted to the yaw plane in order to measure the yaw plane LOS rate as well.

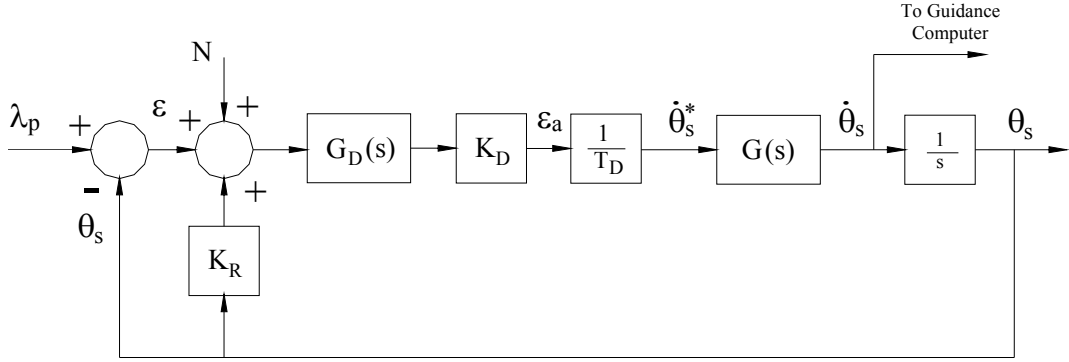


Figure 5.3. Gimballed Seeker Model

As given in Figure 5.3, the noise effects (N) acting on the seeker can be classified as the range independent noises and the range dependent noises. While the major source of the range independent noises is the noises resulting from the components of the gimbal servosystem, the glint and the receiver noises constitute the most significant range dependent noises [94]. As n_g and n_r stand for the standard deviations of the glint and the receiver noises, they can be expressed in terms of the relative distance between the missile and the target ($r_{T/M}$) as

$$n_g = \frac{K_g}{r_{T/M}} \quad (5.11)$$

$$n_r = K_r r_{T/M} \quad (5.12)$$

where K_g and K_r are the glint and the receiver coefficients.

In the model shown in Figure 5.3, $G_D(s)$ can be taken to be unity. Also, since the bandwidth of the gimbal control system is higher than the bandwidth

of the entire control system, $G(s)$ can also be considered to be unity. Hence, the transfer function from λ_p to θ_s can be simply written as

$$\frac{\lambda_p(s)}{\theta_s(s)} = \frac{1}{T_p s + K_p} \quad (5.13)$$

where $T_p = \frac{T_D}{K_D}$ and $K_p = 1 - K_D$.

For the yaw plane LOS rate, equation (5.13) can be adapted as

$$\frac{\lambda_y(s)}{\psi_s(s)} = \frac{1}{T_y s + K_y} \quad (5.14)$$

where ψ_s and λ_y denote the seeker angle in the yaw plane and the yaw plane LOS angle.

5.2.4.2. Strapdown Seekers

The strapdown seekers are directly mounted on the missile body. Therefore, their measurements become relative to the body fixed reference frame of the missile.

In the literature, two different kinds of strapdown seekers are mentioned:

- Beam-Steered Strapdown Seeker Model
- Staring Strapdown Seeker Model

In the former type, the FOV of the detector is enlarged by means of a movable lens called “vario lens”. In this structure, the vario lens slides along a short rail-like guide so as to enlarge the FOV. On the other hand, the lens of the detector is fixed in the latter model that has a narrower FOV than the former one.

The simplified block diagram of a strapdown seeker working in the pitch plane is given in Figure 5.4.

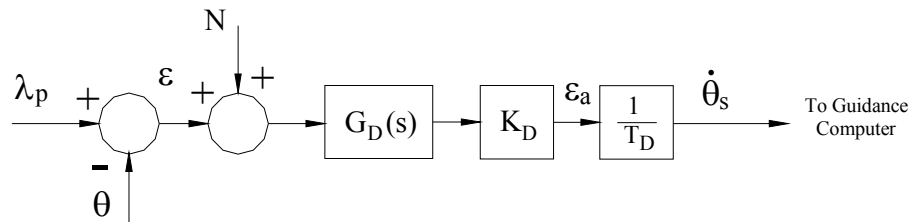


Figure 5.4. Strapdown Seeker Model

5.2.4.3. Comparison of Gimballed and Strapdown Seeker Models

The comparison of gimballed and strapdown seeker models according to some significant criteria is given in Table 1.

Table 1. Comparison of Gimballed and Strapdown Seeker Models [95]

	Gimballed Seeker	Strapdown Seeker
Mounting	Mounted on a two-gimbal platform.	Rigidly mounted on the missile's body, doing away with a gimballed platform
FOV	Up to $\pm 90^\circ$	About $\pm 3^\circ$
Angle and Rate Measurements	LOS angle and LOS angular rate error angles with respect to the ground	LOS angle and LOS angular rate error angles between the the missile centerline and the LOS.

Table 1 (Continued)

Guidance Law Utilization	Proportional Navigation can be easily implemented because of the provision of LOS rate.	Conventional Proportional Navigation Law can not be easily applied.
Measurement Results	Virtually independent of the missile body motion.	Contains the missile body motion.
Major Sources of Measurement Errors	Gyro drift, gimbal friction, gimbal cross-couplings, radome refraction and acceleration sensitivity.	Seeker measurements themselves, glint noise and inherent angle alignment errors.
Cost	Higher than strapdown seeker because of the gimbals.	Low.

5.2.5. Seeker Detector Model

Detector is the heart of every electro-optical system because it converts scene radiation into a measurable electrical signal.

The capability of a detector is defined by the parameter detectivity (D^*). As R , A_d , Δf_e and i_n denote the responsivity, the detector area, the differential noise frequency and the standard deviation of the noise on the detector current, D^* can be formulated as

$$D^* = \frac{R \sqrt{A_d \Delta f_e}}{i_n} \quad (5.15)$$

In fact, D^* is a measure of detector noise. That is, as D^* increases, the noise equivalent differential temperature decreases. Also, real detectors have a D^* that is a function of the operating temperature.

As ε and ε_D denote the error angle between the true LOS angle and the seeker angle, and the detector output signal, there is a nonlinear relationship between them as shown below:

$$\varepsilon_D = K \varepsilon_{DN} \sin\left(\frac{\varepsilon}{\varepsilon_{DN}}\right) + (1 - K) \varepsilon_{UP} \tan\left(\frac{\varepsilon}{\varepsilon_{UP}}\right) \quad (5.16)$$

where

$$\varepsilon_{DN} = \sqrt{\frac{\theta_{(1/2)FOV}^3}{6 \Delta\theta_{FOV}}}$$

$$\varepsilon_{up} = \sqrt{\frac{\theta_{(1/2)FOV}^3}{3 \Delta\theta_{FOV}}}$$

$\theta_{(1/2)FOV}^3$: Sensor half-instantaneous field of view (IFOV) angle

$\Delta\theta_{FOV}$: Sensor half-IFOV deviation

K : Detector gain

Using the Taylor series expansions of the sine and tangent functions, equation (5.12) can be approximated as

$$\frac{\varepsilon_D}{\varepsilon} \cong 1 + (1 - 2K) \left(\frac{\Delta\theta_{\text{FOV}}}{\theta_{(1/2)\text{FOV}}^3} \right) \varepsilon^2 \quad (5.17)$$

Actually, the value of K varies between zero and unity. In most cases, it is taken to be 0.5. In this case, ε_D appears to be equal to ε . In the Laplace domain, this equality leads the detector transfer function $[G_D(s)]$ to become unity.

In some of the applications, ε is calculated from the location of target spot on a four-quadrant detector. As shown in Figure 5.5, ε can be obtained in the following manner:

$$\varepsilon = \sqrt{\varepsilon_y^2 + \varepsilon_p^2} \quad (5.18)$$

where ε_y and ε_p stand for the components of ε in the yaw and pitch planes.

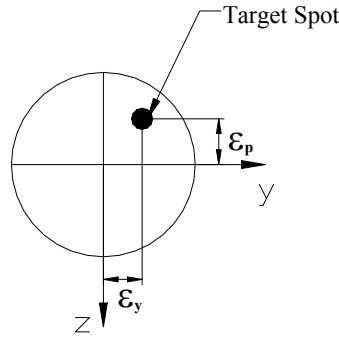


Figure 5.5. Target Spot on a Four-Quadrant Detector

5.3. Target State Estimator

In a missile-target engagement scenario, the seeker of the missile is subjected to several noises and disturbances. Due to those effects, the missile

seeker provides a noisy measurement of the LOS angle. Therefore, the use of a simple digital fading memory filter as a part of the missile guidance system is one of the simplest and most effective ways to get an estimate of the LOS angle and its rate from the noisy measurements. Also, the mentioned state estimator will be used in the prediction of the motion of the target when the target becomes invisible during the guidance phase due to some external effects such as a cloud.

In the state estimator model considered in this study, first, the detection limits of the seeker are defined. Regarding the seeker with a detectable range (r_s) and seeker angle limits in the yaw and pitch planes (ψ_s and θ_s), the receiver of the considered seeker generates nonzero signals provided that all the following conditions are satisfied:

$$\psi - \psi_s \leq \lambda_y \leq \psi + \psi_s, \quad \theta - \theta_s \leq \lambda_p \leq \theta + \theta_s \quad \text{and} \quad r_{T/M} \leq r_s \quad (5.19)$$

where ψ and θ stand for the yaw and pitch angles of the missile. Also, λ_y , λ_p and $r_{T/M}$ denote the yaw and pitch plane components of the LOS angle and the relative distance of the target with respect to the missile. Once all the conditions above are satisfied, the seeker transmits the information of λ_y , λ_p and $r_{T/M}$ quantities to the guidance block. In the determination of the value of r_s , the international visibility code supplied in Table 2 are considered.

Table 2. International Visibility Code [92]

Designation	Visibility (m)
Dense fog	0-50
Thick fog	50-200
Moderate fog	200-500
Light fog	500-1,000
Thin fog	1,000-2,000
Haze	2,000-4,000
Light haze	4,000-10,000
Clear	10,000-20,000
Very clear	20,000-50,000
Exceptionally clear	> 50,000

On the other hand, while the missile is passing through a cloud or when the target is out of the FOV of the seeker, the seeker can not sense the target, i.e., the receiver of the seeker generates zero signals for the location of the target. In such cases, in order to increase the probability of hitting to target, the missile can be made estimate the future behavior of the target. For this reason, a target state estimator is added to the the seeker system. In this study, a first order simple constant gain filter, i.e., a fading memory filter, is designed for the estimation of the target states. Using this filter, the yaw and pitch plane components of the LOS angle (λ_y and λ_p) are estimated as well as the corresponding LOS rates as described below:

$$\hat{\lambda}_{jk} = \hat{\lambda}_{j(k-1)} + \hat{\dot{\lambda}}_{j(k-1)} T_{sj} + G_j \left[\lambda_{jk}^* - \left(\hat{\lambda}_{j(k-1)} + \hat{\dot{\lambda}}_{j(k-1)} T_{sj} \right) \right] \quad (5.20)$$

$$\hat{\dot{\lambda}}_{jk} = \hat{\dot{\lambda}}_{j(k-1)} + \frac{H_j}{T_{sj}} \left[\lambda_{jk}^* - \left(\hat{\lambda}_{j(k-1)} + \hat{\dot{\lambda}}_{j(k-1)} T_{sj} \right) \right] \quad (5.21)$$

where

$j=y$ and p , i.e., yaw and pitch planes

λ_{jk}^* : LOS measurement of the seeker at instant k

$\hat{\lambda}_{jk}$: LOS estimate at instant k

T_{sj} : Sampling time

$$G_j = 1 - \beta_j^2$$

$$H_j = (1 - \beta_j)^2$$

β_j : Memory length

Here, the memory length lies between zero and unity, i.e., $0 < \beta_j < 1$.

If β_j is taken to be one, it means the filter does not take the seeker measurement of the LOS angle into account and works on the previous estimates only. Thus, as β_j is taken closer to zero, the filter accounts more about the LOS measurement. Therefore, for instance, the filter output becomes oscillating for $\beta_j = 0.3$, while a sluggish and lagged signal behaviour is observed for $\beta_j = 0.8$.

In this study, considering the pitch plane estimator, when either of $\lambda_p = \theta - \theta_s$ and $\lambda_p = \theta + \theta_s$ conditions satisfied, the pitch plane memory length (β_p) is taken to be β_s where $0.5 < \beta_s < 1$. On the other hand, β_p is made zero at $\lambda_p = \theta$. This is because the radome refraction effect will be minimum at $\lambda_p = \theta$ and thus only the measurement of the seeker can be

evaluated. Then, the β_p values for the $\theta - \theta_s \leq \lambda_p \leq \theta + \theta_s$ range are computed as follows:

$$\beta_p = \begin{cases} \frac{\beta_s}{\theta_s} (\theta - \lambda_p) & , \text{ for } \theta - \theta_s \leq \lambda_p \leq \theta \\ \frac{\beta_s}{\theta_s} (\lambda_p - \theta) & , \text{ for } \theta \leq \lambda_p \leq \theta + \theta_s \end{cases} \quad (5.22)$$

Similar to the pitch plane, the above procedure is applied to the yaw plane motion of the missile.

Moreover, when the seeker does not supply any signal, λ_{jk}^* is taken to be equal to the last estimate of the estimator.

CHAPTER 6

CASE STUDIES

In this chapter, the numerical parameters used in the models are first given and the models created in the Matlab-Simulink environment are introduced. After the formation of the test configurations as well as the sets of the initial conditions, the results of the performed computer simulations are presented in the form of tables and figures.

6.1. Considered Models

In order to see the performance of the considered guidance laws on different types of missiles, three different missile configurations are regarded in the computer simulations as follows:

- Two-part missile with uncanted tail fins
- Two-part missile with canted tail fins
- Single-part missile with uncanted tail fins

Actually, the first two missiles are the two variants of a two-part missile. Their only difference is the orientations angles of the fixed tail fins.

The numerical values of parameters these missile models are given in Table 3 and Table 4.

Table 3. Parameters of the Two-Part Missiles

Parameter	Symbol	Value
Missile Diameter	d_M	70 mm
Missile Cross-Sectional Area	S_M	3848.5 mm ²
Total Missile Length	L_M	2000 mm
Mass of the Front Body	m_1	10 kg
Mass of the Rear Body	m_2	7.55 kg
Total Missile Mass	m	17.55 kg
Axial Moment of Inertia of the Front Body	I_{a1}	0.01225 kg · m ²
Axial Moment of Inertia of the Rear Body	I_{a2}	0.01225 kg · m ²
Transverse Moment of Inertia of the Missile	I_t	5.855 kg · m ²
Viscous Damping Coefficient of the Bearing	b_t	4 N · m · s
Acceleration Limit	a_{\max}	30 · g
Cant Angle (for the Canted Configuration)	-	1 deg

Table 4. Parameters of the Single-Part Missile

Parameter	Symbol	Value
Missile Diameter	d_M	70 mm
Missile Cross-Sectional Area	S_M	3848.5 mm ²
Missile Length	L_M	2000 mm
Total Missile Mass	m	17.55 kg
Axial Moment of Inertia	I_{al}	0.0215 kg · m ²
Transverse Moment of Inertia of the Missile	I_t	5.855 kg · m ²
Acceleration Limit	a_{max}	30 · g

6.2. Aerodynamic Data

For the computer simulations, the aerodynamic stability derivatives are generated by the Missile Datcom software available at TÜBİTAK-SAGE. However, since the mentioned software can give solutions for only single-part missiles, the considered two-part missile is instantaneously handled as a single-part missile whose control fins and fixed tail fins are oriented at a fixed spin angle with respect to each other. Then, solving the missile aerodynamics for the different values of the spin angle, an aerodynamic data set is obtained for the two-part missile.

For this purpose, first, the aerodynamic coefficients C_x , C_z , C_l and C_m are obtained for the following values of the spin angle (ϕ_s), the elevator deflection (δ_e), the Mach number (M_∞) and the angle of attack (α):

$$\phi_s = 0, 10, 20, 30, 40, 45, 50, 70 \text{ and } 80 \text{ deg}$$

$$\delta_e = -20, -15, -10, -5, 0, 5, 10, 15 \text{ and } 20 \text{ deg}$$

$$M_\infty = 0.5, 1.0 \text{ and } 1.5$$

$$\alpha = -9, -8, -7, -6, -5, -4, -3, -2, -1, 0, 1, 2, 3, 4, 5, 6, 7, 8 \text{ and } 9 \text{ deg}$$

Afterwards, fitting the polynomials given in equations (2.136), (2.138), (2.139) and (2.140) to the obtained C_x , C_z , C_l and C_m values, the stability derivatives C_{z_α} , C_{z_δ} , C_{z_q} , C_{m_α} , C_{m_δ} , C_{m_q} and C_{l_δ} are computed for $M_\infty = 0.5, 1.0$ and 1.5 by changing ϕ_s from 0 to 80 degrees at an amount of 10 degrees.

Then, considering the rotational symmetry property of the missile, the stability derivatives C_{y_β} , C_{y_δ} , C_{y_r} , C_{n_β} , C_{n_δ} and C_{n_r} are found using equations (4.17) through (4.22).

6.3. Guidance and Control System Models

Using the designed transversal and roll autopilots, the yaw, pitch and roll control systems are constructed for the three missile types. As the transversal control systems, the acceleration and angle autopilots are employed. In the models, the roll autopilot is designed at the bandwidth of 20 Hz while the bandwidths of the yaw and pitch autopilots are chosen as 5 Hz. The unit step responses of the designed acceleration and fight path angle control systems for the pitch plane motion of the missile appear as shown in Figure 6. 1 and Figure 6. 2. As seen from the figures, the angle control system has a smaller maximum overshoot than the acceleration control system. However, the settling time of the acceleration control system is shorter than the other.

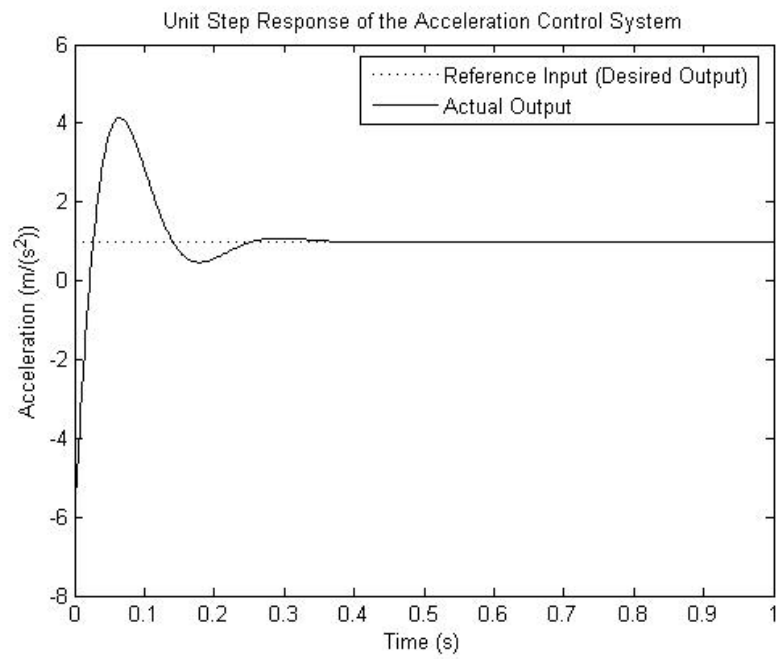


Figure 6. 1. Unit Step Response of the Acceleration Control System

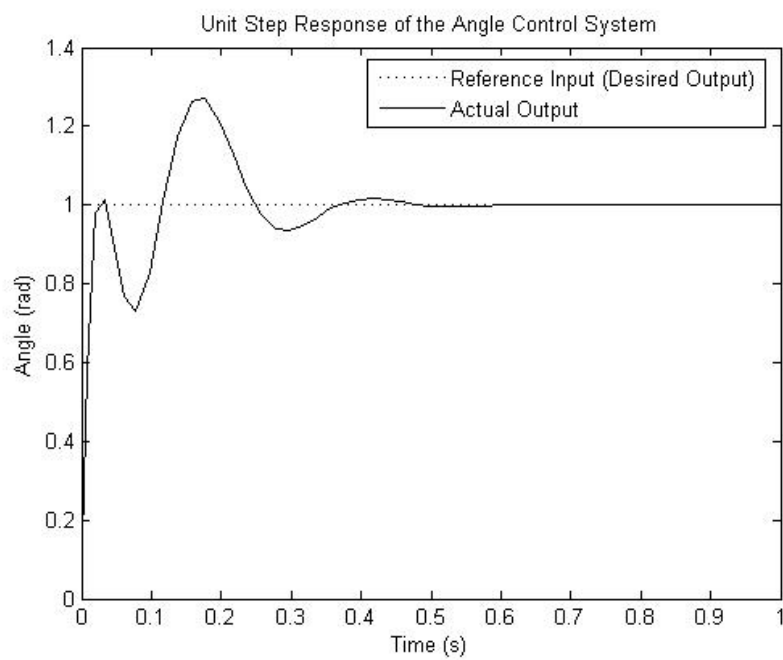


Figure 6. 2. Unit Step Response of the Angle Control System

After designing the control systems on the linearized missile dynamics, the resulting autopilots are applied to the nonlinear missile dynamics. Hence, the unit step responses of the acceleration and the angle control systems in the pitch plane come into the picture as shown in Figure 6. 3 and Figure 6. 4. As seen from the figures, since the initial conditions of the control systems applied to the nonlinear missile dynamics are different from zero, the initial values of the responses are different from those in the linearized control systems. Moreover, although the roll attitude of the missile is assumed to be regulated in the control system design upon the linearized model, the initial roll rates of the front and the rear bodies are different from zero in the computer simulations. For these reasons, the response characteristics of the control systems considering the linearized and the nonlinear missile dynamics are not the same.

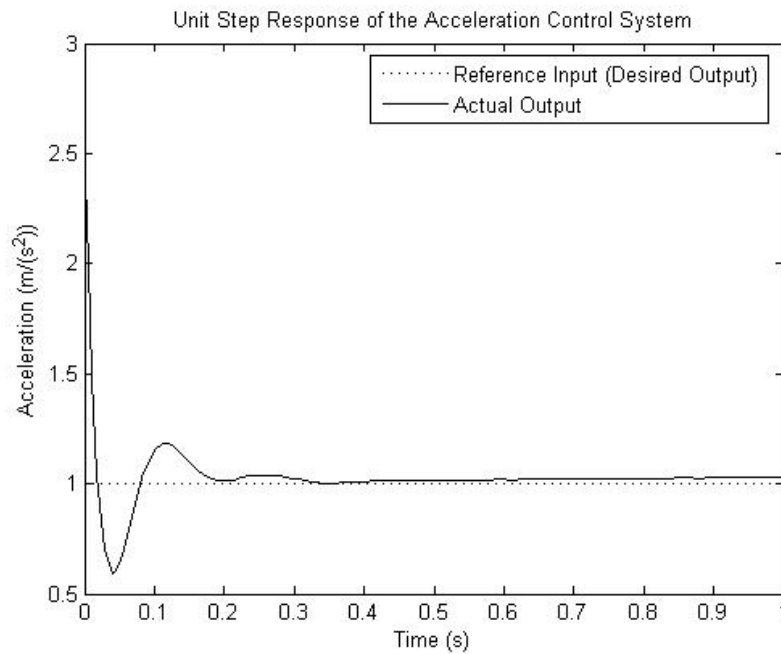


Figure 6. 3. Unit Step Response of the Acceleration Control System with Nonlinear Missile Dynamics

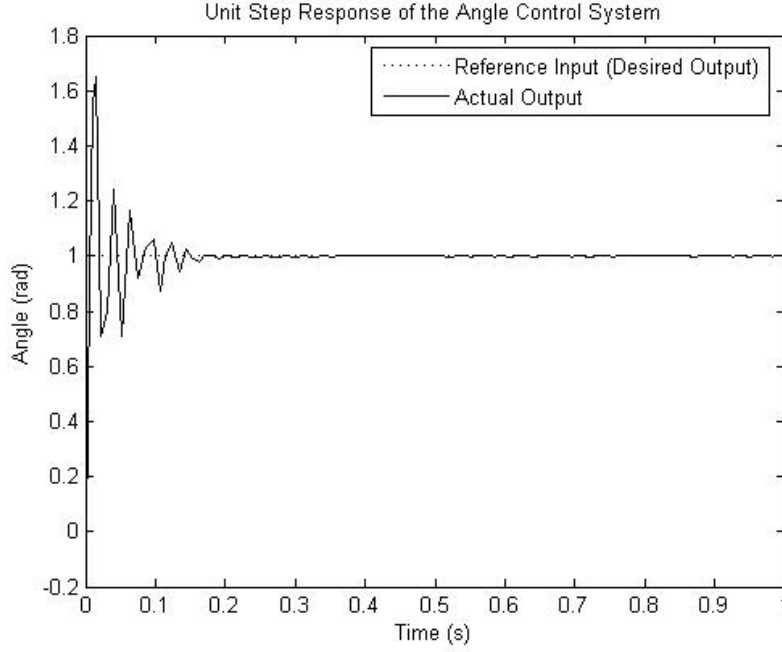


Figure 6. 4. Unit Step Response of the Angle Control System with Nonlinear Missile Dynamics

Then, the models for the target kinematics, the missile-target engagement geometry and the seeker are integrated to the control system models and the entire guidance and control system model is constructed for each missile type separately.

6.4. Simulation Results

In the computer simulations, the Proportional Navigation Guidance (PNG), the Linear Homing Guidance (LHG), and the Parabolic Homing Guidance (PHG) laws are used. Then, regarding these laws for the three missile types, the test configurations are formed as shown in Table 5.

Considering 0 and -20 degrees for the initial heading error of the missile and taking the lateral acceleration of the target as 0 and 0.5g, the test scenarios are constructed as in Table 6.

Table 5. Test Configurations

MISSILE TYPE	GUIDANCE LAW		
	PNG (N=3)	LHG	PHG
Two-part, uncanted	C1	C2	C3
Two-part, canted	C4	C5	C6
Single-part, uncanted	C7	C8	C9

Table 6. Test Scenarios

SCENARIO	HEADING ERROR (deg)	TARGET LATERAL ACCELERATION (g)
S1	0	0
S2	0	0.5
S3	-20	0
S4	-20	0.5

Also, the initial conditions in Table 10 are accounted in the computer simulations.

After constructing the guidance and control system model and setting the initial conditions, the computer simulations are carried out in the Matlab-Simulink environment for all the configurations and scenarios defined above. Hence, the total number of the different situations comes out to be 36. Performing the relevant computer simulations for each of these situations separately, the corresponding terminal miss distance, engagement time, maximum acceleration, and energy consumption values are determined as given in Table 8. In the computer simulations, the ODE 45 solver is used.

Table 7. Initial Conditions

Parameter	Symbol	Value
Position Component of the Target along x axis	x_{T0}	2000 m
Position Component of the Target along y axis	y_{T0}	650 m
Position Component of the Target along z axis	z_{T0}	0
Velocity of the Target	v_{T0}	25 m/s (=90 km/h)
Heading Angle of the Target	η_{t0}	0
Tangential Acceleration Component of the Target	a_T^t	0
Position Component of the Missile along x axis	x_{M0}	1000 m
Position Component of the Missile along y axis	y_{M0}	600 m
Position Component of the Missile along z axis	z_{M0}	200 m
Velocity of the Missile	v_{M0}	408 m/s (= 1.2 Mach)
Heading Angle of the Missile	η_{m0}	0
Flight Path Angle of the Missile	γ_{m0}	
Roll Rate of the Front Body (for the Two-Part Missiles)	p_0	50 rpm
Roll Rate of the Rear Body (for the Two-Part Missiles)	p_{20}	200 rpm
Roll Rate (for the Single-Part Missile)	p_0	150 rpm
Pitch Rate	q_0	0
Yaw Rate	r_0	
Angle of Attack	α_0	
Side-Slip Angle	β_0	

In the simulations, when the relative distance component in $\bar{u}_3^{(0)}$ direction, i.e., Δz , is equal or smaller than 75 cm, it is assumed that the missile-target engagement is terminated. In this case, the terminal miss distance is calculated using the values of the other relative distance components (Δx and Δy) at that instant as

$$d_{\text{miss}} = \sqrt{\Delta x^2 + \Delta y^2} \quad (6.1)$$

Thus, the time passing from the beginning of the engagement to the end of the engagement is taken to be the engagement time.

The maximum acceleration is obtained as the resultant of the missile acceleration components expressed in the wind frame (F_w).

Also, the total energy consumption of each situation is calculated as

$$E_{\text{tot}} = \int_{t_0}^{t_F} P_{\text{ins}} dt \quad (6.2)$$

where $P_{\text{ins}} = |Y v| + |Z w| + |L_1 p| + |M q| + |N r|$ is defined as the instantaneous power consumption.

Table 8. Simulation Results

Scen.	Conf.	Terminal Miss Distance (m)	Engagement Time (s)	Maximum Acceleration (g)	Total Energy Consumption (kJ)
S1	C1	4.840	3.047	2.951	12.257
	C2	2.435	3.052	57.154	2.755
	C3	7.645	3.040	12.928	33.514
	C4	4.854	3.051	2.954	12.305
	C5	2.852	3.057	57.317	2.736
	C6	7.960	3.044	12.795	33.415
	C7	5.310	3.272	5.562	24.331
	C8	3.553	3.216	57.317	32.082
	C9	10.536	3.231	14.748	46.748
S2	C1	4.632	3.038	3.084	13.415
	C2	3.430	3.039	57.154	2.699
	C3	7.171	3.031	11.936	29.677
	C4	4.704	3.042	3.086	13.462
	C5	3.453	3.043	57.154	2.725
	C6	7.376	3.035	11.855	29.569
	C7	5.439	3.262	12.338	49.217
	C8	3.472	3.201	57.317	44.293
	C9	9.592	3.222	12.854	44.867
S3	C1	5.578	3.288	16.528	217.395
	C2	3.205	3.049	942.950	172.717
	C3	3.473	3.299	12.109	228.143
	C4	5.025	3.295	16.528	217.165
	C5	3.546	3.053	942.950	172.716
	C6	3.811	3.303	12.109	227.846
	C7	6.857	3.613	16.528	224.044
	C8	3.355	3.238	942.316	156.197
	C9	5.192	3.723	12.109	278.941
S4	C1	5.597	3.306	16.528	239.068
	C2	3.325	3.039	942.950	172.852
	C3	3.387	3.325	12.702	263.109
	C4	5.096	3.312	16.528	238.855
	C5	3.359	3.043	942.950	172.655
	C6	3.554	3.330	12.702	262.900
	C7	6.972	3.656	16.528	255.258
	C8	3.229	3.218	943.129	215.950
	C9	4.364	3.788	12.702	353.138

The missile-target engagements in the pitch and yaw planes are submitted in the following figures for the configurations C1, C2 and C3 for all

the considered scenarios as well as the change of the relevant command accelerations in time.

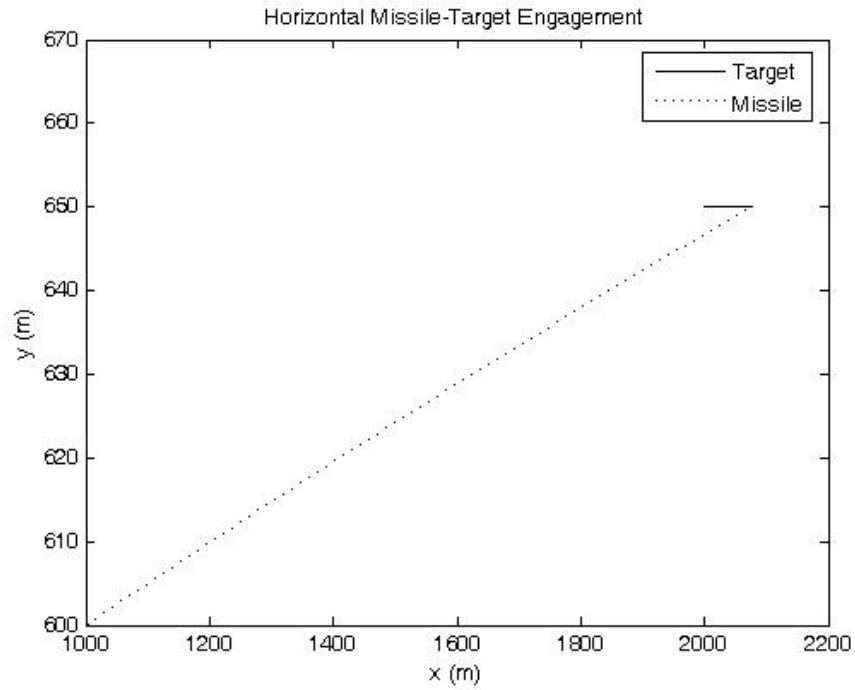


Figure 6. 5. Horizontal Missile-Target Engagement in the S1-C1 Situation

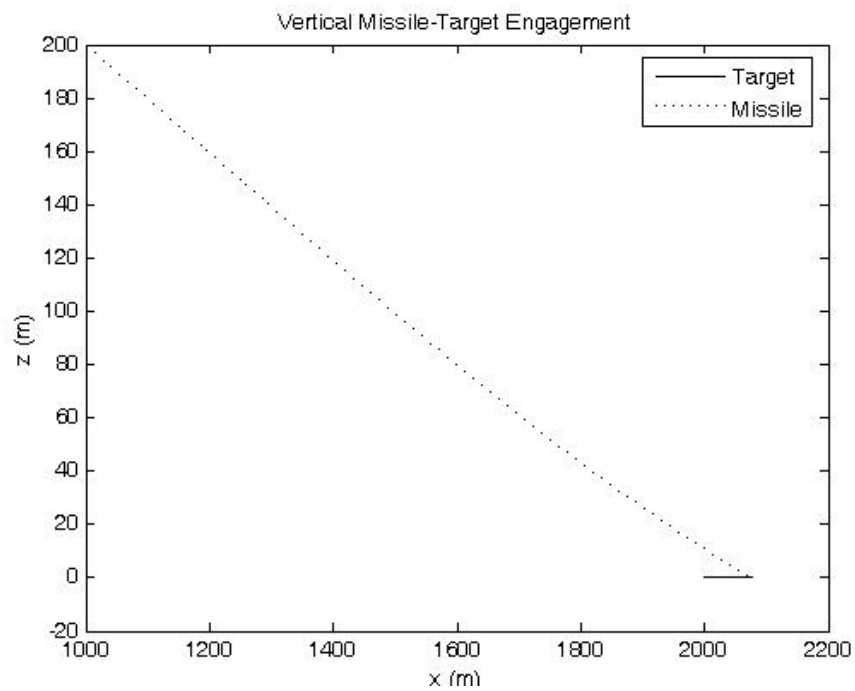


Figure 6. 6. Vertical Missile-Target Engagement in the S1-C1 Situation

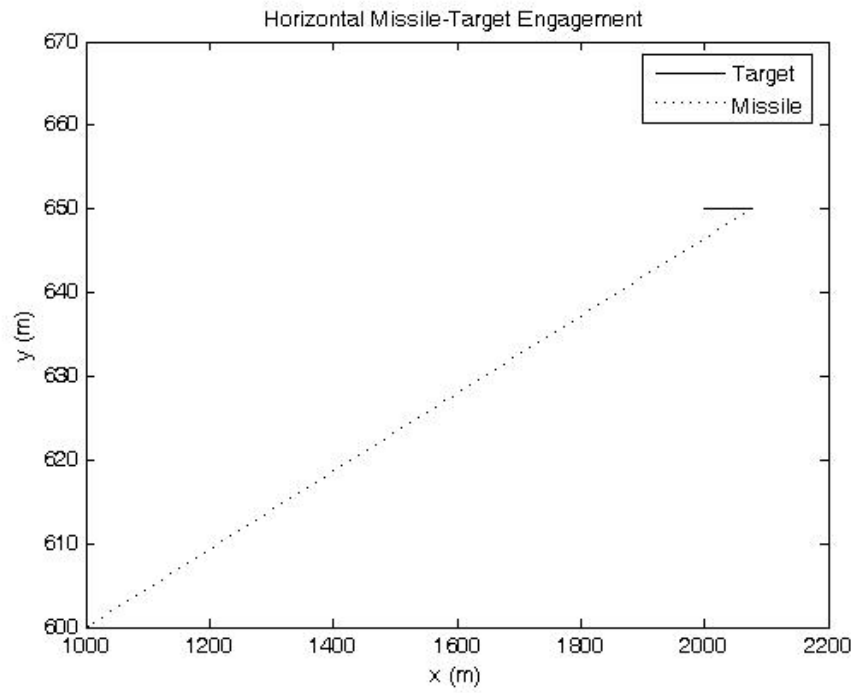


Figure 6. 7. Horizontal Missile-Target Engagement in the S1-C2 Situation

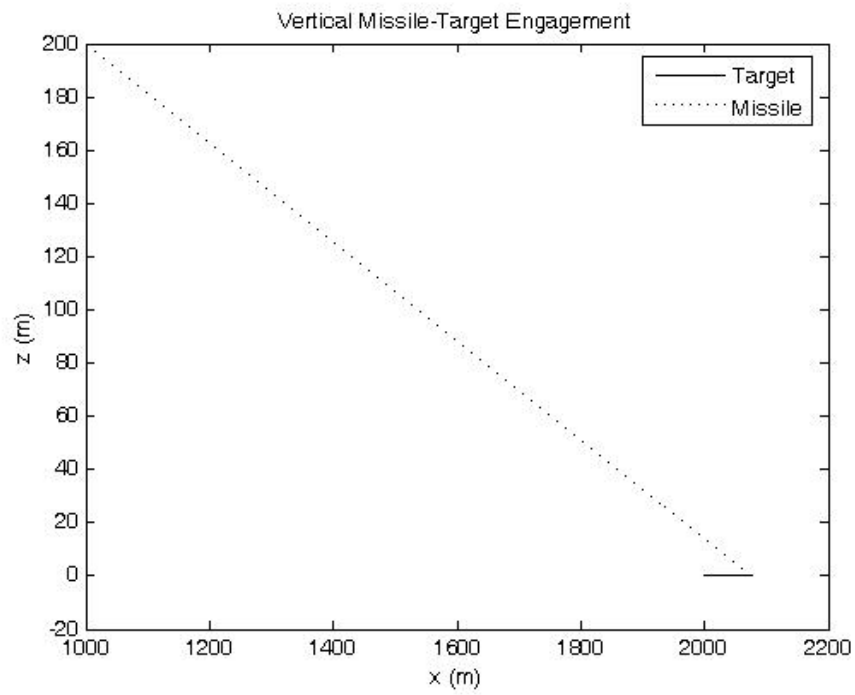


Figure 6. 8. Vertical Missile-Target Engagement in the S1-C2 Situation

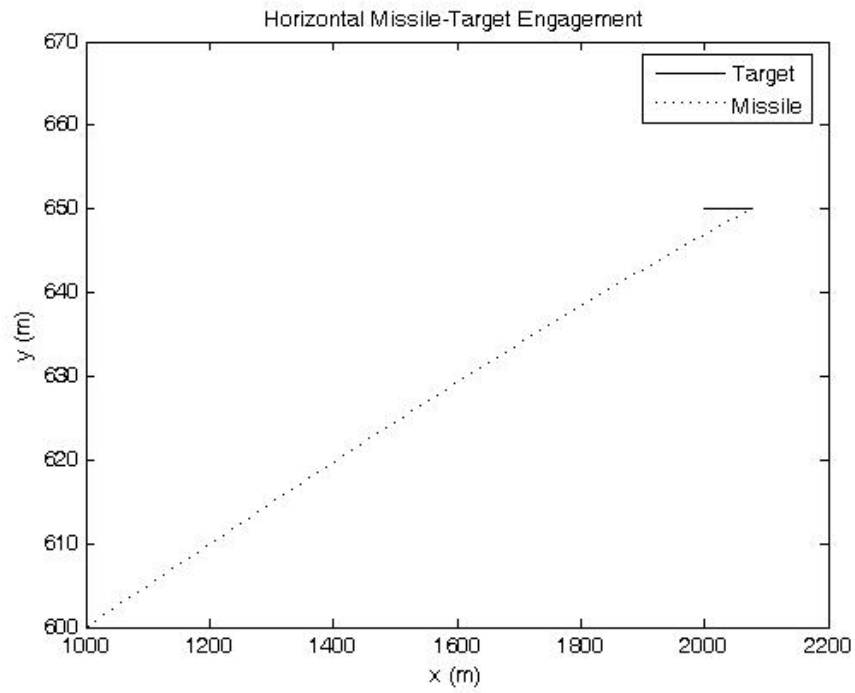


Figure 6. 9. Horizontal Missile-Target Engagement in the S1-C3 Situation

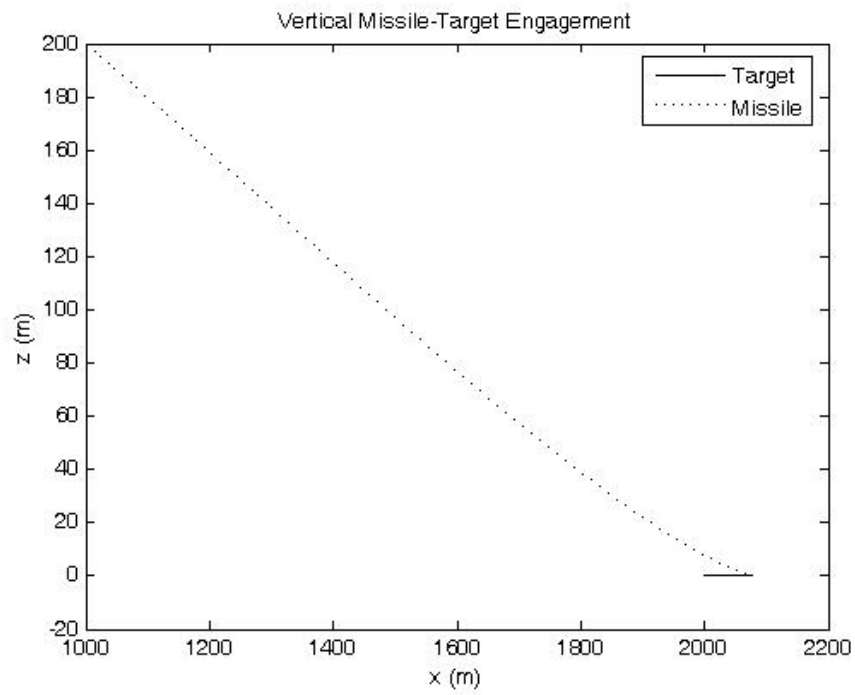


Figure 6. 10. Vertical Missile-Target Engagement in the S1-C3 Situation

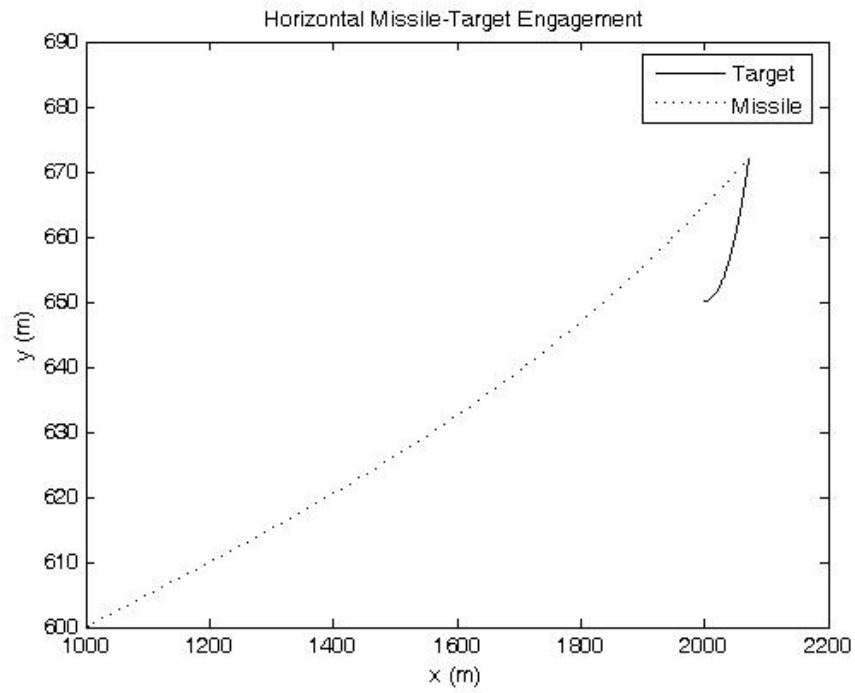


Figure 6. 11. Horizontal Missile-Target Engagement in the S2-C1 Situation

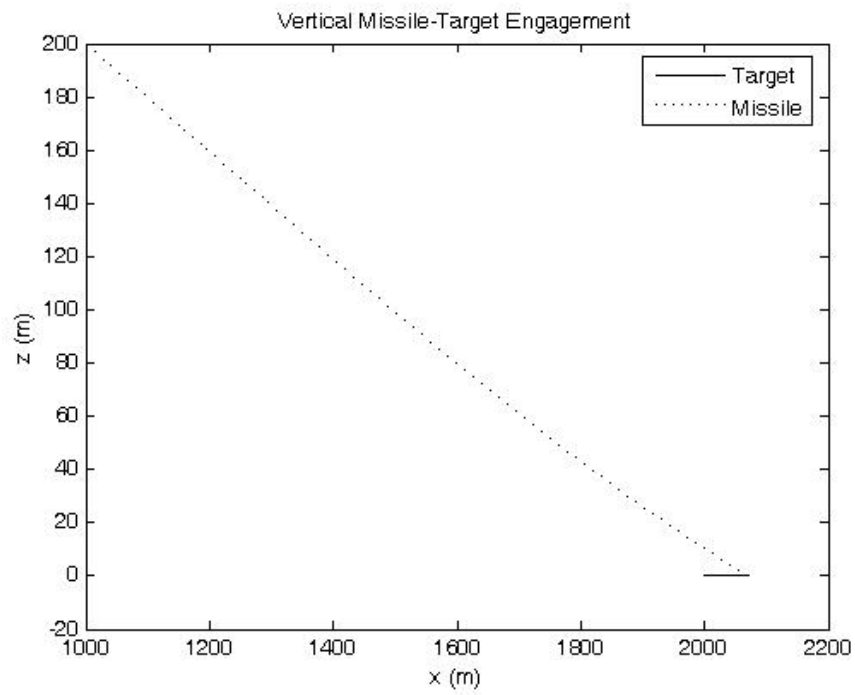


Figure 6. 12. Vertical Missile-Target Engagement in the S2-C1 Situation

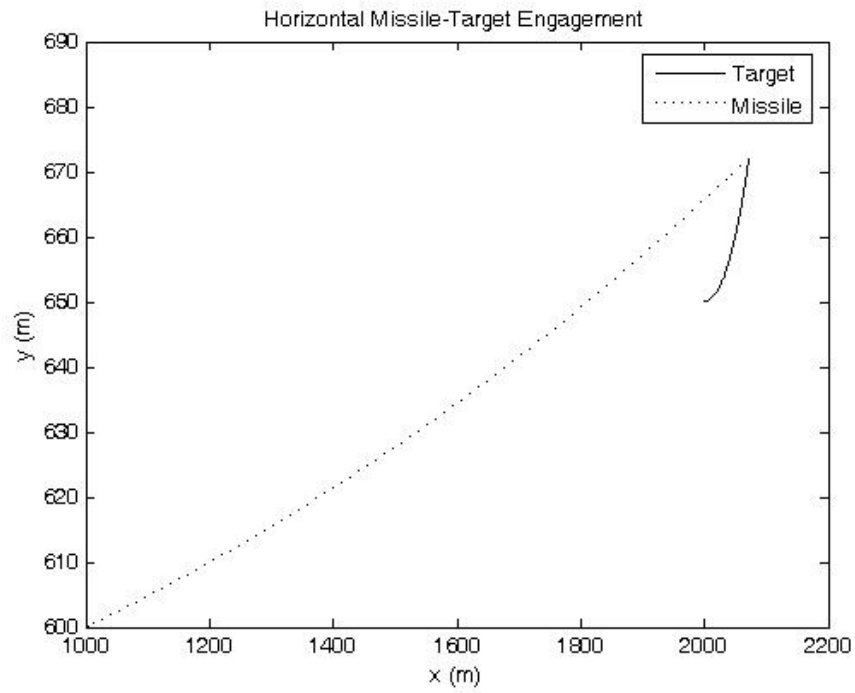


Figure 6. 13. Horizontal Missile-Target Engagement in the S2-C2 Situation

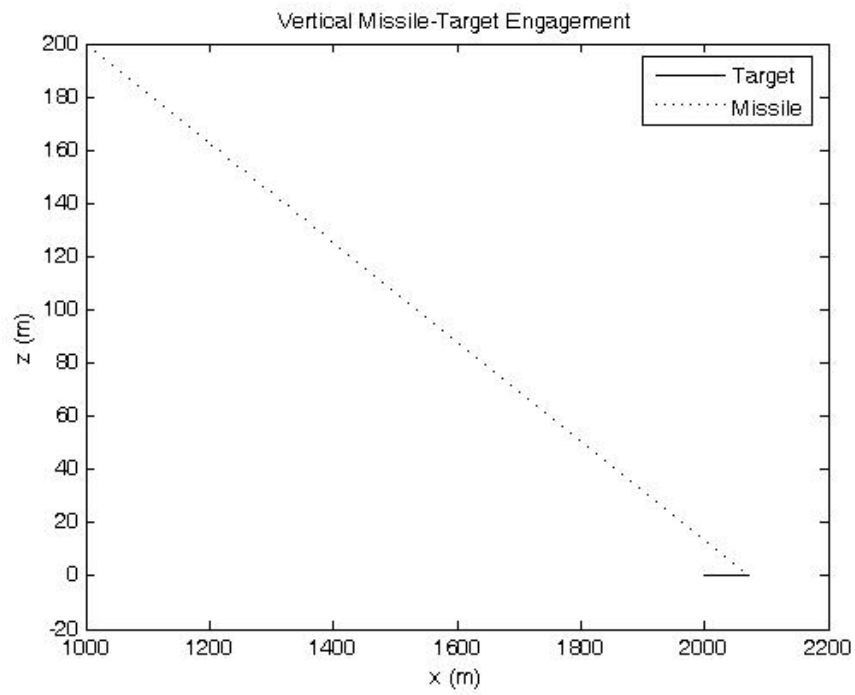


Figure 6. 14. Vertical Missile-Target Engagement in the S2-C2 Situation

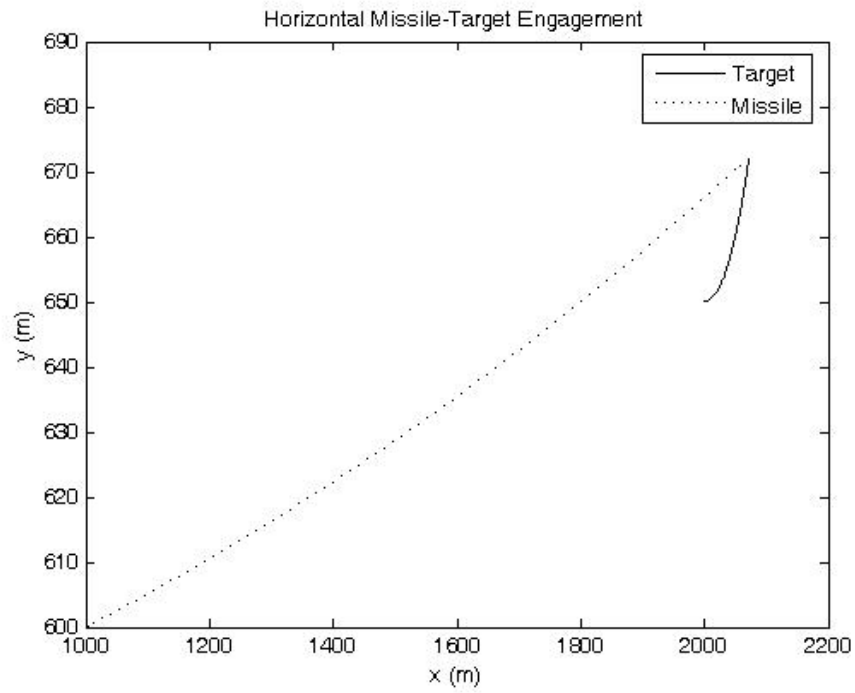


Figure 6. 15. Horizontal Missile-Target Engagement in the S2-C3 Situation

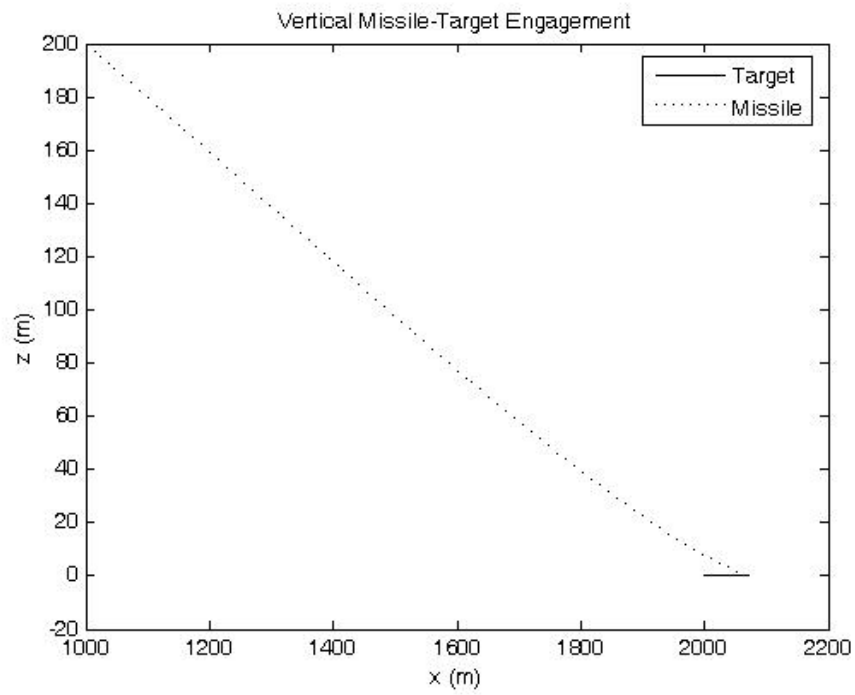


Figure 6. 16. Vertical Missile-Target Engagement in the S2-C3 Situation

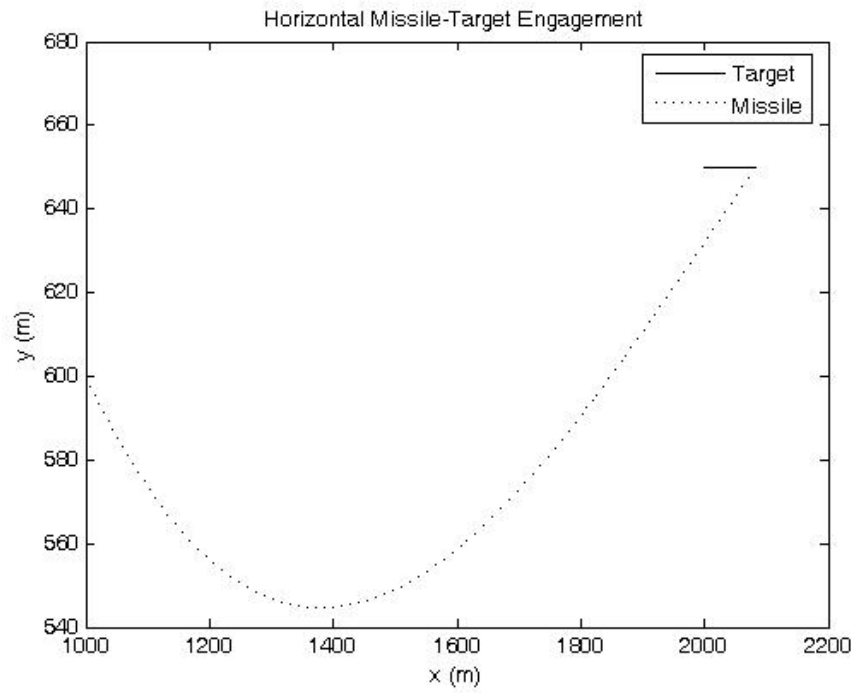


Figure 6. 17. Horizontal Missile-Target Engagement in the S3-C1 Situation

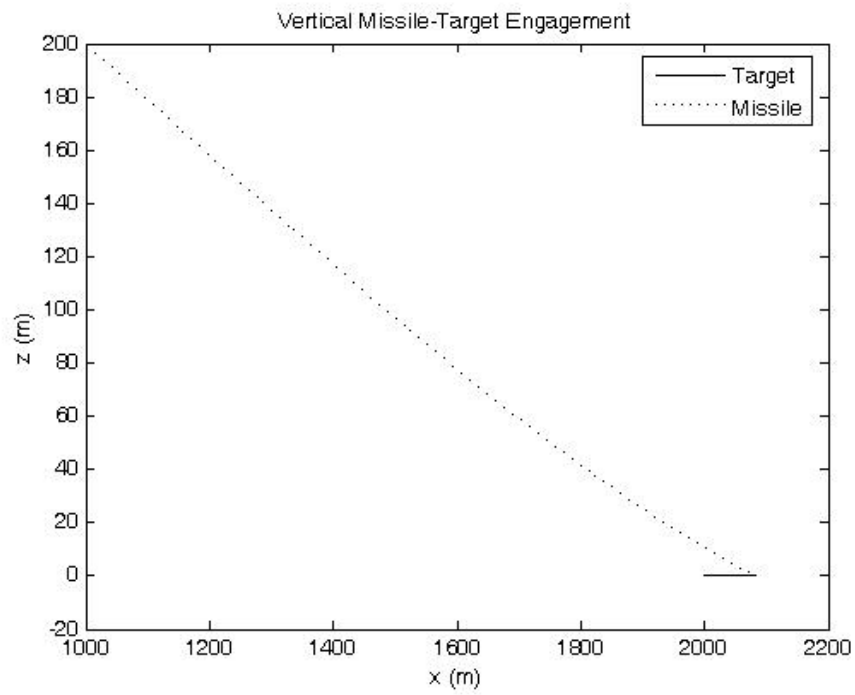


Figure 6. 18. Vertical Missile-Target Engagement in the S3-C1 Situation

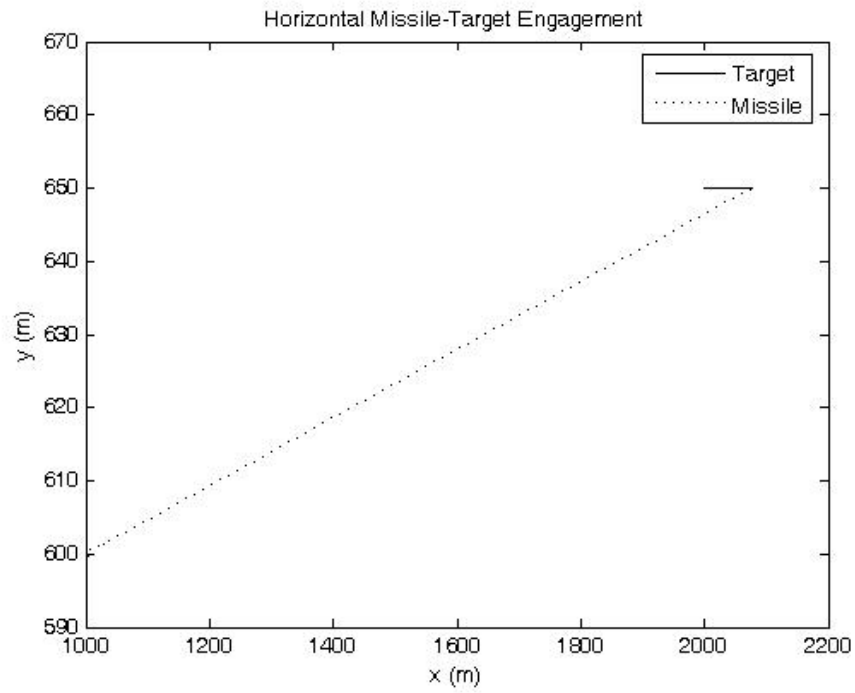


Figure 6. 19. Horizontal Missile-Target Engagement in the S3-C2 Situation

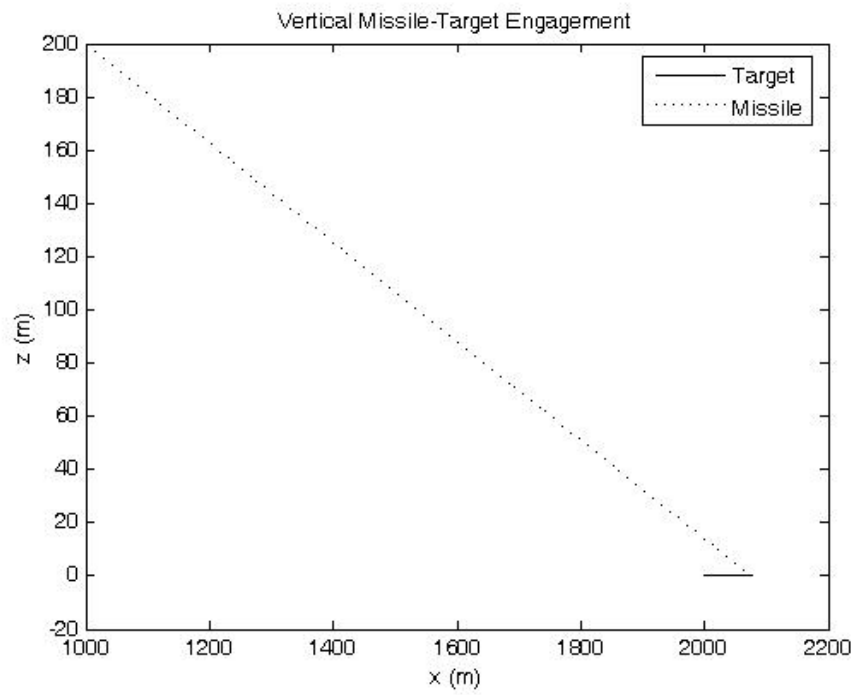


Figure 6. 20. Vertical Missile-Target Engagement in the S3-C2 Situation

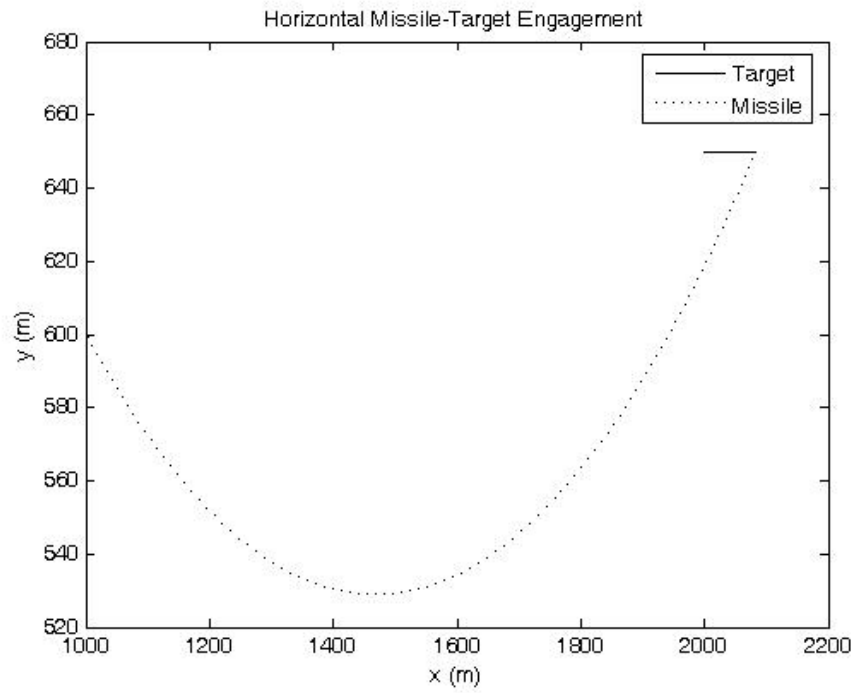


Figure 6. 21. Horizontal Missile-Target Engagement in the S3-C3 Situation

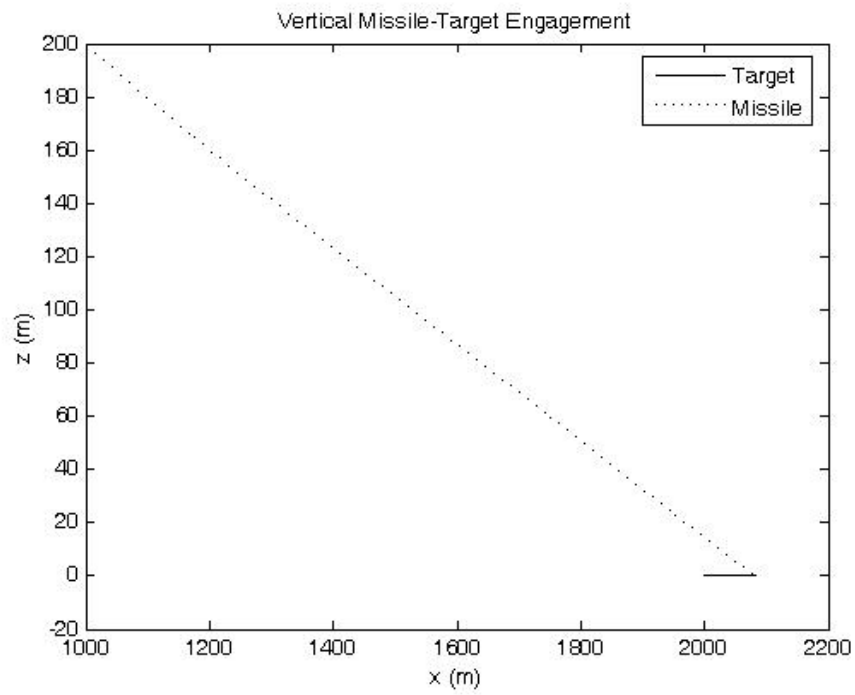


Figure 6. 22. Vertical Missile-Target Engagement in the S3-C3 Situation

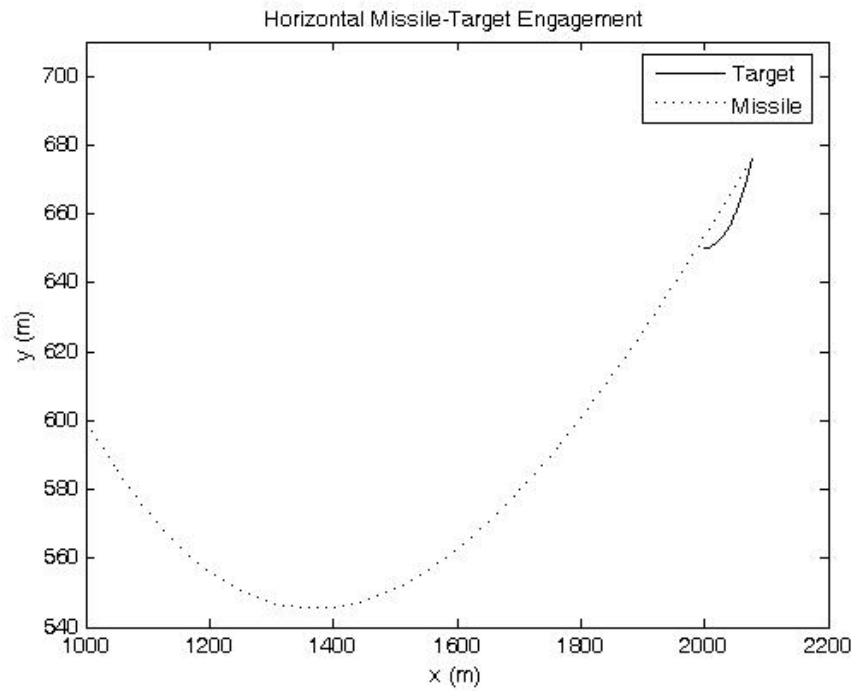


Figure 6. 23. Horizontal Missile-Target Engagement in the S4-C1 Situation

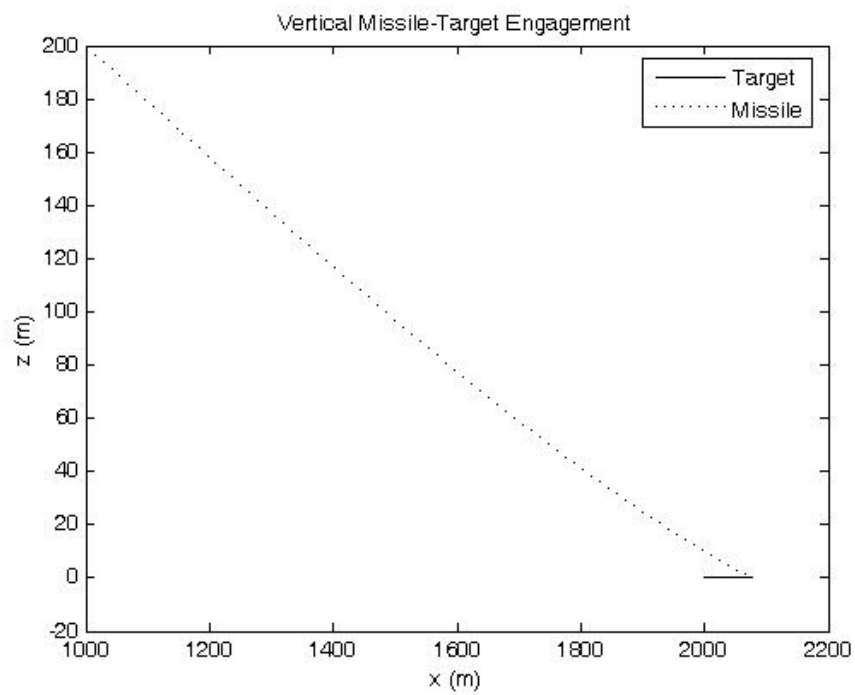


Figure 6. 24. Vertical Missile-Target Engagement in the S4-C1 Situation

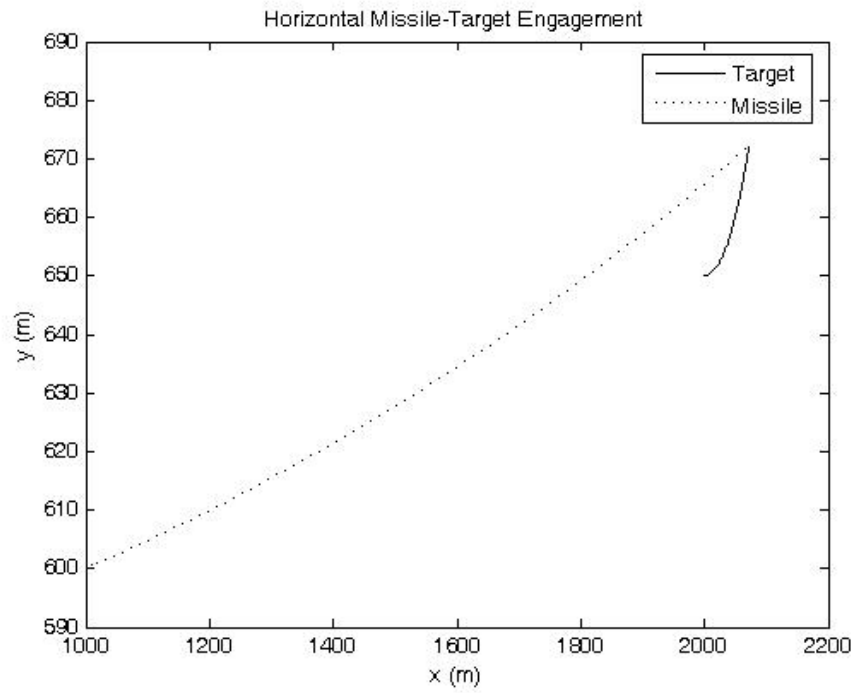


Figure 6. 25. Horizontal Missile-Target Engagement in the S4-C2 Situation

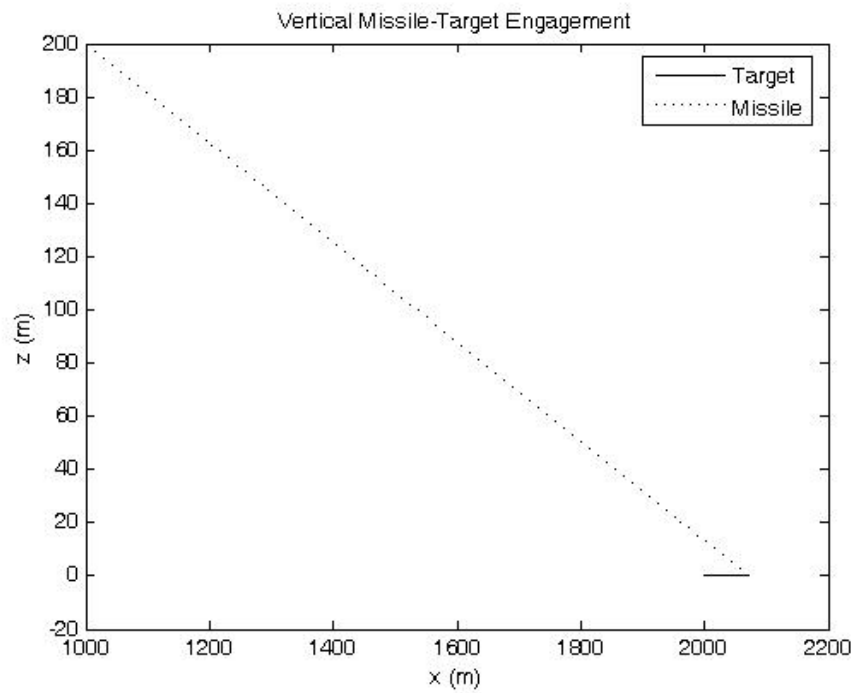


Figure 6. 26. Vertical Missile-Target Engagement in the S4-C2 Situation

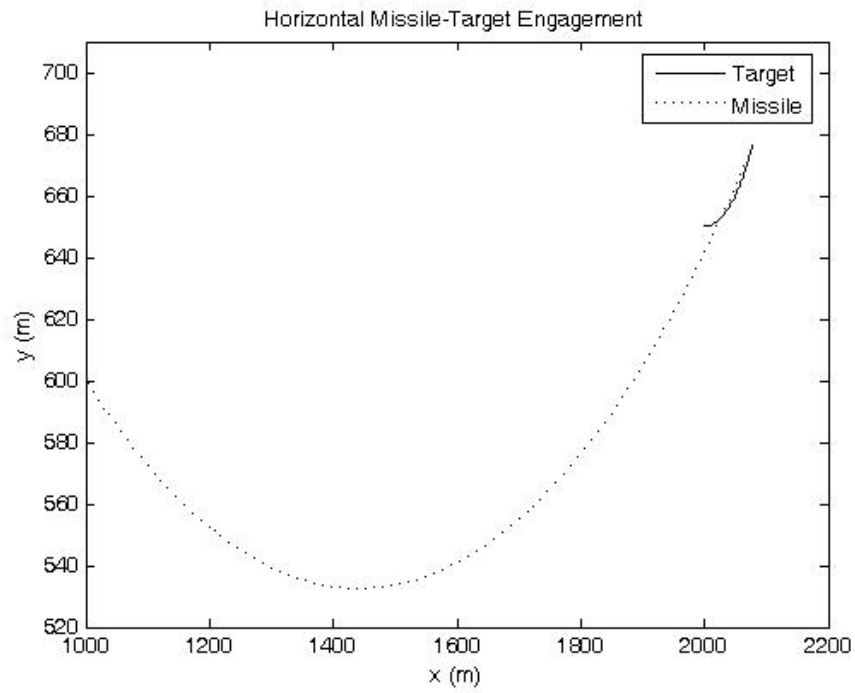


Figure 6. 27. Horizontal Missile-Target Engagement in the S4-C3 Situation

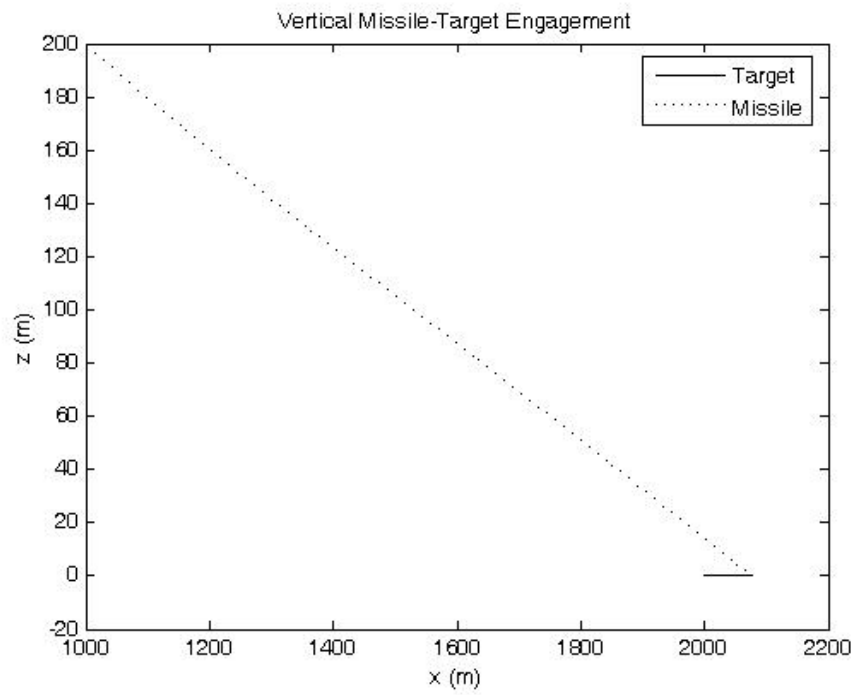


Figure 6. 28. Vertical Missile-Target Engagement in the S4-C3 Situation

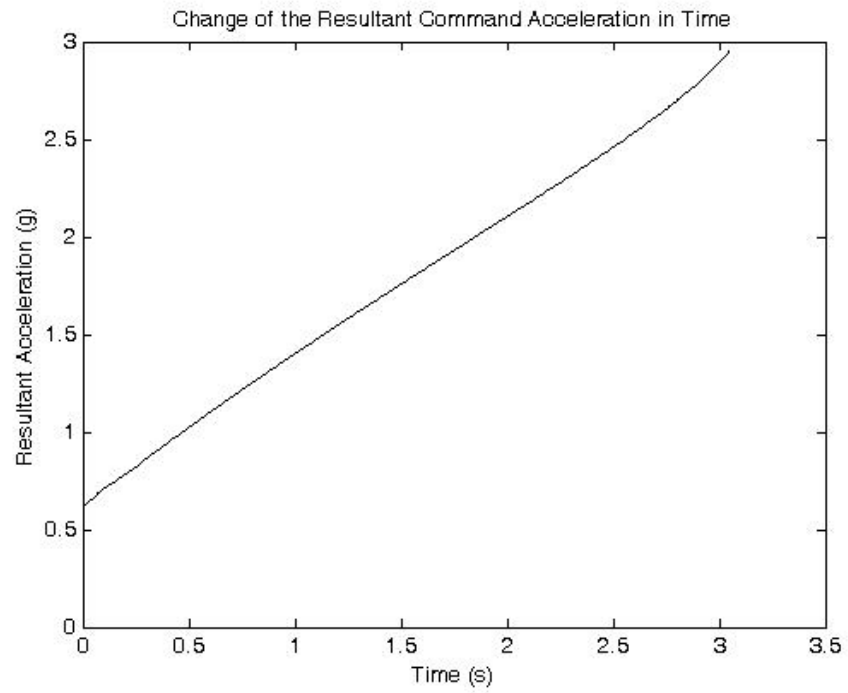


Figure 6. 29. Change of the Resultant Command Acceleration for S1-C1 Situation

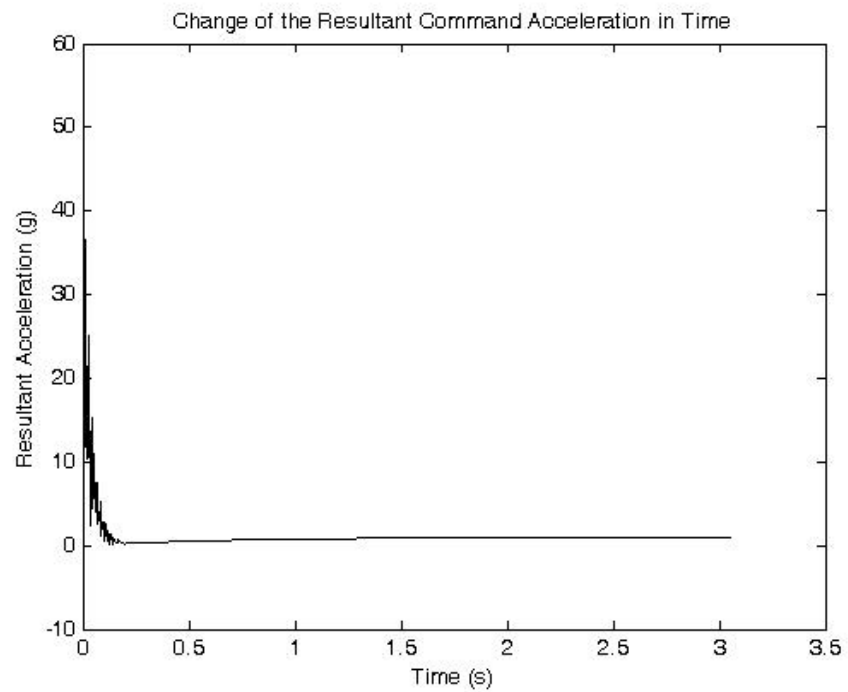


Figure 6. 30. Change of the Resultant Command Acceleration for S1-C2 Situation

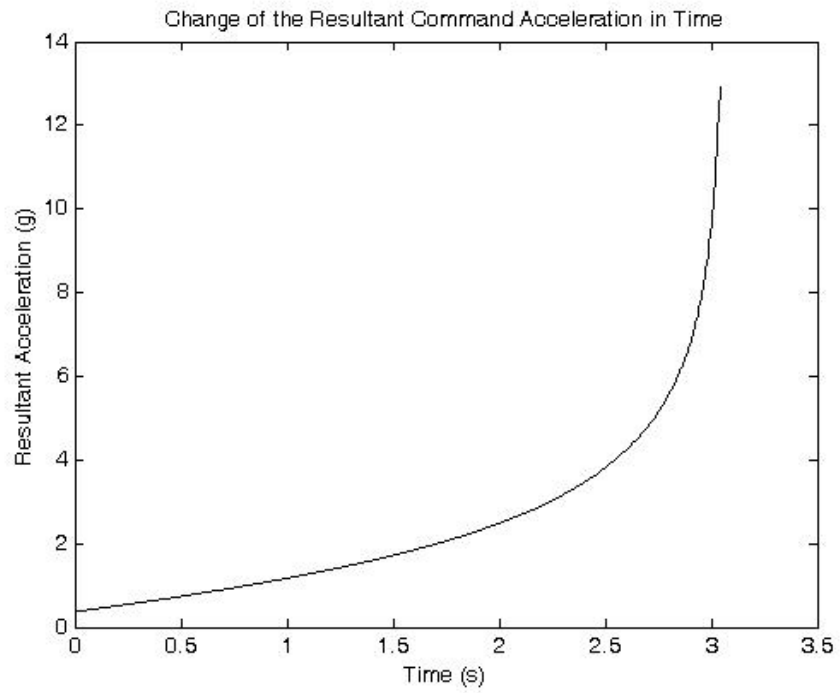


Figure 6. 31. Change of the Resultant Command Acceleration for S1-C3 Situation

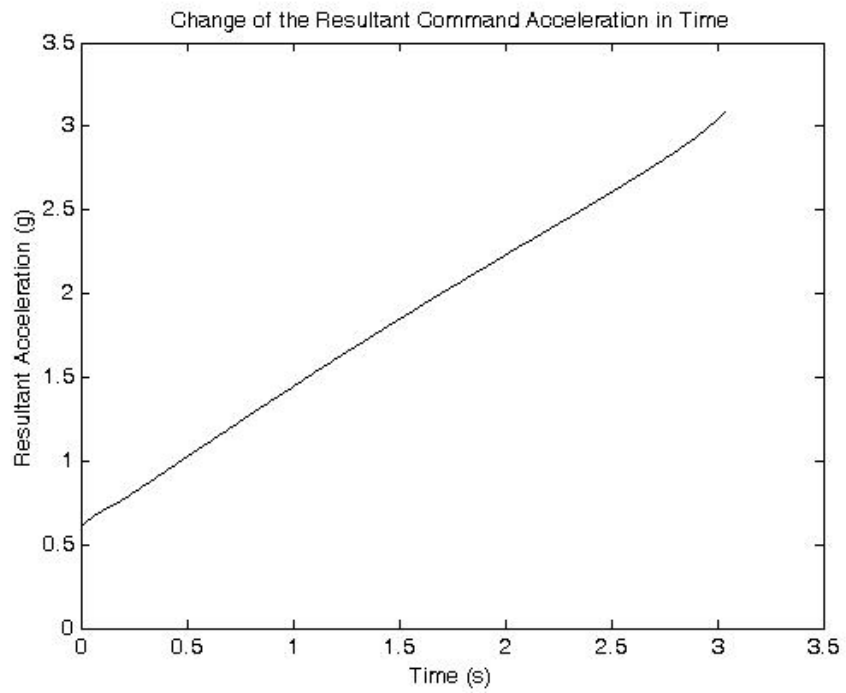


Figure 6. 32. Change of the Resultant Command Acceleration for S2-C1 Situation

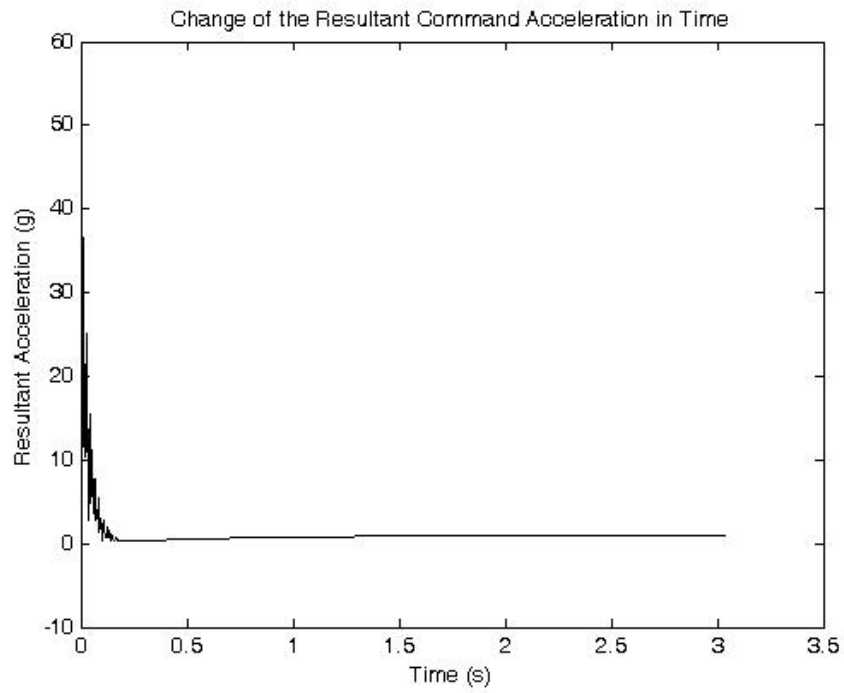


Figure 6. 33. Change of the Resultant Command Acceleration for S2-C2 Situation

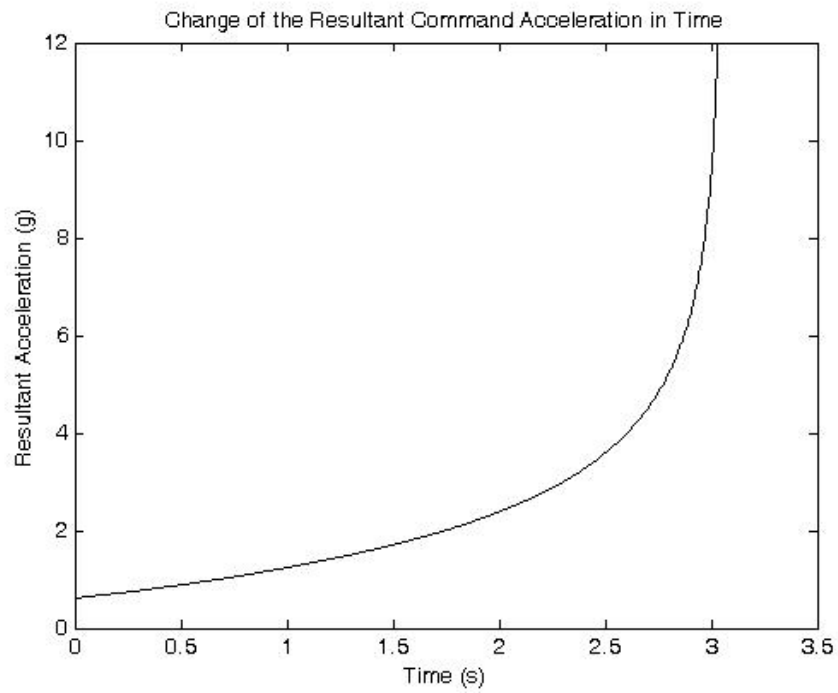


Figure 6. 34. Change of the Resultant Command Acceleration for S2-C3 Situation

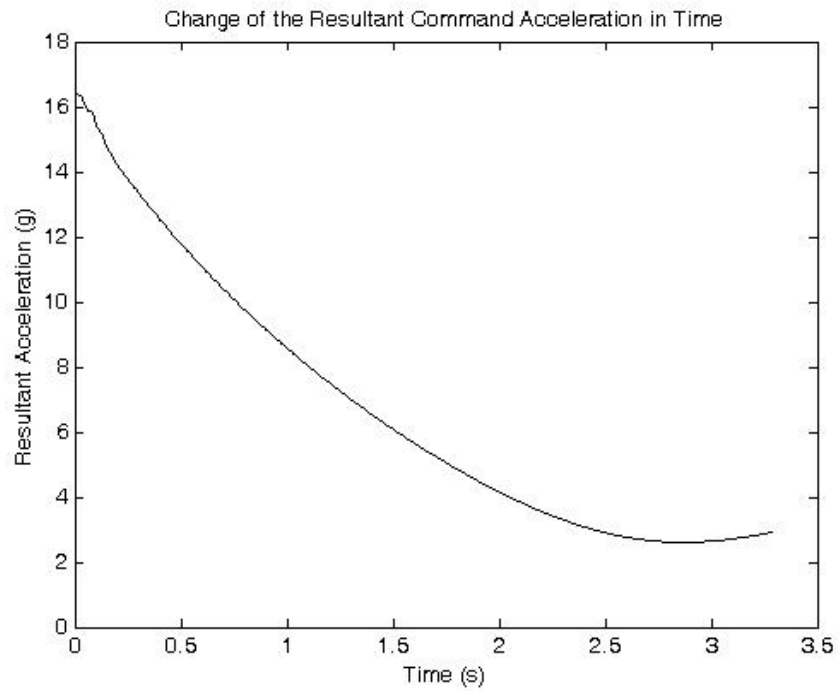


Figure 6. 35. Change of the Resultant Command Acceleration for S3-C1 Situation

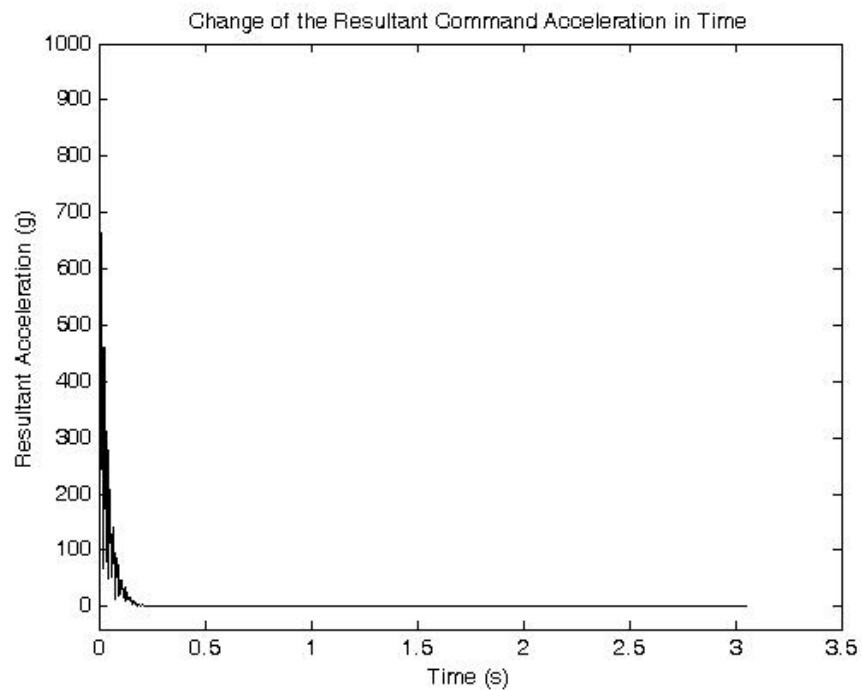


Figure 6. 36. Change of the Resultant Command Acceleration for S3-C2 Situation

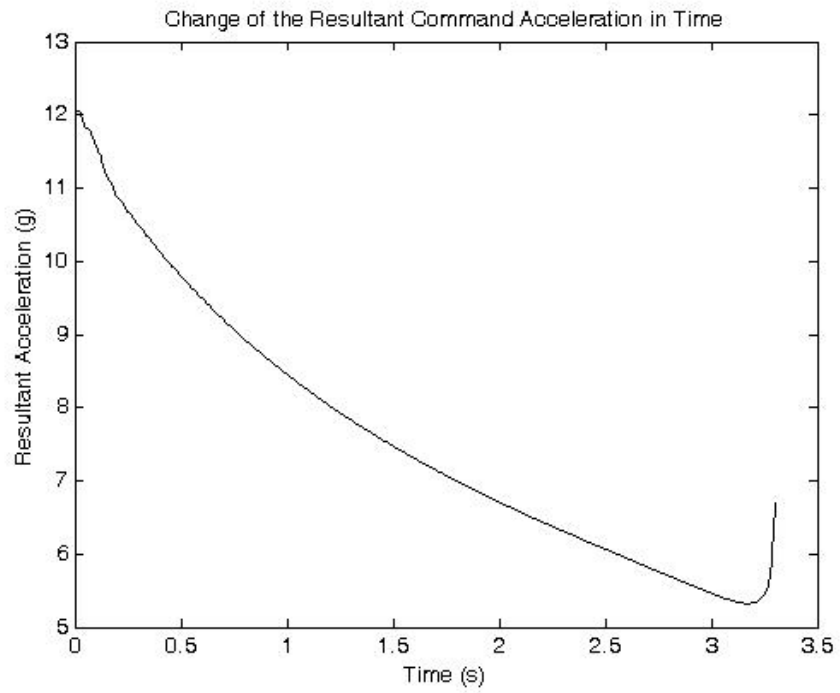


Figure 6. 37. Change of the Resultant Command Acceleration for S3-C3 Situation

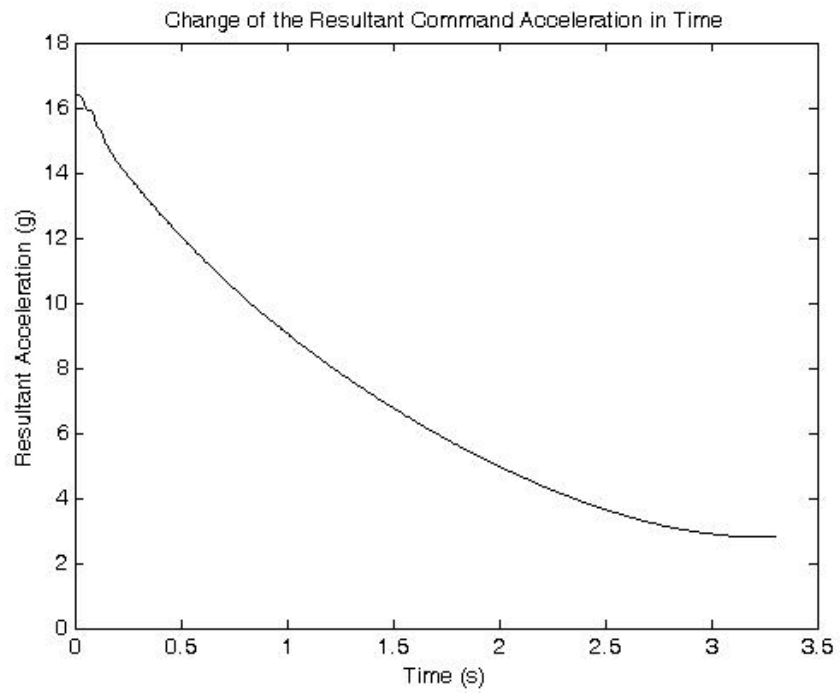


Figure 6. 38. Change of the Resultant Command Acceleration for S4-C1 Situation

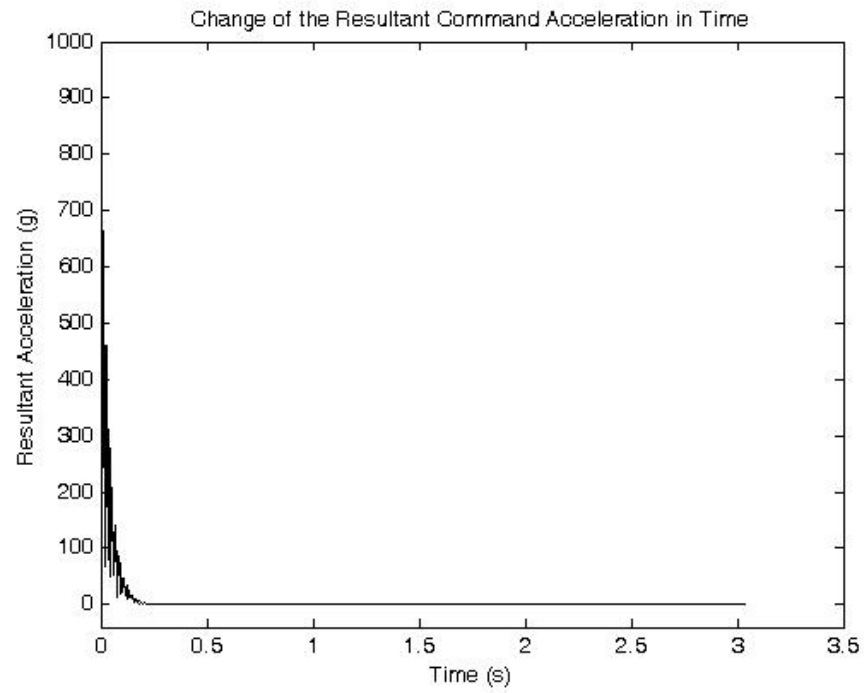


Figure 6. 39. Change of the Resultant Command Acceleration for S4-C2 Situation

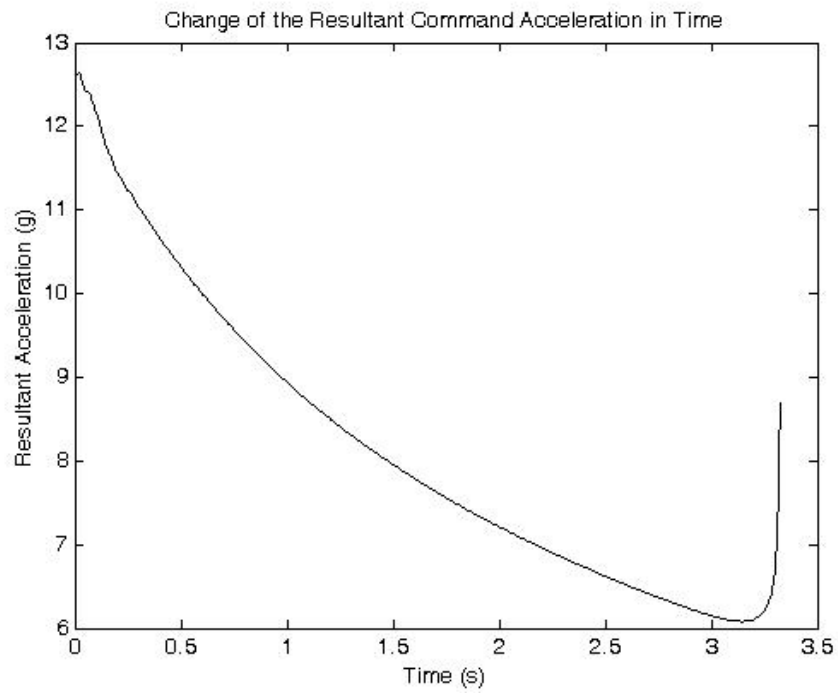


Figure 6. 40. Change of the Resultant Command Acceleration for S4-C3 Situation

Looking at Table 8, the LHG law is better than the PHG law in the sense of the minimum terminal miss distance, the minimum engagement time and the smallest energy consumption. Thus, in order to compare with the PNG law, the sensitivity of the LHG law to the information of the target position components and the target velocity is examined. Here, the S1-C2 and S2-C2 situations are considered. The results of this examination is given in Table 9 and Table 10.

Table 9. Simulation Results for the Target Parameter Uncertainties for
S1-C2 Situation

Amount of Uncertainty in Target Position (%)	Amount of Uncertainty in Target Velocity (%)	Terminal Miss Distance (m)	Engagement Time (s)	Maximum Acceleration (g)	Total Energy Consumption (kJ)
0	0	2.435	3.052	57.154	2.755
1	0	18.448	3.120	65.207	2.978
-1	0	24.522	2.982	53.403	2.820
5	0	105.172	3.399	110.962	5.074
-5	0	111.411	2.710	89.367	4.399
0	1	3.126	3.050	57.649	2.950
0	-1	3.000	3.051	56.990	2.930
0	-5	2.868	3.050	55.657	2.897
0	-10	3.597	3.048	53.997	2.859
0	-20	3.955	3.047	50.677	2.776
0	-50	4.276	3.046	40.717	2.576
0	-100 ($v_T = 0$)	5.695	3.041	24.115	2.286

Table 10. Simulation Results for the Target Parameter Uncertainties
for S2-C2 Situation

Amount of Uncertainty in Target Position (%)	Amount of Uncertainty in Target Velocity (%)	Terminal Miss Distance (m)	Engagement Time (s)	Maximum Acceleration (g)	Total Energy Consumption (kJ)
0	0	3.430	3.039	57.154	2.699
-1	0	25.024	2.970	53.403	2.813
0	-5	3.722	3.038	55.657	2.888
0	-10	3.238	3.040	53.997	2.856
0	-100 ($v_T = 0$)	4.744	3.036	24.115	2.319

As seen from Table 9 and Table 10, the success of the LHG law is strongly dependent on the measurement of the target position. On the other hand, the measurement accuracy of the target velocity does not affect the results much more. In fact, this is because the target speed is much smaller than the missile speed. Conversely, regarding an air target whose speed is much greater than an surface target, it is expected for the results to be more sensitive to the measurement accuracy of the target velocity. For example, keeping the initial positions of the missile and the target as the same, and taking the target velocity and lateral acceleration as 100 m/s and g, the engagement results the values in Table 11. In these simulations, the five cases are considered:

- i. No uncertainty in the target velocity information
- ii. 20% uncertainty in the target velocity information
- iii. 30% uncertainty in the target velocity information
- iv. 50% uncertainty in the target velocity information
- v. No target velocity information

Looking at Table 11, it is seen that as the amount of the uncertainty increases, the terminal miss distance grows up too. On the other hand, the engagement time, the maximum acceleration, and the total energy consumption values become smaller as the uncertainty in the target velocity information increases.

Table 11. Simulation Results against a Faster Target

Amount of Uncertainty in Target Position (%)	Amount of Uncertainty in Target Velocity (%)	Terminal Miss Distance (m)	Engagement Time (s)	Maximum Acceleration (g)	Total Energy Consumption (kJ)
0	0	3.329	4.074	156.930	7.369
0	-20	5.726	4.061	130.360	7.367
0	-30	7.252	4.057	117.077	5.550
0	-50	10.224	4.042	90.516	5.226
0	-100	20.505	4.002	24.115	3.327

As seen above, the most important drawback of the LHG law is the amount of the initial acceleration commands. If they can be lowered, the LHG law will be very competitive to the PNG law. In order to decrease the amount of the maximum lateral acceleration components, the bandwidths of the yaw and the pitch autopilots can be adjusted as a function of time as

$$f_c(t) = \begin{cases} a \cdot t + b & , \text{ for } t_0 \leq t < t_F \\ f_c(t_F) & , \text{ for } t \geq t_F \end{cases} \quad (6.3)$$

where $a = \frac{f_c(t_0) - f_c(t_F)}{t_0 - t_F}$ and $b = \frac{f_c(t_F)t_0 - f_c(t_0)t_F}{t_0 - t_F}$.

Choosing $t_0 = 0$, $f_c(t_0) = 1$ Hz and $f_c(t_F) = 5$ Hz, the results in Table 12 and Table 13 are obtained for $t_F = 0.5$ s and $t_F = 1$ s :

Table 12. Simulation Results with Varying-Bandwidth Autopilots of the C2
Configuration for $t_F = 0.5$ s

Situation	Terminal Miss Distance (m)	Engagement Time (s)	Maximum Acceleration (g)	Total Energy Consumption (kJ)
S1-C2	4.640	3.043	9.351	2.363
S2-C2	4.224	3.035	9.063	2.348
S3-C2	3.034	3.054	80.660	20.981
S4-C2	4.874	3.038	81.317	20.868

Table 13. Simulation Results with Varying-Bandwidth Autopilots of the C2
Configuration for $t_F = 1$ s

Situation	Terminal Miss Distance (m)	Engagement Time (s)	Maximum Acceleration (g)	Total Energy Consumption (kJ)
S1-C2	2.997	3.049	6.193	2.349
S2-C2	2.473	3.041	6.251	2.323
S3-C2	3.224	3.057	65.611	25.689
S4-C2	2.648	3.049	66.132	25.183

As seen from Table 12 and Table 13, the maximum command acceleration and the total energy consumption values are very smaller than those in the case of the constant-bandwidth autopilots while the terminal miss distance becomes larger. Also, the engagement time values are slightly greater. Comparing the results obtained for $t_F = 0.5$ s and $t_F = 1$ s, the terminal miss distance and the maximum acceleration values happen to be smaller as t_F is enlarged. However, the engagement time and the total energy consumption increase.

As an example to the varying-bandwidth application, the graphs about the bandwidth change, the command acceleration history, and the horizontal engagement geometry are given in Figure 6. 41, Figure 6. 42, and Figure 6. 43 for the S2-C2 situation with $t_F = 1$ s.

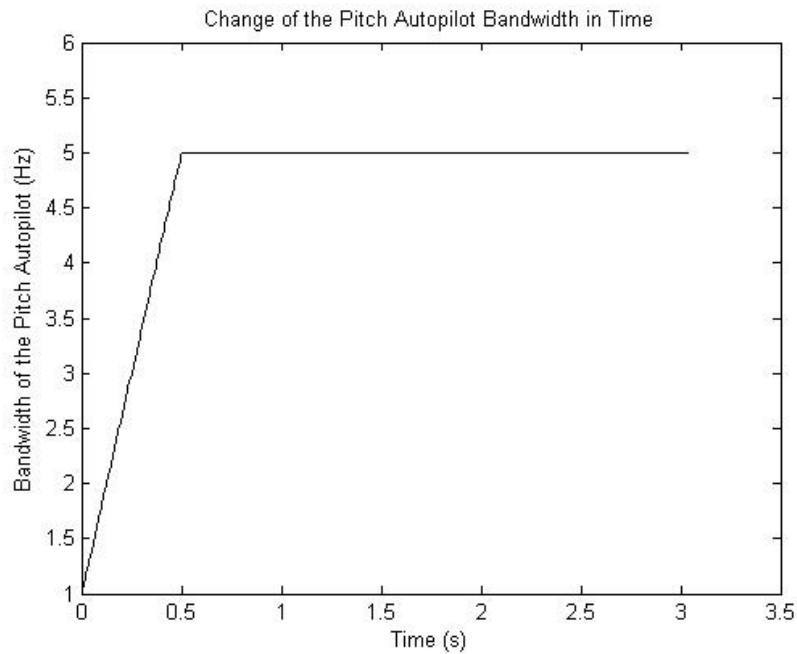


Figure 6. 41. Change of the Pitch Autopilot Bandwidth for S2-C2 Situation for $t_F = 1$ s

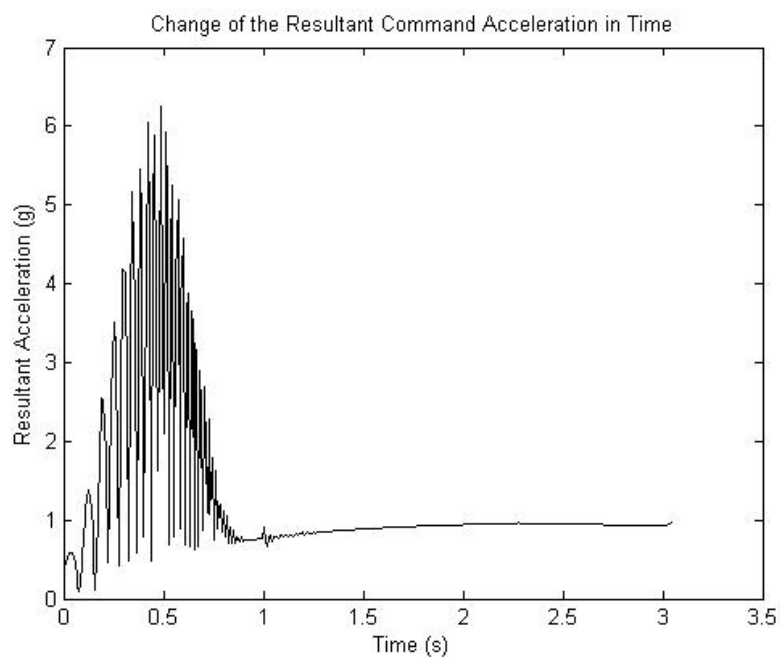


Figure 6. 42. Change of the Resultant Command Acceleration for S2-C2 Situation for $t_F = 1$ s

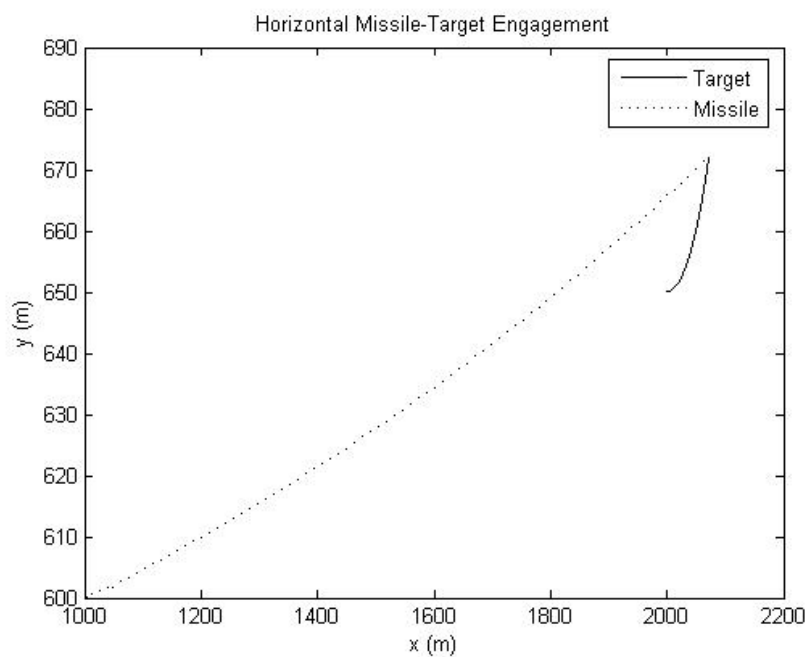


Figure 6. 43. Horizontal Missile-Target Engagement in the S2-C2 Situation for $t_F = 1$ s

In order to see the effect of the wind on the success of the considered guidance laws, two different wind profiles are applied to the missile-target engagement geometry. Assuming the initial heading error of the missile is zero and the target is not maneuvering, the results submitted in Table 14 and Table 15 are determined. As seen, the wind with the components of -1 m/s does not affect the success of the guidance laws much more. On the other hand, as the velocity components of the wind become -7 m/s, the terminal miss distance, the engagement time, the maximum acceleration, and the total energy consumption attain larger values.

Table 14. Simulation Results for the S1 Scenario for $u_w = v_w = -1$ m/s and

$$w_w = 0$$

Situation	Terminal Miss Distance (m)	Engagement Time (s)	Maximum Acceleration (g)	Total Energy Consumption (kJ)
S1-C1	4.937	3.043	2.924	12.200
S1-C2 (constant f_c)	3.507	3.011	88.787	93.217
S1-C2 (varying f_c , $t_F = 1$ s)	3.193	3.047	6.561	2.556
S1-C3	8.050	3.035	12.276	32.794

Table 15. Simulation Results for the S1 Scenario for $u_w = v_w = -7 \text{ m/s}$ and

$$w_w = 0$$

Situation	Terminal Miss Distance (m)	Engagement Time (s)	Maximum Acceleration (g)	Total Energy Consumption (kJ)
S1-C1	7.131	3.047	2.943	17.125
S1-C2 (constant f_c)	3.894	3.055	117.916	25.942
S1-C2 (varying f_c , $t_F = 1 \text{ s}$)	4.711	3.052	11.174	6.315
S1-C3	14.920	3.024	11.103	41.558

CHAPTER 7

DISCUSSION AND CONCLUSION

In this study, the dynamic modeling, guidance, and control of a two-part missile structure is dealt with. Here, the considered missile consists of two separate bodies that are connected to each other by means of a roller bearing. In this scheme, calling the bodies as the front and the rear bodies, the front one is the controlled body while the rear one is left uncontrolled.

In Chapter 2, the governing differential equations of motion of the mentioned missile are derived. For this purpose, first, the equations of motion of the bodies are written separately. Then, using the kinematic and dynamic constraints, these equations are collected so as to get the equations of motion of the entire missile. This way, the seven differential equations describing the motion of the missile are obtained. While the six of them describe the spatial motion of the missile, the seventh one is for the free rotation of the rear body about its body axis. In this model, the interaction between the bodies is provided by the roller bearing.

After the dynamic modeling, the aerodynamic model of the missile is constructed using the Missile Datcom software available in TÜBİTAK-SAGE. However, since the mentioned software can model only single-part munitions,

the considered missile is taken as a single-part missile whose tail fins have a relative orientation with respect to the control fins at an amount of the spin angle. Here, the spin angle is defined as the orientation of the rear body relative to the front one. Then, running the software for the different values of the spin angle from zero to 90° degrees within the selected ranges of the Mach number, the angle of attack (α), and the elevator deflection (δ_e), the sets of aerodynamic coefficients are obtained considering the pitch plane motion of the missile. These sets are then augmented by adding the aerodynamic coefficients related to the pitch rate (q). Thus, the augmented sets of the aerodynamic coefficients are constructed, where each set contains the coefficients for a specific pair of the Mach number and the spin angle. Then, fitting linear polynomials in terms of α , δ_e and q to each of the sets separately, the aerodynamic stability derivatives are calculated for the pitch plane motion of the missile. The results are then tabulated for the pairs of the Mach number and the spin angle. Using the tabulated data, the yaw plane aerodynamic stability derivatives are also found regarding the rotational symmetry property of the missile. In the computer simulations, the stability derivatives are taken from the look-up tables depending on the current values of the Mach number and the spin angle.

In Chapter 2, the design of an electro-mechanical control actuation system is explained as well.

As a following work, the guidance laws that are considered in this study are formulated in Chapter 3. First, the three-dimensional formulation of the Proportional Navigation Guidance (PNG) law is completed. Unlike the spatial derivation of the PNG law which is done in the line-of-sight frame in almost all the previous studies, the guidance commands are generated in the wind frame in this study. This way, the expressions for the guidance commands are made simpler and the guidance command in the velocity vector direction is

automatically eliminated. Thus, the two guidance commands perpendicular to the missile velocity vector are obtained. In this derivation, the effective navigation ratios for the guidance commands are expressed in a dyadic form that is called the *effective navigation ratio dyadic*. In order to apply the generated guidance commands that are in the form of acceleration to the missile, the measured acceleration components of the missile that are expressed in the missile body frame are transformed into the wind frame. Conversely, if the guidance commands were converted to the missile body frame instead, an axial guidance command would exist in the missile body frame. In such a case, the axial command could not be realized by the missile due to the lack of a controllable thrust. For this reason, expressing the measured acceleration components in the wind frame is a more logical way. In the second part of the derivation, the planar interpretation of the PNG law is carried out.

After the derivation of the PNG law, the *Linear Homing Guidance* (LHG) law is proposed as the first alternative to the PNG. In this approach, it is intended to keep the missile always on the collision triangle that is formed by the missile, the target, and the predicted intercept point. For this purpose, the guidance commands are generated so as to orient the missile velocity vector toward the predicted intercept point at which the missile-target collision will occur after a while. Unlike the PNG law, the guidance commands of the present law are in the form of the flight path angles of the missile. Moreover, this law needs the position and the velocity information of the target. As explained below, the success of the LHG is strongly dependent on the accuracy of the target position information. On the other hand, as long as surface targets are considered as in this study, the measurement errors in the target velocity do not affect the resulting miss distance and the engagement time values so much. After completing its general derivation, the planar interpretation of the LHG law is done. Considering the pitch plane motion of the missile, the guidance command to the missile flight path angle is obtained. Then, simplifying the

guidance command expression with the small angle assumption and taking the time derivative of the resulting equation, the guidance law is turned into the Velocity Pursuit Guidance (VPG) law with the addition of the target normal acceleration. In fact, this implies that the VPG law can not put the missile to the collision triangle unless the lateral acceleration information of the target is used. Next, making the definition of the *acceleration advantage factor* (AAF) as the proportion of the missile's lateral acceleration component to the target's lateral acceleration component in the pitch plane, the simplified planar form of the LHG law is rendered to the PNG law. In this form, the effective navigation ratio (ENR) of the PNG law appears as a fractional function of the AAF. As the value of the AAF is one, the ENR becomes infinity. Moreover, for the values of the AAF smaller than one, the ENR takes negative values. Therefore, in order to guide the missile toward the target, the AAF value must be greater than one. Actually, this says that the lateral acceleration component of the missile must strictly be greater than the normal acceleration component of the target in order to achieve a successful intercept. Afterwards, the LHG law is converted into the form of the Augmented Proportional Navigation Guidance (APNG) law by rearranging the guidance law expression. Like the PNG variant, the APNG law form also indicates that the normal acceleration of the missile must exceed the normal acceleration of the target in order to conclude the engagement with a collision.

The *Parabolic Homing Guidance* (PHG) is proposed as the second alternative to the PNG law. In this method, the missile is driven to the predicted intercept point with the target by means of a parabolic trajectory. In order to keep the missile on the planned trajectory, the necessary guidance commands are generated in the form of lateral acceleration components. Actually, this method differs from the LHG law with the shape of the planned trajectory. In other words, while the LHG poses a linear path toward the predicted intercept point, the PHG law upgrades the trajectory to a parabola. Unless the initial

position of the missile is just opposite to the target, this method guides the missile toward the predicted intercept point. However, as mentioned below, the PHG law causes larger miss distance and greater engagement time values than the LHG law. Conversely, it is superior to the LHG law in terms of the maximum acceleration level of the missile. Similar to the previous guidance laws, the planar treatment of the PHG is also done.

At the end of Chapter 3, the kinematic relationships for the missile-target engagement geometry are written.

In Chapter 4, the roll and transversal autopilots of the missile are designed based on the transfer functions obtained in Chapter 2. As the roll autopilot is constructed to regulate the roll attitude of the front body, the transversal autopilots are designed to realize the guidance commands generated by the considered guidance law in the yaw and the pitch planes. In this sense, the transversal autopilots include the acceleration, the rate, and the angle autopilots. In the computer simulations, the acceleration autopilot is preferred to obey the acceleration commands produced by the PNG and the PHG laws. For the cases in which the LHG law is used, the angle autopilot is utilized. Moreover, an anti-windup scheme is used along with the autopilots in order to compensate the windup effects of the integrators in the controllers. Since some amount of rotation will occur in the roll direction due to the manufacturing errors and the aerodynamic effects, a roll resolving scheme is added to the overall control architecture as well. After designing the pitch, the yaw, and the roll control systems, they are applied on the nonlinear missile dynamics using the Matlab-Simulink software. Then, looking at the unit step responses of the yaw and the pitch control systems, it is seen that their initial values and oscillatory behaviors are different from the linearized forms. Actually, this is because the initial conditions of the control systems considering the nonlinear missile dynamics are nonzero. Also, the roll attitude of the missile is not yet nullified at the beginning.

In Chapter 5, the target kinematics is modeled for a typical surface target. Although the Earth's surface is not flat, the altitude of the target is taken to be constant in the computer simulations to simplify the engagement geometry. In fact, using the same equations of the target kinematics, the motion of the target over a non-flat surface can also be modeled. Next, the basic seeker types are introduced and they are compared according to certain criteria. Finally, a simple digital fading memory filter is modeled as a target state estimator. In this model, the memory length of the filter that varies between zero and one is designed to be varying with respect to the length of the relative distance between the missile and the target, and the atmospheric conditions. Namely, as the missile is approaching the target, the memory length is decreased in order to increase the weight of the measured data in the estimations. Also, if the seeker can not provide any signal about the line-of-sight rate due to some atmospheric phenomenon such as a cloud, the memory length becomes one so that the last estimate can be used rather than zero signal.

In Chapter 6, the case studies carried out using the developed models are explained. In these studies, a two-part missile with canted tail fins and a single-body missile with uncanted tail fins are taken into account as well as the considered two-part missile with uncanted tail fins. Thus, the entire guidance and control system models are constructed for all the three types of the missiles regarding the guidance laws. Here, the PNG, the LHG, and the PHG laws are considered. Hence, as each configuration includes a missile type and a guidance law, totally nine simulation configurations are conducted. After defining the initial conditions, the test scenarios are established for the initial heading error values of 0 and -20 degrees, and for the lateral acceleration of the target of 0 and 0.5g. As each test scenario involves one initial heading error value and one target acceleration, four different scenarios are built up. This way, 36 different situations are set up for the computer simulations. Terminal miss distance,

engagement time, maximum acceleration and total energy consumption are selected as the comparison criteria for these situations.

At the end of the computer simulations performed in the Matlab-Simulink environment, it is seen that the LHG yields the minimum terminal miss distance compared to the PNG, and the PHG laws. In this sense, the PHG law appears as the worst one. Moreover, the LHG causes the smallest engagement times. However, the engagement times of the other laws are quite close to them. Looking at the acceleration characteristics, the maximum acceleration demand of the LHG is much larger than the others in all the situations. This is because the initial acceleration requirement of the LHG is very high in order to put the missile onto the collision triangle. Once the missile sits on the collision triangle, the amount of the required acceleration considerably decreases. While the LHG is the worst one in terms of the maximum value of the command accelerations, its average acceleration is very smaller than the PNG and the PHG laws. Furthermore, the part of the acceleration graph after the initial peak is almost flat for the LHG law. Hence, its total energy consumption is very low compared to the other laws. Unlike the LHG law, the acceleration demands of the PNG and the PHG laws grow as the missile approaches the target when the initial heading error of the missile is zero. On the other hand, if the initial heading error is different from zero, then the missile acceleration is required maximum at the beginning and it gradually decreases as the missile approaches the target. When the missile is near the intercept point, the acceleration demand begins growing again. In the PNG and the PHG laws, the difference between the minimum and the maximum acceleration values is not so large unlike the LHG.

When the results are interpreted in terms of the considered missile configurations, the two-part uncanted missile configurations yield the smallest values for all the four criteria. In this sense, the worst one is the single-part missile configurations.

Evaluating the simulation results globally, the LHG is seen to be the best one in terms of the minimum terminal miss distance, the minimum engagement time and the smallest total energy consumption. In the sense of the missile configurations, the two-part uncanted missile configuration with the LHG law appears as the best one. Also, the results of the PNG are quite close to the results of the LHG. On the other hand, the success of the LHG is strictly dependent on the accuracy of the information of the target position. As shown in Chapter 6, the measurement error in the target position even at an amount of 1% increases the terminal miss distance about 10 times. However, as long as a surface target is considered, the accuracy of the target velocity information does not affect on the terminal miss distance so much. As the target speed is increased, the sensitivity of the LHG to the target speed information grows, too. Here, looking at the results of the computer simulations about the uncertain target velocity information for a faster target, it is seen that the engagement time, the maximum acceleration, and the total energy consumption values are reversely proportional to the amount of the uncertainty.

In order to damp the initial acceleration peak of the LHG law, the bandwidths of the yaw and the pitch autopilots can be adjusted within a specified time interval. Namely, starting from a lower value, their bandwidths are linearly increased up to specified values during the considered intervals. Once the interval is ended, the bandwidth values are set to their final values. This way, the maximum value of the missile acceleration can be considerably decreased as explained above.

Briefly, the contributions of this study can be listed as follows:

- The dynamic model of a two-part missile is constructed as a novelty in this field.

- For the two-part missile structure, the aerodynamic model is completed regarding different Mach number and spin angle values.
- The three-dimensional derivation of the PNG law is carried out in a more systematic manner.
- The LHG and the PHG laws are proposed as alternatives to the PNG law, and their formulations are completed.
- In order to improve the performance of the proposed LHG law, a structure with varying-bandwidth yaw and pitch autopilots is suggested and the superiority of this approach is demonstrated.
- The acceleration, the rate, and the angle autopilots are designed in order to realize the guidance commands generated by the guidance laws mentioned above. In this sense, the design of the angle autopilot is another novelty of this study.
- The computer simulations are performed in order to see the performance of the considered guidance laws on both the two and the single-part missiles. This way, it is shown that the two-part uncanted missile gives the best results along with the LHG law.
- The effect of the wind on the considered guidance laws is evaluated.

As the future work, the LHG and the PHG laws can be applied against faster targets such as air targets under different conditions and their performance can be examined. Also, a blended guidance algorithm regarding the PNG and the LHG laws can be examined in order to decrease the initial acceleration demand of the missile as well as the terminal miss distance. Another forthcoming study can be a comprehensive error analysis for each of

the PNG, the LHG, and the PHG laws. Eventually, an advanced filter such as a Kalman filter can be used in the guidance and control system to estimate the target states and the performance of the resulting system can be compared with the guidance and control system constructed in this study.

REFERENCES

- [1]. Özgören, M. K., *Seminar Notes on Dynamics and Control of Guided Missiles*, Middle East Technical University Continuing Education Center, February 21, 1991
- [2]. Frarr, D. j., “*Control of Missile Airframes*”, British Aerospace Dynamics Group Report, 1979
- [3]. Zarchan, P., *Tactical and Strategic Missile Guidance*, Vol. 157, Progress in Aeronautics and Astronautics, AIAA, Washington DC, 1994
- [4]. Lin, C. F., *Modern Navigation, Guidance and Control Processing*, Prentice Hall Publication, Englewood Cliffs, New Jersey, 1991
- [5]. Berglund, E., “*Guidance and Control Technology*”, RTO SCI Lecture Series on Technologies for Future Precision Strike Missile Systems, Atlanta, USA, pp. 1-10, March 2000
- [6]. Tanrikulu, Ö., “*Non-Linear Flight Dynamics of Unguided Missiles*”, Ph.D. Thesis, Middle East Technical University, Türkiye, 1999
- [7]. Mahmutyazıcıoğlu, G., “*Dynamics and Control Simulation of an Inertially Guided Missile*”, M.Sc. Thesis, Middle East Technical University, Türkiye, 1994
- [8]. Acar, Ş.U., “*Trajectory Tracking by Means of Homing Guidance Methods*”, M.Sc. Thesis, Middle East Technical University, Türkiye, 1996

- [9]. Tiriyaki, K., "*Polynomial Guidance Laws and Dynamic Flight Simulation Studies*", M.Sc. Thesis, Middle East Technical University, Türkiye, 2002
- [10]. Şahin, K. D., "*A Pursuit Evasion Game between an Aircraft and a Missile*", M.Sc. Thesis, Middle East Technical University, Türkiye, 2002
- [11]. Vural, A. Ö., "*Fuzzy Logic Guidance System Design for Guided Missiles*", M.Sc. Thesis, Middle East Technical University, Türkiye, 2003
- [12]. Mendanhall, M. R., Perkins, S. C. and Lesieutre, D. J., "*Prediction of the Nonlinear Aerodynamic Characteristics of Maneuvering Missiles*", Journal of Spacecraft, Vol. 24, pp. 394-402, September-October 1987
- [13]. McFarland, M. B. and Calise, A. J., "*Neural Adaptive Nonlinear Autopilot Design for an Agile Anti-Air Missiles*", Proceedings of the AIAA Guidance, Navigation and Control Conference, San Diego, California, July 1996
- [14]. Babu, K. R., Sarma, I. G. and Swamy, K. N., "*Two Robust Homing Missile Guidance Laws Based on Sliding Mode Control Theory*", IEEE Proceedings, pp. 540-547, 1994
- [15]. Mickle, M. C. and Zhu, J. J., "*Skid to Turn Control of the APKWS Missile using Trajectory Linearization Technique*", Proceedings of the American Control Conference, Arlington, VA, pp. 3346-3351, June 25-27, 2001

- [16]. Han, D., Balakrishnan, S. N. and Ohlmeyer, E. J., “*Optimal Midcourse Guidance Law with Neural Networks*”, Proceedings of the IFAC 15th Triennial World Congress, Barcelona, Spain, 2002
- [17]. Lin, C. L. and Chen, Y. Y., “*Design of Advanced Guidance Law against High Speed Attacking Target*”, Proceeding of National Science Council, ROC(A), Vol. 23, No. 1, pp. 60-74, 1999
- [18]. Pastrick, H. L., Seltzer, S. M. and Warren, M. E., “*Guidance Laws for Short- Range Tactical Missiles*”, Journal of Guidance and Control, Vol. 4, No. 2, March- April 1981
- [19]. Wang, Q., Lin, C. F. and D’Souza, C. N., “*Optimality-Based Midcourse Guidance*”, Proceedings of the American Institute of Aeronautics and Astronautics, pp. 1734-1737, 1993
- [20]. Serakos, D. and Lin, C. F., “*Linearized Kappa Guidance*”, Proceedings of the American Control Conference, Baltimore, Maryland, pp. 3293-3297, June 1994
- [21]. Vermishev, Y. K., *Fundamentals of Missile Guidance*, Translation Division Foreign Technology Division, 1969
- [22]. Menon, P. K., Sweriduk, G. D. and Ohlmeyer, E. J., “*Optimal Fixed-Interval Integrated Guidance-Control Laws for Hit-to-Kill Missiles*”, AIAA Guidance, Navigation and Control Conference, Austin, USA, August 11-14, 2003
- [23]. Zarchan, P., “*Ballistic Missile Defense Guidance and Control Issues*”, Science and Global Security, Vol. 8, pp. 99-124, 1998

- [24]. *System Engineering/Guidance Fundamentals 2*, Martin Marietta Training Notes, 1993

- [25]. Heap, E., “*Methodology of Research into Command-to-Line-of-Sight and Homing Guidance*”, Proceeding of the Royal Aircraft Establishment, Farnborough, Hants, U.K., 1995

- [26]. Shinar, J., “Homing of Rolling Missile against a Manoeuvring Target”, Israel Journal of Technology, Vol. 11, No. 3, pp. 117-130, 1973

- [27]. Yang, C. D., Hsiao, F.B. and Yeh, F. B., “*Generalized Guidance Law for Homing Missiles*”, IEEE Transactions on Aerospace and Electronic Systems, Vol. AES-25, No. 2, pp. 197-212, March 1989

- [28]. Nesline, F. W. and Zarchan, P., “*A New Look at Classical vs Modern Homing Missile Guidance*”, AIAA Guidance and Control Conference, Boulder, Colo., August 6-8, 1979

- [29]. Guelman, M., “*Missile Acceleration in Proportional Navigation*”, IEEE Transactions on Aerospace and Electronic Systems, pp. 462-463, May 1973

- [30]. *Guidance and Control Systems*, Naval Weapon Systems Presentation, October 2001

- [31]. Choi, J. Y., Chwa, D. and Cho, H. P., “*Nonlinear Adaptive Guidance Considering Target Uncertainties and Control Loop Dynamics*”, IEEE Proceedings, 2001

- [32]. Özkan, B., Özgören, M. K. and Mahmutyazıcıoğlu, G., “*Guidance and Control of a Homing Missile Pursuing a Moving Target*” (in Turkish), the Advanced Technologies in Aeronautics Symposium (HİTEK-2004), İstanbul, Türkiye, December 9-10, 2004
- [33]. Özkan, B., Özgören, M. K. and Mahmutyazıcıoğlu, G., “*Comparison of the Well-Known Guidance Methods for Laser Guided Missiles*” (in Turkish), the Proceedings of the 12th National Machine Theory Symposium (UMTS-2005), Kayseri, T held in June, 2005 in Kayseri, Türkiye, pp. 431-440, June 9-11, 2005
- [34]. Yang, C. D. and Yang, C. C., “*Optimal Pure Proportional Navigation for Maneuvering Targets*”, IEEE Transactions on Aerospace and Electronic Systems, Vol. 33, No. 3, pp. 949-957, July 1997
- [35]. Adler, F., “*Missile Guidance by Three-Dimensional Proportional Navigation*”, Journal of Applied Physics, Vol. 27, No. 5, pp. 500-507, May 1956
- [36]. Tyan, F., “*A Unified Approach to Missile Guidance Laws: A 3D Extension*”, Proceedings of the American Control Conference, Anchorage AK, USA, pp. 1711-1716, May 8-10, 2002
- [37]. Moon, J., Kim, K. and Kim, Y., “*Design of Missile Guidance Law via Variable Structure Control*”, Journal of Guidance, Control and Dynamics, Vol. 24, No. 4, pp. 659-664, July-August 2001

- [38]. Lin, C. L. and Su, H. W., "*Intelligent Control Theory in Guidance and Control System Design: an Overview*", Proceedings of the National Science Council ROC(A), Vol. 24, No. 1, pp. 15-30, 2000

- [39]. Chen, H. Y., "*3D Nonlinear H_2/H_∞ Adaptive Guidance Law for Homing Missiles*", Proceedings 16th IFAC Symposium on Automatic Control in Aerospace, Saint-Petersburg, Russia, Vol. 2, pp. 23-26, June 14-18, 2004

- [40]. Mehrandezh, M., Sela, N. M., Fenton, R. G. and Benhabib, B., "*Robotic Interception of Moving Objects Using an Augmented Ideal Proportional Navigation Guidance Technique*", IEEE Transactions on Systems, Man, and Cybernetics-Part A: Systems and Humans, Vol. 30, No. 3, pp. 238-250, May 2000

- [41]. Kirk, D. E., *Optimal Control Theory-An Introduction*, Prentice-Hall Inc., 1970

- [42]. Shinar, J. and Shima, T., "*Nonorthodox Guidance Law Development Approach for Intercepting Maneuvering Targets*", Journal of Guidance, Control and Dynamics, Vol. 25, No. 4, pp. 658-666, July-August 2002

- [43]. Kim, K. B. and Kwon, W. H., "*Differential Game Missile Guidance Laws via Receding Horizon Control without Time-to-Go*", Proceeding of School of Electrical Engineering, Seoul National University, Korea, 1997

- [44]. Kim, K. B., Yoon, T. W. and Kwon, W. H., "*Receding Horizon Guidance Laws for Constrained Missiles with Autopilot Lags*", Control Engineering Practice, No.9, pp. 1107-1115, 2001

- [45]. Shinar, J., "*On the Optimal Estimator of Randomly Maneuvering Targets for Terminal Guidance*", Proceedings 16th IFAC Symposium on Automatic Control in Aerospace, Saint-Petersburg, Russia, Vol. 2, pp. 11-16, June 14-18, 2004

- [46]. Song, C., Ryoo, C. K., Tahk, M. J. and Cho, H., "*Optimal Guidance Law for Impact Angle Control*", Proceedings 16th IFAC Symposium on Automatic Control in Aerospace, Saint-Petersburg, Russia, Vol. 2, pp. 91-96, June 14-18, 2004

- [47]. Tsao, L. P. and Lin, C. S., "*A New Optimal Guidance Law for Short-Range Homing Missiles*", Proceedings of the National Science Council ROC(A), Vol. 24, No. 6, pp. 422-426, 2000

- [48]. Cheng, P., "*A Short Survey on Pursuit-Evasion Games*", Proceeding of Department of Computer Science, University of Illinois at Urbana-Champaign, 2003

- [49]. Lin, C. F., *Advanced Control Systems Design*, Prentice Hall Series in Advanced Navigation, Guidance and Control and Their Applications, Prentice-Hall Inc., 1994

- [50]. Ménéec, S. L., “*Extensive Comparison between Quantitative Pursuit Evasion Game Guidance Law and PNS*”, Proceedings 16th IFAC Symposium on Automatic Control in Aerospace, Saint-Petersburg, Russia, Vol. 2, pp. 51-55, June 14-18, 2004
- [51]. Gurfil, P., Jodorkovsky, M. and Guelman, M., “*Neoclassical Guidance for Homing Missiles*”, Journal of Guidance, Control and Dynamics, Vol. 24, No. 3, pp. 452-459, May-June 2001
- [52]. Zhou, K. and Doyle, J. C., *Essentials of Robust Control*, Prentice-Hall Inc., 1998
- [53]. Kim, Y. K. and Jeon, G. J., “*Error Reduction of Sliding Mode Control Using Sigmoid-Type Nonlinear Interpolation in the Boundary Layer*”, International Journal of Control, Automation, and Systems, Vol. 2, No. 4, pp. 523-529, December 2004
- [54]. Shieh, C. S., “*Tunable H_∞ Robust Guidance Law for Homing Missiles*”, IEE Proceedings on Control Theory Applications, Vol. 151, No. 1, pp. 103-107, January 2004
- [55]. Yang, C. D. and Chen, H. Y., “*Three-Dimensional Nonlinear H_∞ Guidance Law*”, International Journal of Robust and Nonlinear Control, No. 11, pp. 109-129, 2001

- [56]. Yang, C. D. and Chen, H. Y., "*H_∞ Guidance Law with Maneuvering Targets*", Proceedings of the 36th Conference on Decision and Control, pp. 2549-2550, San Diego, California, USA, December 1997
- [57]. Jamshidi, M., "*Tools for Intelligent Control: Fuzzy Controllers, Neural Networks and Genetic Algorithms*", Proceedings of Royal Society, No. 361, pp. 1781-1808, 2003
- [58]. Passino, K. M., "*Intelligent Control: An Overview of Techniques*", Proceeding of the Department of Electrical Engineering, The Ohio State University, USA, 2001
- [59]. Kuljaca, O., Swamy, N., Lewis, F. L. and Kwan, C. M., "*Design and Implementation of Industrial Neural Network Controller Using Backstepping*", Proceedings of the 40th IEEE Conference on Decision and Control, Orlando, Florida, USA, pp. 2709-2714, December 2001
- [60]. Xin, M., Balakrishnan, S. N. and Ohlmeyer, E. J., "*Integrated Guidance and Control of Missiles with θ -D Method*", Proceeding of the Naval Surface Weapon Center, USA, 2002
- [61]. Menon, P. K. and Yousefpor, M., "*Design of Nonlinear Autopilots for High Angle of Attack Missiles*", Proceeding of the Optimal Synthesis, 1996

- [62]. Blakelock, J. H., *Automatic Control of Aircraft and Missiles*, John Wiley & Sons Inc., 1965

- [63]. *Control Actuation System Workshop/System Analysis Reference*, Martin Marietta Training Notes, 1993

- [64]. Chwa, D. K. and Choi, J. Y., “*New Parametric Affine Modeling and Control for Skid-to-Turn Missiles*”, IEEE Transactions on Control Systems Technology, Vol. 9, No. 2, pp. 335-347, March 2001

- [65]. *Control Actuation System Design*, Martin Marietta Training Notes, 1993

- [66]. Lee, H. C., Choi, Y. S. and Choi, J. W., “*Autopilot Design for Agile Missile using Time-Varying Control Technique*”, Proceedings 16th IFAC Symposium on Automatic Control in Aerospace, Saint-Petersburg, Russia, Vol. 2, pp. 103-108, June 14-18, 2004

- [67]. Sreenuch, T., Tsourdos, A., Hughes, E. J. and White, B. A., “*Multi-Objective Frequency Loop-Shaping of a Lateral Missile Autopilot*”, Proceedings 16th IFAC Symposium on Automatic Control in Aerospace, Saint-Petersburg, Russia, Vol. 2, pp. 17-22, June 14-18, 2004

- [68]. Janardhanan, S. and Bandyopadhyay, B., “*Tracking of LTI Systems with Unstable Zero Dynamics using Multirate Output Feedback based*

- Sliding Mode Control*”, Proceeding of the Interdisciplinary Programme in Systems and Control Engineering, Indian Institute of Technology, Bombay, India, 2004
- [69]. Goodwin, G. C., “*A Brief Overview of Nonlinear Control*”, Proceeding of the Centre for Integrated Dynamics and Control, Department of Electrical and Computer Engineering, The University of Newcastle, Australia, 2002
- [70]. Helton, J. W. and James, M. R., “*Extending H_∞ Control to Nonlinear Systems*”, Bulletin of the American Mathematical Society, Vol. 38, No. 1, pp. 93-96, October 2, 2000
- [71]. Liu, R., “*Nonlinear Control of Electro-Hydraulic Servosystems: Theory and Experiment*”, M.Sc. Thesis, University of Illinois at Urbana Champaign, USA, 1998
- [72]. Härkegård, O., “*Backstepping and Control Allocation with Applications to Flight Control*”, Ph.D. Thesis, Linköping University, Sweden, 2003
- [73]. Aguiar, A. P., Hespanha, J. P. and Kokotovic', P. V., “*Path-Following for Non-Minimum Phase System Removes Performance Limitations*”, Proceeding of the Center for Control Engineering and Computation, University of California, Santa Barbara, USA, 2004

- [74]. Menon, P. K. and Ohlmeyer, E. J., "*Computer-Aided Synthesis of Nonlinear Autopilots for Missiles*", Nonlinear Studies, Vol. 11, No. 2, pp. 173-198, 2004
- [75]. Sharma, M. and Ward, D. G., "*Flight-Path Angle Control via Neuro-Adaptive Backstepping*", Report of the American Institute of Aeronautics and Astronautics, USA, 2002
- [76]. Thukral, A. and Innocenti, M., "*A Sliding Mode Missile Pitch Autopilot Synthesis for High Angle of Attack Maneuvering*", IEEE Transactions on Control Systems Technology, Vol. 6, No. 3, pp. 359-371, May 1998
- [77]. Kim, K., "*The Control of Nonlinear Nonminimum Phase Systems*", Report of the Coordinate Systems Laboratory, Electrical and Computer Engineering, University of Illinois at Urbana-Champaign, USA, December 8, 2000
- [78]. Shtessel, Y. B. and Shkolnikov, I. A., "*Non-Minimum Phase Tracking on Sliding Modes*", Proceeding of the Department of Alabama in Huntsville, USA, 1998
- [79]. Calise, A. J., Sharma, M. and Corban, J. E., "*An Adaptive Autopilot Design for Guided Munitions*", Proceeding of American Institute of Aeronautics and Astronautics, 2000
- [80]. Chen, G. and Ying, H., "*On the Stability of Fuzzy PI Control Systems*", Proceeding of the Institute of Space Systems Operations, University of Houston, USA, 1993

- [81]. White, B. A., Blumel, A. L. and Hughes, E. J., "*A Robust Fuzzy Autopilot Design using Multi-Criteria Optimization*", International Journal of Fuzzy Systems, Vol. 2, No. 2, pp. 129-138, June 2000
- [82]. Sutton, R. and Craven, P. J., "*A Fuzzy Autopilot Design Approach That Utilizes Non-Linear Consequent Terms*", Journal of Marine Science and Technology, Vol. 9, No. 2, pp. 65-74, 2001
- [83]. Rago, C. and Mehra, R. K., "*Robust Adaptive Target State Estimation for Missile Guidance using the Interacting Multiple Model Kalman Filter*", IEEE Proceedings, 2000
- [84]. Tchamova, A. and Semerdjiev, T., "*Fuzzy Logic Approach to Estimating Tendencies in Target Behavior*", Journal of Information and Security, Vol. 9, pp. 58-69, 2002
- [85]. Lefebvre, T., Bruyninckx, H. and Schutter, J. D., "*Kalman Filters for Non-linear Systems: A Comparison of Performance*", International Journal of Control, Vol. 77, No. 7, pp. 639-653, May 10, 2004
- [86]. Menon, P. K. and Sharma, V., "*Adaptive Target State Estimation Using Neural Networks*", Optimal Synthesis Inc. Report, 1999

- [87]. Vanicek, P. and Omerbašić, M., “*Does a Navigation Algorithm Have to Use Kalman Filter?*”, Proceeding of the Department of Geodesy and Geomatics Engineering, University of New Brunswick, Canada, 1997
- [88]. Öhr, J., *Anti-Windup and Control of Systems with Multiple Input Saturations-Tools, Solutions and Case Studies*, Dissertation for the degree of Doctor of Philosophy, Uppsala University, 2003
- [89]. Visioli, A., “*Modified Anti-Windup Scheme for PID Controllers*”, IEE Proceedings on Control Theory Applications, Vol. 150, No. 1, pp. 49-54, January 2003
- [90]. Lim, H., Park, K. J., Park, E. C. and Choi, C. H., “*Proportional-Integral Active Queue Management with an Anti-Windup Compensator*”, Proceedings of the 2002 Conference on Information Sciences and Systems, Princeton University, March 20-22, 2002
- [91]. Nudelman, G. and Kulesky, R., “*New Approach for Anti-Windup in Cascade Control System*”, Proceeding of the Israel Electric Corporation Ltd., Generation and Transmission Group, 2001
- [92]. Holst, G. C., *Electro-Optical Imaging System Performance*, Second Edition, Spie Optical Engineering Press, USA, 2000
- [93]. Fleeman, E. L., *Tactical Missile Design*, American Institute of Aeronautics and Astronautics, Inc., 2001

- [94]. Lin, C. L. and Su, H. W., “*Adaptive Fuzzy Gain Scheduling in Guidance System Design*”, Journal of Guidance, Control and Dynamics, Vol. 24, No. 4, pp. 683-692, July-August 2001

- [95]. Vergez, P. L. and McClendon, J. R., “Optimal Control and Estimation for Strapdown Seeker Guidance of Tactical Missiles”, Department of the US Air Force Air Force Armament Laboratory (AFSC), February 1982

- [96]. Ogata, K., *Modern Control Engineering*, Prentice-Hall International Inc., 1990

- [97]. Kuo, B. C., *Automatic Control Systems*, Prentice-Hall Inc., 1995

APPENDIX

POLYNOMIALS THAT CAN BE USED IN POLE PLACEMENT¹

The pole placement technique is one of the methods used in the design of control systems. Basically, it is based on the placement of the poles of a closed loop system to the desired locations on the left-hand side of the complex plane. This way, it is guaranteed for the closed loop control system to be stable. Especially when the number of the controller parameters to be determined is equal to the order of the closed loop system, i.e., the highest power of the characteristic polynomial, the pole placement is a very powerful technique.

In the pole placement, the poles can be located according to certain patterns defined by some polynomials. Among them, the Butterworth and Chebyshev polynomials are the most popular ones. Using these polynomials, the poles that make the closed loop system stable can be put on the left-hand-side of the complex plane so as to set the bandwidth of the closed system (ω_c) as well. The expressions for the polynomials in terms of the Laplace operator “s” are given in Table A1.1 and Table A1.2 up to the fourth-order.

¹ Erickson, R.W., “*Filter Circuits*”, ECEN 2260, 2001

Table A1.1. Butterworth Polynomials

Order	Polynomial
1	$1 + \frac{s}{\omega_c}$
2	$1 + \sqrt{2} \frac{s}{\omega_c} + \left(\frac{s}{\omega_c}\right)^2$
3	$\left(1 + \frac{s}{\omega_c}\right) \left(1 + \frac{s}{\omega_c} + \left(\frac{s}{\omega_c}\right)^2\right)$
4	$\left(1 + 0.7654 \frac{s}{\omega_c} + \left(\frac{s}{\omega_c}\right)^2\right) \left(1 + 1.848 \frac{s}{\omega_c} + \left(\frac{s}{\omega_c}\right)^2\right)$

Table A1.2. Chebyshev Polynomials

Order	Polynomial
1	$1 + \frac{s}{\omega_c}$
2	$\sqrt{2} \left(1 + 0.7654 \left(\frac{s}{0.8409 \omega_c}\right) + \left(\frac{s}{0.8409 \omega_c}\right)^2\right)$
3	$\left(1 + \left(\frac{s}{0.2980 \omega_c}\right)\right) \left(1 + 0.3254 \left(\frac{s}{0.9159 \omega_c}\right) + \left(\frac{s}{0.9159 \omega_c}\right)^2\right)$
4	$\sqrt{2} \left(1 + 0.1789 \left(\frac{s}{0.9502 \omega_c}\right) + \left(\frac{s}{0.9502 \omega_c}\right)^2\right) \cdot \left(1 + 0.9276 \left(\frac{s}{0.4425 \omega_c}\right) + \left(\frac{s}{0.4425 \omega_c}\right)^2\right)$

When these two types of polynomials are compared, it can be seen that a Butterworth polynomial of some degree leads to a flatter response than the Chebyshev polynomial of the same degree. It means that the magnitude curve

remains almost constant at zero dB up to the corner frequency, i.e., desired bandwidth value, in the Bode magnitude diagram as shown in Figure A1.1. In this figure, the vertical axis represents the magnitude of the output to input ratio in terms of dB.

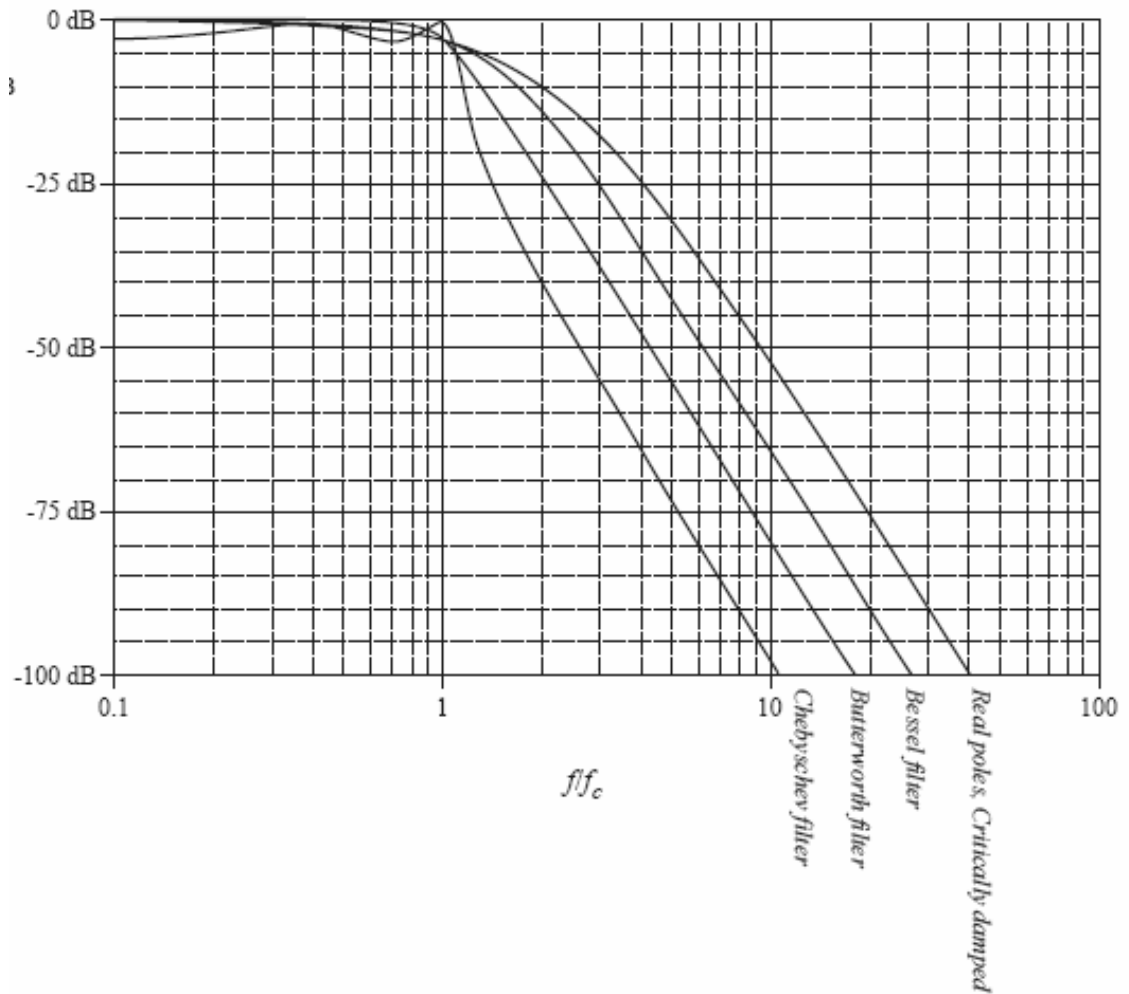


Figure A1.1. Comparison of Certain Fourth Order Polynomials

Moreover, the Butterworth polynomial allows the designer to place poles on a semi-circle with the radius of ω_c that makes the poles far away to the left-hand-side of the complex plane from the pole locations proposed by the ellipse of the

Chebyshev polynomial. The example pole locations proposed by the fourth-order Butterworth and Chebyshev polynomials are shown in Figure A1.2.

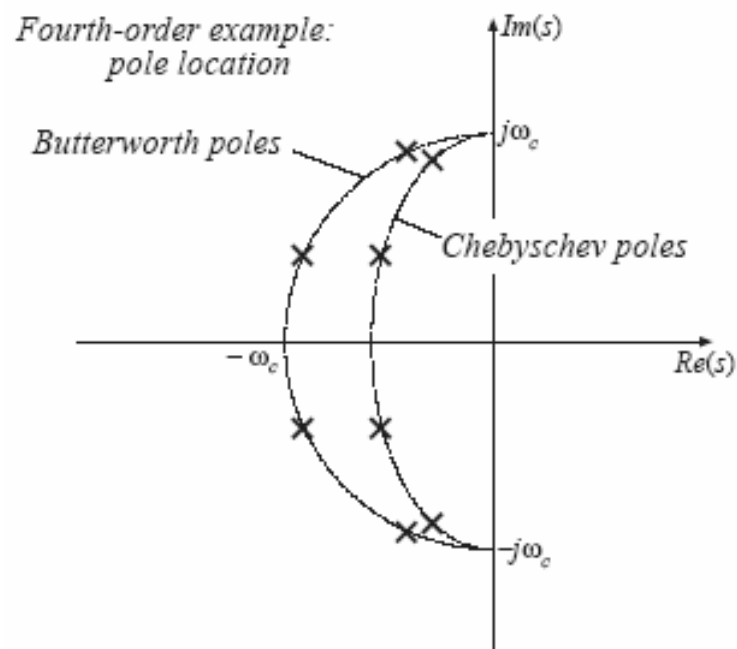


Figure A1.2. Pole Locations Proposed by the Fourth-Order Butterworth and Chebyshev Polynomials

CURRICULUM VITAE

PERSONAL INFORMATION :

Surname : ÖZKAN

Name : Bülent

Date of birth : 03 November 1974

Place of birth : Taşköprü/Kastamonu - TÜRKİYE

Nationality : Turkish

Work address : TUBİTAK-SAGE
Turkish Scientific & Technical Research Council
Defense Industries Research & Development Institute
P.K. 16, 06261 Mamak – ANKARA / TÜRKİYE
Tel: +90 (312) 590 91 28
Fax: +90 (312) 590 91 48-49
E-mail: bozkan@sage.tubitak.gov.tr

Marital status : Married

EDUCATION :

<i>School</i>	<i>Years</i>	<i>Diploma, Subject and Grade</i>
<u>Primary School</u>		
27 Mayıs İlkokulu, Taşköprü, Kastamonu, TÜRKİYE	1980 - 1985	Primary School Diploma, 5.00/5.00
<u>Secondary & High School</u>		
Taşköprü Lisesi, Taşköprü, Kastamonu, TÜRKİYE	1985 - 1991	Secondary & High School Diploma, 9.45/10.00 (First degree)
<u>University</u>		
Gazi University, Department of Mechanical Engineering, Ankara, TÜRKİYE	1991 - 1995	B.Sc. , 73.92 / 100.00 (First degree)
METU, English Preparation School, Ankara, TÜRKİYE	1995-1996	-
METU, Department of Mechanical Engineering, Ankara, TÜRKİYE	1996 - 1999	M.Sc. , “ Dynamic Modeling and Control of Two Coordinated Robot Manipulators”, 3.21 / 4.00
METU, Department of Mechanical Engineering, Ankara, TÜRKİYE	1999 - 2005	Phd. , “Dynamic Modeling, Guidance, and Control of Homing Missiles”, 3.56 / 4.00

LANGUAGE SKILLS :

Native Language : Turkish

Other Languages : English (upper intermediate), German (beginner)

INTERNATIONAL JOURNAL ARTICLE:

1. Özkan, B., and M. K. Özgören, "*Invalid joint arrangements and actuator related singular configurations of a system of two cooperating SCARA manipulators*", Journal of Mechatronics, Vol. 11, 2001, pp. 491-507.

INTERNATIONAL CONFERENCE PAPERS:

2. Özkan, B., and M. K. Özgören, "*Torque Related Singular Configurations of a Planar System of Two Coordinated Manipulators*", MATIMAREN's 8th International Machine Design and Production Conference (UMTIK'98), METU, Ankara, Türkiye, 1998.
3. Özkan, B., and M. K. Özgören, "*Actuator Related Singular Configurations of a System of Two Cooperating SCARA Manipulators*", 6th International Conference on Mechatronics and Machine Vision in Practice (M2VIP), METU, Ankara, Türkiye, 1999.
4. Özkan, B., and M. K. Özgören, "*Optimization of the Driving Torques of the System of Two Coordinated 3R Manipulators*", MATIMAREN's 9th International Machine Design and Production Conference (UMTIK 2000), METU, Ankara, Türkiye, 2000.

5. Özkan, B., and Özgören, M. K., "*ASCs of Two RPR Robots*", 6th International Conference on Mechatronic Design and Modelling (MDM 2002), METU, Cappadocia, Türkiye, September 4-6, 2002.

NATIONAL CONFERENCE PAPERS:

6. Özkan, B., Özgören, M. K., "*Birlikte Çalışan Düzlemsel İki DKD Robot Kolun Eyletimsel Tekil Durumları*", 10. Ulusal Makina Teorisi Sempozyumu, Selçuk Üniversitesi, Konya, Türkiye, Eylül 2001.
7. Özkan, B., Özgören, M. K., "*Birlikte Çalışan İki Düzlemsel Robot Kolun En Az Enerji Tüketimiyle Denetlenmesi*", 10. Ulusal Makina Teorisi Sempozyumu, Selçuk Üniversitesi, Konya, Türkiye, Eylül 2001.
8. Özkan, B., Özgören, M. K., "*Birlikte Çalışan İki Düzlemsel Robot Kolun Eyletimsel Tekil Durumları Etrafında Denetimi*", TOK'2001 Otomatik Kontrol Ulusal Toplantısı, Uludağ Üniversitesi, Bursa, Türkiye, Ekim 2001.
9. Özkan, B., Özgören, M. K., Mahmutyazıcıoğlu, G., "*Hareketli Bir Hedefi Takip Eden Lazer Güdümlü Bir Füzenin Güzüm ve Kontrolü*", Havacılıkta İleri Teknolojiler Sempozyumu (HİTEK-2004), Hava Harp Okulu Komutanlığı, İstanbul, Türkiye, Aralık 2004.
10. Özkan, B., Özgören, M. K., Mahmutyazıcıoğlu, G., "*Lazer Güdümlü Bir Füze Uygulanabilecek Belli Başlı Güzüm Yöntemleri*", 12. Ulusal Makina Teorisi Sempozyumu, Erciyes Üniversitesi, Kayseri, Türkiye, Haziran 2005.

WORK EXPERIENCE :

Organization	Years	Job
<i>METU</i> , Department of Mechanical Engineering, Ankara, TÜRKİYE	Aug. 1996 – Aug.. 2000	Research Assistant
<i>TÜBİTAK-SAGE</i> , Mechanical System Engineering Group / Mechanical Design Division, Ankara, TÜRKİYE	Aug. 2000 - Jan. 2002	Researcher
<i>TÜBİTAK-SAGE</i> , Weapon Systems and Control Technologies Group / Mechatronics Division, Ankara, TÜRKİYE	Jan. 2002 – Nov. 2002	Researcher
<i>TÜBİTAK-SAGE</i> , Weapon Systems and Control Technologies Group / Mechatronics Division, Ankara, TÜRKİYE	Nov. 2002 – ...	Senior Researcher